Johann Wolfgang von Goethe Universität Frankfurt

Institut für theoretische Physik

Master thesis

Evaluating Gauge Corrections to Leptogenesis

Author:
Andreas Halsch

Supervisor:
Prof. Dr. Owe Philipsen

January 4, 2018

Contents

1 Introduction

1.1 Motivation

The most successful scenario of modern cosmology to explain the origin of our universe is the Big-Bang scenario. The Big-Bang model describes the evolution of the universe from an initial singularity in an accelerated expansion. In 1927 the idea of a linearly expanding universe has been proposed by Georges Lemaître [Lem27] and it has become famous as "Hubble expansion of the universe" named after the US-American physicist Edwin Hubble who first measured the Hubble constant by investigating the redshift of spiral galaxies in 1929 [Hub29]. Most recent analysis lead to the Nobel prize of physics in 2011 for S. Perlmutter, B.P. Schmidt and A.G. Riess for proving that the expansion of the universe is actually accelerated [Bah+99]. The most successful model in cosmology explaining the accelerated universe and several other observations as for example the cosmic background radiation is the ΛCDM model. It requires not only a cosmological constant Λ that might be connected to dark energy but also a new, not yet discovered, matter named cold dark matter (CDM) [Bam+12]. Nevertheless cosmology remains a highly interesting topic of modern physics with various open problems. One of the most famous problems will be attacked in this thesis: It is still open to explain the origin of the baryon-to-antibaryon distribution in the universe. Latest measurements, as for example the Wilkinson Microwave Anisotropy Probe (WMAP), could measure the net-baryon (baryons minus antibaryons) to photon ratio as a small positive number. Two fundamental questions arise from this measurement: Why has the ratio the observed small value and why is it a positive quantity? The positive number gives evidence that there is more matter in our universe then antimatter arising the question of the origin of this asymmetry.

This leads to a fundamental problem: When considering the Big-Bang model one starts with symmetric initial conditions for particles and antiparticles. As a result, no matter would remain due to annihilation effects. On the other hand, non-symmetric initial conditions are ineffective because of the inflationary phase and non-perturbative effects in the Standard Model of elementary particle physics (SM). All these effects erasing a preexisting (or dynamically generated) baryon asymmetry are referred to as washout. In context of a preexisting asymmetry the washout is so strong that an enormous initial asymmetry would be required to arrive at the measured value making it an unlikely scenario. A possible way out is the idea of a dynamical process generating a baryon asymmetry during the expansion of the universe. In 1967 Andrei Dmitrijewitsch Sakharov formulated three necessary conditions such a process has to fulfill [Sak67] to generate a finite asymmetry.

Up to date numerous processes fulfilling the Sakharov conditions have been discussed. One of the most successful candidates is the model of thermal Leptogenesis we have chosen as our preferred model. Thermal Leptogenesis requires an extension of the Standard Model: Three additional heavy right handed neutrinos are added to the SM Lagrangian. These additional fermions couple to standard model Higgs fields and leptons and they are introduced with a Majorana mass term. Majorana particles are their own antiparticles making it possible to decay into leptons and anti-leptons. The change of temperature due to the Hubble expansion leads to a decay of the Majorana neutrino at temperatures of the mass scale. The out-of-equilibrium decay is CP-violating such that a lepton asymmetry is generated. The lepton asymmetry is later converted into a baryon asymmetry via nonperturbative effects in the SM known as sphaleron transitions.

Thermal Leptogenesis is closely linked to parameters in the neutrino sector that can eventually be tested experimentally. For example the neutrinoless double beta decay is a promising candidate. On top of that the seesaw mechanism uses the presence of very heavy neutrinos to explain the very light ordinary neutrino masses observed in neutrino oscillation experiments. At the moment neither thermal Leptogenesis nor any other theory explaining the baryon asymmetry in the universe has been tested successfully in an experiment. The topic remains a challenging problem both experimentally and theoretically.

Since thermal Leptogenesis requires an out-of-equilibrium process, most of the theoretical descriptions are done by making use of Boltzmann equations. In 2011 A. Anisimov and W. Buchmüller presented a full quantum mechanical treatment of the problem [Ani+11] based on Kadanoff-Baym equations [KB62] and the Schwinger-Keldysh formalism [Sch61; Kel64]. In contrast to Boltzmann equations, where the involved collision terms are calculated from zero temperature S-matrix elements, the quantum mechanical ansatz is based completely on Green functions including temperature and memory effects. By introducing thermal widths for SM propagators it was possible to show that the Boltzmann result could be reproduced. Nevertheless a more systematic treatment of gauge corrections in the quantum mechanical approach is still missing.

The aim of this thesis is to provide such a systematic treatment and investigate the effect of SM corrections in quantum mechanical thermal Leptogenesis especially by focusing on electroweak gauge corrections. A first approach has been presented in a PhD thesis by Janine Hütig, a former member of the group of Prof. Owe Philipsen at the Goethe Universität Frankfurt [Hüt13].

This work continues the PhD thesis by presenting an approximation for the gauge corrected result that allows to solve the remaining equation numerically. It is structured the following way:

In this first section a brief overview on various models explaining the baryon asymmetry in the universe is presented, focusing especially on the model of thermal Leptogenesis.
In the next section basic concepts of statistical quantum field theory are presented focusing on nonequilibrium field theory and the real time formalism. The final part of the section is a short review of the calculation for the nonequilibrium Majorana propagator as presented in [Ani+11].
In the third section SM corrections to the Majorana self energy are discussed. It is pointed out that resummation is needed and for this purpose hard thermal loop (HTL) resummation and collinear thermal loop (CTL) resummation are discussed. For CTL resummation a recursion relation to calculate the gauge corrected self energy is developed. This part is based on previous works by A. Ansisimov, D. Besak and D. Bödecker [BB10; ABB11].
In the forth section a measure for the amount of asymmetry called lepton number matrix is calculated following [Ani+11]. In this step the asymmetry causing diagrams need to be identified. The calculation leads to a final expression without SM corrections.
The aim of the fifth section is to include corrections to the lepton number matrix from section 4. As a result the gauge corrected Majorana decay width is presented as well as gauge corrections to the asymmetry-causing diagrams following the discussion in [Hüt13]. Finally, after taking all corrections into account, a full gauge corrected result of the lepton number matrix is presented.
In section 6 the numerical procedure for the calculation of the gauge corrected Majorana self energy is presented following [ABB11].
Section 7 motivates an approximation for the gauge corrected lepton number matrix leading to a result that can be treated numerically. For this purpose the infinite time limit of the lepton number matrix is discussed and the dominating parts of the integral are investigated.
The final section 8 presents the numerical results. After introducing the numerical setup and explaining the program structure the thermalization of the Lepton number matrix is investigated by comparing the results from different algorithms. Next the thermalized result is calculated as a function of temperature. The result is compared to a previous results from [Ani+11] obtained in a different more phenomenological way. Next the time dependence of our result is compared to the time dependence obtained by [Ani+11]. Finally the gauge corrected lepton number matrix is calculated as a function of time and temperature. Again the result is compared to [Ani+11].
There are 4 appendices attached: The first two give an overview on the Feynman rules and the propagators. The third one presents the lengthy result of the gauge corrected lepton number matrix when carrying out all time integrations. The final appendix gives details on the result from [Ani+11] used in section 8 to compare the gauge corrected result to.

1.2 The Baryon Asymmetry

The observation of a baryon asymmetry in the universe is a frequently discussed problem of modern physics. As pointed out in the introduction, starting with symmetric initial conditions in a Big-Bang scenario would lead to no baryon asymmetry due to annihilation $b + \bar{b} \to \gamma\gamma$. As a result there would be no matter left in the universe nowadays.

Latest measurements as for example by the WMAP-collaboration give

$$\eta_B^{\mathrm{WMAP}} = \frac{n_b - n_{\bar{b}}}{n_\gamma} = (6.19 \pm 0.15) \cdot 10^{-10} \tag{1}$$

as value for the baryon to antibaryon to photon ratio [Kom+11]. This is a positive small number making clear that the amount of baryons is larger than the amount of antibaryons in the universe. Note that the smallness of the value shows that the universe is dominated by photons instead of baryons.

Considering large regions of antimatter in the universe that could not be observed yet does not solve the problem since intersecting regions would be measurable due to radiation from annihilation. On top of that an initial asymmetry would have to be extremely large to arrive at the measured value. During inflation the baryon number density is reduced at least by a factor order of 10^{60} [DK03] making such a scenario very unlikely. As a result the inflationary phase would washout an initial asymmetry together with SM effects explained later.

Most likely the asymmetry arises during the expansion of the universe for example by a decay of a heavy particle existing only in the early universe at high energies.

A first theoretical approach on such a process has been presented by Andrei Dimitrijewitsch Sakharov in 1967. He formulated 3 necessary conditions a dynamical process has to fulfill to create a baryon asymmetry. These condition became famous as the 3 **Sakharov conditions** [Sak67]:

- **Baryon number violation**: Keeping the baryon number constant could obviously not lead to an asymmetry.
- **C- and CP-violation**: Even if a process violates baryon number conservation a zero net baryon number is kept if not both C and CP is violated. The reason for that is that in the absence of a preference of matter over antimatter both will be produced at the same ratio leading to a zero net baryon number.
- **Departure from thermal equilibrium**: In equilibrium the entropy is maximized when the chemical potentials associated with non conserved quantum numbers vanish. As a result the phase space densities for baryons and antibaryons are necessarily identical and no asymmetry survives [KT90].

There have been numerous models considered fulfilling the Sakharov conditions and leading to a baryon asymmetry. A very short overview will be given in the following.

1.2.1 Baryon Asymmetry in the Standard Model

In 1976 t'Hooft et al. [t H76a; t H76b] discovered nonperturbative processes in the SM that could violate baryon number conservation. On one hand the **Instantons**. These are vacuum solutions in a non-Abelian gauge theory that can change the sum of baryon and lepton number $B + L$ while keeping $B - L$ constant. On the other hand there is another nonperturbative process with such an ability in the SM appearing in the electroweak symmetric phase at temperatures $T \gtrsim 100$ GeV. It is known as saddle point solution or **Sphaleron** process. Both processes are solutions of the field equations of a non-Abelian gauge theory. The topology of the vacuum of such a gauge theory known as θ-vacuum is a non trivial periodic structure. The Instanton solution is a tunneling between different minima of the vacuum. For the Sphaleron process the SM is in its electroweak symmetric phase and the barrier separating neighboring minima can be surmounted. These processes change the Chern-Simons-number by $\Delta N_{CS} = 3$ leading to a change of the baryon number ΔB.

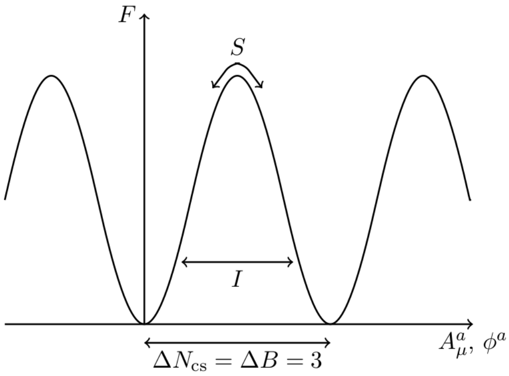

Figure 1: Schematic Structure of the θ-vacuum for the free energy F as a function of the Higgs field ϕ^a and gauge fields A^a_μ with Instanton and Sphaleron transitions c.f. [Hüt13, p. 7]

With the Sphaleron processes at hand the first Sakharov condition is fulfilled and one could wonder if it is possible to describe the generation of a baryon asymmetry completely with the SM. Experimentally a source of CP-violation has been observed in the Quark sector given by the neutral Kaon decay [Fan+99]. Unluckily the amount of CP-violation is too small to explain the observed asymmetry. At least eight orders of magnitude are missing [HS95]. Departure from equilibrium could be provided by a phase transition. In the SM the electroweak phase transition could be the candidate. It shows that a first order phase transition is required to obtain a baryon number $B \neq 0$. Up to date lattice simulations have set an upper limit on the Higgs mass to guarantee a first order phase transition $m_H = 66.5 \pm 1.4$ GeV [CFH99]. The latest measured value of the Higgs mass $m_H = 125.09(24)$ GeV [Pat+16] lies beyond this estimate making a crossover the most likely scenario for the phase transition. Nevertheless the order of the phase transition is still a frequently discussed topic. The theory of electroweak Baryogenesis requires an extra CP violating factor that could be provided by an extension of the Higgs sector for example by adding two further CP-violating Higgs doublets or in the framework of the MSSM (Minimal Supersymmetric Standard Model) [MR12]. Besides the difficulties on the order of the electroweak phase transition these models often require a large number of new parameters.

1.2.2 GUT Baryogenesis

In grand unified theories the electroweak and the strong interaction would be unified in a non-Abelian gauge group as for example SU(5) or SO(10) [Lan81]. The energy scale of such a theory is estimated to be at least at the order of 10^{14} GeV or larger. A baryon asymmetry is generated by a CP-violating out-of-equilibrium decay of a super heavy boson from the underlying gauge group that decays into baryons and antibaryons. Besides the very high energy scale the main problem of such a theory is that the asymmetry is washed out by the Sphaleron processes. These processes still occur at lower energies where most of the bosons already decayed.

1.2.3 Affleck-Dine Baryogenesis

In 1984 Affleck and Dine published a mechanism [AD85] defined for a SU(5) GUT based on a many parameter set of vacuum expectation values for scalar quarks and leptons. Such a setup is naturally implemented in supersymmetric models. The generation of an asymmetry appears after the supersymmetry breaking and the inflationary phase. In this case quarks and leptons can have a large non zero expectation value that can be connected to a generation of an asymmetry. Nevertheless this model is highly non trivial and difficult to falsify. The question arises if a more "natural" model exists.

1.3 The Model of thermal Leptogenesis

A successful model to attack the problem of baryon asymmetry is thermal Leptogenesis. It extends the SM by adding 3 additional right-handed electroweak singlet fermions to the SM Lagrangian. These particles are considered to be very heavy with masses beyond $M \gtrsim 10^8$ GeV. The mass term has the structure of a Majorana mass term. Majorana particles are their own antiparticles making it possible for them to decay to particles as well as antiparticles. Of course they do not carry an electric charge and can be identified as right-handed heavy Majorana neutrinos.

This Ansatz has the advantage that it could solve two problems of particle physics:

On one hand the very light but finite mass of ordinary neutrinos in the SM could be explained via the **See-Saw mechanism** [BPY05]. The Majorana mass term does not affect the gauge symmetry properties of the SM. The presence of a very heavy neutrino relates the Dirac mass matrix m_D to the Majorana mass matrix M_R via the Eigenstates of the complete mass matrix. With the mass matrix given as

$$M = \begin{pmatrix} 0 & m_D \\ m_D & M_R \end{pmatrix}, \tag{2}$$

integrating out the heavy neutrinos defines an effective mass given here for only one neutrino generation ($M_R \equiv M_1$)

$$\tilde{m}_1 \approx \frac{m_D^2}{M_1}. \tag{3}$$

Due to the heaviness of the Majorana neutrinos the effective mass $\tilde{m}_1$ of the ordinary neutrinos turns out to be very small.

On the other hand at temperatures $T \sim M$ the **CP-violating out-of-equilibrium decay** of the Majorana neutrinos can generate a lepton asymmetry. This was first proposed by Fukugita and Yanagida [FY86] in 1986. After generating a lepton asymmetry it is possible to convert it to a baryon asymmetry by making use of the Sphaleron processes.

The new introduced right-handed electroweak singlet fermions are denoted as $\nu_{R,i}$, $i = \{1,2,3\}$ and they couple to the SM Higgs doublet ϕ as well as to SM left-handed lepton doublets $l_{L,i}$ via Yukawa couplings λ leading to the following Lagrangian

$$\mathcal{L} = \mathcal{L}_{SM} + \bar{\nu}_{R,i}\mathrm{i}\partial\!\!\!/\nu_{R,j} + \bar{l}_{L,i}\tilde{\phi}\lambda^*_{ij}\nu_{R,j} + \bar{\nu}_{R,j}\lambda_{ij}l_{L,i}\phi - \frac{1}{2}M_{i,j}(\bar{\nu^c}_{R,i}\nu_{R,j} + \bar{\nu}_{R,j}\nu^c_{R,i}). \tag{4}$$

We have introduced the notation $\nu^c_{R,i} = C\nu^T_{R,i}$ with $C = \mathrm{i}\gamma_2\gamma_0$ being the charge conjugation matrix and $\tilde{\phi} = \mathrm{i}\sigma_2\phi$.

From the electroweak singlets the Majorana neutrinos are defined as

$$N_i = \nu_{R,i} + \nu^c_{R,i}. \tag{5}$$

Since they are their own antiparticle they couple to SM leptons and antileptons making it possible to decay in both. As a result the decay process violates lepton number conservation. This satisfies the first Sakharov condition.

The departure from equilibrium arises due to the effect of Hubble expansion. When the temperature drops to $T \lesssim M$ with M being the mass scale of the heavy neutrinos the neutrinos are not able to follow the rapid change of the equilibrium distribution. A too large number of heavy neutrinos compared to thermal equilibrium is the result. At temperatures $T \sim M$ the system then equilibrates due to the decay of the out-of-equilibrium particles. Since this is a CP-violating process a finite lepton asymmetry is generated (for a review see [BPY05]).

To understand the mechanism of Leptogenesis it is crucial to study the CP-violation of the heavy neutrino decay. This has to be done by studying the dynamics of the heavy neutrinos. In this case the CP-violation is an interference effect of tree level and loop graphs manifesting itself in complex Yukawa couplings.

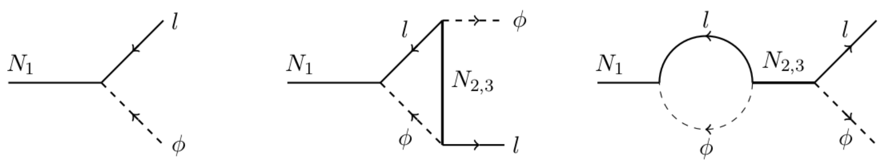

Figure 2: Tree level and 1-loop graphs leading to a complex Yukawa coupling causing CP violation via interference effects. [Hüt13, p. 10]

At temperature $T = 0$ one can define a parameter measuring the amount of CP-violation

$$\epsilon_i := \frac{\Gamma(N_i \to \phi l) - \Gamma(N_i \to \bar{\phi}\bar{l})}{\Gamma(N_i \to \phi l) + \Gamma(N_i \to \bar{\phi}\bar{l})}. \tag{6}$$

For simplicity we restrict our model to a strict mass hierarchy with heavy neutrino masses M_i given as $M_1 \ll M_2, M_3$. A calculation of the interference between tree level and loop graphs leads to the coupling giving the amount of CP-violation. A detailed analysis can be found in [CRV96].

$$\epsilon_1 \simeq -\frac{3}{16\pi} \sum_{k=2}^{3} \frac{\mathrm{Im}\left[(\lambda^\dagger \lambda)^2_{k1}\right]}{(\lambda^\dagger \lambda)_{11}} \frac{M_1}{M_k} + \mathcal{O}\left(\left(\frac{M_1}{M_k}^{\frac{3}{2}}\right)\right). \tag{7}$$

At finite temperature calculations are even more involving. A hard thermal loop corrected result can for example be found in [GHK10; KP12a; KP12b]. In this work we want to study the effects of SM corrections in a systematic quantum treatment.

The main problem of Leptogenesis is the postulate of a new particle living on an energy scale that is yet experimentally out of range. On top of that the coupling is expected to be very weak making measurements even more difficult. An indirect test could be provided by the neutrinoless double beta decay [Hal+76], but at the moment only small masses are experimentally in range.

Never the less there are interesting constraints on the model of Leptogenesis. Besides the heavy neutrino mass M and the effective mass $\tilde{m}$ it is possible to define the mass scale $\bar{m}^2 = m_1^2 + m_2^2 + m_3^2$ with m_i being the masses of the ordinary neutrinos. In the past Leptogenesis has been studied by making use of Boltzmann equations and it was possible to find a maximal asymmetry as function of the mass parameters. It should of course be close to the observed asymmetry [BPY05]

$$\eta_B \leq \eta_B^{\max}(\tilde{m}_1, M_1, \bar{m}). \tag{8}$$

This sets a bound on the mass parameters given as [BDP03]

$$m_i < 0.1\ eV, \qquad M_1 > 4 \times 10^8\ GeV. \tag{9}$$

For a zero initial abundance of the heavy neutrino N_1 one receives an even larger value of

$$M_1 > 2 \times 10^9\ GeV. \tag{10}$$

Note that the other two heavy neutrinos require an even larger mass due to the assumption of mass hierarchy. The lower bound for the ordinary neutrinos is not affected by the hierarchy assumption.

1.4 The effective Model

A first approach is an effective theory formulated by integrating out the two heavier neutrinos N_2 and N_3. After defining $N_1 := N$ and $M_1 := M$ the effective Lagrangian has the following form (leaving out kinetic parts) [BF00]

$$\mathcal{L} \sim \bar{l}_{L,i}\tilde{\phi}\lambda^*_{i1}N + N^T\lambda_{i1}Cl_{L,i}\phi - \frac{1}{2}MN^TCN + \frac{1}{2}\eta_{ij}l^T_{L,i}\phi Cl_{L,j}\phi + \frac{1}{2}\eta^*_{ij}\bar{l}_{L,i}\tilde{\phi}C\bar{l}^T_{L,j}\tilde{\phi}. \tag{11}$$

The remaining heavy neutrino N is weakly coupled to SM particles with small Yukawa couplings $\lambda_{i1} \ll 1$. By integrating out the heavier neutrinos we have defined an effective coupling

$$\eta_{ij} := \sum_{k=2}^{3} \lambda_{ik}\frac{1}{M_k}\lambda^T_{kj}. \tag{12}$$

Most analyses of thermal Leptogenesis are formulated in terms of Boltzmann equations. Assuming small number densities justifies the use of Maxwell-Boltzmann statistics and the Boltzmann equations can be written as [BDP02; Bar+00]

$$\begin{aligned}\frac{dN_{N_1}}{dz} &= -(D+S)(N_{N_1} - N^{eq}_{N_1}), \\ \frac{dN_{B-L}}{dz} &= -\epsilon_1 D(N_{N_1} - N^{eq}_{N-1}) - WN_{B-L},\end{aligned} \tag{13}$$

with the dimensionless parameter $z = M_1/T$. The number densities N are calculated in a portion of co-moving volume containing one photon at temperatures $T \gg M$.

D denotes the decay and inverse decay processes of the Majorana neutrino generating a Lepton asymmetry and S are scattering processes of the heavy neutrino. The scattering processes do not appear in the $B - L$ equation since they do not directly change the lepton number. W denotes the so called washout processes that play a crucial role. As implied by their name washout processes tend to erase a created Lepton asymmetry. The final lepton asymmetry is the result of a competition between washout and production processes.

The importance of washout is closely connected to the decay parameter K originally introduced in the context of GUT Baryogenesis. It gives information if the decay is out of equilibrium. It is defined as a function of the decay rate and the Hubble expansion[1] [2]

$$K := \frac{\Gamma_D(z \to \infty)}{H(z=1)} = \frac{\tilde{m_1}}{m_*}. \tag{14}$$

In this step we have further introduced the equilibrium neutrino mass m_* given by

$$m_* = \frac{16\pi^{\frac{5}{2}}\sqrt{g_*}}{3\sqrt{5}}\frac{v^2}{M_{\text{Pl}}} \simeq 1.08 \times 10^{-3}\ eV, \tag{15}$$

as a function of the total number of degrees of freedom in the SM $g_* = 106.75$, the Planck mass M_{Pl} and the Higgs VEV denoted as v.

Far out-of-equilibrium K is very small because the Hubble expansion is dominating ($K \ll 1$). As a result decays occur at very small temperatures $z \gg 1$ and the produced asymmetry is not reduced by washout effects on a significant level. This scenario is referred to as the **weak washout regime**.

On the opposite for $K \gg 1$ the asymmetry is generated at high temperatures and efficiently washed out. This is the **strong washout regime**.

The issue of washout has been attacked in several publications using a Boltzmann approach on Leptogenesis for example see [BDP05].

[1] Remember that the Hubble expansion takes the system out of equilibrium.

[2] $z = M/T$, so $z \to \infty$ corresponds to $T = 0$ and $z = 1$ to $T \sim M$ the temperature scale where Leptogenesis happens

In this work we are having a look at Leptogenesis using a purely quantum mechanical treatment. In particular we want to investigate SM corrections focusing on gauge corrections. Instead of Boltzmann equations we have to use equations from nonequilibrium statistical field theory known as Kadanoff-Baym equations. These equations make use of the Schwinger Keldysh formalism to obtain real time nonequilibrium propagators. The basic ideas and techniques of nonequilibrium QFT will be presented in the next section.

In thermal Leptogenesis the departure from equilibrium is provided by the Hubble expansion of the universe. At temperatures $T \sim M$ this leads to an excess of the Majorana neutrino abundance compared to the equilibrium thermal abundance of the heavy neutrinos. As a result the neutrino decays to SM leptons and Higgs fields generating a lepton asymmetry. This asymmetry generating decay competes with numerous processes as for example scattering processes that diminish the generated asymmetry. After a short time these washout processes are no longer in equilibrium and the asymmetry is "frozen in".

The described process of Leptogenesis starts with a thermal distribution of heavy neutrinos. In the standard picture of Leptogenesis the Majorana neutrinos need to be produced first at temperatures $T > M$ by thermal scatterings in the early universe [Bio+17]. During this production a first lepton asymmetry is created, that is later completely washed out. Afterwards when the equilibrium distribution of the heavy neutrino is reached and the temperature drops to $T \sim M$ the process described above takes place.

By making use of Boltzmann analysis it could be observed in [BDP02] that for a physical set of Leptogenesis parameters $M = 10^{10}$ GeV, $\tilde{m}_1 = 10^{-3}$ eV, $\epsilon = 10^{-6}$ the first asymmetry created during the production of the heavy neutrinos is of the same size as the final asymmetry (compare to figure 3). As a result it is possible to investigate the generation of a lepton asymmetry starting with a zero initial abundance of heavy neutrinos. For the given parameters it could be observed that the first and the final lepton asymmetry is at the same order of magnitude.

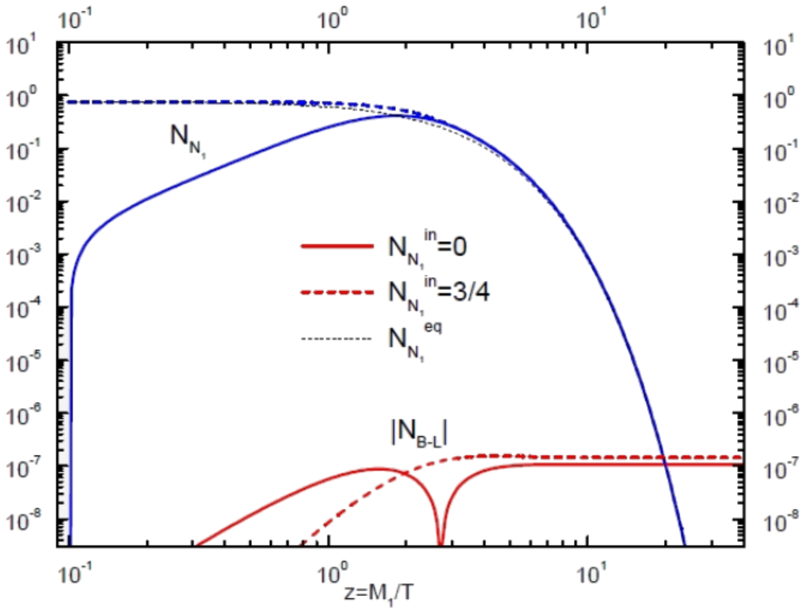

Figure 3: Generated Lepton asymmetry as a function of the initial abundance of the neutrino N by making use of the model parameters $M = 10^{10}$ GeV, $\tilde{m}_1 = 10^{-3}$ eV, $\epsilon = 10^{-6}$. [Hüt13, p. 14]

When investigating the generation of the first asymmetry the effect of Hubble expansion can be neglected and the temperature of the thermal bath of SM fields can be kept constant. This is based on a discussion made by [Ani+11] allowing a full quantum mechanical treatment of the generation of a lepton asymmetry. Since the first and the final asymmetry are of the same size calculating the first asymmetry gives information about the final asymmetry of the system.

As mentioned, after the first asymmetry is created and before the generation of the final asymmetry takes place the first asymmetry is washed out efficiently. This allows us to neglect washout when considering the generation of the first asymmetry.

This scenario can of course also be investigated by making use of Boltzmann equations. The equations can for example be found in [HPW09] by neglecting washout and Hubble expansion. The equation for the Majorana neutrino distribution f_N has the following form $\left(\int_{\vec{q}} = \int \frac{d^3q}{(2\pi)^3 2q_0)}\right)$

$$\frac{\partial}{\partial t} f_N(t, \omega_{\vec{p}}) = -\frac{2}{\omega_{\vec{p}}} \int_{\vec{q},\vec{k}} (2\pi)^4 \delta^4(k+q-p)(\lambda^\dagger\lambda)_{11} p \cdot k \\ \times [f_N(t, \omega_{\vec{p}})(1-f_l(k))(1+f_\phi(q)) - f_l(k) f_\phi(q)(1-f_N(t,\omega_{\vec{p}}))]. \tag{16}$$

All other distribution functions in the equation are equilibrium Fermi- and Bose distribution functions f_l and f_ϕ. Note that $\omega_{\vec{p}} = \sqrt{M^2 + \vec{p}^2}$ is on shell and k, q denote the energies of l and ϕ. The matrix element of the decay process obtained by investigating CP-violation $|M(N(p) \to l(k)\phi(q))|^2 = 2(\lambda^\dagger\lambda) p \cdot k$ can for example be found in [BF00].

Neglecting the momentum dependence of the heavy neutrino distribution and using a zero initial abundance given as $f_N(0, \omega_{\vec{p}}) = 0$ one obtains the following solution of the Boltzmann equation

$$f_N(t, \omega_{\vec{p}}) = f_N^{eq}(\omega_{\vec{p}})(1 - e^{-\Gamma_{\vec{p}} t}). \tag{17}$$

The thermal width is given as a sum of decay and inverse decay widths and has the following form

$$\Gamma_{\vec{p}} = (\lambda^\dagger\lambda)_{11} \frac{2}{\omega_{\vec{p}}} \int_{\vec{k},\vec{q}} (2\pi)^4 \delta^4(k+q-p) p \cdot k (1 - f_l(k) + f_\phi(q)). \tag{18}$$

With the equilibrium distribution of the heavy neutrino, given as Fermi-distribution.

To compute the lepton asymmetry we require an equation for the lepton distribution function. It is given by

$$\frac{\partial}{\partial t} f_l(t,k) = -\frac{1}{2k} \int_{\vec{q},\vec{p}} (2\pi)^4 \delta^4(k+q-p) \\ [|M(l\phi \to N)|^2 f_l(k) f_\phi(q)(1 - f_N(t,\omega_{\vec{p}})) - |M(N \to l\phi)|^2 f_N(t,\omega_{\vec{p}})(1-f_l(k))(1+f_\phi(q))]. \tag{19}$$

Solving the equation assuming no initial asymmetry $f_{L,i}(0,k) = 0$ leads to the following result

$$f_{L,i}(t,k) = f_{l,i}(t,k) - f_{\bar{l},i}(t,k) = -\epsilon_{ii} \frac{1}{k} \int_{\vec{p},\vec{q}} (2\pi)^4 \delta^4(k+q-p) p \cdot k (1 - f_l(k) + f_\phi(q)) f_N^{eq}(\omega_{\vec{p}}) \frac{1 - e^{-\Gamma_{\vec{p}} t}}{\Gamma_{\vec{p}}}, \tag{20}$$

where the coupling has been defined as

$$\epsilon_{ii} = \frac{3}{16\pi} \mathrm{Im}(\lambda_{i1}^* (\eta\lambda^*)_{j1}) M. \tag{21}$$

It is directly connected to the parameter obtained previously when analyzing the amount of CP-violation in our effective model

$$\epsilon = \sum_{k=2}^{3} \frac{\epsilon_{ii}}{(\lambda^\dagger\lambda)_{11}}. \tag{22}$$

It will be interesting to compare the quantum mechanical result to the structure of this non gauge corrected Boltzmann result.

2 Nonequilibrium Quantum Field Theory

In our model we consider one out-of-equilibrium heavy Majorana neutrino weakly coupled to a thermal bath of SM leptons and Higgs fields. For this reason calculations have to be performed using technics of statistical quantum field theory to derive the propagators. In the following section a short review of statistical QFT will be given and the calculation of the nonequilibrium Majorana propagator will be motivated. A detailed presentation can be found in [Ani+11] or [Men10].

2.1 Statistical Quantum Field Theory

For a thermodynamic system described by the statistical ensemble a density matrix ρ can be defined as [Ani+11]

$$\rho := \frac{e^{-\beta H}}{\mathrm{tr}\left(e^{-\beta H}\right)} = \frac{e^{-\beta H}}{Z[\beta]}. \tag{23}$$

With the Hamilton operator H of the system and the inverse temperature $\beta = 1/T$. An observable is now measured by calculating the expectation value of the corresponding operator

$$\langle \mathcal{O} \rangle = \mathrm{tr}(\rho \mathcal{O}) = \frac{1}{Z[\beta]} \mathrm{tr}(\mathcal{O} e^{-\beta H}). \tag{24}$$

Leptogenesis is considered to be a process in the early universe at high temperatures above the electroweak scale. As a result the SM is in its symmetric phase with the Higgs fields given as massless real scalar fields. The two characteristic functions for massless scalar fields are the spectral function Δ^- and the statistical propagator Δ^+

$$\begin{aligned} \Delta^-(x_1, x_2) &= \mathrm{i} \left\langle [\phi(x_1), \phi(x_2)] \right\rangle, \\ \Delta^+(x_1, x_2) &= \frac{1}{2} \left\langle \{\phi(x_1), \phi(x_2)\} \right\rangle. \end{aligned} \tag{25}$$

The spectral function is the Fourier transform of the spectral density, which characterizes the density of quantum mechanical states in phase space. The statistical propagator gives information about the occupation number of states.

Further one can define two two-point functions referred to as Wightman functions

$$\begin{aligned} \Delta^>(x_1, x_2) &= \left\langle \phi(x_1)\phi(x_2) \right\rangle, \\ \Delta^<(x_1, x_2) &= \left\langle \phi(x_2)\phi(x_1) \right\rangle. \end{aligned} \tag{26}$$

It is now straight forward to define the time ordered propagator

$$\Delta(x_1, x_2) = \langle T(\phi(x_1)\phi(x_2)) \rangle = \Theta(x_1 - x_2)\Delta^>(x_1, x_2) + \Theta(x_2 - x_1)\Delta^<(x_1, x_2). \tag{27}$$

The Wightman functions are connected to the statistical and spectral propagator the following way

$$\begin{aligned} \Delta^-(x_1, x_2) &= \mathrm{i}(\Delta^>(x_1, x_2) - \Delta^<(x_1, x_2)), \\ \Delta^+(x_1, x_2) &= \frac{1}{2}(\Delta^>(x_1, x_2) + \Delta^<(x_1, x_2)). \end{aligned} \tag{28}$$

Since the spectral function is defined by making use of a commutator for field operators ϕ one obtains the following boundary conditions after making use of the condition for canonical quantization

$$\begin{aligned} \Delta^-(x_1, x_2)|_{t_1 = t_2} &= 0, \\ \partial_{t_1}\Delta^-(x_1, x_2)|_{t_1 = t_2} &= \delta(\vec{x_1} - \vec{x_2}), \\ \partial_{t_1}\partial_{t_2}\Delta^-(x_1, x_2)|_{t_1 = t_2} &= 0. \end{aligned} \tag{29}$$

It is important to notice that these conditions do not depend on physical initial conditions yet. Physical initial conditions enter only as the boundary conditions for the statistical propagator Δ^+.

Recalling the effective Lagrangian of our model the neutrino couples also to left-handed leptons. For these Weyl fields it is possible to define the statistical propagator and the spectral function in an analogous way

$$
\begin{aligned}
(S^-_{L,ij})_{\alpha\beta}(x_1,x_2) &= \mathrm{i}\left\langle\{l_{L,i\alpha}(x_1),\bar{l}_{L,j\beta}(x_2)\}\right\rangle, \\
(S^+_{L,ij})_{\alpha\beta}(x_1,x_2) &= \frac{1}{2}\left\langle[l_{L,i\alpha}(x_1),\bar{l}_{L,j\beta}(x_2)]\right\rangle,
\end{aligned}
\tag{30}
$$

keeping in mind that the commutator has to be replaced by an anticommutator for fermions.

The fields are denoted with flavour indices i, j and spinor indices α, β, the index L denotes left-handed leptons. The definition of Wightman functions stays the same as in the bosonic case, as well as the connection between Wightman functions and statistical propagator or spectral function.

Finally the heavy Majorana neutrino propagator can be defined in analogy to the lepton propagator

$$
\begin{aligned}
G^-_{\alpha\beta}(x_1,x_2) &= \mathrm{i}\left\langle\{N_\alpha(x_1),N_\beta(x_2)\}\right\rangle, \\
G^+_{\alpha\beta}(x_1,x_2) &= \frac{1}{2}\left\langle[N_\alpha(x_1),N_\beta(x_2)]\right\rangle.
\end{aligned}
\tag{31}
$$

2.2 The Real Time Formalism

As known from the Sakharov conditions departure from thermal equilibrium is a necessary condition to create a baryon asymmetry or an initial lepton asymmetry later transformed into a baryon asymmetry. The heavy Majorana neutrino has to be out-of-equilibrium. The corresponding out-of-equilibrium correlation function $G^\pm$ can be obtained by making use of the Schwinger-Keldysh formalism [Kel64]. In the Schwinger-Keldysh formalism Green functions are calculated along a special time integration contour $\mathcal{C}$ in the complex time-plane. The reason for that is that nonequilibrium processes are initial value problems. In equilibrium quantum field theory S-matrix elements are calculated by sending the initial and final time to $t_i \to -\infty$ and $t_f \to \infty$. By contrast for a nonequilibrium processes the system is prepared in a known initial state at time $t_i = 0$. Since the system is not in equilibrium there is no information on the system before the initial time so taking the limit $t_i \to -\infty$ is not possible. Instead one can only have a look at the final state of the system by sending $t_f \to \infty$ but keeping t_i fixed. Since the only information about the system is at initial time it is intuitive that the contour $\mathcal{C}$ in the complex x^0-plane has to begin and end at t_i. It is referred to as Keldysh contour.

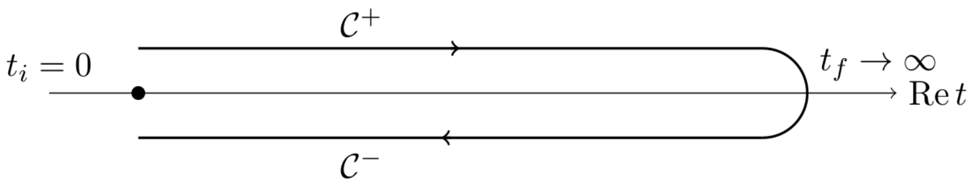

Figure 4: Keldysh contour $\mathcal{C}$ in the complex time plane used to compute nonequilibrium propagators [Hüt13, p.20]. Starting point is a known configuration at $t_i = 0 + \mathrm{i}\epsilon$ the integration is then performed parallel to the real axis up to $t_f \to \infty + \mathrm{i}\epsilon$ denoted as $\mathcal{C}^+$ and then in opposite direction from $t_f \to \infty - \mathrm{i}\epsilon$ to $t_i = 0 - \mathrm{i}\epsilon$, denoted as $\mathcal{C}^-$. The physical correlation function is obtained in the limit $\epsilon \to 0$.

The Green function of the heavy neutrino calculated along the Keldysh contour is denoted as $G_\mathcal{C}$ and given as

$$
G_\mathcal{C}(x_1,x_2) = \Theta_\mathcal{C}(x_1^0,x_2^0)G^>(x_1,x_2) + \Theta_\mathcal{C}(x_2^0,x_1^0)G^<(x_1,x_2). \tag{32}
$$

The path ordering along the Keldysh contour is enforced by the Θ-functions.

The Green function satisfies the following equation of motion given as Schwinger-Dyson equation [Bel11]

$$C(\mathrm{i}\not{\partial}_1 - M)G_{\mathcal{C}}(x_1, x_2) - \mathrm{i}\int_{\mathcal{C}} C\Sigma_{\mathcal{C}}(x_1, x')G_{\mathcal{C}}(x', x_2)d^4x' = \mathrm{i}\delta_{\mathcal{C}}(x_1 - x_2), \tag{33}$$

where $C\Sigma_{\mathcal{C}}(x_1, x')$ is the self energy on the contour and a charge conjugation matrix C has been factorized out. It can also be decomposed by making use of the Θ-functions

$$\Sigma_{\mathcal{C}}(x_1, x_2) = \Theta_{\mathcal{C}}(x_1^0, x_2^0)\Sigma^{>}(x_1, x_2) + \Theta_{\mathcal{C}}(x_2^0, x_1^0)\Sigma^{<}(x_1, x_2). \tag{34}$$

Having a closer look at the Schwinger-Dyson equation shows that both time coordinates of $G_{\mathcal{C}}$ and $\Sigma_{\mathcal{C}}$ can lie on the upper branch of the Keldysh contour. In this case one denotes G^{11} and this is the familiar time-ordered Feynman propagator. Never the less there are 3 more possibilities as for example both time coordinates on the lower branch or a mixing between branches leading to a total number of 4 propagators. Since the upper branch is "earlier" than the lower branch one obtains

$$\begin{aligned}
G^{12}(x_1, x_2) &= G^{<}(x_1, x_2), \\
G^{21}(x_1, x_2) &= G^{>}(x_1, x_2), \\
G^{11}(x_1, x_2) &= G^{+}(x_1, x_2) - \frac{\mathrm{i}}{2}\mathrm{sgn}(x_1^0 - x_2^0)G^{-}(x_1, x_2), \\
G^{22}(x_1, x_2) &= G^{+}(x_1, x_2) + \frac{\mathrm{i}}{2}\mathrm{sgn}(x_1^0 - x_2^0)G^{-}(x_1, x_2).
\end{aligned} \tag{35}$$

The propagator can now be written as a 2×2 matrix, with the indices G^{kl} referred to as contour indices. This is of course also the case for the self energy Σ^{kl}.

The self energy fulfills the same relations introduced previously connecting Wightman functions and the statistical propagator and spectral function

$$\begin{aligned}
\Sigma^{-}(x_1, x_2) &= \mathrm{i}(\Sigma^{>}(x_1, x_2) - \Sigma^{<}(x_1, x_2)), \\
\Sigma^{+}(x_1, x_2) &= \frac{1}{2}(\Sigma^{>}(x_1, x_2) + \Sigma^{<}(x_1, x_2)).
\end{aligned} \tag{36}$$

Splitting the Schwinger-Dyson equation above in terms of contour indices finally leads to a set of two coupled differential equations for $G^{\pm}_{\vec{p}}$ known as Kadanoff-Baym equations

$$C(\mathrm{i}\gamma^0\partial_{t_1} - \vec{p}\vec{\gamma} - M)G^{-}_{\vec{p}}(t_1, t_2) = -\int_{t_1}^{t_2} C\Sigma^{-}_{\vec{p}}(t_1, t')G^{-}_{\vec{p}}(t', t_2)dt', \tag{37}$$

$$C(\mathrm{i}\gamma^0\partial_{t_1} - \vec{p}\vec{\gamma} - M)G^{+}_{\vec{p}}(t_1, t_2) = -\int_{t_i}^{t_2} C\Sigma^{+}_{\vec{p}}(t_1, t')G^{-}_{\vec{p}}(t', t_2)dt' + \int_{t_i}^{t_1} C\Sigma^{-}_{\vec{p}}(t_1, t')G^{+}_{\vec{p}}(t', t_2)dt', \tag{38}$$

with the spacial components transformed to momentum space. There are important properties of the Kadanoff-Baym equations:

- The Kadanoff-Baym equation is an exact equation containing all quantum and non-Markovian effects. There has not been made any assumption on the size of the deviation from equilibrium. As a result it is valid for arbitrary nonequilibrium initial states which can be parametrized by Gaussian initial conditions [Ani+11, p. 13]. This is the case in this work because the generated lepton asymmetry is calculated to leading order in Yukawa coupling by making use of 2-point functions of the heavy neutrino only.
- As mentioned previously the physical initial conditions at t_i enter only via the statistical propagator or more precisely in the equation of the statistical propagator (38).
- The state of a nonequilibrium system is characterized in terms of quantum mechanical correlation functions $G^{\pm}$ instead of distribution functions. The interactions enter as corrections to the self energies $\Sigma^{\pm}$ making it necessary to identify the corresponding self energy diagrams.

It is also possible to calculate equilibrium propagators using a contour in the complex x^0-plane. As mentioned earlier for a system in thermal equilibrium, S-matrix elements are calculated by sending $t_i \to -\infty$ and $t_f \to \infty$. Further it is well known from the imaginary time formalism that the complex time is connected to the inverse temperature β. The resulting time integration contour can for example be found in [Bel11]. It has the following form:

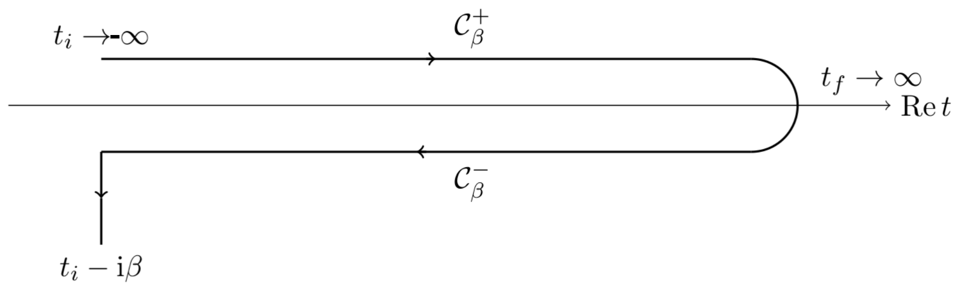

Figure 5: Time integration contour $\mathcal{C}_\beta$ to calculate equilibrium propagators in real time formalism [Hüt13, p. 24]. Integration starts at $t_i \to -\infty + \mathrm{i}\epsilon$ parallel to the real time axis up to $t_f \to \infty + \mathrm{i}\epsilon$ denoted as $\mathcal{C}_\beta^+$ and then backwards from $t_f \to \infty - \mathrm{i}\epsilon$ to $t_i \to -\infty - \mathrm{i}\epsilon$, denoted as $\mathcal{C}_\beta^-$, finishing at $t_i - \mathrm{i}\beta$. Again the physical propagator is obtained in the limit $\epsilon \to 0$.

A straightforward calculation leads to the equilibrium propagators.

2.3 Equilibrium Propagators

For the calculation of our nonequilibrium Majorana neutrino propagator we are dealing with one particle, the heavy Majorana neutrino, that is weakly coupled to a thermal bath of SM Higgs fields and leptons. As pointed out in section 1.4 the thermal bath of SM fields is kept at a constant temperature, because the SM interactions keep the thermal bath in equilibrium. This is the case because at temperatures $T \sim M$ the timescale of SM interactions $\tau_{SM} \sim 1/(g^2 T)$ is much shorter then the equilibration time $\tau_N \sim (\lambda^2 M)$ of the heavy neutrino due to the weakness of the Yukawa coupling $\lambda \ll 1$. As a result this governs the the generation of the lepton asymmetry, since $\tau_{SM} \ll \tau_N$ allows the assumption that the background medium equilibrates instantaneously on the timescale of the heavy neutrino, leaving open the details of the equilibration process [Ani+11, p. 13].

In the effective Lagrangian only massless left-handed leptons couple to the Majorana neutrino so there will be no mass term involved in the lepton propagator. On top of that at temperatures where Leptogenesis takes place the SM is in its electroweak symmetric phase leading to massless Higgs fields.

It is well known from equilibrium statistical QFT that correlation functions of spatially homogeneous systems only depend on spacetime differences. Further the propagators fulfill the Kubo-Martin-Schwinger (KMS) relations known as

$$\Delta^<_{\vec{k}}(\omega) = e^{-\beta\omega} \Delta^>_{\vec{k}}(\omega), \qquad S^<_{\vec{k}}(\omega) = -e^{-\beta\omega} S^>_{\vec{k}}(\omega). \tag{39}$$

Together with the connection between Wightman functions and the statistical function and spectral propagator this implies

$$\begin{aligned} \Delta^+_{\vec{k}}(\omega) &= -\mathrm{i}\left(\frac{1}{2} + f_\phi(\omega)\right)\Delta^-_{\vec{k}}(\omega) = -\frac{\mathrm{i}}{2}\coth\left(\frac{\beta\omega}{2}\right)\Delta^-_{\vec{k}}(\omega), \\ S^+_{\vec{k}}(\omega) &= -\mathrm{i}\left(\frac{1}{2} - f_l(\omega)\right)S^-_{\vec{k}}(\omega) = -\frac{\mathrm{i}}{2}\tanh\left(\frac{\beta\omega}{2}\right)S^-_{\vec{k}}(\omega). \end{aligned} \tag{40}$$

The distribution functions are classic Fermi- and Bose-distribution functions

$$f_\phi(\omega) = \frac{1}{e^{\beta\omega} - 1}, \qquad f_l(\omega) = \frac{1}{e^{\beta\omega} + 1}, \tag{41}$$

yet ω is not fixed at the on-shell value denoted as $\omega_{\vec{k}}$.

Calculating the propagators using the time integration contour presented in the last section leads to the desired equilibrium propagators ($q = |\vec{q}|$, $k = |\vec{k}|$ [Bel11]

$$\Delta^-_{\vec{q}}(y) = \frac{1}{q}\sin(qy), \tag{42}$$

$$\Delta^+_{\vec{q}}(y) = \frac{1}{2q}\coth\left(\frac{\beta q}{2}\right)\cos(qy), \tag{43}$$

$$S^-_{L,\vec{k}}(y) = P_L\left(\mathrm{i}\gamma_0\cos(ky) - \frac{\vec{k}\vec{\gamma}}{k}\sin(ky)\right), \tag{44}$$

$$S_{L,\vec{k}}(y)^+ = -\frac{1}{2}P_L\tanh\left(\frac{\beta k}{2}\right)\left(\mathrm{i}\gamma_0\sin(ky) + \frac{\vec{k}\vec{\gamma}}{k}\cos(ky)\right). \tag{45}$$

A detailed list can be found in Appendix B.

2.4 The nonequilibrium Majorana Neutrino Propagator

The calculation of the out-of-equilibrium Majorana propagator is more involved. As explained in the beginning the calculation is an initial value problem that can be treated in real time formalism by making use of the Keldysh contour.

As pointed out, we consider the heavy neutrino to be weakly coupled to a thermal bath of SM particles. Keeping the thermal bath in equilibrium and at constant temperature allows us to compute the self energy Σ of the Majorana neutrino from equilibrium propagators of bath fields only. All backreactions can be neglected [Ani+11, chap. 4]. This corresponds to a truncation in the perturbative expansion in Yukawa coupling λ where corrections are suppressed due to the smallness of the coupling and the number of degrees of freedom in the bath. The corresponding Feynman graph of the self energy up to one loop order is given as:

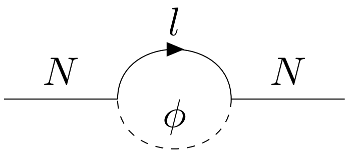

Figure 6: Leading order one loop contribution to the Majorana neutrino self energy.

Note that the diagram is time-translation invariant since the SM equilibrium propagators are time-translation invariant. As a result the spectral function of the heavy neutrino is time-translation invariant $G^-_{\vec{p}}(t_1, t_2) \equiv G^-_{\vec{p}}(t_1 - t_2)$.

Having a first look at the equation for the spectral function of the Majorana neutrino and using the time-translation invariance leads to

$$C(\mathrm{i}\gamma^0\partial_y - \vec{p}\vec{\gamma} - M)G^-_{\vec{p}}(y) - \int_0^y C\Sigma^-_{\vec{p}}(y-y')G^-_{\vec{p}}(y')dy' = 0. \tag{46}$$

This equation can be simplified further by introducing the Laplace-transform

$$\tilde{G}^-_{\vec{k}}(s) := \int_0^\infty e^{-sy}G^-_{\vec{k}}(y)dy, \qquad \tilde{\Sigma}^-_{\vec{p}}(s) := \int_0^\infty e^{-sy}\Sigma^-_{\vec{p}}(y)dy. \tag{47}$$

The equation simplifies to

$$\left(\mathrm{i}\gamma^0 s - \vec{p}\vec{\gamma} - M - \tilde{\Sigma}^-_{\vec{p}}(s)\right)\tilde{G}^-_{\vec{p}}(s) = \mathrm{i}\gamma^0 G^-_{\vec{p}}(0). \tag{48}$$

This is an algebraic equation that can be solved easily. The final propagator can then be obtained by calculating the inverse Laplace transformation given as

$$G^-_{\vec{p}}(y) = \int_{\mathcal{C}_\mathcal{B}} e^{sy}\tilde{G}^-_{\vec{p}}(s)\frac{ds}{2\pi\mathrm{i}}. \tag{49}$$

The integration contour $\mathcal{C}_\mathcal{B}$ is known as Bromwitch contour.

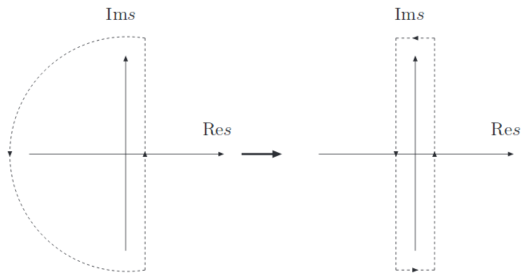

Figure 7: Bromwitch contour: The contour part parallel to the imaginary s axis is chosen with all singularities to its left and then the contour is closed via a semicircle with $\mathrm{Re}(s) < 0$ taking all singularities into account.

The Laplace transform of the self energy Σ is analytic for real s but has a discontinuities across the imaginary axis [Ani+11, p. 18]. One can define a spectral representation exploiting this fact

$$\tilde{\Sigma}^-_{\vec{p}}(s) := \mathrm{i}\int\limits_{-\infty}^{\infty}\frac{\Sigma^-_{\vec{p}}(p_0)}{\mathrm{i}s - p_0}\frac{dp_0}{2\pi}. \tag{50}$$

Known for example from [Sch14] the retarded and advanced self energy is then given as

$$\tilde{\Sigma}^-_{\vec{p}}(-\mathrm{i}\omega + \epsilon) = \Sigma^R_{\vec{p}}(\omega), \tag{51}$$

$$\tilde{\Sigma}^-_{\vec{p}}(-\mathrm{i}\omega - \epsilon) = \Sigma^A_{\vec{p}}(\omega). \tag{52}$$

The discontinuity determines the total self energy

$$\mathrm{disc}\tilde{\Sigma}^-_{\vec{p}}(-\mathrm{i}\omega) = \tilde{\Sigma}^-_{\vec{p}}(-\mathrm{i}\omega + \epsilon) - \tilde{\Sigma}^-_{\vec{p}}(-\mathrm{i}\omega - \epsilon) = \Sigma^-_{\vec{p}}(\omega). \tag{53}$$

The real part is given as the principal value integral and in total we have

$$\tilde{\Sigma}^-_{\vec{p}}(-\mathrm{i}\omega \pm \epsilon) = \mathrm{i}\mathcal{P}\int\limits_{-\infty}^{\infty}\frac{\Sigma^-(p_0)}{\omega - p_0}\frac{dp_0}{2\pi} \pm \frac{1}{2}\Sigma^-_{\vec{p}}(\omega). \tag{54}$$

Calculating the inverse spectral function $G^-_{\vec{p}}(y)$ by solving the inverse Laplace transformation along the Bromwich contour and applying a Fourier transformation then leads to the spectral density

$$\rho_{\vec{p}}(\omega) = \left(\frac{-\mathrm{i}}{\not{p} - M - \frac{1}{2}\Sigma^-_{\vec{p}}(\omega)} - \frac{-\mathrm{i}}{\not{p} - M + \frac{1}{2}\Sigma^-_{\vec{p}}(\omega)}\right)C^{-1}. \tag{55}$$

It has been assumed that the divergent contribution of the real part has already been absorbed into mass and wave function renormalization, so that $\rho_{\vec{p}}$ is a renormalized quantity.

The result of the one loop self energy is well known and can for example be found in [Wel83]

$$\Sigma^-_{\vec{p}}(\omega) = 2\mathrm{i}(\lambda^\dagger\lambda)_{11} \int\int \not{k}\sigma(p;k,q) \frac{d^3k}{(2\pi)^3 2k_0} \frac{d^3q}{(2\pi)^3 2q_0}. \tag{56}$$

Note that $k = (k, \vec{k})$ as well as $q = (q, \vec{q})$ are on-shell, whereas $p = (\omega, \vec{p})$ is still off-shell. The quantity σ is defined as a function of distribution functions and the energy-momentum conservation

$$\sigma(p;k,q) := f_{l,\phi}(k,q)(2\pi)^4 \left(\delta^4(p-k-q) + \delta^4(p+k+q)\right) + \bar{f}_{l,\phi}(k,q)(2\pi)^4 \left(\delta^4(p+k-q) + \delta^4(p-k+q)\right),$$
$$f_{l,\phi}(k,q) := 1 - f_l(k) + f_\phi(q), \qquad \bar{f}_{l,\phi}(k,q) := f_\phi(q) + f_l(k). \tag{57}$$

The properties of the Dirac γ matrices and rotational invariance give rise to the following Ansatz [Ani+11, p. 19]

$$\Sigma^-_{\vec{p}}(\omega) = \mathrm{i}a_{\vec{p}}(\omega)\gamma^0 + \mathrm{i}b_{\vec{p}}(\omega)\vec{p}\vec{\gamma}, \tag{58}$$

defining ($\int_{\vec{k}} := \int \frac{d^3k}{(2\pi)^3 2k_0}$)

$$a_{\vec{p}}(\omega) := 2(\lambda^\dagger\lambda)_{11} \int_{\vec{k},\vec{q}} k\sigma(p;k,q), \tag{59}$$

$$b_{\vec{p}}(\omega) := -2(\lambda^\dagger\lambda)_{11} \frac{1}{\vec{p}^2} \int_{\vec{k},\vec{q}} \vec{p}\cdot\vec{k}\sigma(p;k,q). \tag{60}$$

Using the definition of a and b, as well as the definition of $\sigma(p;k,q)$ one can easily check the following symmetry properties

$$a_{\vec{p}}(-\omega_{\vec{p}}) = a_{\vec{p}}(\omega_{\vec{p}}), \qquad b_{\vec{p}}(-\omega_{\vec{p}}) = -b_{\vec{p}}(\omega_{\vec{p}}). \tag{61}$$

With the help of these definitions the spectral density can be written in the following form

$$\rho_{\vec{p}}(\omega) = \frac{2\omega\Gamma_{\vec{p}}(\omega)}{(\omega^2 - \omega^2_{\vec{p}}) + (\omega\Gamma_{\vec{p}}(\omega))^2} (\not{p} + M)C^{-1}, \tag{62}$$

where the width $\Gamma_{\vec{p}}$ has been defined as

$$\omega\Gamma_{\vec{p}}(\omega) = \omega a_{\vec{p}}(\omega) + \vec{p}^{\,2} b_{\vec{p}}(\omega) = 2(\lambda^\dagger\lambda)_{11} \int_{\vec{k},\vec{q}} p\cdot k\sigma(p;k,q). \tag{63}$$

The width $\Gamma_{\vec{p}}(\omega_{\vec{p}})$ fulfills the following symmetry properties

$$\Gamma_{\vec{p}}(-\omega_{\vec{p}}) = \Gamma_{-\vec{p}}(\omega_{\vec{p}}) = \Gamma_{\vec{p}}(\omega_{\vec{p}}). \tag{64}$$

Note that in the zero width limit the spectral density reduces to the familiar expression from the vacuum

$$\rho_{\vec{p}}(\omega) = 2\pi\mathrm{sgn}(\omega)\delta(p^2 - M^2)(\not{p} + M)C^{-1}. \tag{65}$$

After calculating the inverse Fourier transformation, the final result of $G^-_{\vec{p}}(\omega)$ takes the following form[3].

$$G^-_{\vec{p}}(y) = \left(\mathrm{i}\gamma_0\cos(\omega_{\vec{p}}y) + \frac{M - \vec{p}\vec{\gamma}}{\omega_{\vec{p}}}\sin(\omega_{\vec{p}}y)\right) e^{-\Gamma_{\vec{p}}|y|/2} C^{-1}. \tag{66}$$

In comparison to the free spectral function this result contains an extra thermal damping factor.

[3]The integral can not be solved without an approximation: The form of the integrand function gives rise to a Breit-Wigner approximation valid for small widths $\Gamma \ll M$ [Ani+10]

After calculating the spectral function we have to continue to solve the second Kadanoff-Baym equation for the statistical propagator

$$C(\mathrm{i}\gamma^0\partial_{t_1} - \vec{p}\vec{\gamma} - M)G^+_{\vec{p}}(t_1,t_2) - \int_0^{t_1} C\Sigma^-_{\vec{p}}(t_1,t')G^+_{\vec{p}}(t',t_2)dt' = \underbrace{-\int_0^{t_2} C\Sigma^+_{\vec{p}}(t_1,t')G^-_{\vec{p}}(t',t_2)dt'}_{:=\zeta_{\vec{p}}(t_1-t_2)}, \tag{67}$$

where the initial time has been set to $t_i = 0$ and a source term $\zeta_{\vec{p}}(t_1 - t_2)$ has been defined.

The general solution is a superposition of the homogeneous solution and an inhomogeneous solution called 'memory integral' containing non-Markovian effects

$$C(\mathrm{i}\gamma^0\partial_{t_1} - \vec{p}\vec{\gamma} - M)G^{+,\mathrm{hom}}_{\vec{p}}(t_1,t_2) - \int_0^{t_1} C\Sigma^-_{\vec{p}}(t_1,t')G^{+,\mathrm{hom}}_{\vec{p}}(t',t_2)dt' = 0, \tag{68}$$

$$G^{+,\mathrm{mem}}_{\vec{p}}(t_1,t_2) = \int_0^{t_1}\int_0^{t_2} G^-_{\vec{p}}(t_1-t')\Sigma^+_{\vec{p}}(t'-t'')G^-_{\vec{p}}(t''-t_2)dt''dt', \tag{69}$$

$$G^+_{\vec{p}}(t_1,t_2) = G^{+,\mathrm{hom}}_{\vec{p}}(t_1,t_2) + G^{+,\mathrm{mem}}_{\vec{p}}(t_1,t_2). \tag{70}$$

The memory part can be calculated using the previous result of the statistical propagator, applying a Fourier transformation and neglecting contributions of $\mathcal{O}(\Gamma_{\vec{p}})$[4]. Sticking to the notation of [Ani+11] we change variables from (t_1,t_2) to $(t, y = t_1 - t_2)$. The final result is given as

$$G^{+,\mathrm{mem}}_{\vec{p}}(t,y) = -\frac{1}{2}\tanh\left(\frac{\beta\omega_{\vec{p}}}{2}\right)\left(\mathrm{i}\gamma_0\sin(\omega_{\vec{p}}y) - \frac{M-\vec{p}\vec{\gamma}}{\omega_{\vec{p}}}\cos(\omega_{\vec{p}}y)\right)\left(e^{-\Gamma_{\vec{p}}|y|/2} - e^{-\Gamma_{\vec{p}}t}\right)C^{-1}. \tag{71}$$

Note that in the limit $t \to \infty$ the memory part takes the form of the equilibrium statistical propagator

$$\lim_{t\to\infty} G^{+,\mathrm{mem}}_{\vec{p}}(t,y) = G^{+,\mathrm{eq}}_{\vec{p}}(y) = -\frac{1}{2}\tanh\left(\frac{\beta\omega_{\vec{p}}}{2}\right)\left(\mathrm{i}\gamma_0\sin(\omega_{\vec{p}}y) - \frac{M-\vec{p}\vec{\gamma}}{\omega_{\vec{p}}}\cos(\omega_{\vec{p}}y)\right)e^{-\Gamma_{\vec{p}}|y|/2}C^{-1}. \tag{72}$$

Up to this point no physical boundary conditions have been used in the calculation. The boundary conditions now enter when solving the homogeneous equation as physical boundary conditions for the statistical propagator $G^+_{\vec{p}}(0,0)$.

As motivated in section 1 we consider vacuum initial conditions corresponding to a zero abundance of the heavy Majorana neutrino

$$G^{+,\mathrm{vac}}_{\vec{p}}(0,0) = \frac{M-\vec{p}\vec{\gamma}}{2\omega_{\vec{p}}}C^{-1}. \tag{73}$$

The Kadanoff-Baym equation for the statistical propagator can then be solved in an analogous way as presented previously for the spectral function. One finally obtains the following full solution of the statistical propagator

$$G^+_{\vec{p}}(t,y) = -\left(\mathrm{i}\gamma_0\sin(\omega_{\vec{p}}y) - \frac{M-\vec{p}\vec{\gamma}}{\omega_{\vec{p}}}\cos(\omega_{\vec{p}}y)\right)\left[\frac{1}{2}\tanh\left(\frac{\beta\omega_{\vec{p}}}{2}\right)e^{-\Gamma_{\vec{p}}|y|/2} + f_N^{eq}(\omega_{\vec{p}})e^{-\Gamma_{\vec{p}}t}\right]. \tag{74}$$

All other propagators as for example the Wightman functions are given as linear combinations of the two propagators calculated. Their form can be found in Appendix B.

[4] This corresponds to the approximation made earlier when calculating the inverse Fourier transformation of the spectral function

3 Gauge corrected Majorana Self Energy

In the considered model we are looking at one out-of-equilibrium heavy neutrino N weakly coupled to a thermal bath of SM particles. As explained previously the self energy of the heavy neutrino can be calculated from equilibrium bath field propagators only [Ani+11, p. 16]. The bath fields couple to electroweak gauge fields making it interesting to consider gauge corrections to the Majorana self energy. Unluckily perturbation theory breaks down in thermal field theory and one has to consider resummation. The resummation schemes are distinguished by different momentum scales of the system (for more details see [Bes10]).

3.1 Momentum Scales

There are three different momentum scales relevant in our model:

- **Hard scale:** The momentum of the particle is of order $p \sim T$ and $p^2 \sim T^2$. In this region perturbation techniques familiar from vacuum QFT are valid since the propagating particle is only weakly affected by interactions with the thermal bath.
- **Soft Scale:** The momentum is of order $p \sim gT$. As a result the particle interacts significantly with the thermal bath. These interactions are of order $\mathcal{O}(1)$ and collective excitations arise. These effects are included by making use of thermal masses $m \sim gT$ and thermal widths Γ. These quantities can be calculated using the HTL (Hard Thermal Loop) resummation scheme [Bel11, chap. 7].
- **Lightcone Scale:** In this case the momentum is of order $p \sim T$, but the squared momentum is of order $p^2 \sim g^2T^2$. In this regime additional collinear divergences arise due to interactions with the thermal bath. Similar to the soft scale new masses become important defined as asymptotic masses m_∞. Calculations are done using the Collinear Thermal Loop resummation scheme (CTL) [BB10].

We are working at large temperatures where large momenta are relevant. Typical particle momentum in our system is of order $\mathcal{O}(T)$. The Majorana neutrino belongs to the hard scale and is not influenced by the thermal bath up to leading order, so that its mass M remains a temperature independent parameter. On the contrary in the high temperature regime with $M \lesssim T$ corrections to SM propagators need to be taken into account. They carry hard but nearly lightlike momenta and a treatment involving asymptotic masses is needed [BB10]. Therefore the relation $k^2 \sim g^2T^2$ is strictly needed. As a result SM particles can become heavier then Majorana particles at high temperatures beyond the neutrino mass $T > M$. Nevertheless for $M \lesssim T$ the asymptotic masses are relatively small compared to the momenta of the particles. It is possible to consider the external and internal loop momenta as nearly collinear with angles of the order of the weak coupling $\mathcal{O}(g)$ [ABB11, p. 5].

3.2 Perturbation Theory close to the Lightcone

3.2.1 Thermal Widths and asymptotic Masses

Close to the lightcone only the relation $k^2 \sim g^2T^2$ is strictly needed whereas $k \sim T$. The scalar propagator $\Delta(k)$ can be parametrized in terms of a thermal width $\Gamma(k)$ and the corresponding thermal mass m via [Bes10, p. 18]

$$\Delta(k) = \frac{-1}{k^2 - \Pi(k)} = \frac{-1}{(k_0 + \mathrm{i}\Gamma(k))^2 - \vec{k}^2 - m^2}, \tag{75}$$

with the self energy $\Pi(k)$. To keep a quasi-particle description of the interaction we have to deal with a small rate $\Gamma^2 \ll m^2$ otherwise we are dealing with a broad resonance, such that the interpretation as a particle is not valid anymore [Bes10, p. 19]. One easily arrives at

$$\mathrm{Re}\Pi(k) = m^2, \qquad \mathrm{Im}\Pi(k) = -2\mathrm{i}k_0\Gamma(k). \tag{76}$$

In general we have $m^2 \sim \mathcal{O}(g^2T^2)$ and $k_0\Gamma(k) \sim \mathcal{O}(g^2T^2)$ such that they are equally important, but at sufficiently high temperatures we are dealing with hard loop momentum close to the lightcone. In this case the self energy turns out to be purely real keeping only the thermal mass now referred to as asymptotic mass $m^2 = m_\infty^2$. It should be mentioned that the asymptotic mass is in general not equal to the thermal mass calculated using

HTL resummation, especially for fermions the results differ.

The asymptotic masses of the nearly lightlike SM Higgs fields and leptons have already been calculated in [BB10, p. 76-81] or [Hüt13, App. A] arriving at

$$\begin{aligned} m_{\phi,\infty} &= \frac{1}{16}\left(3g^2 + g'^2 + 4h_t^2 + 8\lambda\right)T^2, \\ m_{l,\infty} &= \frac{1}{16}\left(3g^2 + g'^2\right)T^2, \end{aligned} \tag{77}$$

with g, g' the $SU(2)$ and $U(1)$ gauge group couplings, h_t the coupling to the top quark and λ the Higgs self-coupling. The corrections do not only include gauge corrections but also other SM corrections as a coupling to the quark sector via λ_t.

3.2.2 Lightcone Coordinates

As we deal with hard lightlike momenta for SM particles it is useful to transform momenta to lightcone coordinates. For this purpose the four vector $v := (1, \vec{v})$ is defined, with $\vec{v}^2 = 1$. The transformed coordinates are defined the following way

$$k_{\|} := \vec{k} \cdot \vec{v}, \tag{78}$$

and the remaining perpendicular 2-momentum $\vec{k}_\perp$. The four vector can then be written as

$$k = (k_+, k_-, \vec{k}_\perp), \qquad k_+ = k_0 + k_{\|}, \qquad k_- = k_0 - k_{\|}. \tag{79}$$

Finally we have

$$k^2 = k_+k_- - \vec{k}_\perp^2 = (k_0 + k_{\|})(k_0 - k_{\|}) - \vec{k}_\perp^2 \sim g^2T^2. \tag{80}$$

We choose v such that

$$\vec{k}_\perp \sim gT, \qquad k_+ \sim T, \qquad k_- \sim g^2T. \tag{81}$$

Note that this choice has the feature that parallel components are hard $k_{\|} \sim T$ whereas the perpendicular components are soft $k_\perp \sim gT$.

3.2.3 Collinear thermal Loops

As explained in the beginning, in contrast to HTL resummation, the external momentum p is not considered to be soft but close to the lightcone for CTL resummation. In this approach motivated by [Bes10, Sec. 2.3] generic 1-loop diagrams with external momenta $p_i \sim T,\ i \in \{1, N\}$, $p_i^2 \sim g^2T^2$ are considered with inner loop momentum k. The loop momentum is of the same kind as the external momentum $k \sim T$, $k^2 \sim g^2T^2$ such that $p_i \cdot k \sim g^2T^2$. The momenta are then called collinear. In lightcone coordinates we then have $k_{\|}, p_{i\ \|} \sim T$, $|\vec{k}_\perp|, |\vec{p}_{i\ \perp}| \sim gT$ and the angle between momenta is of order $\mathcal{O}(g)$.

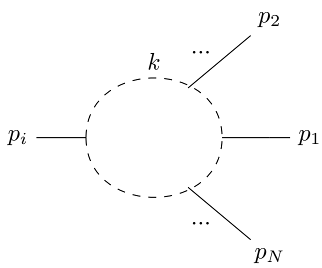

Figure 8: Generic 1-loop diagram used for CTL resummation with external momenta p_i and internal loop momentum k.

We want to investigate gauge corrections for the Majorana self energy, therefore it is sufficient to limit our considerations of external particles to spin-1/2 fermions and spin-1 gauge bosons.

In this case the power counting rules can be found in [Bes10, p. 21] and are given as

- A loop integral gives a g^4 suppression
- A propagator gives $1/(g^2T^2)$
- The vertex contribution of a gauge boson is given by another factor of g
- A Yukawa vertex leads to a further factor of g

For n vertices involving a gauge boson and $m = N - n$ arbitrary vertices our generic 1-loop CTL N-point function is of order

$$\Pi^{(N)}_{\mathrm{CTL}} \sim g^4 \left(\frac{1}{g^2T^2}\right)^N g^n g^N \sim g^{4-m}. \tag{82}$$

In our case of the Majorana self energy we have $m = 2$ external particles that are not gauge particles namely the neutrinos leading to a contribution of order $\mathcal{O}(g^2)$. So at first we are going to have a look at the contribution to the self energy with one additional soft gauge boson.

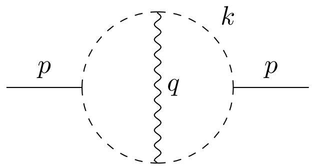

Figure 9: 2-point self energy contribution with one additional soft gauge boson of momentum q.

The corresponding integral expression in imaginary time formalism is given as [Bes10, p. 23]

$$\Pi_{1\ \mathrm{gauge}} \sim g^2 T \sum_{p_0} \int T \sum_{q_0} \int V(p,k,q)\Delta(p)\Delta(p-q)\Delta(p-k+q)\Delta(p-k)\Delta(q) \frac{d^3q}{(2\pi)^3}\frac{d^3p}{(2\pi)^3}, \tag{83}$$

with $V(k,p,q)$ denoting the vertex factor. Following [Bes10] a scalar loop is considered for simplicity but the presented strategy is also valid if one (or both) scalar particles are replaced by fermions. Applying the power counting rules:

- We get an additional g^2 suppression from the new gauge boson vertices.
- Further there is an $1/g^2$ contribution from each new propagator and q is chosen such that $q \cdot p \sim g^2T$.
- There is an additional g^4 factor due to the sum-integral.
- Finally all other contributions from the previous discussions have to be taken into account (choosing of course $N = 2$ and $m = 2$ in (82))

The final result is then given as

$$\Pi_{1\ \mathrm{gauge}} \sim \underbrace{g^2}_{\text{external line vertices}} \underbrace{g^2}_{\text{gauge boson vertices}} \underbrace{\left(\frac{1}{g^2T^2}\right)^5}_{\text{propagators}} \underbrace{(g^4)^2}_{\text{phase space integration}} \sim g^2. \tag{84}$$

Remarkably all additional powers of g have canceled and the correction is of the same order as the tree level. In fact this is still the case when inserting further gauge boson lines leading to ladder diagrams.

Summing up all contributions one arrives at the following ladder diagram for the CTL resummed Majorana self energy with asymptotic masses for equilibrium SM propagators.

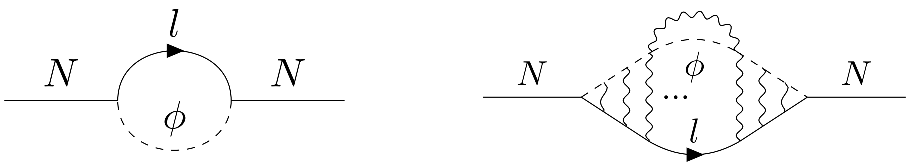

Figure 10: Left: tree level Majorana self energy as known from section 2. Right: gauge corrected ladder diagram of the Majorana self energy with CTL resummation containing propagator and vertex corrections.

3.3 The Landau-Pomeranchuk-Migdal Effect

The presented calculation is closely connected to thermal particle production in terms of the Landau-Pomeranchuk-Migdal effect. The effect was first discovered 1953 by Landau and Pomeranchuk [LP53] and later described by A. Migdal [Mig56] as an effect in electromagnetic showers coming from high-energy cosmic rays. It has shown to be important when describing photon production in the quark gluon plasma (QGP). The effect describes the behavior of a high energetic particle propagating through a thermal medium while undergoing multiple soft scattering processes with the thermal bath. If the formation time of an emitted particle is of the same order as the mean free time between collisions it is not possible anymore to separate events as independent, thus interference arises.
In case of the Majorana neutrino the LPM effect gives information about a thermal production of the Majorana neutrino as investigated in [BB10; ABB11] as well as in the PhD thesis of Denis Besak [Bes10].
For sufficiently high temperatures $T > M$ SM particles are heavier than the Majorana neutrino due to the effect of thermal masses. As a result the Higgs particle can decay into a heavy neutrino. Further the propagation is influenced by the thermal bath because of soft gauge scattering, leading to interference effects of processes as

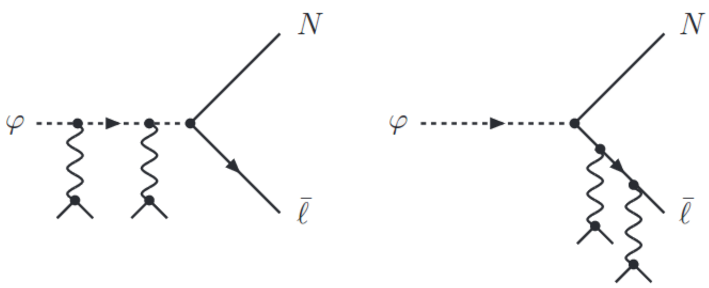

Figure 11: Interfering processes that have to be taken into account when investigating the thermal production of the heavy Majorana neutrinos at temperatures $T > M$ [ABB11, p. 6].

Note that these graphs can be obtained by cutting the ladder diagram (figure 10). The production rate Γ^{prod} per unit time and unit volume can then be calculated via [ABB11, p. 3]

$$\frac{d\Gamma^{\text{prod}}}{d^3k} = \frac{1}{(2\pi)^3 k_0} f_F(k_0) \text{tr}[\not{k} \text{Im}\Sigma^{\text{ret}}(k)], \tag{85}$$

with the retarded self energy $\Sigma^{\text{ret}}(k)$ of the heavy neutrinos. It has to be calculated using the ladder diagram. This turns out to be very useful as a crosscheck of results presented later in section 5.

3.4 Strategy of the Calculation

As presented in the last section corrections to the Majorana self energy are connected to the ladder diagram. In the following we are going to present the strategy for calculating the ladder diagram leading to a result for the self energy including all leading order SM corrections. The calculation is structured the following way [ABB11, p. 7]

- At first the hard field modes are integrated out. As a result asymptotic masses for particles near the lightcone scale are generated and a HTL effective action for soft gauge bosons is defined. Since thermal widths and hard-hard interactions are of order $\mathcal{O}(g^4T)$ they can be neglected.
- Next a current is defined. Starting point is a one-loop diagram with two external Majorana neutrinos and an arbitrary number of soft external gauge bosons. The loop momentum and the external momenta are considered to be nearly collinear. At first the 2-point function without external gauge bosons is calculated. Next it is possible to set up a recursion relation between the n point function and the $(n-1)$ point function obtained by removing one external gauge boson. This is done by making use of a current which is induced by the gauge field background and defined as the integral over all external momenta contracted with the external fields.
- In the last step the soft gauge boson background has to be integrated out. The gauge bosons appear only in self energy insertions leading to thermal widths for lepton and Higgs fields and as rungs in the ladder diagram presented previously. The current now satisfies an integral equation. Finally after stripping of all external fields from the current an integral equation for the desired gauge corrected self energy remains.

3.4.1 Integrating out the hard Modes - SM Propagators with asymptotic Masses

As described the first step of the calculation is to get rid of the hard modes by integrating them out. As a result one obtains a resummed lepton and Higgs propagators with asymptotic masses. For simplicity the subscript ∞ for the asymptotic mass will be dropped in the following. After neglecting contributions of order $\mathcal{O}(g^2T)$ one arrives at the following scalar propagator [BB10, p. 5] and spin-1/2 fermion propagator [BB10, p. 12]

$$\Delta_{\vec{k}}(\omega) = \frac{-1}{k^2 - m_\phi^2}, \tag{86}$$

$$S_{\vec{k}}(\omega) = \frac{\not{k} - \frac{m_l^2}{2k_0}\gamma^0}{k^2 - m_l^2}.$$

Since we only have asymptotic masses the contribution of left- or right-handed leptons flowing in the loop is the same. Therefore it is sufficient to consider only one orientation of fermions in the loop. Sticking with [ABB11] we choose left-handed fermions.

In Weyl basis the gamma matrices have the following form

$$\gamma^0 = \begin{pmatrix} 0 & \mathbb{1}_{2\times 2} \\ \mathbb{1}_{2\times 2} & 0 \end{pmatrix}, \qquad \gamma^k = \begin{pmatrix} 0 & \sigma^k \\ -\sigma^k & 0 \end{pmatrix}, \tag{87}$$

and one can defined the 4-vector

$$k_\mu \cdot \sigma^\mu := k_0 - \sigma^k k_k, \qquad k_\mu \cdot \bar{\sigma}^\mu := k_0 + \sigma^k k_k. \tag{88}$$

By making use of the Weyl basis the lepton propagator S can be written in the following form

$$S_{\vec{p}} = \frac{1}{p^2 - m_l^2} \begin{pmatrix} 0 & p\cdot\sigma - \frac{m_l^2}{2p_0}\mathbb{1}_{2\times 2} \\ p\cdot\bar{\sigma} - \frac{m_l^2}{2p_0}\mathbb{1}_{2\times 2} & 0 \end{pmatrix} := \frac{1}{p^2 - m_l^2} \begin{pmatrix} 0 & \tilde{p}\cdot\sigma \\ \tilde{p}\cdot\bar{\sigma} & 0 \end{pmatrix}, \tag{89}$$

where we have defined

$$\tilde{k} = k - \frac{m_l^2}{2k_0}u, \qquad u = (1, \vec{0}). \tag{90}$$

The projectors in Weyl basis are given as

$$P_L = \frac{\mathbb{1}_{4\times 4} - \gamma^5}{2} = \begin{pmatrix} \mathbb{1}_{2\times 2} & 0 \\ 0 & 0 \end{pmatrix}, \qquad P_R = \frac{\mathbb{1}_{4\times 4} + \gamma^5}{2} = \begin{pmatrix} 0 & 0 \\ 0 & \mathbb{1}_{2\times 2} \end{pmatrix}. \tag{91}$$

Using the projectors we can define the left- and right-handed fermion propagators

$$P_L S_{\vec{k}}(\omega) = \frac{1}{k^2 - m_l^2} \begin{pmatrix} \mathbb{1}_{2\times 2} & 0 \\ 0 & 0 \end{pmatrix} \cdot \begin{pmatrix} 0 & \tilde{k}\cdot\sigma \\ \tilde{k}\cdot\bar{\sigma} & 0 \end{pmatrix} = \frac{1}{k^2 - m_l^2} \tilde{k}\cdot\sigma, \tag{92}$$

$$P_R S_{\vec{k}}(\omega) = \frac{1}{k^2 - m_l^2} \begin{pmatrix} 0 & 0 \\ 0 & \mathbb{1}_{2\times 2} \end{pmatrix} \cdot \begin{pmatrix} 0 & \tilde{k}\cdot\sigma \\ \tilde{k}\cdot\bar{\sigma} & 0 \end{pmatrix} = \frac{1}{k^2 - m_l^2} \tilde{k}\cdot\bar{\sigma}. \tag{93}$$

Note that the only difference between the propagators is a sign in front of the spacial momentum components. A parity transformation then changes left-handed to right-handed.

Since we are only interested in left-handed leptons we can limit our consideration to

$$S^L_{\vec{k}} = \frac{1}{k^2 - m_l^2} \tilde{k}\cdot\sigma. \tag{94}$$

Since the momenta are close to the lightcone we are making use of lightcone coordinates. The scalar propagator can then be written as

$$\Delta_{\vec{k}}(k_0) = \frac{-1}{k^2 - m_\phi^2} = \frac{-1}{k_+ k_- - \vec{k}_\perp^2 - m_\phi^2} = \frac{-1}{(k_0 + k_\parallel)(k_0 - k_\parallel) - \vec{k}_\perp^2 - m_\phi^2}. \tag{95}$$

By making use of collinearity $v\cdot p \sim v\cdot k \sim g^2 T$ it is possible to approximate $k_0 \sim k_\parallel$ [BB10, p. 5].

$$\begin{aligned}\Delta_{\vec{k}}(k_0) = \frac{-1}{k^2 - m_\phi^2} &\approx \frac{-1}{2k_\parallel k_- - \vec{k}_\perp^2 - m_\phi^2} = \frac{1}{2k_\parallel} \frac{-1}{\underbrace{k_0 - k_\parallel}_{=k_0 - \vec{v}\cdot\vec{k} = v\cdot k} - \frac{(\vec{k}_\perp^2 + m_\phi^2)}{2k_\parallel}} = \frac{1}{2k_\parallel} \underbrace{\frac{-1}{v\cdot k - \frac{(\vec{k}_\perp^2 + m_\phi^2)}{2k_\parallel}}}_{:=D_\phi(k)} \\ &\approx \frac{D_\phi(k)}{2k_\parallel}.\end{aligned} \tag{96}$$

The left-handed fermion propagator S^L can be approximated in a similar way

$$S^L_{\vec{k}} = \frac{1}{k^2 - m_l^2} \tilde{k}\cdot\sigma \approx \frac{D_l(k)}{2k_\parallel} \tilde{k}\cdot\sigma. \tag{97}$$

On top of that if the fermion is on-shell $k^2 = m_l^2$, $\tilde{k}$ is lightlike up to higher order terms that have been neglected. Evaluating the loop integral in imaginary time formalism and taking the imaginary part leads to an on-shell fermion propagator allowing to treat $\tilde{k}$ as light-like 4 vector [ABB11, p. 9]. Now it is possible to rewrite S^L in the following form

$$S^L(p) = \eta(\tilde{p})\eta^\dagger(\tilde{p}) D_l(p), \tag{98}$$

by expanding the Weyl spinor η in terms of its coupling g

$$\eta = \left(\mathbb{1}_{2\times 2} - \frac{\vec{\sigma}\cdot\vec{p}_\perp}{2p_\parallel}\right)\begin{pmatrix} 0 \\ 1 \end{pmatrix} + \mathcal{O}(g^2) \quad\to\quad \eta \simeq \eta_0 + \eta_1 + \mathcal{O}(g^2), \qquad \eta_0 = \begin{pmatrix} 0 \\ 1 \end{pmatrix}, \qquad \eta_1 = -\frac{\vec{\sigma}\cdot\vec{p}_\perp}{2p_\parallel}\eta_0. \tag{99}$$

Note that it is sufficient to write $\eta(p)$ instead of $\eta(\tilde{p})$ since the difference is of order $\mathcal{O}(g^2 T)$ and therefore neglectable.

3.4.2 The reduced Self Energy

With the propagators at hand it is now possible to write down the 2-point function referred to as non gauge corrected Majorana self energy

$$\begin{aligned}\Sigma^R_{\vec{p},4\times4}(\omega) = \Sigma_{\vec{p}}(\omega)P_R &= \int S_{\vec{k}}(\omega')\Delta_{\vec{p}-\vec{k}}(\omega-\omega')\frac{d\omega'}{2\pi}\frac{d^3k}{(2\pi)^3}P_R = \int P_L S_{\vec{k}}(\omega')\Delta_{\vec{p}-\vec{k}}(\omega-\omega')\frac{d\omega'}{2\pi}\frac{d^3k}{(2\pi)^3} \\ &= \int S^L_{\vec{k},4\times4}(\omega')\Delta_{\vec{p}-\vec{k}}(\omega-\omega')\frac{d\omega'}{2\pi}\frac{d^3k}{(2\pi)^3}.\end{aligned} \tag{100}$$

Note that we obtain the left-handed self energy when changing $\vec{p}\to-\vec{p}$

$$\begin{aligned}\Sigma^R_{-\vec{p}}(\omega) &= \int S^L_{\vec{k}}(\omega')\Delta_{-\vec{p}-\vec{k}}(\omega-\omega')\frac{d\omega'}{2\pi}\frac{d^3k}{(2\pi)^3} \\ &\overset{\vec{k}\to-\vec{k}}{=} \int S^L_{-\vec{k}}(\omega')\Delta_{-\vec{p}+\vec{k}}(\omega-\omega')\frac{d\omega'}{2\pi}\frac{d^3(-k)}{(2\pi)^3} \\ &= \int S^R_{\vec{k}}(\omega')\Delta_{\vec{p}-\vec{k}}(\omega-\omega')\frac{d\omega'}{2\pi}\frac{d^3k}{(2\pi)^3} = \Sigma^L_{\vec{p}}(\omega),\end{aligned} \tag{101}$$

where we have used $S^R_{-\vec{k}} = S^L_{\vec{k}}$ as pointed out in the last section.

Since Σ is a function of the lepton propagator S^L and the Higgs propagator Δ, it is possible to define the following quantity using the simplifications and approximations of the propagators given before [ABB11, p. 9-10]

$$\Sigma^{ret,R}_{\vec{p}}(\omega) := |\lambda|^2 \int_{-\infty}^{\infty} \eta(\omega,\vec{k})\tilde{\Sigma}(\omega,\vec{k},\vec{p})\frac{d^3k}{(2\pi)^3}, \tag{102}$$

with the Yukawa coupling $|\lambda|^2 = \sum_i (\lambda^\dagger\lambda)_{1i}$ extracted.

The object $\tilde{\Sigma}$ is referred to as reduced self energy and it is calculated by solving

$$\int_{-\infty}^{\infty} S^L(\omega',\vec{k})\Delta(\omega-\omega',\vec{p},\vec{k})\frac{d\omega'}{2\pi} = \eta(k)\int_{-\infty}^{\infty}\eta^\dagger(k)\frac{D_l(k)D_\phi(k-p)}{2(k_\parallel-p_\parallel)}\frac{d\omega'}{2\pi} = \eta(k)\tilde{\Sigma}(p,\vec{k}). \tag{103}$$

With the definition of D_x we have

$$D_l^{-1}(k) = -\left(v\cdot k - \frac{\vec{k}_\perp^2+m_l^2}{2k_\parallel}\right), \qquad D_\phi^{-1}(k-p) = -\left(v\cdot(k-p) - \frac{(\vec{k}_\perp-\vec{p}_\perp)^2+m_\phi^2}{2(k_\parallel-p_\parallel)}\right), \tag{104}$$

$$\begin{aligned}D_l(k) - D_\phi(p-k) &= -\frac{1}{v\cdot k - \frac{\vec{k}_\perp^2+m_l^2}{2k_\parallel}} + \frac{1}{v\cdot(k-p) - \frac{(\vec{k}_\perp-\vec{p}_\perp)^2+m_\phi^2}{2(k_\parallel-p_\parallel)}} \\ &= \frac{-v\cdot(k-p) + \frac{(\vec{k}_\perp-\vec{p}_\perp)^2+m_\phi^2}{2(k_\parallel-p_\parallel)} + v\cdot k - \frac{\vec{k}_\perp^2+m_l^2}{2k_\parallel}}{\left(v\cdot k - \frac{\vec{k}_\perp^2+m_l^2}{2k_\parallel}\right)\left(v\cdot(k-p) - \frac{(\vec{k}_\perp-\vec{p}_\perp)^2+m_\phi^2}{2(k_\parallel-p_\parallel)}\right)} := \frac{\epsilon(p,\vec{k})}{(D_l\cdot D_\phi)^{-1}}.\end{aligned} \tag{105}$$

So ϵ is given as

$$\epsilon(p,\vec{k}) = v\cdot p + \frac{(\vec{k}_\perp-\vec{p}_\perp)^2+m_\phi^2}{2(k_\parallel-p_\parallel)} - \frac{\vec{k}_\perp^2+m_l^2}{2k_\parallel}. \tag{106}$$

Using this we can simplify further

$$\int_{-\infty}^{\infty}\eta(k)\eta^\dagger(k)\frac{D_l(k)D_\phi(k-p)}{2(k_\parallel-p_\parallel)}\frac{d\omega'}{2\pi} = \int_{-\infty}^{\infty}\eta(k)\eta^\dagger(k)\frac{1}{2\epsilon(p,\vec{k})}\frac{D_l(k)-D_\phi(k-p)}{k_\parallel-p_\parallel}\frac{d\omega'}{2\pi} = \eta(k)\tilde{\Sigma}(p,\vec{k}). \tag{107}$$

The calculation of the reduced self energy has already been done in the PhD thesis of Denis Besak [Bes10] using the imaginary time formalism and ending up with

$$\tilde{\Sigma}(p,\vec{k}) = -\frac{d(r)\mathcal{F}(p_\parallel,k_\parallel)}{2\epsilon(p,\vec{k})}\frac{\eta^\dagger(k)}{k_\parallel - p_\parallel}, \tag{108}$$

where $\mathcal{F}(p_\parallel,k_\parallel) = f_F(k_\parallel) + f_B(k_\parallel - p_\parallel)$ is a function of the equilibrium distribution functions and $d(r)$ the dimension of the gauge group representation.

3.4.3 Definition of a Current and Recursion Relation

With this expression for the one loop Majorana self energy at hand we can now continue the calculation by introducing a current J^a_μ. Our aim is to derive a recursion relation for the n-point function. For this purpose the external soft gauge fields are written as $A^a_\mu(q_i)$ with $a = \{1,2,3\}$ and momenta q_i. The current is defined as [BB10, p. 8]

$$J^a_\mu(p) := \int V_\mu(k,k-p)\mathrm{Tr}\left[t^a\hat{J}(p,\vec{k})\right]\frac{d^3k}{(2\pi)^3}, \tag{109}$$

with the vertex factor $V_\mu(k,k-p) = \frac{1}{2k_\parallel}(2k-p)_\mu$ and the gauge group generators t^a. The object $\hat{J}$ is referred to as unintegrated current and defined via

$$\hat{J}(p,\vec{k}) = \sum_{n=2}^{\infty}\prod_{i=1}^{n-1}\int_{q_i} A^{\mu_i}(q_i)(2\pi)^4\delta\left(p - \sum_{j=1}^{n-1} q_j\right)\tilde{\Sigma}^{(n)a_1\dots a_{n-1}}_{\mu_1\dots\mu_{n-1}}(q_1,\dots,q_{n-1},\vec{k})\frac{d^4q_i}{(2\pi)^4}, \tag{110}$$

with the short notation $A^{\mu_i} = t_{a_i}A^{\mu_i}_{a_i}$ and the reduced self energy $\tilde{\Sigma}$. After taking the trace over $SU(2)$ indices we arrive at

$$\mathrm{tr}\hat{J}(p,\vec{k}) = \tilde{\Sigma}(p,\vec{k})N(p). \tag{111}$$

By looking at the vertex structure and making use of partial fraction decomposition and the explicit form of the reduced self energy, it is possible to arrive at a recursion relation for the current

$$\begin{aligned}\epsilon(p,\vec{k})\hat{J}(p,\vec{k}) = &-\frac{1}{2}\mathcal{F}(p_\parallel,k_\parallel)\frac{\eta^\dagger(k)}{k_\parallel - p_\parallel}N(p)\\ &+\int_q[\hat{J}(p-q,\vec{k})V\cdot A(q) - V\cdot A(q)\hat{J}(p-q,\vec{k}-\vec{q})]\frac{d^4q}{(2\pi)^4}.\end{aligned} \tag{112}$$

Note that the recursion relation has the general form $J = N + AJ$. For further details see [ABB11, p. 11-12].

3.4.4 Integrating out the soft gauge Bosons

Finally the soft gauge boson background has to be integrated out. Integrating over the gauge fields A can be done by iterating the recursion relation: $J = N + AJ$ leads to $J = N + A(N + AJ)$ after the first iteration and so on. Integrating over the gauge fields A then leads to contributions as $\langle AAJ\rangle = \langle AA\rangle$ whereas all terms linear in A vanish [ABB11, p. 12-13]. The gauge field propagator is given as

$$\langle A_\mu(q)A_\nu(q')\rangle = \frac{1}{T}\delta_{q_0-q_0',0}(2\pi)^3\delta^3(\vec{q}-\vec{q}\,')(C_2(r)g^2\Delta_{\mu\nu}(q) + y_l^2g'^2\Delta'_{\mu\nu}(q)), \tag{113}$$

derived in imaginary time formalism with the HTL resummed gauge propagators for $SU(2)$ and $U(1)$ respectively. For SU(2) the Casimir operator equals $C_2(r) = 3/4$ and the hypercharge $y_l = -1/2$. Finally after taking the trace over SU(2) indices and stripping of all background fields N we end up with [ABB11, p. 14]

$$\begin{aligned}\mathrm{i}\epsilon(p,\vec{k})\tilde{\Sigma}(p,\vec{k}) = &-\frac{\mathrm{i}}{2}d(r)\mathcal{F}(p_\parallel,k_\parallel)\frac{\eta^\dagger(k)}{k_\parallel - p_\parallel}\\ &+\int\mathcal{C}(\vec{q}_\perp)\left[\tilde{\Sigma}(p,\vec{k}) - \tilde{\Sigma}(p,k_\parallel,\vec{k}_\perp - \vec{q}_\perp)\right]\frac{d^2q_\perp}{(2\pi)^2}.\end{aligned} \tag{114}$$

The kernel $\mathcal{C}$ has been derived by integrating out the A contribution and using the corresponding gauge propagators with HTL resummed Debye mass m_D

$$\mathcal{C}(\vec{q}_\perp) = T\left[C_2(r)g^2\left(\frac{1}{\vec{q}_\perp^{\,2}} - \frac{1}{\vec{q}_\perp^{\,2} + m_D^2}\right) + y_l^2 g'^2\left(\frac{1}{\vec{q}_\perp^{\,2}} - \frac{1}{\vec{q}_\perp^{\,2} + m_D'^2}\right)\right]. \tag{115}$$

Note that the parallel momentum direction $q_\parallel$ as well as the Matsubara sum over q_0 has been solved already.

The Debye masses are given as [ABB11, p. 13]

$$m_D^2 = \frac{11}{6}g^2T^2, \qquad m_D'^2 = \frac{11}{6}g'^2T^2. \tag{116}$$

Looking at the final expression it should be clear that the obtained recursion relation for the self energy can not be solved analytically, moreover a numerical treatment is needed. For this reason it is useful to rewrite the reduced self energy again by parameterizing it using a scalar function ψ and a vector function $\vec{f}$ [Aur+02]

$$\tilde{\Sigma}(p,\vec{k}) \sim \eta^\dagger(k) = \left(-\frac{k_1 + \mathrm{i}k_2}{2k_\parallel}, 1\right) \sim (-\vec{w}\cdot\vec{f}, \psi), \tag{117}$$

with the auxiliary vector $\vec{w} = (1, \mathrm{i})$. Using this parametrization one can write the reduced self energy in the following form [ABB11, p. 15, note the missing factor of 4]

$$\tilde{\Sigma}(p,\vec{k}) = -\frac{\mathrm{i}}{2}\frac{d(r)\mathcal{F}(p_\parallel, k_\parallel)}{k_\parallel - p_\parallel}\begin{pmatrix}\frac{-(f^1+\mathrm{i}f^2)}{4p_\parallel}\\ \psi\end{pmatrix} \tag{118}$$

. Instead of one single equation we then end up with two integral equations for ψ and $\vec{f}$ that have to be solved numerically [ABB11, p. 14]

$$\mathrm{i}\epsilon(p,\vec{k})\vec{f}(\vec{k}_\perp) - \int \mathcal{C}(\vec{q}_\perp)\left[\vec{f}(\vec{q}_\perp) - \vec{f}(\vec{k}_\perp - \vec{q}_\perp)\right]\frac{d^2q_\perp}{(2\pi)^2} = 2\vec{k}_\perp, \tag{119}$$

$$\mathrm{i}\epsilon(p,\vec{k})\psi(\vec{k}_\perp) - \int \mathcal{C}(\vec{q}_\perp)\left[\psi(\vec{q}_\perp) - \psi(\vec{k}_\perp - \vec{q}_\perp)\right]\frac{d^2q_\perp}{(2\pi)^2} = 1. \tag{120}$$

For the integrated self energy one arrives at

$$\Sigma_{\vec{p}}^{ret,R}(\omega) := |\lambda|^2\int\limits_{-\infty}^{\infty}\eta(\omega,\vec{k})\tilde{\Sigma}(\omega,\vec{k},\vec{p})\frac{d^3k}{(2\pi)^3} = -|\lambda|^2\frac{\mathrm{i}}{2}\int\limits_{-\infty}^{\infty}\eta(\omega,\vec{k})\frac{d(r)\mathcal{F}(p_\parallel,k_\parallel)}{k_\parallel - p_\parallel}\begin{pmatrix}\frac{-(f^1+\mathrm{i}f^2)}{4p_\parallel}\\ \psi\end{pmatrix}\frac{d^3k}{(2\pi)^3}. \tag{121}$$

Solving the integral equations for ψ and $\vec{f}$ leads to the desired gauge corrected result of the Majorana self energy.

4 Lepton Asymmetry with the Lepton Number Matrix

The aim of the section is to compute a measure for the generated Lepton asymmetry. For this purpose the calculation follows the strategy developed by Anisimov, Buchmüller et al. in [Ani+11].

4.1 The Lepton Number Matrix

Starting point is the flavor non-diagonal lepton current in a spacial homogeneous system. It is obtained from the statistical lepton propagator [Ani+11, p. 24]

$$j^{\mu}_{ij}(x) = -\mathrm{tr}\left[\gamma^{\mu} S^{+}_{L,ij}(x,x')\right]_{x'\to x}. \tag{122}$$

The zeroth component of this current is referred to as flavor non-diagonal lepton number matrix

$$L_{\vec{k},ij}(t,t) = -\mathrm{tr}\left[\gamma_0 S^{+}_{\vec{k},L,ij}(t,t')\right]_{t'\to t}. \tag{123}$$

For free fields in equilibrium it is possible to show that the flavor diagonal part of the matrix is connected to the equilibrium distribution functions of leptons and anti-leptons

$$L_{\vec{k},ii}(t) = f_{li}(t,\vec{k}) - f_{\bar{l},i}(t,\vec{k}). \tag{124}$$

In section 2 the Kadanoff-Baym equations had been presented. An important feature of the equations was that interactions enter as corrections to the self energy $\Sigma^{\pm}$ in nonequilibrium QFT. This is why the lepton number matrix is going to be calculated from self energy corrections to the statistical propagator S^{+}. These corrections involve the out-of-equilibrium Majorana neutrino and are closely connected to the CP-violating processes investigated in section 1. Details on the corrections will be given in the next subsection. The corresponding Kadanoff-Baym equations have the following form [Ani+11, p. 25]

$$(\mathrm{i}\gamma^0\partial_t - \vec{k}\vec{\gamma})S^{+}_{\vec{k},L,ij}(t,t') = \int_0^t \Pi^{-}_{\vec{k}}(t,t_1)S^{+}_{\vec{k},L,ij}(t_1,t')dt_1 - \int_0^{t'} \Pi^{+}_{\vec{k}}(t,t_1)S^{-}_{\vec{k},L,ij}(t_1,t')dt_1, \tag{125}$$

$$S^{+}_{\vec{k},L,ij}(t,t')(-\mathrm{i}\gamma^0\overleftarrow{\partial_{t'}} - \vec{k}\vec{\gamma}) = -\int_0^{t'} S^{+}_{\vec{k},L,ij}(t,t_1)\Pi^{-}_{\vec{k}}(t_1,t')dt_1 + \int_0^{t} S^{-}_{\vec{k},L,ij}(t,t')\Pi^{+}_{\vec{k}}(t_1,t')dt_1, \tag{126}$$

where the self energy correction to S is denoted as $\Pi^{\pm}$.

4.2 CP-Violation from Self Energy Corrections

There are numerous self energy corrections to the statistical lepton propagator involving a heavy Majorana neutrino. Most of the diagrams are referred to as washout diagrams and do not lead to the intended lepton asymmetry. As a result the relevant diagrams have to be identified.

As explained in the first section CP-violation is a non trivial effect caused by interference of tree level and loop graphs. It manifests itself in the imaginary part of the complex Yukawa couplings λ. For our effective model with two of three Majorana neutrinos integrated out the amount of CP-violation is given as [Ani+11, p. 7]

$$\epsilon := -\epsilon_1 \simeq \frac{3}{16\pi}\sum_{j=2}^{3}\frac{\mathrm{Im}\left[(\lambda^{\dagger}\lambda)^2_{j1}\right]}{(\lambda^{\dagger}\lambda)_{11}}\frac{M_1}{M_j} + o\left(\left(\frac{M_1}{M_j}\right)^{\frac{3}{2}}\right) = \frac{3}{16\pi}M\sum_i\frac{\mathrm{Im}(\lambda^*_{i1}(\eta\lambda^*)_{i1})}{(\lambda^{\dagger}\lambda)_{11}} = \frac{3}{16\pi}M\frac{\mathrm{Im}((\lambda^{\dagger}\eta\lambda^*)_{11})}{(\lambda^{\dagger}\lambda)_{11}}, \tag{127}$$

with effective coupling η and $M_1 \equiv M$.

There are two two-loop self energy corrections leading to the same coupling structure known from the analysis of CP-violation in section 1: [Ani+11, figure 7]

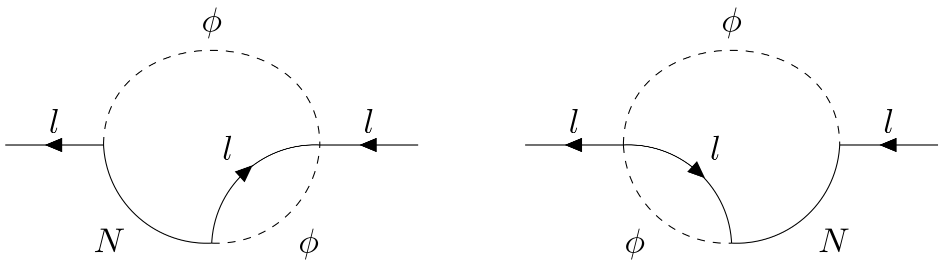

Figure 12: CP violating two-loop contributions to the lepton self energy $\Pi^{\pm}$ leading to a non zero lepton asymmetry.

From now on these diagrams will be referred to as CP-violating diagrams. The couplings can be found by applying the Feynman rules from Appendix A. The two-lepton-two-Higgs effective vertex leads to a factor η_{ij} or its conjugate, the lepton-Higgs-Majorana vertex to a factor of λ_{i1} or its conjugate. All in all the complete diagram leads to a factor of $\mathrm{Im}(\lambda^*_{i1}(\eta\lambda^*)_{i1})$ reproducing the (unnormalized) result known from the analysis of the CP-violating out-of-equilibrium decay.
The integral expressions of these diagrams can easily be derived using the propagators and Feynman rules given in the appendices A and B. All other one- or two-loop self energy corrections are washout processes. Higher order contributions are neglected in this approach.

4.3 Flavor diagonal Lepton Number Matrix

We can continue the derivation by taking the time derivative of the lepton number matrix [Gar+10] and using the Kadanoff-Baym equation from section 2

$$\begin{aligned}
\partial_t L_{\vec{k},ij}(t,t) &= \mathrm{i}\ \mathrm{tr}[(\mathrm{i}\gamma_0\partial_t + \mathrm{i}\gamma_0\partial_{t'})S^+_{\vec{k},L,ij}(t,t')]_{t'\to t} \\
&= \mathrm{i}\ \mathrm{tr}[(\mathrm{i}\gamma_0\partial_t - \vec{k}\vec{\gamma})S^+_{\vec{k},L,ij}(t,t') + S^+_{\vec{k},L,ij}(t,t')(\mathrm{i}\gamma_0\overleftarrow{\partial_{t'}} + \vec{k}\vec{\gamma})] \\
&= \mathrm{i}\ \mathrm{tr}\Bigg[\int_0^t \Pi^-_{\vec{k},ij}(t,t_1)S^+_{\vec{k},L}(t_1,t')dt_1 - \int_0^{t'} \Pi^+_{\vec{k},ij}(t,t_1)S^-_{\vec{k},L}(t_1,t)dt_1 \\
&\qquad \int_0^{t'} S^+_{\vec{k},L}(t,t_1)\Pi^-_{\vec{k},ij}(t_1,t')dt_1 - \int_0^t S^-_{\vec{k},L}(t,t_1)\Pi^+_{\vec{k},ij}(t_1,t')dt_1\Bigg].
\end{aligned} \tag{128}$$

Integrating the whole expression with respect to t and using identities for the integration domains and the trace we obtain the following result [Ani+11, p. 26]

$$L_{\vec{k},ij}(t,t) = \mathrm{i}\int_0^t\int_0^{t_1} \mathrm{tr}\left[\Pi^-_{\vec{k},ij}(t_1,t_2)S^+_{\vec{k},L}(t_2,t_1) - \Pi^+_{\vec{k},ij}(t_2,t_1)S^-_{\vec{k},L}(t_2,t_1)\right]dt_2dt_1. \tag{129}$$

With the connection between spectral function and statistical propagator and the Wightman functions it is possible to rewrite the result

$$L_{\vec{k},ij}(t,t) = -\int_0^t\int_0^{t_1} \mathrm{tr}\left[\Pi^{>}_{\vec{k},ij}(t_1,t_2)S^{<}_{\vec{k},L}(t_2,t_1) - \Pi^{<}_{\vec{k},ij}(t_1,t_2)S^{>}_{\vec{k},L}(t_2,t_1)\right]dt_2dt_1. \tag{130}$$

Anisimov, Buchmüller et al. have shown that the equilibrium part of the heavy neutrino propagator does not contribute to the asymmetry [Ani+11, p. 27]. So when calculating the lepton asymmetry to leading order in Yukawa coupling λ it is sufficient to keep only the deviation from equilibrium, denoted for the lepton self energy as $\delta\Pi$

$$L_{\vec{k},ij}(t,t) = \mathrm{i} \int_0^t \int_0^{t_1} \mathrm{tr}\left[\delta\Pi^-_{\vec{k},ij}(t_1,t_2) S^+_{\vec{k},L}(t_2-t_1) - \delta\Pi^+_{\vec{k},ij}(t_1,t_2) S^-_{\vec{k},L}(t_2-t_1)\right] dt_2 dt_1. \tag{131}$$

The expression $\delta\Pi^\pm$ is obtained from the two CP-violating loop graphs

$$\delta\Pi_{\vec{k},ij}(t_1,t_2) = \Pi^{(1)}_{\vec{k},ij}(t_1,t_2) + \Pi^{(2)}_{\vec{k},ij}(t_1,t_2). \tag{132}$$

The couplings can be factorized out by using the Feynman rules from Appendix A [Ani+11, p. 28]

$$\Pi^{(1)}_{\vec{k},ij}(t_1,t_2) = -3\mathrm{i}\lambda^*_{i1}(\eta\lambda^*)_{j1}\Pi^{(1)}_{\vec{k}}(t_1,t_2), \tag{133}$$

$$\Pi^{(2)}_{\vec{k},ij}(t_1,t_2) = 3\mathrm{i}(\eta^*\lambda)_{i1}\lambda_{j1}\Pi^{(2)}_{\vec{k}}(t_1,t_2). \tag{134}$$

As pointed out in the beginning, for equilibrium fields the flavor diagonal part of the lepton number matrix is connected to the lepton distribution functions. Since we are most interested in the distribution of leptons to antileptons we are setting $i = j$ and look at the diagonal elements of the lepton number matrix. Using various identities for the lepton and Higgs propagator as well as some trace identities that can be found in [Ani+11, p. 28-29] we arrive at

$$L_{\vec{k},ii}(t,t) = 12\underbrace{\mathrm{Im}(\lambda^*_{i1}(\eta\lambda^*)_{i1})}_{:=\lambda_{ii}} \int_0^t \int_0^t Re\left[tr\left(\Pi^{(1)\,>}_{\vec{k}}(t_1,t_2) S^<_{\vec{k}}(t_2-t_1)\right)\right] dt_1 dt_2. \tag{135}$$

Note that the result is proportional to the coupling known from the analysis of CP-violation and of course known from Boltzmann analysis.

Since both diagrams lead to the same contribution it is sufficient to calculate the correction to the lepton self energy Π given by the first of the two CP-violating diagrams. Using the Feynman rules and the short notation $y_{ij} = t_i - t_j$ leads to [Ani+11, p. 28],[Hüt13, p. 54]

$$\begin{aligned}\Pi^{(1)\,>}_{\vec{k}}(t_1,t_2) = \int\int\int\int\int \tilde{G}_{\vec{p}}(t_1,t_3)\left[S^{11}_{\vec{k}'}(y_{23})\Delta^{11}_{\vec{q}'}(y_{23}) - S^<_{\vec{k}'}(y_{23})\Delta^<_{\vec{q}'}(y_{23})\right]\Delta^<_{\vec{q}}(y_{21})P_L \\ (2\pi)^3\delta(\vec{p}-\vec{k}'-\vec{q}')(2\pi)^3\delta(\vec{p}+\vec{k}+\vec{q})\frac{d^3p}{(2\pi)^3}\frac{d^3q}{(2\pi)^3}\frac{d^3q'}{(2\pi)^3}\frac{d^3k'}{(2\pi)^3}dt_3.\end{aligned} \tag{136}$$

Due to chiral projections at the vertices only the scalar part of the Majorana propagator contributes [Ani+11, p. 28]

$$\tilde{G}_{\vec{p}}(t_1,t_3) = \frac{M}{\omega_{\vec{p}}}\cos(\omega_{\vec{p}}(t_1-t_3)) f^{eq}_N(\omega_{\vec{p}}) e^{-\Gamma_{\vec{p}}\frac{t_1+t_3}{2}}. \tag{137}$$

The lepton propagator S and the Higgs propagator Δ fulfill the following identities [Hüt13].

$$S^{11}(x,,y) = S^+(x,y) - \frac{\mathrm{i}}{2}\mathrm{sgn}\left(x^0-y^0\right)S^-(x,y), \tag{138}$$

$$\Delta^{11}(x,y) = \Delta^+(x,y) - \frac{\mathrm{i}}{2}\mathrm{sgn}\left(x^0-y^0\right)\Delta^-(x,y), \tag{139}$$

$$S^-(x,y) = \mathrm{i}\left(S^>(x,y) - S^<(x,y)\right), \tag{140}$$

$$S^+(x,y) = \frac{1}{2}\left(S^>(x,y) + S^<(x,y)\right), \tag{141}$$

$$\Delta^-(x,y) = \mathrm{i}\left(\Delta^>(x,y) - \Delta^<(x,y)\right), \tag{142}$$

$$\Delta^+(x,y) = \frac{1}{2}\left(\Delta^>(x,y) + \Delta^<(x,y)\right). \tag{143}$$

Combining these equations leads to

$$S^{11}(x,y) = \frac{1}{2}\left(S^{>}(x,y) + S^{<}(x,y)\right) + \frac{1}{2}\mathrm{sgn}\left(x^0 - y^0\right)\left(S^{>}(x,y) - S^{<}(x,y)\right), \tag{144}$$

$$\Delta^{11}(x,y) = \frac{1}{2}\left(\Delta^{>}(x,y) + \Delta^{<}(x,y)\right) + \frac{1}{2}\mathrm{sgn}\left(x^0 - y^0\right)\left(\Delta^{>}(x,y) - \Delta^{<}(x,y)\right). \tag{145}$$

Since lepton and Higgs fields are in equilibrium the propagator depends only on the time difference $y_{23} = t_2 - t_3$. Transforming spacial components to momentum space then leads to

$$S^{11}_{\vec{k}'}(y_{23}) = \frac{1}{2}\left(S^{>}_{\vec{k}'}(y_{23}) + S^{<}_{\vec{k}'}(y_{23})\right) + \frac{1}{2}\mathrm{sgn}(y_{23})\left(S^{>}_{\vec{k}'}(y_{23}) - S^{<}_{\vec{k}'}(y_{23})\right), \tag{146}$$

$$\Delta^{11}_{\vec{q}'}(y_{23}) = \frac{1}{2}\left(\Delta^{>}_{\vec{q}'}(y_{23}) + \Delta^{<}_{\vec{q}'}(y_{23})\right) + \frac{1}{2}\mathrm{sgn}(y_{23})\left(\Delta^{>}_{\vec{q}'}(y_{23}) - \Delta^{<}_{\vec{q}'}(y_{23})\right), \tag{147}$$

$$\begin{aligned} S^{11}_{\vec{k}'}(y_{23})\Delta^{11}_{\vec{q}'}(y_{23}) = &\left[\frac{1}{2}\left(S^{>}_{\vec{k}'}(y_{23}) + S^{<}_{\vec{k}'}(y_{23})\right) + \frac{1}{2}\mathrm{sgn}(y_{23})\left(S^{>}_{\vec{k}'}(y_{23}) - S^{<}_{\vec{k}'}(y_{23})\right)\right] \\ &\times \left[\frac{1}{2}\left(\Delta^{>}_{\vec{q}'}(y_{23}) + \Delta^{<}_{\vec{q}'}(y_{23})\right) + \frac{1}{2}\mathrm{sgn}(y_{23})\left(\Delta^{>}_{\vec{q}'}(y_{23}) - \Delta^{<}_{\vec{q}'}(y_{23})\right)\right] \\ &= \frac{1}{4}\left(S^{>}_{\vec{k}'}(y_{23}) + S^{<}_{\vec{k}'}(y_{23})\right)\left(\Delta^{>}_{\vec{q}'}(y_{23}) + \Delta^{<}_{\vec{q}'}(y_{23})\right) \\ &+ \frac{1}{4}\left(S^{>}_{\vec{k}'}(y_{23}) - S^{<}_{\vec{k}'}(y_{23})\right)\left(\Delta^{>}_{\vec{q}'}(y_{23}) - \Delta^{<}_{\vec{q}'})(y_{23})\right) \\ &+ \frac{1}{4}\mathrm{sgn}(y_{23})\left(S^{>}_{\vec{k}'}(y_{23}) - S^{<}_{\vec{k}'}(y_{23})\right)\left(\Delta^{>}_{\vec{q}}(y_{23}) + \Delta^{<}_{\vec{q}}(y_{23})\right) \\ &+ \frac{1}{4}\mathrm{sgn}(y_{23})\left(S^{>}_{\vec{k}'}(y_{23}) + S^{<}_{\vec{k}'}(y_{23})\right)\left(\Delta^{>}_{\vec{q}}(y_{23}) - \Delta^{<}_{\vec{q}}(y_{23})\right) \\ &= \frac{1}{2}\left(S^{>}_{\vec{k}'}(y_{23})\Delta^{>}_{\vec{q}}(y_{23}) + S^{<}_{\vec{k}'}(y_{23})\Delta^{<}_{\vec{q}}(y_{23})\right) \\ &+ \frac{1}{2}\mathrm{sgn}(y_{23})\left(S^{>}_{\vec{k}'}(y_{23})\Delta^{>}_{\vec{q}}(y_{23}) - S^{<}_{\vec{k}'}(y_{23})\Delta^{<}_{\vec{q}}(y_{23})\right), \end{aligned} \tag{148}$$

$$\begin{aligned} S^{11}_{\vec{k}'}(y_{23})\Delta^{11}_{\vec{q}'}(y_{23}) - S^{<}_{\vec{k}'}(y_{23})\Delta^{<}_{\vec{q}}(y_{23}) = &\underbrace{\frac{1}{2}\left(1 + \mathrm{sgn}(y_{23})\right)}_{\Theta(y_{23})} S^{>}_{\vec{k}'}(y_{23})\Delta^{>}_{\vec{q}}(y_{23}) \\ &- \underbrace{\frac{1}{2}\left(1 + \mathrm{sgn}(y_{23})\right)}_{\Theta(y_{23})} S^{<}_{\vec{k}'}(y_{23})\Delta^{<}_{\vec{q}}(y_{23}) \\ &= \Theta(y_{23})\left(S^{>}_{\vec{k}'}(y_{23})\Delta^{>}_{\vec{q}}(y_{23}) - S^{<}_{\vec{k}'}(y_{23})\Delta^{<}_{\vec{q}}(y_{23})\right). \end{aligned} \tag{149}$$

From the calculation of the Majorana neutrino propagator in section 2 the object

$$\Sigma^{<}_{\vec{k}',\vec{q}}(y_{23}) \equiv S^{<}_{\vec{k}'}(y_{23})\Delta^{<}_{\vec{q}}(y_{23}) \tag{150}$$

is well known as the neutrino self energy.

Using the cyclicity of the trace and combining all results, the lepton number matrix can be written in the following form (for simplicity using the short notation $\int_{\vec{p}} = \int \frac{d^3p}{(2\pi)^3}$)

$$\begin{aligned} L_{\vec{k},ii}(t,t) = 12\lambda_{ii} \int_0^t \int_0^t \int_0^{t_2} \int_{\vec{p},\vec{k}',\vec{q},\vec{q}'} &\tilde{G}_{\vec{p}}(t_1,t_3)\mathrm{Re}\left[\mathrm{tr}\left(\Sigma^{>}_{\vec{k},\vec{q}}(y_{21})\left(\Sigma^{>}_{\vec{k}',\vec{q}'}(y_{23}) - \Sigma^{<}_{\vec{k}',\vec{q}'}(y_{23})\right)P_L\right)\right] \\ &\times (2\pi)^3\delta(\vec{p} - \vec{k}' - \vec{q}')(2\pi)^3\delta(\vec{p} + \vec{k} + \vec{q})\; dt_3 dt_2 dt_1. \end{aligned} \tag{151}$$

As pointed out in the beginning, for free fields in equilibrium the lepton number matrix is equivalent to the distribution functions of leptons and anti-leptons

$$L_{\vec{k},ii}(t,t) = f_{li}(k) - f_{\bar{l}i}(k). \tag{152}$$

Our aim is to implement gauge corrections to the Lepton number matrix. For later purpose we are going to integrate out the $\vec{k}$ dependency and obtain an integrated lepton number matrix. This corresponds to a change from distribution functions to particle densities [Dev+17]

$$L_{ii}(t,t) = n_{li} - n_{\bar{l}i}. \tag{153}$$

The full out-of-equilibrium result takes the following form

$$\begin{aligned} L_{ii}(t,t) = 12\lambda_{ii} \int_0^t \int_0^t \int_0^{t_2} \int_{\vec{p},\vec{k},\vec{k}',\vec{q},\vec{q}'} \tilde{G}_{\vec{p}}(t_1,t_3) \mathrm{Re}\left[\mathrm{tr}\left(\Sigma^{>}_{\vec{k},\vec{q}}(y_{21})\left(\Sigma^{>}_{\vec{k}',\vec{q}'}(y_{23}) - \Sigma^{<}_{\vec{k}',\vec{q}'}(y_{23})\right) P_L\right)\right] \\ \times (2\pi)^3\delta(\vec{p}-\vec{k}'-\vec{q}')(2\pi)^3\delta(\vec{p}+\vec{k}+\vec{q})\; dt_3 dt_2 dt_1. \end{aligned} \tag{154}$$

The result can be simplified further by making use of the KMS-relations, well known from thermal field theory.

4.3.1 Simplification of L_{ii} using KMS-Relations

In momentum space the KMS-relations have the following form [Bel11]

$$\begin{aligned} \Delta^{<}_{\vec{q}}(\omega) &= e^{-\beta\omega}\Delta^{>}_{\vec{q}}(\omega), \\ S^{<}_{\vec{k}}(\omega) &= -e^{-\beta\omega}S^{>}_{\vec{k}}(\omega). \end{aligned} \tag{155}$$

Transforming the Majorana self energy to Fourier space leads to

$$\Sigma^{<}_{\vec{k}',\vec{q}}(y_{23}) = S^{<}_{\vec{k}'}(y_{23})\Delta^{<}_{\vec{q}}(y_{23}) \;\rightarrow\; \Sigma^{<}_{\vec{k}',\vec{q}}(\omega_{21}) = \int_{-\infty}^{\infty} S^{<}_{\vec{k}'}(\omega')\Delta^{<}_{\vec{q}}(\omega_{21}-\omega')\frac{d\omega}{2\pi}, \tag{156}$$

by using the convolution theorem.

Now we can use the KMS-relations:

$$\begin{aligned} \Sigma^{<}_{\vec{k}',\vec{q}}(\omega_{21}) = \int_{-\infty}^{\infty} S^{<}_{\vec{k}'}(\omega')\Delta^{<}_{\vec{q}}(\omega_{21}-\omega')\frac{d\omega}{2\pi} &= -\int_{-\infty}^{\infty} S^{>}_{\vec{k}'}(\omega')\Delta^{>}_{\vec{q}}(\omega_{21}-\omega')e^{-\beta(\omega'+\omega_{21}-\omega')}\frac{d\omega}{2\pi} \\ &= -e^{-\beta\omega_{21}}\Sigma^{>}_{\vec{k}',\vec{q}}(\omega_{21}). \end{aligned} \tag{157}$$

Transforming the complete Lepton number matrix to Fourier space then leads to

$$\begin{aligned} L_{ii}(t,t) = 12\lambda_{ii} \int_0^t \int_0^t \int_0^{t_2} \int_{-\infty}^{\infty} \int_{-\infty}^{\infty} \int_{\vec{p},\vec{k},\vec{k}',\vec{q},\vec{q}'} \tilde{G}_{\vec{p}}(t_1,t_3)(2\pi)^3\delta(\vec{p}-\vec{k}'-\vec{q}')(2\pi)^3\delta(\vec{p}+\vec{k}+\vec{q}) \\ \times \mathrm{Re}\left[\mathrm{tr}\left(\Sigma^{>}_{\vec{k},\vec{q}}(\omega_{21})\left(\Sigma^{>}_{\vec{k}',\vec{q}'}(\omega_{23}) - \Sigma^{<}_{\vec{k}',\vec{q}'}(\omega_{23})\right) P_L\right) e^{-i(\omega_{21}y_{21}+\omega_{23}y_{23})}\right] \frac{d\omega_{21}}{2\pi}\frac{d\omega_{23}}{2\pi} dt_3 dt_2 dt_1, \end{aligned} \tag{158}$$

and after making use of the KMS-relations we find

$$\begin{aligned} L_{ii}(t,t) = 12\lambda_{ii}\; \mathrm{Re}\Bigg[\int_0^t \int_0^t \int_0^{t_2} \int_{-\infty}^{\infty} \int_{-\infty}^{\infty} \int_{\vec{p},\vec{k},\vec{k}',\vec{q},\vec{q}'} \tilde{G}_{\vec{p}}(t_1,t_3)(2\pi)^3\delta(\vec{p}-\vec{k}'-\vec{q}')(2\pi)^3\delta(\vec{p}+\vec{k}+\vec{q}) \\ \underbrace{(-e^{-\beta\omega_{23}}-1)}_{-f_F(\omega_{23})^{-1}} \mathrm{tr}\left(\Sigma^{<}_{\vec{k},\vec{q}}(\omega_{23})\Sigma^{<}_{\vec{k}',\vec{q}'}(\omega_{23}) P_L\right) e^{-i(\omega_{21}y_{21}+\omega_{23}y_{23})}\frac{d\omega_{21}}{2\pi}\frac{d\omega_{23}}{2\pi} dt_3 dt_2 dt_1 \Bigg]. \end{aligned} \tag{159}$$

Another very useful identity for the self energy found in [Bel11] is the following

$$\Sigma^{<}_{\vec{k},\vec{q}}(\omega) = -2f_F(\omega)\mathrm{Im}\Sigma^{\mathrm{ret}}_{\vec{k},\vec{q}}(\omega), \tag{160}$$

so we have

$$\begin{aligned} L_{ii}(t,t) = -48\lambda_{ii}\ \mathrm{Re}\Bigg[\int_0^t\int_0^t\int_0^{t_2}\int_{-\infty}^{\infty}\int_{-\infty}^{\infty}\int_{\vec{p},\vec{k},\vec{k}',\vec{q},\vec{q}'} \tilde{G}_{\vec{p}}(t_1,t_3)(2\pi)^3\delta(\vec{p}-\vec{k}'-\vec{q}')(2\pi)^3\delta(\vec{p}+\vec{k}+\vec{q}) \\ f_F(\omega_{21})\mathrm{tr}\left(\mathrm{Im}\Sigma^{\mathrm{ret}}_{\vec{k},\vec{q}}(\omega_{23})\mathrm{Im}\Sigma^{\mathrm{ret}}_{\vec{k}',\vec{q}'}(\omega_{23})P_L\right)e^{-i(\omega_{21}y_{21}+\omega_{23}y_{23})}\ \frac{d\omega_{21}}{2\pi}\frac{d\omega_{23}}{2\pi}dt_3dt_2dt_1\Bigg] \\ = -48\lambda_{ii}\int_0^t\int_0^t\int_0^{t_2}\int_{-\infty}^{\infty}\int_{-\infty}^{\infty}\int_{\vec{p},\vec{k},\vec{k}',\vec{q},\vec{q}'} \tilde{G}_{\vec{p}}(t_1,t_3)(2\pi)^3\delta(\vec{p}-\vec{k}'-\vec{q}')(2\pi)^3\delta(\vec{p}+\vec{k}+\vec{q}) \\ f_F(\omega_{21})\mathrm{tr}\left(\mathrm{Im}\Sigma^{\mathrm{ret}}_{\vec{k},\vec{q}}(\omega_{23})\mathrm{Im}\Sigma^{\mathrm{ret}}_{\vec{k}',\vec{q}'}(\omega_{23})P_L\right)\mathrm{Re}\left[e^{-i(\omega_{21}y_{21}+\omega_{23}y_{23})}\right]\ \frac{d\omega_{21}}{2\pi}\frac{d\omega_{23}}{2\pi}dt_3dt_2dt_1. \end{aligned} \tag{161}$$

Plugging in the Majorana propagator $\tilde{G}$ and leaving out short notation finally leads to

$$\begin{aligned} L_{ii}(t,t) = -48\lambda_{ii}\int_0^t\int_0^t\int_0^{t_2}\int\int\int\int\int\int_{-\infty}^{\infty}\int_{-\infty}^{\infty}\underbrace{\frac{M}{\omega_{\vec{p}}}\cos(\omega_{\vec{p}}y_{13})f_F(\omega_{\vec{p}})e^{-\Gamma_{\vec{p}}\frac{t_1+t_3}{2}}}_{\tilde{G}\ \text{Majorana propagator}} \\ \underbrace{f_F(\omega_{21})\mathrm{tr}\left(\mathrm{Im}\Sigma^{\mathrm{ret}}_{\vec{k},\vec{q}}(\omega_{23})\mathrm{Im}\Sigma^{\mathrm{ret}}_{\vec{k}',\vec{q}'}(\omega_{23})P_L\right)\mathrm{Re}\left[e^{-i(\omega_{21}y_{21}+\omega_{23}y_{23})}\right]}_{\text{Majorana self energy}} \\ \underbrace{(2\pi)^3\delta(\vec{p}-\vec{k}'-\vec{q}')(2\pi)^3\delta(\vec{p}+\vec{k}+\vec{q})}_{\text{momentum conservation}}\frac{d\omega_{21}}{2\pi}\frac{d\omega_{23}}{2\pi}\frac{d^3q}{(2\pi)^3}\frac{d^3q'}{(2\pi)^3}\frac{d^3k}{(2\pi)^3}\frac{d^3k'}{(2\pi)^3}\frac{d^3p}{(2\pi)^3}dt_3dt_2dt_1. \end{aligned} \tag{162}$$

Especially the Majorana self energy part can be simplified further by making use of the projector P_L.

4.4 Left- and right-handed Projection

Since we are working with lepton and Higgs fields that carry no mass (or only thermal mass) it is possible to write the self energy in the following form [Ani+11, p. 19]

$$\mathrm{Im}\Sigma^{\mathrm{ret}}_{\vec{p}}(\omega_{21}) = \frac{1}{2}(a_{\vec{p}}(\omega_{21})\gamma^0 + b_{\vec{p}}(\omega_{21})\vec{p}\vec{\gamma}) = \frac{1}{2}\begin{pmatrix} 0 & a_{\vec{p}}(\omega_{21})\mathbb{1}_{2\times2}+b_{\vec{p}}(\omega_{21})p_k\sigma^k \\ a_{\vec{p}}(\omega_{21})\mathbb{1}_{2\times2}-b_{\vec{p}}(\omega_{21})p_k\sigma^k & 0\end{pmatrix}, \tag{163}$$

where the Weyl representation of the γ-matrices has been used. Recalling the projectors in Weyl representation:

$$P_L = \frac{\mathbb{1}_{4\times4}-\gamma^5}{2} = \begin{pmatrix}\mathbb{1}_{2\times2} & 0\\ 0 & 0\end{pmatrix},\qquad P_R = \frac{\mathbb{1}_{4\times4}+\gamma^5}{2} = \begin{pmatrix}0 & 0\\ 0 & \mathbb{1}_{2\times2}\end{pmatrix}, \tag{164}$$

it is possible to use the following two identities in the expression of L_{ii}

$$\mathrm{Im}\Sigma^{ret}_{\vec{k},\vec{q}}(\omega_{21})P_L = P_R\mathrm{Im}\Sigma^{ret}_{\vec{k},\vec{q}}(\omega_{21}) = P_R^2\mathrm{Im}\Sigma^{ret}_{\vec{k},\vec{q}}(\omega_{21}) = P_R\mathrm{Im}\Sigma^{ret}_{\vec{k},\vec{q}}(\omega_{21})P_L, \tag{165}$$

$$\mathrm{tr}\left(\mathrm{Im}\Sigma^{ret}_{\vec{k},\vec{q}}(\omega_{21})\mathrm{Im}\Sigma^{ret}_{\vec{k}',\vec{q}'}(\omega_{23})P_L\right) = \mathrm{tr}\left(\mathrm{Im}\Sigma^{ret}_{\vec{k},\vec{q}}(\omega_{21})P_R\mathrm{Im}\Sigma^{ret}_{\vec{k}',\vec{q}'}(\omega_{23})P_L\right), \tag{166}$$

or in detail

$$\begin{aligned} \mathrm{Im}\Sigma^{ret}_{\vec{k}',\vec{q}'}(\omega_{23})P_L &= \frac{1}{2}\begin{pmatrix} 0 & a_{\vec{p}}(\omega_{21})\mathbb{1}_{2\times2}+b_{\vec{p}}(\omega_{21})p_k\sigma^k \\ a_{\vec{p}}(\omega_{21})\mathbb{1}_{2\times2}-b_{\vec{p}}(\omega_{21})p_k\sigma^k & 0\end{pmatrix}\begin{pmatrix}\mathbb{1}_{2\times2} & 0\\ 0 & 0\end{pmatrix} \\ &= \begin{pmatrix} 0 & 0 \\ \underbrace{\frac{1}{2}(a_{\vec{p}}(\omega_{21})\mathbb{1}_{2\times2}-b_{\vec{p}}(\omega_{21})p_k\sigma^k)}_{:=\mathrm{Im}\Sigma^{ret,L}_{\vec{k}',\vec{q}'}(\omega_{23})} & 0\end{pmatrix} \to \mathrm{Im}\Sigma^{ret,L}_{\vec{k}',\vec{q}'}(\omega_{23}). \end{aligned} \tag{167}$$

The P_R projection can be obtained in a similar way. In general the self energy has the following form

$$\mathrm{Im}\Sigma^{\mathrm{ret}}_{\vec{p}}(\omega_{21}) = \frac{1}{2}(a_{\vec{p}}(\omega_{21})\gamma^0 + b_{\vec{p}}(\omega_{21})\vec{p}\vec{\gamma}) = \begin{pmatrix} 0 & \mathrm{Im}\Sigma^{\mathrm{ret},R}_{\vec{p}}(\omega_{21}) \\ \mathrm{Im}\Sigma^{\mathrm{ret},L}_{\vec{p}}(\omega_{21}) & 0 \end{pmatrix}. \tag{168}$$

Note that this Ansatz corresponds to the symmetry observed earlier in section 3.4.2 when changing $\vec{p} \to -\vec{p}$. The prefactors $b_{-\vec{p}} = b_{\vec{p}}$ and $a_{-\vec{p}} = a_{\vec{p}}$ are both symmetric [Ani+11, p. 19] leading to

$$\mathrm{Im}\Sigma^{\mathrm{ret},R}_{-\vec{p}} = \frac{1}{2}(a_{-\vec{p}}\mathbb{1}_{2\times 2} - b_{-\vec{p}}p_k\sigma^k) = \frac{1}{2}(a_{\vec{p}}\mathbb{1}_{2\times 2} - b_{\vec{p}}p_k\sigma^k) = \mathrm{Im}\Sigma^{\mathrm{ret},L}_{\vec{p}}. \tag{169}$$

As a result the trace reduces to a 2×2 trace and we have

$$\mathrm{tr}\left(\mathrm{Im}\Sigma^{ret}_{\vec{k},\vec{q}}(\omega_{21})\mathrm{Im}\Sigma^{ret}_{\vec{k}',\vec{q}'}(\omega_{23})P_L\right) = \mathrm{tr}\left(\mathrm{Im}\Sigma^{ret,R}_{\vec{k},\vec{q}}(\omega_{21})\mathrm{Im}\Sigma^{ret,L}_{\vec{k}',\vec{q}'}(\omega_{23})\right). \tag{170}$$

Note that the trace and the momentum conservation part are the only $\vec{k}, \vec{k}', \vec{q}, \vec{q}'$ dependent parts.

Putting everything together gives the following integral

$$\begin{aligned} L_{ii}(t,t) = -48\lambda_{ii} & \int_0^t \int_0^t \int_0^{t_2} \int\int\int\int\int \int_{-\infty}^{\infty} \int_{-\infty}^{\infty} \frac{M}{\omega_{\vec{p}}} \cos(\omega_{\vec{p}} y_{13}) f_F(\omega_{\vec{p}}) e^{-\Gamma_{\vec{p}}\frac{t_1+t_3}{2}} \\ & f_F(\omega_{21}) \mathrm{tr}\left(\mathrm{Im}\Sigma^{\mathrm{ret},R}_{\vec{k},\vec{q}}(\omega_{23})\mathrm{Im}\Sigma^{\mathrm{ret},L}_{\vec{k}',\vec{q}'}(\omega_{23})\right) \mathrm{Re}\left[e^{-i(\omega_{21}y_{21}+\omega_{23}y_{23})}\right] \\ & (2\pi)^3\delta(\vec{p}-\vec{k}'-\vec{q}')(2\pi)^3\delta(\vec{p}+\vec{k}+\vec{q})\frac{d^3q}{(2\pi)^3}\frac{d^3q'}{(2\pi)^3}\frac{d^3k}{(2\pi)^3}\frac{d^3k'}{(2\pi)^3}\frac{d^3p}{(2\pi)^3}\frac{d\omega_{21}}{2\pi}\frac{d\omega_{23}}{2\pi}dt_3dt_2dt_1. \end{aligned} \tag{171}$$

The aim of the next section is to systematically include gauge corrections to this result of the lepton number matrix.

5 The gauge corrected Lepton Number Matrix

There are two parts of the lepton number matrix where gauge corrections need to be taken into account to arrive at a full gauge corrected result. On one hand the decay width $\Gamma_{\vec{p}}$ of the heavy neutrino and on the other hand the CP-violating diagrams.

5.1 The gauge corrected Majorana Decay Width

Recalling the calculation of the heavy neutrino propagator, the Majorana self energy can be written in the following form [Ani+11, p. 19]

$$\Sigma^-_{\vec{p}}(\omega) = \mathrm{i}a_{\vec{p}}(\omega)\gamma^0 + \mathrm{i}b_{\vec{p}}(\omega)\vec{p}\cdot\vec{\gamma}. \tag{172}$$

The decay width was connected to a and b via

$$\omega\Gamma_{\vec{p}}(\omega) = \omega a_{\vec{p}}(\omega) + \vec{p}^{\,2} b_{\vec{p}}(\omega). \tag{173}$$

Using these two equations, a simple calculation leads to a connection between Γ and Σ^-

$$\begin{aligned}
tr\left(-\mathrm{i}\not{p}\Sigma^-_{\vec{p}}\right) &= tr\left(-\mathrm{i}\not{p}(\mathrm{i}a_{\vec{p}}(\omega)\gamma^0 + \mathrm{i}b_{\vec{p}}(\omega)\vec{p}\vec{\gamma})\right) = tr\left(\not{p}a_{\vec{p}}(\omega)\gamma^0 + \not{p}b_{\vec{p}}(\omega)\vec{p}\vec{\gamma}\right) = tr\left(\not{p}a_{\vec{p}}(\omega)\gamma^0\right) + tr\left(\not{p}b_{\vec{p}}(\omega)\vec{p}\vec{\gamma}\right)\\
&= tr\left(\left(\gamma^0\right)^2\omega a_{\vec{p}}(\omega)\right) + \underbrace{tr\left(-\gamma^0\vec{\gamma}\vec{p}a_{\vec{p}}(\omega)\right)}_{=0} + \underbrace{tr\left(\gamma^0\vec{\gamma}\vec{p}\omega b_{\vec{p}}(\omega)\right)}_{=0} + tr\left(-(\vec{\gamma}\vec{p})^2 b_{\vec{p}}(\omega)\right)\\
&= 4\omega a_{\vec{p}}(\omega) + tr(\underbrace{-\vec{\gamma}^2}_{=\mathbb{1}}\vec{p}^{\,2} b_{\vec{p}}(\omega)) = 4\omega a_{\vec{p}}(\omega) + 4\vec{p}^2 b_{\vec{p}}(\omega)\\
&= 4\omega\Gamma_{\vec{p}}(\omega).
\end{aligned} \tag{174}$$

Further in section 2 we introduced the spectral representation of the self energy [Ani+11, p. 17]

$$\hat{\Sigma}^-_{\vec{p}}(s) := \mathrm{i}\int_{-\infty}^{\infty} \frac{\Sigma^-_{\vec{p}}(p_0)}{\mathrm{i}s - p_0}\frac{dp_0}{2\pi\mathrm{i}}. \tag{175}$$

The retarded self energy is connected to the spectral representation via

$$\Sigma^{\mathrm{ret}}_{\vec{p}}(\omega) = \hat{\Sigma}^-_{\vec{p}}(-\mathrm{i}\omega + \epsilon). \tag{176}$$

All in all $\hat{\Sigma}$ and Σ are connected the following way

$$\hat{\Sigma}^-_{\vec{p}}(-\mathrm{i}\omega + \epsilon) = i\mathcal{P}\int_{-\infty}^{\infty} \frac{\Sigma^-(p_0)}{\omega - p_0}\frac{dp_0}{2\pi} + \frac{1}{2}\Sigma^-_{\vec{p}}(\omega), \tag{177}$$

with the real part given as principal value integral [Ani+11, p. 18].

Taking the imaginary part then leads to

$$\mathrm{Im}\left(\hat{\Sigma}^-_{\vec{p}}(-\mathrm{i}\omega + \epsilon)\right) = \mathrm{Im}\left(\Sigma^{\mathrm{ret}}_{\vec{p}}(\omega)\right) = \frac{1}{2\mathrm{i}}\Sigma^-_{\vec{p}}(\omega). \tag{178}$$

By making use of this connection for the retarded self energy Σ^{ret} and the self energy Σ^- we obtain

$$\mathrm{tr}\left(-\mathrm{i}\not{p}\Sigma^-_{\vec{p}}(\omega)\right) = \mathrm{tr}\left(2\not{p}\mathrm{Im}\left(\Sigma^{\mathrm{ret}}_{\vec{p}}(\omega)\right)\right) = 4\omega\Gamma_{\vec{p}}(\omega), \tag{179}$$

so finally the decay width is given as

$$\Gamma_{\vec{p}}(\omega) = \frac{1}{2\omega}\mathrm{tr}\left(\not{p}\mathrm{Im}\left(\Sigma^{\mathrm{ret}}_{\vec{p}}(\omega)\right)\right). \tag{180}$$

This can be simplified further using the Weyl basis for gamma matrices with $\not{p} = \omega\gamma^0 - \vec{p}\cdot\vec{\gamma}$

$$p_\mu \gamma^\mu = \begin{pmatrix} 0 & p_0 \mathbb{1} + p_i\sigma^i \\ p_0\mathbb{1} - p_i\sigma^i & 0 \end{pmatrix} = \begin{pmatrix} 0 & \sigma\cdot p \\ \bar{\sigma}\cdot p & 0 \end{pmatrix}. \tag{181}$$

Recalling the splitting of the retarded self energy Σ^{ret} into left- and right-handed self energy from section 4

$$\mathrm{Im}\left(\Sigma^{\mathrm{ret}}_{\vec{p}}(\omega)\right) = \begin{pmatrix} 0 & \mathrm{Im}\left(\Sigma^{\mathrm{ret},R}_{\vec{p}}(\omega)\right) \\ \mathrm{Im}\left(\Sigma^{\mathrm{ret},L}_{\vec{p}}(\omega)\right) & 0 \end{pmatrix}, \tag{182}$$

we end up with

$$\Gamma_{\vec{p}}(\omega) = \frac{1}{2\omega}\mathrm{tr}\left(\not{p}\,\mathrm{Im}\left(\Sigma^{\mathrm{ret}}_{\vec{p}}(\omega)\right)\right) = \frac{1}{2\omega}\mathrm{tr}\left(\begin{pmatrix} 0 & \sigma\cdot p \\ \bar{\sigma}\cdot p & 0 \end{pmatrix}\cdot\begin{pmatrix} 0 & \mathrm{Im}\left(\Sigma^{\mathrm{ret},R}_{\vec{p}}(\omega)\right) \\ \mathrm{Im}\left(\Sigma^{\mathrm{ret},L}_{\vec{p}}(\omega)\right) & 0 \end{pmatrix}\right). \tag{183}$$

Since left- and right-handed contributions lead to the same result we get an extra factor of 2 and can finally write

$$\Gamma_{\vec{p}}(\omega) = \frac{1}{\omega}\mathrm{tr}\left(\bar{\sigma}\cdot p\;\mathrm{Im}\left(\Sigma^{\mathrm{ret},R}_{\vec{p}}(\omega)\right)\right). \tag{184}$$

In section 3 we developed a procedure to include gauge corrections to the Majorana self energy. This was done by formulating two integral equations for the two functions ψ and $\vec{f}$, motivated by calculating a ladder diagram for the Majorana self energy containing all leading order gauge corrections. The developed decay width is given as the imaginary part of the Majorana self energy, thus gauge corrections are implemented by solving the integral equations using

$$\Sigma^{ret,R}_{\vec{p}}(\omega) = -|\lambda|^2\frac{\mathrm{i}}{2}\int\limits_{-\infty}^{\infty}\eta(\omega,\vec{k})\frac{d(r)\mathcal{F}(p_\parallel,k_\parallel)}{k_\parallel - p_\parallel}\begin{pmatrix} \frac{-(f^1+\mathrm{i}f^2)}{4p_\parallel} \\ \psi \end{pmatrix}\frac{d^3k}{(2\pi)^3}. \tag{185}$$

The result is the desired gauge corrected decay width.

We can further simplify by choosing a frame with $\vec{p}_\perp = 0$ [Hüt13, p. 73]

$$\bar{\sigma}\cdot p = \begin{pmatrix} p_0 + p_3 & p_1 - \mathrm{i}p_2 \\ p_1 + \mathrm{i}p_2 & p_0 - p_3 \end{pmatrix} \overset{\vec{p}_\perp = 0}{=} \begin{pmatrix} p_+ & 0 \\ 0 & p_- \end{pmatrix}. \tag{186}$$

The decay width then simplifies to

$$\begin{aligned} \Gamma_{\vec{p}} \sim \mathrm{tr}\left[\bar{\sigma}\cdot p\;\mathrm{Im}\left(\Sigma^{\mathrm{ret},R}_{\vec{p}}(\omega)\right)\right] &= -\frac{|\lambda|^2}{2}\mathrm{tr}\left[\begin{pmatrix} p_+ & 0 \\ 0 & p_- \end{pmatrix}\mathrm{Im}\left(\mathrm{i}\int\limits_{-\infty}^{\infty}\eta(\omega,\vec{k})\frac{d(r)\mathcal{F}(p_\parallel,k_\parallel)}{k_\parallel - p_\parallel}\begin{pmatrix} \frac{-(f^1+\mathrm{i}f^2)}{4p_\parallel} \\ \psi \end{pmatrix}\frac{d^3k}{(2\pi)^3}\right)\right] \\ &= -\frac{|\lambda|^2 d(r)}{2}\int\limits_{-\infty}^{\infty}\frac{\mathcal{F}(p_\parallel,k_\parallel)}{k_\parallel - p_\parallel}\mathrm{tr}\left[\begin{pmatrix} p_+ & 0 \\ 0 & p_- \end{pmatrix}\mathrm{Re}\left(\eta(\omega,\vec{k})\begin{pmatrix} \frac{-(f^1+\mathrm{i}f^2)}{4p_\parallel} \\ \psi \end{pmatrix}\right)\right]\frac{d^3k}{(2\pi)^3}. \end{aligned} \tag{187}$$

Recalling a few equations for η from section 3

$$\eta \approx \eta_0 + \eta_1, \qquad \eta_0 = \begin{pmatrix} 0 \\ 1 \end{pmatrix}, \qquad \eta_1 = -\frac{\vec{\sigma}\cdot\vec{k}_\perp}{2k_\parallel}\eta_0, \tag{188}$$

and using the Pauli matrices leads to

$$\eta_1 = -\frac{\sigma_1 k_1 + \sigma_2 k_2}{2k_\parallel}\begin{pmatrix} 0 \\ 1 \end{pmatrix} = -\frac{1}{2k_\parallel}\begin{pmatrix} k_1 - \mathrm{i}k_2 \\ 0 \end{pmatrix}. \tag{189}$$

So we have the following result for η

$$\eta = \eta_0 + \eta_1 = \begin{pmatrix} -\frac{k_1 - \mathrm{i}k_2}{2k_\parallel} \\ 1 \end{pmatrix}. \tag{190}$$

Expanding it then leads to

$$\mathrm{Re}\left(\eta(\omega,\vec{k})\begin{pmatrix} \frac{-(f^1+\mathrm{i}f^2)}{4p_\parallel} \\ \psi \end{pmatrix}\right) = \mathrm{Re}\left(\begin{pmatrix} -\frac{k_1-\mathrm{i}k_2}{2k_\parallel} \\ 1 \end{pmatrix}\begin{pmatrix} \frac{-(f^1+\mathrm{i}f^2)}{4p_\parallel} & ,\psi \end{pmatrix}\right) = \mathrm{Re}\left(\begin{pmatrix} \frac{(k_1-\mathrm{i}k_2)(f^1+\mathrm{i}f^2)}{8k_\parallel^2} & -\frac{k_1-\mathrm{i}k_2}{2k_\parallel}\psi \\ -\frac{f^1+\mathrm{i}f^2}{4k_\parallel} & \psi \end{pmatrix}\right). \tag{191}$$

The real part is taken by calculating $\mathrm{Re}(\Sigma) = \frac{1}{2}(\Sigma + \Sigma^\dagger)$

$$\begin{aligned} \mathrm{Re}\left(\eta(\omega,\vec{k})\begin{pmatrix} \frac{-(f^1+\mathrm{i}f^2)}{4p_\parallel} \\ \psi \end{pmatrix}\right) &= \frac{1}{2}\left[\begin{pmatrix} \frac{(k_1-\mathrm{i}k_2)(f_1+\mathrm{i}f_2)}{8k_\parallel^2} & -\frac{k_1-\mathrm{i}k_2}{2k_\parallel}\psi \\ -\frac{f^1+\mathrm{i}f^2}{4k_\parallel} & \psi \end{pmatrix} + \begin{pmatrix} \frac{(k_1+\mathrm{i}k_2)(f_1^*-\mathrm{i}f_2^*)}{8k_\parallel^2} & -\frac{f_1^*+\mathrm{i}f_2^*}{4k_\parallel} \\ -\frac{k_1+\mathrm{i}k_2}{2k_\parallel}\psi^* & \psi^* \end{pmatrix}\right] \\ &= \frac{1}{2}\begin{pmatrix} \frac{(k_1-\mathrm{i}k_2)(f_1+\mathrm{i}f_2)+(k_1+\mathrm{i}k_2)(f_1^*-\mathrm{i}f_2^*)}{8k_\parallel^2} & -\frac{k_1-\mathrm{i}k_2}{2k_\parallel}\psi - \frac{f_1^*+\mathrm{i}f_2^*}{4k_\parallel} \\ -\frac{f^1+\mathrm{i}f^2}{4k_\parallel} - \frac{k_1+\mathrm{i}k_2}{2k_\parallel}\psi^* & \psi+\psi^* \end{pmatrix} \\ &= \frac{1}{2}\begin{pmatrix} \frac{2\mathrm{Re}(\vec{k}_\perp\vec{f})+2k_2\mathrm{Im}(f_1)-2k_1\mathrm{Im}(f_2)}{8k_\parallel^2} & -\frac{k_1-\mathrm{i}k_2}{2k_\parallel}\psi - \frac{f_1^*+\mathrm{i}f_2^*}{4k_\parallel} \\ -\frac{f^1+\mathrm{i}f^2}{4k_\parallel} - \frac{k_1+\mathrm{i}k_2}{2k_\parallel}\psi^* & 2\mathrm{Re}(\psi) \end{pmatrix}. \end{aligned} \tag{192}$$

The decay width is then given as

$$\begin{aligned} \Gamma_{\vec{p}}(\omega) &= -\frac{|\lambda|^2 d(r)}{2\omega}\int_{-\infty}^{\infty}\frac{\mathcal{F}(p_\parallel,k_\parallel)}{k_\parallel - p_\parallel}\mathrm{tr}\left[\begin{pmatrix} p_+ & 0 \\ 0 & p_- \end{pmatrix}\begin{pmatrix} \frac{\mathrm{Re}(\vec{k}_\perp\vec{f})+k_2\mathrm{Im}(f_1)-k_1\mathrm{Im}(f_2)}{8k_\parallel^2} & -\frac{k_1-\mathrm{i}k_2}{4k_\parallel}\psi - \frac{f_1^*+\mathrm{i}f_2^*}{8k_\parallel} \\ -\frac{f^1+\mathrm{i}f^2}{8k_\parallel} - \frac{k_1+\mathrm{i}k_2}{4k_\parallel}\psi^* & \mathrm{Re}(\psi) \end{pmatrix}\right]\frac{d^3k}{(2\pi)^3} \\ &= -\frac{|\lambda|^2 d(r)}{2\omega}\int_{-\infty}^{\infty}\frac{\mathcal{F}(p_\parallel,k_\parallel)}{k_\parallel - p_\parallel}\left[p_+\frac{\mathrm{Re}(\vec{k}_\perp\vec{f})+k_2\mathrm{Im}(f_1)-k_1\mathrm{Im}(f_2)}{8k_\parallel^2} + p_-\mathrm{Re}(\psi)\right]\frac{d^3k}{(2\pi)^3}. \end{aligned} \tag{193}$$

The presented result can be compared to the thermal Majorana neutrino production rate calculated by Anisimov, Bödecker et al. [ABB11]. We will come back to this expression later when discussing the solution of the integral equations.

5.2 Gauge corrected CP-violating Diagrams

Further we need to investigate gauge corrections to the CP-violating diagrams discussed earlier in section 4. On one hand there are corrections to the Higgs and lepton propagator:

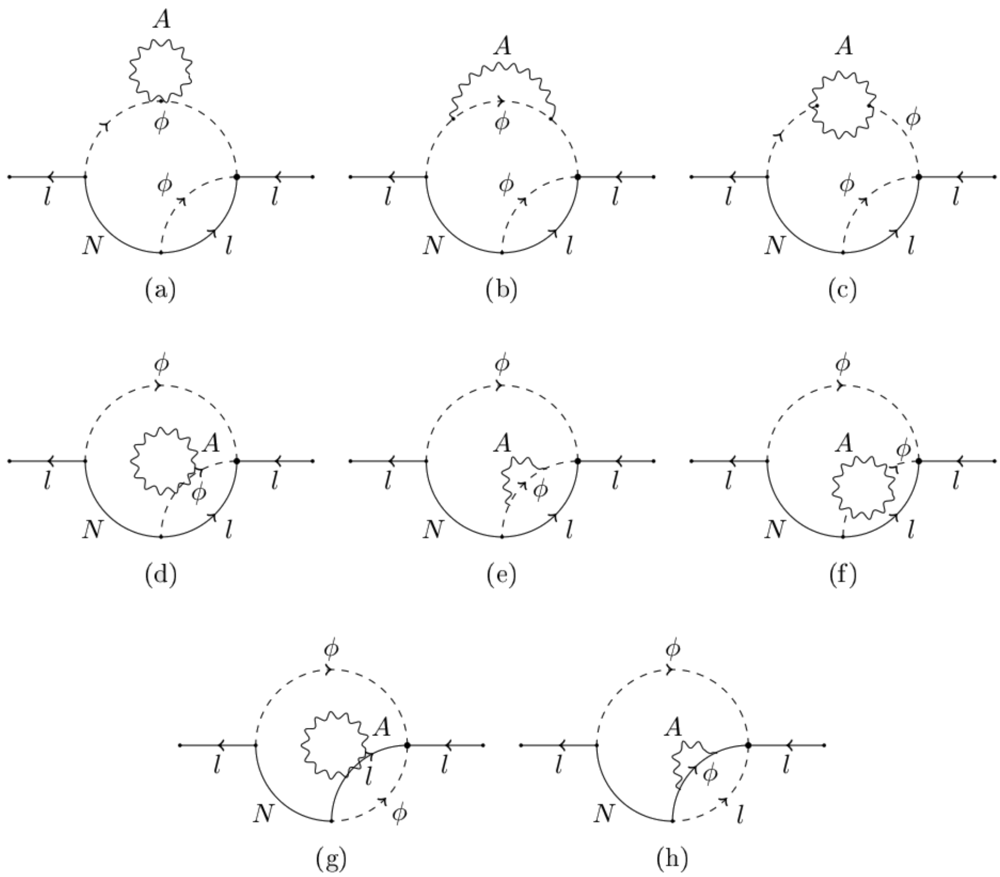

Figure 13: Three loop diagrams with gauge corrections for the Higgs (a)-(e) and lepton propagator (f)-(h) [Hüt13, p. 52].

As pointed out in section 3, these contributions are included using HTL resummation for momenta close to the lightcone leading to the asymptotic masses m_ϕ and m_l.

Further vertex corrections need to be taken into account. The possible three-loop corrections are shown in the following picture

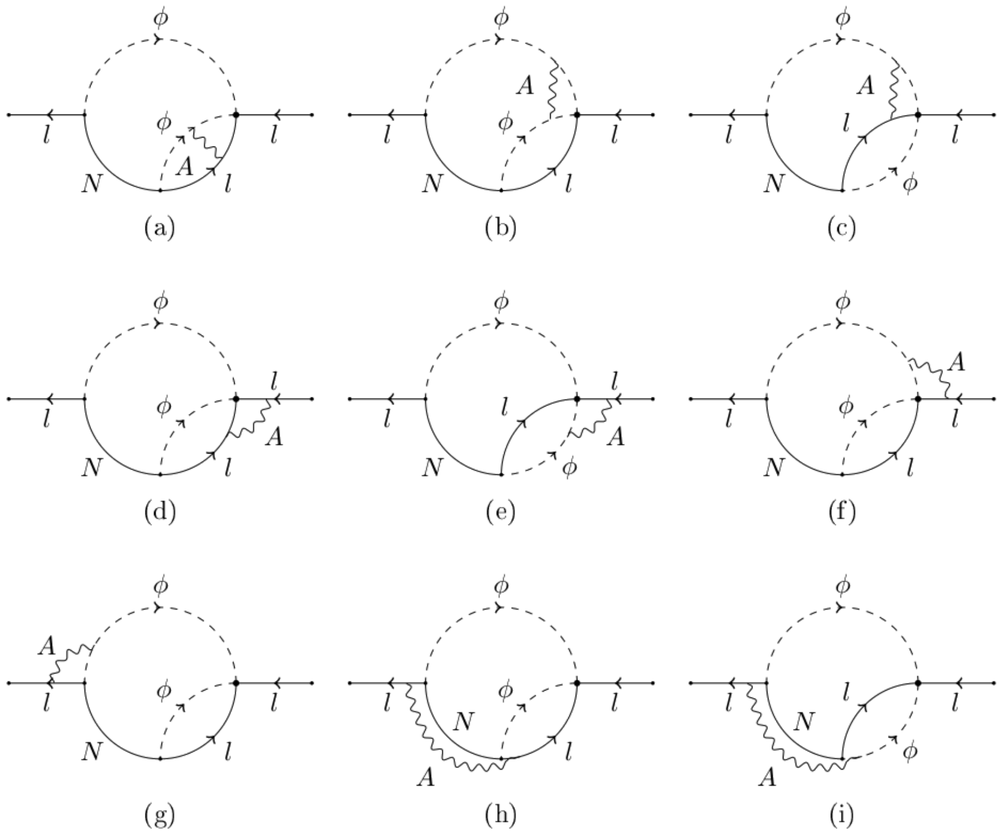

Figure 14: Three loop vertex corrections to the CP-violating diagram [Hüt13, p. 53].

An idea how to include all these contributions was first presented in the PhD thesis of J. Hütig [Hüt13]. The procedure to include the corrections works the following way: At first, for a better visualization, the Majorana line is reinserted at the effective vertex in the CP-violating diagram but actually the heavier neutrinos N_2 and N_3 are left integrated out keeping the effective vertex. Now the outer line is closed by integrating over the external momentum. This leads to the following diagram referred to as cylindrical diagram [Hüt13, p. 51-52].

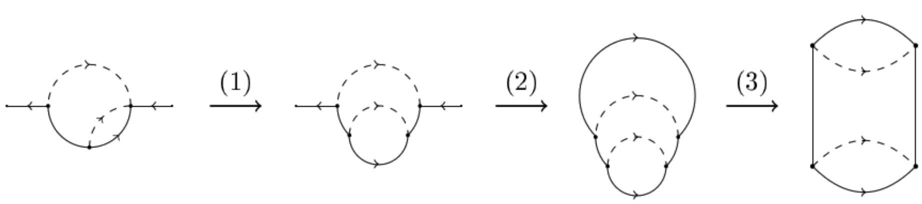

Figure 15: Systematic approach to include all gauge corrections [Hüt13]: In step (1) the effective Majorana line is reinserted, in step (2) the outer lepton line is closed, step (3) just changes the visualization.

It is now possible to identify the top and the bottom of the cylindrical diagram with the Majorana self energy known from calculations before. Gauge corrections can now be implemented by making use of the results for the gauge corrected Majorana self energy from section 3. Note that this corresponds to not only taking all 3-loop corrections into account but also higher loop order corrections since they are of the same order in the gauge coupling g. All in all we are left with the following gauge corrected cylindrical diagram

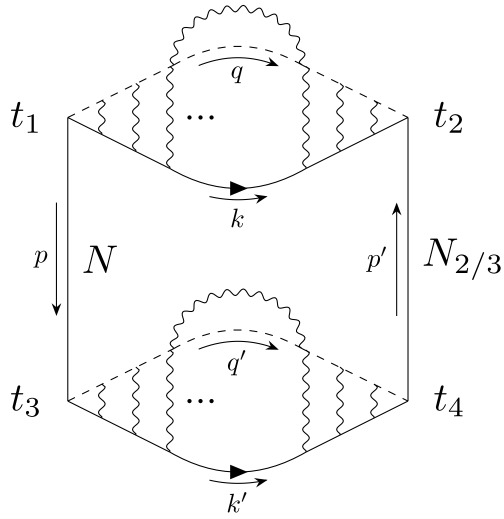

Figure 16: Gauge corrected cylindrical diagram containing all gauge contributions for a consistent treatment of gauge corrections to the Lepton number matrix.

Keep in mind that the line on the right hand side is integrated out and the effective vertex is given by $t_2 \equiv t_4$.

Comparing the diagram to the 3-loop vertex corrections from figure 15 shows that the contributions (a), (f) and (g) are obviously included. Further all other contributions are included as well since they are treated as soft external gauge bosons for the Majorana self energy in the resummation procedure from section 3. In short all leading order gauge corrections to the CP-violating diagrams are included when calculating the presented diagram [Hüt13, p. 53]. It is now also clear why we had to integrate $L_{ii\vec{k}}$ over the external momentum $\vec{k}$ in section 4.

The result of the lepton number matrix without corrections had the following form

$$\begin{aligned} L_{ii}(t,t) = -48\lambda_{ii} \int_0^t \int_0^t \int_0^{t_2} \int \int \int \int \int \int_{-\infty}^{\infty} \int_{-\infty}^{\infty} \frac{M}{\omega_{\vec{p}}} \cos(\omega_{\vec{p}} y_{13}) f_F(\omega_{\vec{p}}) e^{-\Gamma_{\vec{p}} \frac{t_1+t_3}{2}} \\ f_F(\omega_{21}) \mathrm{tr}\left(\mathrm{Im}\Sigma^{\mathrm{ret},R}_{\vec{k},\vec{q}}(\omega_{23}) \mathrm{Im}\Sigma^{\mathrm{ret},L}_{\vec{k}',\vec{q}'}(\omega_{23})\right) \mathrm{Re}\left[e^{-i(\omega_{21}y_{21}+\omega_{23}y_{23})}\right] \\ (2\pi)^3\delta(\vec{p}-\vec{k}'-\vec{q}')(2\pi)^3\delta(\vec{p}+\vec{k}+\vec{q}) \frac{d\omega_{21}}{2\pi} \frac{d\omega_{23}}{2\pi} \frac{d^3q}{(2\pi)^3} \frac{d^3q'}{(2\pi)^3} \frac{d^3k}{(2\pi)^3} \frac{d^3k'}{(2\pi)^3} \frac{d^3p}{(2\pi)^3} dt_3 dt_2 dt_1. \end{aligned} \tag{194}$$

The part of the lepton number matrix where the gauge corrections in context of the cylindrical diagram have to be implemented is

$$\int \int \int \int \mathrm{tr}\left(\mathrm{Im}\Sigma^{ret,R}_{\vec{k},\vec{q}}(\omega_{21}) \mathrm{Im}\Sigma^{ret,L}_{\vec{k}',\vec{q}'}(\omega_{23})\right) (2\pi)^3\delta(\vec{p}-\vec{k}'-\vec{q}')(2\pi)^3\delta(\vec{p}+\vec{k}+\vec{q}) \frac{d^3k}{(2\pi)^3} \frac{d^3k'}{(2\pi)^3} \frac{d^3q}{(2\pi)^3} \frac{d^3q'}{(2\pi)^3}. \tag{195}$$

At first we can use the momentum conservation by integrating out q and q'.

$$\int\int\int\int \mathrm{tr}\left(\mathrm{Im}\Sigma^{ret,R}_{\vec{k},\vec{q}}(\omega_{21})\mathrm{Im}\Sigma^{ret,L}_{\vec{k}',\vec{q}\,'}(\omega_{23})\right)(2\pi)^3\delta(\vec{p}-\vec{k}'-\vec{q}\,')(2\pi)^3\delta(\vec{p}+\vec{k}+\vec{q})\frac{d^3k}{(2\pi)^3}\frac{d^3k'}{(2\pi)^3}\frac{d^3q}{(2\pi)^3}\frac{d^3q'}{(2\pi)^3} \tag{196}$$

$$= \int\int \mathrm{tr}\left(\mathrm{Im}\Sigma^{ret,R}_{\vec{k},-\vec{p}-\vec{k}}(\omega_{21})\mathrm{Im}\Sigma^{ret,L}_{\vec{k}',\vec{p}-\vec{k}'}(\omega_{23})\right)\frac{d^3k}{(2\pi)^3}\frac{d^3k'}{(2\pi)^3} = \mathrm{tr}\left(\mathrm{Im}\Sigma^{\mathrm{ret},R}_{-\vec{p}}(\omega_{21})\mathrm{Im}\Sigma^{\mathrm{ret},L}_{\vec{p}}(\omega_{23})\right).$$

As previously seen in section 4.4 the only difference between left- and right-handed self energy is the sign of the spacial momentum components. We can simplify using

$$\mathrm{tr}\left(\mathrm{Im}\Sigma^{\mathrm{ret},R}_{-\vec{p}}(\omega_{21})\mathrm{Im}\Sigma^{\mathrm{ret},L}_{\vec{p}}(\omega_{23})\right) = \mathrm{tr}\left(\mathrm{Im}\Sigma^{\mathrm{ret},R}_{-\vec{p}}(\omega_{21})\mathrm{Im}\Sigma^{\mathrm{ret},R}_{-\vec{p}}(\omega_{23})\right). \tag{197}$$

Since $\Gamma_{\vec{p}}(\omega)$ is invariant under a change $\vec{p}\to-\vec{p}$ we can write

$$\mathrm{tr}\left(\mathrm{Im}\Sigma^{\mathrm{ret},R}_{-\vec{p}}(\omega_{21})\mathrm{Im}\Sigma^{\mathrm{ret},R}_{-\vec{p}}(\omega_{23})\right) \overset{\vec{p}\to-\vec{p}}{\to} \mathrm{tr}\left(\mathrm{Im}\Sigma^{\mathrm{ret},R}_{\vec{p}}(\omega_{21})\mathrm{Im}\Sigma^{\mathrm{ret},R}_{\vec{p}}(\omega_{23})\right), \tag{198}$$

regarding the complete lepton number matrix.

Keep in mind that the coupling is already factorized out, so in this case the corrected Σ is given as

$$\mathrm{Im}\left(\Sigma^{\mathrm{ret},R}_{\vec{p}}(\omega)\right) = -\frac{d(r)}{2}\int\frac{\mathcal{F}(p_\parallel,k_\parallel)}{k_\parallel-p_\parallel}\begin{pmatrix}\frac{\mathrm{Re}(\vec{k}_\perp\vec{f})+k_2\mathrm{Im}(f_1)-k_1\mathrm{Im}(f_2)}{8k_\parallel^2} & -\frac{k_1-\mathrm{i}k_2}{4k_\parallel}\psi-\frac{f_1^*+\mathrm{i}f_2^*}{8k_\parallel} \\ -\frac{f^1+\mathrm{i}f^2}{8k_\parallel}-\frac{k_1+\mathrm{i}k_2}{4k_\parallel}\psi^* & \mathrm{Re}(\psi)\end{pmatrix}\frac{d^3k}{(2\pi)^3}. \tag{199}$$

Putting everything together and using $d(r)=2$ leads to

$$\begin{aligned}\mathrm{tr}\left(\mathrm{Im}\Sigma^{\mathrm{ret},R}_{\vec{p}}(\omega_{21})\mathrm{Im}\Sigma^{\mathrm{ret},R}_{\vec{p}}(\omega_{23})\right) = &\int\int\frac{\mathcal{F}(p_\parallel,k_\parallel)}{k_\parallel-p_\parallel}\frac{\mathcal{F}(p_\parallel,k'_\parallel)}{k'_\parallel-p_\parallel} \\ &\mathrm{tr}\left[\begin{pmatrix}\frac{\mathrm{Re}(\vec{k}_\perp\vec{f})+k_2\mathrm{Im}(f_1)-k_1\mathrm{Im}(f_2)}{8k_\parallel^2} & -\frac{k_1-\mathrm{i}k_2}{4k_\parallel}\psi-\frac{f_1^*+\mathrm{i}f_2^*}{8k_\parallel} \\ -\frac{f_1+\mathrm{i}f_2}{8k_\parallel}-\frac{k_1+\mathrm{i}k_2}{4k_\parallel}\psi^* & \mathrm{Re}(\psi)\end{pmatrix}\right. \\ &\left.\begin{pmatrix}\frac{\mathrm{Re}(\vec{k}'_\perp\vec{f}')+k_2\mathrm{Im}(f'_1)-k_1\mathrm{Im}(f'_2)}{8(k'_\parallel)^2} & -\frac{k'_1-\mathrm{i}k'_2}{4k'_\parallel}\psi'-\frac{(f'_1)^*+\mathrm{i}(f'_2)^*}{8k'_\parallel} \\ -\frac{f'_1+\mathrm{i}f'_2}{8k'_\parallel}-\frac{k'_1+\mathrm{i}k'_2}{4k'_\parallel}(\psi')^* & \mathrm{Re}(\psi')\end{pmatrix}\right]\frac{d^3k}{(2\pi)^3}\frac{d^3k'}{(2\pi)^3}.\end{aligned} \tag{200}$$

As well as for the gauge corrected decay width, a numerical treatment is needed.

5.3 Solving the Integral Equations

In section 3 we developed the following integral equations for ψ and $\vec{f}$

$$\mathrm{i}\epsilon(p,\vec{k})\vec{f}(\vec{k}_\perp) - \int\mathcal{C}(\vec{q}_\perp)\left[\vec{f}(\vec{q}_\perp)-\vec{f}(\vec{k}_\perp-\vec{q}_\perp)\right]\frac{d^2q_\perp}{(2\pi)^2} = 2\vec{k}_\perp, \tag{201}$$

$$\mathrm{i}\epsilon(p,\vec{k})\psi(\vec{k}_\perp) - \int\mathcal{C}(\vec{q}_\perp)\left[\psi(\vec{q}_\perp)-\psi(\vec{k}_\perp-\vec{q}_\perp)\right]\frac{d^2q_\perp}{(2\pi)^2} = 1. \tag{202}$$

To simplify these equation it is useful to have a closer look at ϵ. Recalling its definition and using a frame with $\vec{p}_\perp=0$ we can rewrite

$$\epsilon(p,\vec{k}) \overset{\vec{p}_\perp=0}{=} \underbrace{v\cdot p}_{=\omega-p_\parallel=p_-} + \frac{\vec{k}_\perp+m_\phi^2}{2(k_\parallel-p_\parallel)} - \frac{\vec{k}_\perp^2+m_l^2}{2k_\parallel} \overset{\vec{p}_\perp=0}{=} \alpha(k_\parallel,p_\parallel)+\beta(k_\parallel,p_\parallel)\vec{k}_\perp^2 := \beta(M_{\mathrm{eff}}^2+\vec{k}_\perp^2), \tag{203}$$

with

$$\alpha(k_\parallel, p_\parallel) := -\frac{m_l^2}{2k_\parallel} + \frac{m_\phi^2}{2(k_\parallel - p_\parallel)} + p_- \qquad \beta(k_\parallel, p_\parallel) := \frac{p_\parallel}{2k_\parallel(k_\parallel - p_\parallel)}. \tag{204}$$

M_{eff}^2 is then given as $M_{\text{eff}}^2 = \frac{\alpha}{\beta}$ and takes the following form

$$M_{\text{eff}}^2 = \frac{m_l^2(p_\parallel - k_\parallel) + m_\phi^2 k_\parallel + 2k_\parallel(\omega - p_\parallel)(k_\parallel - p_\parallel)}{p_\parallel}. \tag{205}$$

Further we apply a Fourier transformation

$$\psi(\vec{k}_\perp) = \int \psi(\vec{b}) e^{-\mathrm{i}\vec{k}_\perp \vec{b}} d^2 b, \qquad \psi(\vec{b}) = \int \psi(\vec{k}_\perp) e^{\mathrm{i}\vec{k}_\perp \vec{b}} \frac{d^2 k_\perp}{(2\pi)^2}. \tag{206}$$

Using the result for ϵ and the Fourier transformation of ψ we can reformulate the integral equation of ψ. Keep in mind that there are two very useful features of the Fourier transformation used here

- **Linear operators become derivative operators:**

$$\int \psi(\vec{k}_\perp) \vec{k}_\perp^2 e^{\mathrm{i}\vec{k}_\perp \vec{b}} \frac{d^2 k_\perp}{(2\pi)^2} = -\Delta_{\vec{b}} \int \psi(\vec{k}_\perp) e^{\mathrm{i}\vec{k}_\perp \vec{b}} \frac{d^2 k_\perp}{(2\pi)^2} = -\Delta_{\vec{b}} \psi(\vec{b}). \tag{207}$$

- **The convolution theorem:**

$$\int\int \mathcal{C}(\vec{q}_\perp) e^{\mathrm{i}\vec{k}_\perp \vec{b}} \psi(\vec{k}_\perp - \vec{q}_\perp) e^{\mathrm{i}\vec{k}_\perp \vec{b}} \frac{d^2 q_\perp}{(2\pi)^2} \frac{d^2 k_\perp}{(2\pi)^2} = \int \mathcal{C}(\vec{q}_\perp) \left(\int \psi(\vec{k}_\perp - \vec{q}_\perp) e^{\mathrm{i}\vec{k}_\perp \vec{b}} \frac{d^2 k_\perp}{(2\pi)^2} \right) \frac{d^2 q_\perp}{(2\pi)^2} \tag{208}$$

$$\overset{\text{substitute: } \vec{z} = \vec{k}_\perp - \vec{q}_\perp}{=} \int \mathcal{C}(\vec{q}_\perp) \left(\int \psi(\vec{z}) e^{\mathrm{i}(\vec{z} + \vec{q}_\perp)\vec{b}} \frac{d^2 z}{(2\pi)^2} \right) \frac{d^2 q_\perp}{(2\pi)^2} = \int \mathcal{C}(\vec{q}_\perp) e^{\mathrm{i}\vec{q}_\perp \vec{b}} \frac{d^2 q_\perp}{(2\pi)^2} \int \psi(\vec{z}) e^{\mathrm{i}\vec{z}\vec{b}} \frac{d^2 z}{(2\pi)^2}$$

$$= \mathcal{C}(\vec{b}) \psi(\vec{b}).$$

Now the integral equation is given as differential equation of the following form [Hüt13, Appendix B]

$$-\mathrm{i}\beta(\Delta_{\vec{b}} - M_{\text{eff}}^2)\psi(\vec{b}) - \underbrace{\left(\int \mathcal{C}(\vec{q}_\perp) \frac{d^2 q_\perp}{(2\pi)^2} - \mathcal{C}(\vec{b}) \right)}_{:= \mathcal{K}(\vec{b})} \psi(\vec{b}) = \delta^{(2)}(\vec{b}). \tag{209}$$

Due to rotational invariance one has $\psi(\vec{b}) = \psi(b)$ and $\mathcal{K}(\vec{b}) = \mathcal{K}(b)$ [Hüt13, p. 76]. Using the Δ operator in cylindrical coordinates yields the following ordinary differential equation for $b > 0$

$$-\mathrm{i}\beta \left(\partial_b^2 + \frac{1}{b}\partial_b - M_{\text{eff}}^2 \right) \psi(b) - \mathcal{K}(b)\psi(b) = 0. \tag{210}$$

It is possible to treat $\vec{f}$ in the same way as presented for ψ using the Ansatz $\vec{f}(\vec{b}) = h(b)\vec{b}$ [Hüt13, p. 76]. The right-hand side of the equation is then given as $-2\mathrm{i}\nabla_{\vec{b}}\delta^{(2)}(\vec{b})$. The full equation for $b > 0$ reads

$$-\mathrm{i}\beta \left(\partial_b^2 + \frac{3}{b}\partial_b - M_{\text{eff}}^2 \right) h(b) - \mathcal{K}(b)h(b) = 0. \tag{211}$$

The last part remaining is the calculation of $\mathcal{K}(b)$. This is done by integrating $\mathcal{C}(\vec{q}_\perp)$ with respect to $\vec{q}_\perp$, as well as by calculating the Fourier transform $\mathcal{C}(b)$. This has to be done using dimensional regularization and is presented in [Hüt13, p. 76-77] in detail. The calculation leads to

$$\mathcal{K}(b) = T[C_2(r)g^2 D(m_D b) + y_l^2 (g')^2 D(m'_D b)]. \tag{212}$$

In the calculation a new function D has been introduced given as

$$D(x) = \frac{1}{2\pi}\left[\gamma_E + \ln\left(\frac{x}{2}\right) + K_0(x) \right]. \tag{213}$$

Here $K_0(x)$ is the modified Bessel function of the second kind and γ_E the Euler-Mascheroni constant.

5.3.1 Boundary Conditions and limiting Behavior

To apply the Fourier transformation ψ and $\vec{f}$ have to fulfill the following limiting behavior

$$\lim_{b\to\infty} \psi(b) = 0 \qquad \lim_{b\to\infty} \vec{f}(\vec{b}) = 0. \tag{214}$$

Further we have to investigate the limiting behavior for small b. One shows that [Hüt13, p. 77]

$$\lim_{b\to 0} \mathcal{K}(b) \sim D(b) \sim b^2 \to 0, \tag{215}$$

thus in the limit $b \to 0$ the differential equations simplify to

$$\begin{aligned} \Delta_{\vec{b}}\psi(\vec{b}) &= \frac{\mathrm{i}}{\beta}\delta^{(2)}(\vec{b}), \\ \Delta_{\vec{b}}\vec{f}(\vec{b}) &= \frac{2}{\beta}\nabla_{\vec{b}}\delta^{(2)}(\vec{b}). \end{aligned} \tag{216}$$

The solution of these equations can easily be derived via separation of variables arriving at the following limiting solutions for ψ and $\vec{f}$ in the case $b \to 0$

$$\begin{aligned} \psi(\vec{b}) &= \frac{\mathrm{i}}{2\pi\beta}\ln(b) + \mathcal{O}(b^0), \\ \vec{f}(\vec{b}) &= \frac{1}{\pi\beta}\frac{\vec{b}}{b^2} + \mathcal{O}(b) \to h(b) = \frac{1}{\pi\beta}\frac{1}{b^2} + \mathcal{O}(b^0). \end{aligned} \tag{217}$$

Looking at the limiting behavior for $b \to 0$ it can be noticed that only $\mathrm{Re}(\psi(b))$ and $\mathrm{Im}(\vec{f}(b)) = \vec{b}\mathrm{Im}(h(b))$ stay regular for $b \to 0$ while $\mathrm{Im}(\psi(b))$ and $\mathrm{Re}(\vec{f}(b)) = \vec{b}\mathrm{Re}(h(b))$ are singular.
The first corrections $\tilde{h}$ and $\tilde{\psi}$ have to fulfill the equations

$$\begin{aligned} (\Delta_{\vec{b}} - M_{\text{eff}}^2)\tilde{\psi}(b) &= \tilde{\psi}''(b) + \frac{\tilde{\psi}'(b)}{b} - M_{\text{eff}}^2\tilde{\psi}(b) = 0, \\ (\Delta_{\vec{b}} - M_{\text{eff}}^2)\tilde{h}(b) &= \tilde{h}''(b) + 3\frac{\tilde{h}'(b)}{b} - M_{\text{eff}}^2\tilde{h}(b) = 0, \end{aligned} \tag{218}$$

and since $\mathcal{K}(b) = b^2\ln(b) \to 0$ for $b \to 0$ one obtains $\tilde{\psi}'(b) \to 0$ and $\tilde{h}'(b) \to 0$ for $b \to 0$.

5.3.2 The perpendicular Momentum Integration

In the following we are going to focus on the contributions after solving the perpendicular momentum integral

$$\int \frac{d^3k}{(2\pi)^3} = \int_{-\infty}^{\infty} \int \frac{d^2k_\perp}{(2\pi)^2}\frac{dk_\parallel}{2\pi}. \tag{219}$$

The Dirac delta distribution can be defined as [Hüt13, p. 84]

$$\delta^{(2)}(\vec{b}) := \int e^{\pm\mathrm{i}\vec{k}_\perp\vec{b}}\frac{d^2k_\perp}{(2\pi)^2}. \tag{220}$$

We have to solve integrals of the form

$$\int \begin{pmatrix} \frac{\mathrm{Re}(\vec{k}_\perp\vec{f})+k_2\mathrm{Im}(f_1)-k_1\mathrm{Im}(f_2)}{8k_\parallel^2} & -\frac{k_1-\mathrm{i}k_2}{4k_\parallel}\psi - \frac{f_1^*+\mathrm{i}f_2^*}{8k_\parallel} \\ -\frac{f_1+\mathrm{i}f_2}{8k_\parallel} - \frac{k_1+\mathrm{i}k_2}{4k_\parallel}\psi^* & \mathrm{Re}(\psi) \end{pmatrix} \frac{d^2k_\perp}{(2\pi)^2}. \tag{221}$$

At first let us have a look at

$$\int \mathrm{Re}(\vec{k}_\perp \cdot \vec{f}(\vec{k}_\perp))\frac{d^2k_\perp}{(2\pi)^2} = \int k_1\mathrm{Re}(f_1(\vec{k}_\perp)) + k_2\mathrm{Re}(f_2(\vec{k}_\perp))\frac{d^2k}{(2\pi)^2}. \tag{222}$$

Introducing the Fourier transformation of $\vec{f}$ and replacing the linear k_i with a derivative operator acting on the integral kernel then leads to [Hüt13, p. 84]

$$\int \mathrm{Re}\left[\mathrm{i}\int\left(f_1(\vec{b})\frac{d}{db_1}+f_2(\vec{b})\frac{d}{db_2}\right)e^{-\mathrm{i}\vec{k}_\perp\vec{b}}d^2b\right]\frac{d^2k_\perp}{(2\pi)^2} = -\mathrm{Re}\left[\int \mathrm{i}\delta^{(2)}(\vec{b})\left(\frac{f_1(\vec{b})}{db_1}+\frac{f_2(\vec{b})}{db_2}\right)d^2b\right] \tag{223}$$
$$= \lim_{b\to 0}\mathrm{Im}\left(\nabla_{\vec{b}}\cdot\vec{f}(\vec{b})\right),$$

where partial integration has been used. Using the Ansatz $\vec{f}(\vec{b}) = h(b)\vec{b}$ finally leads to

$$\int \mathrm{Re}(\vec{k}_\perp\cdot\vec{f}(\vec{k}_\perp))\frac{d^2k_\perp}{(2\pi)^2} = \lim_{b\to 0}\mathrm{Im}(2h(b)+bh'(b)) = \lim_{b\to 0}\mathrm{Im}(2h(b)) := 2\mathrm{Im}[c_{2,h}(\omega,k_\parallel,p_\parallel)] \tag{224}$$

The $\mathrm{Im}(bh'(b))$ contribution has to vanish due to the limiting behavior of $h'(b)$ in the limit $b\to 0$ as described in the last section. The $\mathcal{O}(1/b^2)$ part of the limiting function is purely real and therefore the imaginary part must be at least of order $\mathcal{O}(b)$. As a result $h'(b)$ is at least of order $\mathcal{O}(1)$[5], so $\mathrm{Im}(bh'(b))$ vanishes in the limit $b\to 0$.

The same can be done for the $\mathrm{Re}(\psi)$ contribution

$$\int \mathrm{Re}(\psi(\vec{k}_\perp))\frac{d^2k_\perp}{(2\pi)^2} = \mathrm{Re}\left[\int \delta^{(2)}(\vec{b})\psi(\vec{b})d^2b\right] = \lim_{b\to 0}\mathrm{Re}(\psi(b)) := \mathrm{Re}[c_{2,\psi}(\omega,k_\parallel,p_\parallel)]. \tag{225}$$

The remaining contribution on the diagonal is given as

$$\int k_2\mathrm{Im}(f_1(\vec{k}_\perp)) - k_1\mathrm{Im}(f_2(\vec{k}_\perp))\frac{d^2k_\perp}{(2\pi)^2}. \tag{226}$$

With the Ansatz $\vec{f}(\vec{b}) = \vec{b}h(b)$ from rotational invariance we get

$$\begin{aligned}\int k_2\mathrm{Im}(f_1(\vec{k}_\perp)) - k_1\mathrm{Im}(f_2(\vec{k}_\perp))\frac{d^2k_\perp}{(2\pi)^2} &= \int \mathrm{Im}\left[\int\left(k_2f_1(\vec{b})-k_1f_2(\vec{b})\right)e^{-\mathrm{i}\vec{k}_\perp\vec{b}}d^2b\right]\frac{d^2k_\perp}{(2\pi)^2} \\ &= -\int \mathrm{Im}\left[\int \mathrm{i}\left(\frac{f_1(\vec{b})}{db_2}-\frac{f_2(\vec{b}}{db_1}\right)e^{-\mathrm{i}\vec{k}_\perp\vec{b}}d^2b\right]\frac{d^2k_\perp}{(2\pi)^2} \\ &= -\int \mathrm{Im}\left[\int \mathrm{i}\left(\frac{b_1h(b)}{db_2}-\frac{b_2h(b)}{db_1}\right)e^{-\mathrm{i}\vec{k}_\perp\vec{b}}d^2b\right]\frac{d^2k_\perp}{(2\pi)^2} \\ &= -\int \mathrm{Im}\left[\int \mathrm{i}\left(\frac{b_1b_2}{b}h'(b)-\frac{b_2b_1}{b}h'(b)\right)e^{-\mathrm{i}\vec{k}_\perp\vec{b}}d^2b\right]\frac{d^2k_\perp}{(2\pi)^2} = 0.\end{aligned} \tag{227}$$

Further we have to take a look at the contributions on the off-diagonal of the matrix

$$\begin{aligned}\int f_i(\vec{k}_\perp)\frac{d^2k_\perp}{(2\pi)^2} &= \int \mathrm{Re}f_i(\vec{k}_\perp)+\mathrm{i}\mathrm{Im}f_i(\vec{k}_\perp)\frac{d^2k_\perp}{(2\pi)^2} \\ \int k_i\psi(\vec{k}_\perp)\frac{d^2k_\perp}{(2\pi)^2} &= \int k_i\mathrm{Re}\psi(\vec{k}_\perp)+\mathrm{i}k_i\mathrm{Im}\psi(\vec{k}_\perp)\frac{d^2k_\perp}{(2\pi)^2},\end{aligned} \tag{228}$$

where $i\in 1,2$. In detail we have

$$\int \mathrm{Im}f_i(\vec{k}_\perp)\frac{d^2k_\perp}{(2\pi)^2} = \mathrm{Im}\left[\int \delta^{(2)}(\vec{b})f_i(\vec{b})d^2b\right] = \lim_{\vec{b}\to 0}\mathrm{Im}(f_i(\vec{b})) = 0. \tag{229}$$

Again this is clear from the limiting behavior of $\vec{f}$.

[5] Keep in mind that the first correction $\tilde{h}'(b)$ also vanishes.

Further we have

$$\int \mathrm{Re} f_i(\vec{k}_\perp) \frac{d^2k_\perp}{(2\pi)^2} = \mathrm{Re}\left[\int \delta^{(2)}(\vec{b}) f_i(\vec{b}) d^2b\right] = \lim_{\vec{b}\to 0} \mathrm{Re}(f_i(\vec{b})), \tag{230}$$

$$\begin{aligned} \int k_i \mathrm{Im}(\psi(\vec{k}_\perp)) \frac{d^2k_\perp}{(2\pi)^2} &= \int \mathrm{Im}\left[\int \psi(\vec{k}_\perp) k_i e^{\mathrm{i}\vec{k}_\perp \vec{b}} d^2b\right] \frac{d^2k_\perp}{(2\pi)^2} = -\mathrm{Im}\left[\int \mathrm{i}\delta^{(2)}(\vec{b}) \frac{d\psi(\vec{b})}{db_i} d^2b\right] \\ &= -\lim_{b\to 0} \mathrm{Re}\left(\frac{d\psi(b)}{db_i}\right) = -\lim_{b\to 0} \frac{b_i}{b} \mathrm{Re}\left(\psi'(b)\right), \end{aligned} \tag{231}$$

$$\begin{aligned} \int k_i \mathrm{Re}(\psi(\vec{k}_\perp)) \frac{d^2k_\perp}{(2\pi)^2} &= \int \mathrm{Re}\left[\int \psi(\vec{k}_\perp) k_i e^{\mathrm{i}\vec{k}_\perp \vec{b}} d^2b\right] \frac{d^2k_\perp}{(2\pi)^2} = -\mathrm{Re}\left[\int \mathrm{i}\delta^{(2)}(\vec{b}) \frac{d\psi(\vec{b})}{db_i} d^2b\right] \\ &= \lim_{b\to 0} \mathrm{Im}\left(\frac{d\psi(b)}{db_i}\right) = \lim_{b\to 0} \frac{b_i}{b} \mathrm{Im}\left(\psi'(b)\right). \end{aligned} \tag{232}$$

Having a closer look at the limiting behavior again we see that all these terms are $1/b$ divergent [Hüt13, p. 56]. This is not a problem because the divergence appears in the temperature independent part of the self energy. The only temperature dependent part is the function $\mathcal{F}$ that only depends on the parallel momentum components

$$\mathcal{F}(p_\parallel, k_\parallel) = f_F(p_\parallel) + f_B(k_\parallel - p_\parallel) = \frac{1}{e^{\beta p_\parallel} + 1} + \frac{1}{e^{\beta(k_\parallel - p_\parallel)} - 1} \overset{T=0}{=} \Theta(-p_\parallel) - \Theta(k_\parallel - p_\parallel). \tag{233}$$

Getting rid of the $T = 0$ divergent parts then leads to vanishing off-diagonal elements [Hüt13, p. 56].

All in all after renormalization and perpendicular momentum integration we are left with

$$\int \begin{pmatrix} \frac{\mathrm{Re}(\vec{k}_\perp \vec{f}) + k_2 \mathrm{Im}(f_1) - k_1 \mathrm{Im}(f_2)}{8k_\parallel^2} & -\frac{k_1 - \mathrm{i}k_2}{4k_\parallel}\psi - \frac{f_1^* + \mathrm{i}f_2^*}{8k_\parallel} \\ -\frac{f_1 + \mathrm{i}f_2}{8k_\parallel} - \frac{k_1 + \mathrm{i}k_2}{4k_\parallel}\psi^* & \mathrm{Re}(\psi) \end{pmatrix} \frac{d^2k_\perp}{(2\pi)^2} = \begin{pmatrix} \frac{\mathrm{Im}(c_{2,h}(\omega, p_\parallel, k_\parallel))}{4k_\parallel^2} & 0 \\ 0 & \mathrm{Re}(c_{2,\psi}(\omega, p_\parallel, k_\parallel)) \end{pmatrix}. \tag{234}$$

The self energy part in the lepton number matrix has the following form now

$$\begin{aligned} \mathrm{tr}\left(\mathrm{Im}\Sigma_{\vec{p}}^{\mathrm{ret},R}(\omega_{21}) \mathrm{Im}\Sigma_{\vec{p}}^{\mathrm{ret},R}(\omega_{23})\right) &= \int_{-\infty}^{\infty}\int_{-\infty}^{\infty} \frac{\mathcal{F}(p_\parallel, k_\parallel)}{k_\parallel - p_\parallel} \frac{\mathcal{F}(p_\parallel, k'_\parallel)}{k'_\parallel - p_\parallel} \mathrm{tr}\left[\begin{pmatrix} \frac{\mathrm{Im}(c_{2,h}(\omega_{21}, p_\parallel, k_\parallel))}{4k_\parallel^2} & 0 \\ 0 & \mathrm{Re}(c_{2,\psi}(\omega_{21}, p_\parallel, k_\parallel)) \end{pmatrix}\right. \\ &\qquad \left.\begin{pmatrix} \frac{\mathrm{Im}(c_{2,h}(\omega_{23}, p_\parallel, k'_\parallel))}{4k'^2_\parallel} & 0 \\ 0 & \mathrm{Re}(c_{2,\psi}(\omega_{23}, p_\parallel, k'_\parallel)) \end{pmatrix}\right] \frac{dk_\parallel}{2\pi} \frac{dk'_\parallel}{2\pi} \\ &= \int_{-\infty}^{\infty}\int_{-\infty}^{\infty} \frac{\mathcal{F}(p_\parallel, k_\parallel)}{k_\parallel - p_\parallel} \frac{\mathcal{F}(p_\parallel, k'_\parallel)}{k'_\parallel - p_\parallel} \left[\mathrm{Re}(c_{2,\psi}(\omega_{21}, p_\parallel, k_\parallel)) \mathrm{Re}(c_{2,\psi}(\omega_{23}, p_\parallel, k'_\parallel))\right. \\ &\qquad \left. + \frac{1}{16k_\parallel^2 k'^2_\parallel} \mathrm{Im}(c_{2,h}(\omega_{21}, p_\parallel, k_\parallel)) \mathrm{Im}(c_{2,h}(\omega_{23}, p_\parallel, k'_\parallel))\right] \frac{dk_\parallel}{2\pi} \frac{dk'_\parallel}{2\pi}. \end{aligned} \tag{235}$$

Since this is the only part of L_{ii} that is $k_\parallel$ and $k'_\parallel$ dependent it is very useful to define

$$\sigma_h(\omega, p_\parallel) := \int_{-\infty}^{\infty} \frac{\mathcal{F}(p_\parallel, k_\parallel)}{4k_\parallel^2(k_\parallel - p_\parallel)} \mathrm{Im}(c_{2,h}(\omega, p_\parallel, k_\parallel)) \frac{dk_\parallel}{2\pi}, \tag{236}$$

$$\sigma_\psi(\omega, p_\parallel) := \int_{-\infty}^{\infty} \frac{\mathcal{F}(p_\parallel, k_\parallel)}{k_\parallel - p_\parallel} \mathrm{Re}(c_{2,\psi}(\omega, p_\parallel, k_\parallel)) \frac{dk_\parallel}{2\pi}. \tag{237}$$

5.4 Calculating the gauge corrected Majorana Decay Width

Previously we have presented how to solve the integral equations for the gauge corrected Majorana neutrino self energy.

The gauge corrected decay width was given as

$$\Gamma_{\vec{p}}(\omega_{\vec{p}}) = -\frac{|\lambda|^2 d(r)}{2\omega_{\vec{p}}} \int \frac{\mathcal{F}(p_\parallel, k_\parallel)}{k_\parallel - p_\parallel} \left[p_+ \frac{\mathrm{Re}(\vec{k}_\perp \vec{f}) + k_2 \mathrm{Im}(f_1) - k_1 \mathrm{Im}(f_2)}{8k_\parallel^2} + p_- \mathrm{Re}(\psi) \right] \frac{d^3k}{(2\pi)^3}. \tag{238}$$

Following the results from the previous section the perpendicular momentum components can be integrated out leading to

$$\begin{aligned}\Gamma_{\vec{p}}(\omega_{\vec{p}}) &= -\frac{|\lambda|^2 d(r)}{2\omega_{\vec{p}}} \int\limits_{-\infty}^{\infty} \frac{\mathcal{F}(p_\parallel, k_\parallel)}{k_\parallel - p_\parallel} \left[\frac{\omega_{\vec{p}} + p_\parallel}{4k_\parallel^2} \mathrm{Im}(c_{2,h}(\omega_{\vec{p}}, p_\parallel, k_\parallel)) + (\omega_{\vec{p}} - p_\parallel) \mathrm{Re}(c_{2,\psi}(\omega_{\vec{p}}, p_\parallel, k_\parallel)) \right] \frac{dk_\parallel}{2\pi} \\ &= -\frac{|\lambda|^2 d(r)}{2\omega_{\vec{p}}} \left((\omega_{\vec{p}} + p_\parallel) \sigma_h(\omega_{\vec{p}}, p_\parallel) + (\omega_{\vec{p}} - p_\parallel) \sigma_\psi(\omega_{\vec{p}}, p_\parallel) \right).\end{aligned} \tag{239}$$

As pointed out earlier it is possible to compare this result for the gauge corrected Majorana decay width to the thermal production rate developed by Anisimov, Bödecker et al. [ABB11].

The result from the paper has the following form [ABB11, p. 15]

$$\frac{d\Gamma^{\mathrm{prod}}}{d^3p} = -\frac{d(r)|\lambda|^2}{(2\pi)^3 2p} \int \frac{1}{p - k_\parallel} f_F(k_\parallel) f_B(p - k_\parallel) \mathrm{Re} \left[\frac{p}{2k_\parallel^2} \vec{p}_\perp \cdot \vec{f} + \frac{M^2}{p} \psi \right] \frac{d^3k}{(2\pi)^3}. \tag{240}$$

Note that there are two important differences between the results:
The thermal production rate is given as a differential rate, giving evidence on produced particles per unit time and unit volume. On top of that a further approximation called lightlike approximation has been used in [ABB11] ($p_\parallel = p$)

$$\omega_{\vec{p}} \approx p_\parallel, \qquad p_+ = \omega_{\vec{p}} + p_\parallel \approx 2p_\parallel, \qquad p_- = \omega_{\vec{p}} - p_\parallel \approx \frac{M^2}{2p_\parallel}. \tag{241}$$

Applying the lightlike approximation to the gauge corrected decay width[6] leads to

$$\Gamma_{\vec{p}}^{\mathrm{light}} = -\frac{|\lambda|^2 d(r)}{2p_\parallel} \left(2p_\parallel \sigma_h(\omega_{\vec{p}}, p_\parallel) + \frac{M^2}{2p_\parallel} \sigma_\psi(\omega_{\vec{p}}, p_\parallel) \right). \tag{242}$$

Comparing both expression then leads to

$$\frac{d\Gamma^{\mathrm{prod}}}{d^3p} \frac{1}{f_F(p) T |\lambda|^2} = \frac{2}{(2\pi)^3 T |\lambda|^2} \Gamma_{\vec{p}}^{\mathrm{light}}. \tag{243}$$

The result of the thermal production rate calculated in [ABB11] is split into a helicity flip part and a non flip part by defining

$$\frac{d\Gamma^{\mathrm{prod,\ hel}}}{d^3p} \frac{1}{f_F(p) T |\lambda|^2} = -\frac{d(r)}{(2\pi)^3 T p_\parallel} 2p_\parallel \sigma_h(\omega_{\vec{p}}, p_\parallel), \tag{244}$$

$$\frac{d\Gamma^{\mathrm{prod,\ non}}}{d^3p} \frac{1}{f_F(p) T |\lambda|^2} = -\frac{d(r)}{(2\pi)^3 T p_\parallel} \frac{M^2}{2p_\parallel} \sigma_\psi(\omega_{\vec{p}}, p_\parallel). \tag{245}$$

[6] This also has an effect on M_{eff}^2 which is then given as $M_{\mathrm{eff}}^2 = [k_\parallel (k_\parallel - p_\parallel) M^2 - p_\parallel (k_\parallel - p_\parallel) m_l^2 + p_\parallel k_\parallel m_\phi^2]/p_\parallel^2$.

It is now possible to compare the result of the gauge corrected decay width to the result of the thermal production rate from [ABB11] to check the numerical program.

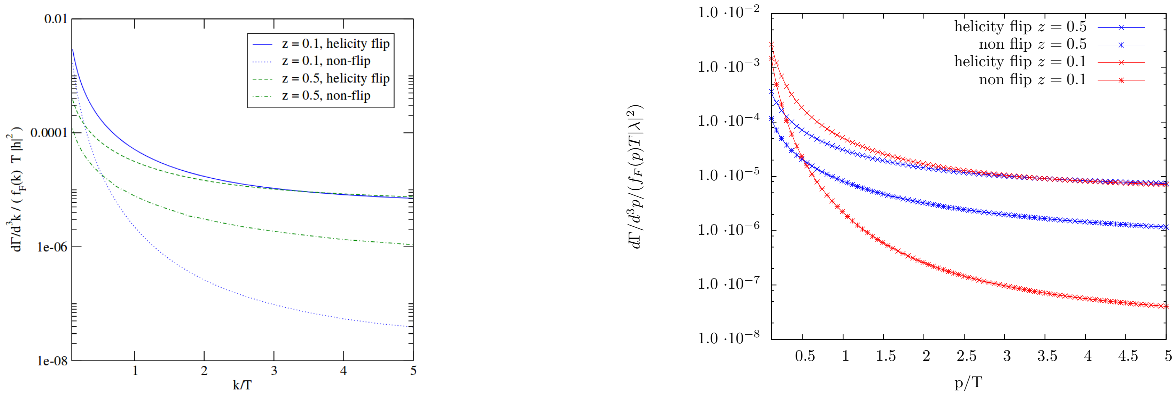

Figure 17: Left: Result of Γ^{prod} from [ABB11, p. 19] for fixed $M = 10^7$ GeV. Right: Result for Γ^{prod} calculated with the *GSL QAG* adaptive integration algorithm with a relative tolerance of $tol_{\text{rel}} = 10^{-2}$ (For further details see section 8).

Note that [ABB11] uses the label k for the Majorana neutrino momentum. The comparison of the two graphs shows perfect agreement. The algorithm explained later in section 6 and 8 is implemented correctly to the program leading to good results.

When calculating L_{ii} we are also integrating over the neutrino momentum p. Because of that it is not consistent to use the lightlike approximation since it is motivated in terms of large momenta. Investigating the effect of the approximation leads to the following graph

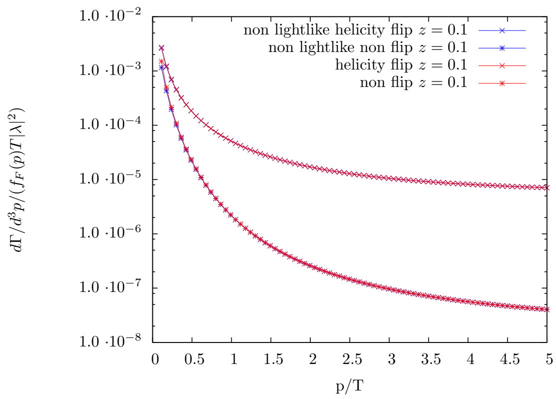

Figure 18: Comparing Γ^{prod} with and without lightlike approximation with fixed $M = 10^7$ GeV.

One can clearly notice that the results differ only for small momenta p. Although the effect is rather small all results of L_{ii} are calculated without the use of the lightlike approximation in this thesis.

An investigation of the effect of the lightlike approximation on the result for L_{ii} has been done in the Master thesis of Frederik Depta, proving that the difference is marginal.

5.5 Full gauge corrected Result

The gauge corrected Majorana self energy contribution in L_{ii} was given as

$$\operatorname{tr}\left(\mathrm{Im}\Sigma_{\vec{p}}^{\mathrm{ret},R}(\omega_{21})\mathrm{Im}\Sigma_{\vec{p}}^{\mathrm{ret},R}(\omega_{23})\right) = \int_{-\infty}^{\infty}\int_{-\infty}^{\infty} \frac{\mathcal{F}(p_\parallel,k_\parallel)}{k_\parallel - p_\parallel}\frac{\mathcal{F}(p_\parallel,k'_\parallel)}{k'_\parallel - p_\parallel} \left[\frac{1}{16k_\parallel^2(k'_\parallel)^2}\mathrm{Im}(c_{2,h}(\omega_{21},p_\parallel,k_\parallel))\mathrm{Im}(c_{2,h}(\omega_{23},p_\parallel,k'_\parallel)) + \mathrm{Re}(c_{2,\psi}(\omega_{21},p_\parallel,k_\parallel))\mathrm{Re}(c_{2,\psi}(\omega_{23},p_\parallel,k'_\parallel))\right]\frac{dk_\parallel}{2\pi}\frac{dk'_\parallel}{2\pi} = \sigma_h(\omega_{21},p_\parallel)\sigma_h(\omega_{23},p_\parallel) + \sigma_\psi(\omega_{21},p_\parallel)\sigma_\psi(\omega_{23},p_\parallel). \tag{246}$$

This has to be implemented in the final, not corrected result for the lepton number matrix L_{ii} from section 4

$$L_{ii}(t,t) = -48\lambda_{ii}\int_0^t\int_0^t\int_0^{t_2}\int_{-\infty}^{\infty}\int_{-\infty}^{\infty}\int\int\int\int\int \frac{M}{\omega_{\vec{p}}}\cos(\omega_{\vec{p}}y_{13})f_F(\omega_{\vec{p}})e^{-\Gamma_{\vec{p}}\frac{t_1+t_3}{2}} f_F(\omega_{21})\operatorname{tr}\left(\mathrm{Im}\Sigma_{\vec{k},\vec{q}}^{\mathrm{ret},R}(\omega_{23})\mathrm{Im}\Sigma_{\vec{k}',\vec{q}'}^{\mathrm{ret},L}(\omega_{23})\right)\mathrm{Re}\left[e^{-i(\omega_{21}y_{21}+\omega_{23}y_{23})}\right] (2\pi)^3\delta(\vec{p}-\vec{k}'-\vec{q}')(2\pi)^3\delta(\vec{p}+\vec{k}+\vec{q})\frac{d^3q}{(2\pi)^3}\frac{d^3q'}{(2\pi)^3}\frac{d^3k}{(2\pi)^3}\frac{d^3k'}{(2\pi)^3}\frac{d^3p}{(2\pi)^3}\frac{d\omega_{21}}{2\pi}\frac{d\omega_{23}}{2\pi}dt_3dt_2dt_1. \tag{247}$$

Putting everything together now leads to a result for the lepton number matrix include all leading order gauge corrections

$$L_{ii}(t,t) = -\frac{24}{\pi^2}\lambda_{ii}\int_0^t\int_0^t\int_0^{t_2}\int_{-\infty}^{\infty}\int_{-\infty}^{\infty}\int_0^{\infty}\frac{M}{\omega_{\vec{p}}}\cos(\omega_{\vec{p}}y_{13})f_F(\omega_{\vec{p}})f_F(\omega_{21})e^{-\Gamma_{\vec{p}}(\omega_{\vec{p}})\frac{t_1+t_3}{2}}\mathrm{Re}\left[e^{-i(\omega_{21}y_{21}+\omega_{23}y_{23})}\right] \left[\sigma_h(\omega_{21},p)\sigma_h(\omega_{23},p)+\sigma_\psi(\omega_{21},p)\sigma_\psi(\omega_{23},p)\right]p^2dp\frac{d\omega_{21}}{2\pi}\frac{d\omega_{23}}{2\pi}dt_3dt_2dt_1. \tag{248}$$

Keep in mind that the gauge corrected expression of the Majorana decay width $\Gamma_{\vec{p}}$ has to be used. The next step is to calculate the lepton number matrix numerically. For this purpose an algorithm is needed to obtain the c_2-coefficients by solving the integral equations leading to the σ contributions. Such an algorithm will be presented in the next section.

6 The numerical Algorithm to calculate the gauge Corrections

In the following the procedure to calculate the σ contributions is going to be presented. The idea of the algorithm follows the results presented in [ABB11, Appendix A] and [Hüt13, Appendix B]. The aim of the section is to develop two ordinary differential equations for ψ and $\vec{f}$ that can be solved easily using a C++ program.

6.1 Recipe of the Calculation

In the previous section we have simplified the integral equations for ψ and $\vec{f} = \vec{b}h(b)$ as far as possible ending up with the following differential equations

$$\begin{aligned} -\mathrm{i}\beta \left(\partial_b^2 + \frac{1}{b}\partial_b - M_{\text{eff}}^2\right)\psi(b) - \mathcal{K}(b)\psi(b) = 0, \\ -\mathrm{i}\beta \left(\partial_b^2 + \frac{3}{b}\partial_b - M_{\text{eff}}^2\right)h(b) - \mathcal{K}(b)h(b) = 0. \end{aligned} \tag{249}$$

To keep it short only the strategy for ψ is going to be presented here in detail. The calculation for $h(b)$ can be done in the same way. The following steps are made [Hüt13, p. 78]

1. At first ψ is split into a tree-level and a higher order part

$$\psi(b) = \psi_0(b) + \psi_1(b), \tag{250}$$

   with $\psi_0(b)$ being the solution of the equation

$$-\mathrm{i}\beta \left(\partial_b^2 + \frac{1}{b}\partial_b - M_{\text{eff}}^2\right)\psi_0(b) = 0. \tag{251}$$

2. The general solution ψ_1 is a superposition of a particular solution of the inhomogeneous equation $\psi_1^{(p)}$ and homogeneous solutions $\psi_1^{(1)/(2)}$

$$\psi_1(b) = \psi_1^{(p)}(b) + a_1\psi_1^{(1)}(b) + a_2\psi_1^{(2)}(b). \tag{252}$$

3. It will be shown that $a_1 = 0$ and

$$a_2 = -\lim_{b\to\infty} \frac{\psi_1^{(p)}(b)}{\psi_1^{(2)}(b)}. \tag{253}$$

4. After choosing initial values for $b \to \infty$ the following algorithm is implemented:
   - The homogeneous equation for $\psi_1(b)$ is solved with initial values $\psi_1^{(1)/(2)}(0) = 1$ and $\psi_1^{(1)/(2)\prime}(0) = 0$, this leads to $\psi_1^{(2)}$.
   - The inhomogeneous equation for $\psi_1(b)$ is solved using the initial conditions $\psi_1^{(p)}(0) = \mathrm{i}$ and $\psi_1^{(p)\prime}(0) = 0$, this leads to $\psi_1^{(p)}$.
5. Finally the results for $\psi_1^{(p)}$ and $\psi_1^{(2)}$ are used to calculate a_2 which is directly connected to c_2.

The main difference in the calculation of $h(b)$ is a different choice of initial conditions in step 4, choosing

$$h_1^{(1)/(2)}(0) = \mathrm{i}, \qquad h_1^{(1)/(2)\prime}(0) = 0, \qquad h_1^{(p)}(0) = 1, \qquad h_1^{(p)\prime}(0) = 0. \tag{254}$$

6.2 Solving the Equation for ψ_0

The solution of

$$-\mathrm{i}\beta\left(\partial_b^2+\frac{1}{b}\partial_b-M_{\text{eff}}^2\right)\psi_0(b)=0 \tag{255}$$

is given as [Hüt13, p. 79]

$$\psi_0(b)=d_1J_0\left(\mathrm{i}b\sqrt{M_{\text{eff}}^2}\right)+d_2Y_0\left(-\mathrm{i}b\sqrt{M_{\text{eff}}^2}\right),\qquad d_1,d_2\in\mathbb{C}, \tag{256}$$

with the Bessel functions J_n of the first and Y_n of the second kind.

It is important to notice that M_{eff}^2 can become negative recalling its definition

$$M_{\text{eff}}^2=\frac{m_l^2(p_\parallel-k_\parallel)+m_\phi^2k_\parallel+2k_\parallel(\omega-p_\parallel)(k_\parallel-p_\parallel)}{p_\parallel}. \tag{257}$$

There are two cases to look at:

1. $M_{\text{eff}}^2\geq 0\rightarrow\sqrt{M_{\text{eff}}^2}=M_{\text{eff}}$.

   In this case the Bessel functions have a purely complex argument and they can be rewritten in the following form

$$J_0\left(\mathrm{i}b\sqrt{M_{\text{eff}}^2}\right)\rightarrow I_0\left(bM_{\text{eff}}\right),\qquad Y_0\left(-\mathrm{i}b\sqrt{M_{\text{eff}}^2}\right)\rightarrow K_0\left(bM_{\text{eff}}\right). \tag{258}$$

   Their limiting behavior for $b\rightarrow 0$ is given as

$$\begin{aligned}K_0(b)&\overset{b\rightarrow 0}{\rightarrow}-\ln(b),\\ I_0(b)&\overset{b\rightarrow 0}{\rightarrow}\frac{1}{\Gamma(1)}=1,\end{aligned} \tag{259}$$

   such that in the case $b\rightarrow 0$ the solution takes the following form

$$\psi_0(b)=d_1^{(1)}I_0\left(bM_{\text{eff}}\right)+d_2^{(1)}K_0\left(bM_{\text{eff}}\right)\overset{b\rightarrow 0}{\rightarrow}d_1^{(1)}-d_2^{(1)}\ln(bM_{\text{eff}}). \tag{260}$$

   The limiting behavior of ψ discussed in section 5.3.1 was given as

$$\psi(b)\sim\frac{\mathrm{i}}{2\pi\beta}\ln(b)+\mathcal{O}(b^0). \tag{261}$$

   Comparing both results then leads to

$$\psi_0(b)=d_1^{(1)}I_0(bM_{\text{eff}})-\frac{\mathrm{i}}{2\pi\beta}K_0(bM_{\text{eff}}). \tag{262}$$

2. $M_{\text{eff}}^2<0\rightarrow\sqrt{M_{\text{eff}}^2}=\mathrm{i}M_{\text{eff}}$.

   Now the Bessel functions only depend on real values. For their limiting behavior one can observe

$$\begin{aligned}J_0(b)&\overset{b\rightarrow 0}{\rightarrow}\frac{\left(\frac{b}{2}\right)^0}{\Gamma(1)}=1,\\ Y_0(b)&\overset{b\rightarrow 0}{\rightarrow}\frac{2}{\pi}\ln(b).\end{aligned} \tag{263}$$

   Again after comparing this with the limiting behavior of ψ from section 5.3.1 we arrive at

$$\psi_0(b)=d_1^{(2)}J_0(M_{\text{eff}}b)+\frac{\mathrm{i}}{4\beta}Y_0(M_{\text{eff}}b). \tag{264}$$

Further the limiting behavior for $b \to \infty$ needs to be investigated. Since I_0 is divergent for $b \to \infty$ we have to set $d_1^{(1)} = 0$ leading to a purely imaginary solution. On top of that the transition between the two regions of M_{eff}^2 needs to be continuous. Since the $M_{\text{eff}}^2 \geq 0$ is now purely imaginary we need to set $d_1^{(2)} = 0$ as well to obtain continuity [Hüt13, p. 80]. The two purely imaginary solutions are then given as

$$\psi_0(b) = -\frac{\mathrm{i}}{2\pi\beta} K_0\left(\sqrt{M_{\text{eff}}^2} b\right) \qquad M_{\text{eff}}^2 \geq 0, \tag{265}$$

$$\psi_0(b) = \frac{\mathrm{i}}{4\beta} Y_0\left(\sqrt{|M_{\text{eff}}^2|} b\right) \qquad M_{\text{eff}}^2 < 0. \tag{266}$$

6.3 Equation for $\psi_1^{(1)/(2)}$

We have made the Ansatz

$$\begin{aligned} \psi(b) &= \psi_0(b) + \psi_1(b), \qquad \text{with} \\ \psi_1(b) &= a_1 \psi_1^{(1)}(b) + a_2 \psi_1^{(2)}(b) + \psi_1^{(p)}(b). \end{aligned} \tag{267}$$

The solution of the homogeneous equation is given by $\psi_1^{(1)/(2)}$

$$-\mathrm{i}\beta \left(\partial_b^2 + \frac{1}{b}\partial_b - M_{\text{eff}}^2\right) \psi_1^{(1)/(2)}(b) - \mathcal{K}(b)\psi_1^{(1)/(2)}(b) = 0. \tag{268}$$

After taking a look at the limiting behavior of ψ_1 we can simplify further by making a subtle choice of initial conditions. As already mentioned in section 5.3.1 the $D(b)$ contributions in $\mathcal{K}(b)$ have the following limiting behavior for $b \to 0$: $D(b) \sim b^2 \ln(b)$. Further the ψ_0 solution constructed in the last section is regular and shows the same limiting behavior. Thus ψ_1 has to be regular for $b \to 0$. By making an adequate choice of initial conditions we set [Hüt13, p. 80]

$$\psi_1^{(1)} \overset{b\to 0}{\sim} -\frac{\mathrm{i}}{2\pi\beta}\ln(b) \quad (\sim K_0(b)), \qquad \psi_1^{(2)} \overset{b\to 0}{\sim} \text{regular} \quad (\sim I_0(b)). \tag{269}$$

For the correct limiting behavior of $\psi(b)$ in the limit $b \to \infty$ we need

$$\begin{aligned} \lim_{b\to\infty} \psi(b) = 0 \quad &\to \quad \lim_{b\to\infty} \psi_1(b) = 0, \\ \lim_{b\to\infty} \psi_1(b) = 0 = &\underbrace{a_1 \psi_1^{(1)}(b)}_{\sim a_1 b^2 \ln(b) \to a_1 \overset{!}{=} 0} + a_2 \underbrace{\psi_1^{(2)}(b)}_{\sim \text{regular}} + \psi_1^{(p)}(b), \end{aligned} \tag{270}$$

leading to

$$a_2 = -\lim_{b\to\infty} \frac{\psi_1^{(p)}(b)}{\psi_1^{(2)}(b)}. \tag{271}$$

Using the initial conditions

$$\psi_1^{(1)/(2)}(0) = 1, \qquad \psi_1^{(1)/(2)\prime}(0) = 0, \tag{272}$$

leads to the solution $\psi_1^{(2)}$ when solving the homogeneous equation since $a_1 = 0$

$$-\mathrm{i}\beta \left(\partial_b^2 + \frac{1}{b}\partial_b - M_{\text{eff}}^2\right) \psi_1^{(2)}(b) - \mathcal{K}(b)\psi_1^{(2)}(b) = 0. \tag{273}$$

It is possible to split the equation into two real-valued equations using $\psi_1^{(2)}(b) = \psi_{1,r}^{(2)}(b) + \mathrm{i}\psi_{1,i}^{(2)}(b)$ since all other functions are real valued functions

$$\begin{aligned} \left(\partial_b^2 + \frac{1}{b}\partial_b - M_{\text{eff}}^2\right) \psi_{1,r}^{(2)}(b) + \frac{\mathcal{K}(b)}{\beta}\psi_{1,i}^{(2)}(b) = 0, \\ \left(\partial_b^2 + \frac{1}{b}\partial_b - M_{\text{eff}}^2\right) \psi_{1,i}^{(2)}(b) - \frac{\mathcal{K}(b)}{\beta}\psi_{1,r}^{(2)}(b) = 0. \end{aligned} \tag{274}$$

For the initial conditions we then have

$$\begin{aligned}\psi_1^{(2)}(0)=1 \quad &\to \quad \psi_{1,r}^{(2)}(0)+\mathrm{i}\psi_{1,i}^{(2)}(0)=1 \quad \to \quad \psi_{1,r}^{(2)}(0)=1, \quad \psi_{1,i}^{(2)}(0)=0,\\ \psi_1^{(2)\prime}(0)=0 \quad &\to \quad \psi_{1,r}^{(2)\prime}(0)+\mathrm{i}\psi_{1,i}^{(2)\prime}(0)=1 \quad \to \quad \psi_{1,r}^{(2)\prime}(0)=0, \quad \psi_{1,i}^{(2)\prime}(0)=0.\end{aligned} \tag{275}$$

6.4 Solving the inhomogeneous Equation

The remaining inhomogeneous equation takes the following form

$$\begin{aligned}-\mathrm{i}\beta\left(\partial_b^2+\frac{1}{b}\partial_b-M_{\text{eff}}^2\right)(\psi_0(b)+\psi_1^{(p)}(b))-\mathcal{K}(b)(\psi_0(b)+\psi_1^{(p)}(b))=0,\\ \Leftrightarrow -\mathrm{i}\beta\left(\partial_b^2+\frac{1}{b}\partial_b-M_{\text{eff}}^2\right)\psi_1^{(p)}(b)-\mathcal{K}(b)(\psi_0(b)+\psi_1^{(p)}(b))=0.\end{aligned} \tag{276}$$

Solving the equation with initial conditions

$$\psi_1^{(p)}(0)=\mathrm{i}, \qquad \psi_1^{(p)\prime}(0)=0, \tag{277}$$

leads to the solution $\psi_1^{(p)}(b)$. Again this equation can be split into two real-valued ODEs in the same way as presented above

$$\begin{aligned}\left(\partial_b^2+\frac{1}{b}\partial_b-M_{\text{eff}}^2\right)\psi_{1,r}^{(p)}(b)+\frac{\mathcal{K}(b)}{\beta}(\psi_{0,i}(b)+\psi_{1,i}^{(p)}(b))=0,\\ \left(\partial_b^2+\frac{1}{b}\partial_b-M_{\text{eff}}^2\right)\psi_{1,i}^{(p)}(b)-\frac{\mathcal{K}(b)}{\beta}(\psi_{0,r}(b)+\psi_{1,r}^{(p)}(b))=0.\end{aligned} \tag{278}$$

The initial conditions are then given as

$$\begin{aligned}\psi_1^{(p)}(0)=\mathrm{i} \quad &\to \quad \psi_{1,r}^{(p)}(0)+\mathrm{i}\psi_{1,i}^{(p)}(0)=\mathrm{i} \quad \to \quad \psi_{1,r}^{(p)}(0)=0, \quad \psi_{1,i}^{(p)}(0)=1,\\ \psi_1^{(p)\prime}(0)=0 \quad &\to \quad \psi_{1,r}^{(p)\prime}(0)+\mathrm{i}\psi_{1,i}^{(p)\prime}(0)=1 \quad \to \quad \psi_{1,r}^{(p)\prime}(0)=0, \quad \psi_{1,i}^{(p)\prime}(0)=0.\end{aligned} \tag{279}$$

6.5 Calculating the c_2-Coefficients

All in all we now have the following structure of the solution

$$\psi(b)=\psi_0(b)+\psi_1(b)=\begin{cases}-\frac{\mathrm{i}}{2\pi\beta}K_0\left(\sqrt{M_{\text{eff}}^2}b\right)-\left(\lim\limits_{b\to\infty}\frac{\psi_1^{(p)}(b)}{\psi_1^{(2)}(b)}\right)\psi_1^{(2)}(b)+\psi_1^{(p)}(b) & M_{\text{eff}}^2\geq 0\\ \frac{\mathrm{i}}{4\beta}Y_0\left(\sqrt{|M_{\text{eff}}^2|}b\right)-\left(\lim\limits_{b\to\infty}\frac{\psi_1^{(p)}(b)}{\psi_1^{(2)}(b)}\right)\psi_1^{(2)}(b)+\psi_1^{(p)}(b) & M_{\text{eff}}^2<0\end{cases}, \tag{280}$$

with initial conditions

$$\begin{aligned}\psi_1^{(2)}(0)=1 \quad &\to \quad \psi_{1,r}^{(2)}(0)=1, \quad \psi_{1,i}^{(2)}(0)=0,\\ \psi_1^{(2)\prime}(0)=0 \quad &\to \quad \psi_{1,r}^{(2)\prime}(0)=0, \quad \psi_{1,i}^{(2)\prime}(0)=0,\\ \psi_1^{(p)}(0)=\mathrm{i} \quad &\to \quad \psi_{1,r}^{(p)}(0)=0, \quad \psi_{1,i}^{(p)}(0)=1,\\ \psi_1^{(p)\prime}(0)=0 \quad &\to \quad \psi_{1,r}^{(p)\prime}(0)=0, \quad \psi_{1,i}^{(p)\prime}(0)=0.\end{aligned} \tag{281}$$

Using these results it is straight forward to calculate the c_2-coefficient

$$\mathrm{Re}(c_{2,\psi})=\mathrm{Re}\left(\lim_{b\to 0}\psi(b)\right)=\mathrm{Re}\left(-\left(\lim_{b\to\infty}\frac{\psi_1^{(p)}(b)}{\psi_1^{(2)}(b)}\right)\underbrace{\psi_1^{(2)}(0)}_{=1}+\underbrace{\psi_1^{(p)}(0)}_{=\mathrm{i}}\right)=-\lim_{b\to\infty}\mathrm{Re}\left(\frac{\psi_1^{(p)}(b)}{\psi_1^{(2)}(b)}\right). \tag{282}$$

6.6 Procedure for $h(b)$

As mentioned in the beginning the solution for $h(b)$ can be obtained in the same way as presented for $\psi(b)$. The homogeneous solution is given as [Hüt13, p. 81]

$$
\begin{aligned}
h_0(b) &= \frac{M_{\text{eff}}}{\pi\beta b} K_1\left(\sqrt{M_{\text{eff}}^2} b\right) \qquad M_{\text{eff}}^2 \geq 0, \\
h_0(b) &= -\frac{M_{\text{eff}}}{2\beta b} Y_1\left(\sqrt{|M_{\text{eff}}^2|} b\right) \qquad M_{\text{eff}}^2 < 0.
\end{aligned} \tag{283}
$$

Note that $h_0(b)$ is now purely real instead of purely imaginary. Further the previously presented equations also hold for $h(b)$ when replacing $\frac{1}{b}$ with $\frac{3}{b}$

$$
\begin{aligned}
\left(\partial_b^2 + \frac{3}{b}\partial_b - M_{\text{eff}}^2\right) h_{1,r}^{(2)}(b) + \frac{\mathcal{K}(b)}{\beta} h_{1,i}^{(2)}(b) = 0, \\
\left(\partial_b^2 + \frac{3}{b}\partial_b - M_{\text{eff}}^2\right) h_{1,i}^{(2)}(b) - \frac{\mathcal{K}(b)}{\beta} h_{1,r}^{(2)}(b) = 0,
\end{aligned} \tag{284}
$$

$$
\begin{aligned}
\left(\partial_b^2 + \frac{3}{b}\partial_b - M_{\text{eff}}^2\right) h_{1,r}^{(p)}(b) + \frac{\mathcal{K}(b)}{\beta} (h_{0,i}(b) + h_{1,i}^{(p)}(b)) = 0, \\
\left(\partial_b^2 + \frac{3}{b}\partial_b - M_{\text{eff}}^2\right) h_{1,i}^{(p)}(b) - \frac{\mathcal{K}(b)}{\beta} (h_{0,r}(b) + h_{1,r}^{(p)}(b)) = 0.
\end{aligned} \tag{285}
$$

The main difference is given in the choice of initial conditions. The coefficient $c_{2,h}$ is given via the imaginary part of $h(b)$

$$
\text{Im}(c_{2,h}) = \text{Im}\left(\lim_{b\to 0} h(b)\right). \tag{286}
$$

The full solution $h(b)$ has a similar structure compared to the full solution $\psi(b)$

$$
h(b) = h_0(b) + h_1(b) = \begin{cases} \frac{M_{\text{eff}}}{\pi\beta b} K_1\left(\sqrt{M_{\text{eff}}^2} b\right) - \left(\lim\limits_{b\to\infty} \frac{h_1^{(p)}(b)}{h_1^{(2)}(b)}\right) h_1^{(2)}(b) + h_1^{(p)}(b) & M_{\text{eff}}^2 \geq 0 \\ -\frac{M_{\text{eff}}}{2\beta b} Y_1\left(\sqrt{|M_{\text{eff}}^2|} b\right) - \left(\lim\limits_{b\to\infty} \frac{h_1^{(p)}(b)}{h_1^{(2)}(b)}\right) h_1^{(2)}(b) + h_1^{(p)}(b) & M_{\text{eff}}^2 < 0 \end{cases}. \tag{287}
$$

To obtain the imaginary part the following initial conditions are chosen [Hüt13, p. 81]

$$
\begin{aligned}
h_1^{(2)}(0) = \mathrm{i} \quad &\to \quad h_{1,r}^{(2)}(0) = 0, \quad h_{1,i}^{(2)}(0) = 1, \\
h_1^{(2)\prime}(0) = 0 \quad &\to \quad h_{1,r}^{(2)\prime}(0) = 0, \quad h_{1,i}^{(2)\prime}(0) = 0, \\
h_1^{(p)}(0) = 1 \quad &\to \quad h_{1,r}^{(p)}(0) = 1, \quad h_{1,i}^{(p)}(0) = 0, \\
h_1^{(p)\prime}(0) = 0 \quad &\to \quad h_{1,r}^{(p)\prime}(0) = 0, \quad h_{1,i}^{(p)\prime}(0) = 0.
\end{aligned} \tag{288}
$$

The coefficient $c_{2,h}$ is then given as

$$
\text{Im}(c_{2,h}) = \text{Im}\left(\lim_{b\to 0} h(b)\right) = \text{Im}\left(-\left(\lim_{b\to\infty} \frac{h_1^{(p)}(b)}{h_1^{(2)}(b)}\right) \underbrace{h_1^{(2)}(0)}_{=\mathrm{i}} + \underbrace{h_1^{(p)}(0)}_{=1}\right) = -\lim_{b\to\infty} \text{Im}\left(\frac{h_1^{(p)}(b)}{h_1^{(2)}(b)}\right). \tag{289}
$$

6.7 ODE Solver

We arrived at 4 ordinary differential equations of second order for ψ and h where always two of them are coupled. To solve these equations numerically we have to transform them to first order equations by making use of

$$\frac{d^2f(x)}{dx^2}+g(x)\frac{df(x)}{dx}=r(x)\quad\rightarrow\quad\frac{df(x)}{dx}:=z(x),\quad\frac{dz(x)}{dx}=r(x)-g(x)z(x). \tag{290}$$

The complete set of equations for $\psi_1^{(2)}$ is then given as

$$\begin{aligned}\partial_b\psi_{1,r}^{(2)}(b)&=z_r^{(2)}(b),\\ \partial_b\psi_{1,i}^{(2)}(b)&=z_i^{(2)}(b),\\ \partial_b z_{1,r}^{(2)}(b)&=-\frac{1}{b}z_{1,r}^{(2)}(b)+M_{\text{eff}}^2\psi_{1,r}^{(2)}(b)-\frac{\mathcal{K}(b)}{\beta}\psi_{1,i}^{(2)}(b),\\ \partial_b z_{1,i}^{(2)}(b)&=-\frac{1}{b}z_{1,i}^{(2)}(b)+M_{\text{eff}}^2\psi_{1,i}^{(2)}(b)+\frac{\mathcal{K}(b)}{\beta}\psi_{1,r}^{(2)}(b),\end{aligned} \tag{291}$$

with initial conditions

$$\psi_{1,r}^{(2)}(0)=1,\quad\psi_{1,i}^{(2)}(0)=0,\quad z_r^{(2)}(0)=0,\quad z_i^{(2)}(0)=0. \tag{292}$$

The complete set of equations for $\psi_1^{(p)}$ is given as

$$\begin{aligned}\partial_b\psi_{1,r}^{(p)}(b)&=z_r^{(p)}(b),\\ \partial_b\psi_{1,i}^{(p)}(b)&=z_i^{(p)}(b),\\ \partial_b z_{1,r}^{(p)}(b)&=-\frac{1}{b}z_{1,r}^{(p)}(b)+M_{\text{eff}}^2\psi_{1,r}^{(p)}(b)-\frac{\mathcal{K}(b)}{\beta}(\psi_{0,i}(b)+\psi_{1,i}^{(p)}(b)),\\ \partial_b z_{1,i}^{(p)}(b)&=-\frac{1}{b}z_{1,i}^{(p)}(b)+M_{\text{eff}}^2\psi_{1,i}^{(p)}(b)+\frac{\mathcal{K}(b)}{\beta}(\psi_{0,r}(b)+\psi_{1,r}^{(p)}(b)),\end{aligned} \tag{293}$$

with initial conditions

$$\begin{aligned}&\psi_{1,r}^{(p)}(0)=0,\quad\psi_{1,i}^{(p)}(0)=1,\quad z_r^{(p)}(0)=0,\quad z_i^{(p)}(0)=0,\\ &\psi_{0,r}(b)=0,\quad\psi_{0,i}(b)=\begin{cases}-\frac{1}{2\pi\beta}K_0\left(\sqrt{M_{\text{eff}}^2}b\right) & M_{\text{eff}}^2\geq 0\\ \frac{1}{4\beta}Y_0\left(\sqrt{|M_{\text{eff}}^2|}b\right) & M_{\text{eff}}^2<0\end{cases}.\end{aligned} \tag{294}$$

The complete set of equations for $h_1^{(2)}$ is given as

$$\begin{aligned}\partial_b h_{1,r}^{(2)}(b)&=y_r^{(2)}(b),\\ \partial_b h_{1,i}^{(2)}(b)&=y_i^{(2)}(b),\\ \partial_b y_{1,r}^{(2)}(b)&=-\frac{3}{b}y_{1,r}^{(2)}(b)+M_{\text{eff}}^2h_{1,r}^{(2)}(b)-\frac{\mathcal{K}(b)}{\beta}h_{1,i}^{(2)}(b),\\ \partial_b y_{1,i}^{(2)}(b)&=-\frac{3}{b}y_{1,i}^{(2)}(b)+M_{\text{eff}}^2h_{1,i}^{(2)}(b)+\frac{\mathcal{K}(b)}{\beta}h_{1,r}^{(2)}(b),\end{aligned} \tag{295}$$

with initial conditions

$$h_{1,r}^{(2)}(0)=0,\quad h_{1,i}^{(2)}(0)=1,\quad y_r^{(2)}(0)=0,\quad y_i^{(2)}(0)=0. \tag{296}$$

And finally the complete set of equations for $h_1^{(p)}$ is given as

$$\begin{aligned}
\partial_b h_{1,r}^{(p)}(b) &= y_r^{(p)}(b), \\
\partial_b h_{1,i}^{(p)}(b) &= y_i^{(p)}(b), \\
\partial_b y_{1,r}^{(p)}(b) &= -\frac{3}{b} y_{1,r}^{(p)}(b) + M_{\text{eff}}^2 h_{1,r}^{(p)}(b) - \frac{\mathcal{K}(b)}{\beta}(h_{0,i}(b) + h_{1,i}^{(p)}(b)), \\
\partial_b y_{1,i}^{(p)}(b) &= -\frac{3}{b} y_{1,i}^{(p)}(b) + M_{\text{eff}}^2 h_{1,i}^{(p)}(b) + \frac{\mathcal{K}(b)}{\beta}(h_{0,r}(b) + h_{1,r}^{(p)}(b)),
\end{aligned} \tag{297}$$

with initial conditions

$$\begin{aligned}
&\psi_{1,r}^{(p)}(0) = 0, \quad \psi_{1,i}^{(p)}(0) = 1, \quad z_r^{(p)}(0) = 0, \quad z_i^{(p)}(0) = 0, \\
&\psi_{0,i}(b) = 0, \quad \psi_{0,r}(b) = \begin{cases} \frac{M_{\text{eff}}}{\pi\beta b} K_1\left(\sqrt{M_{\text{eff}}^2} b\right) & M_{\text{eff}}^2 \geq 0 \\ -\frac{M_{\text{eff}}}{2\beta b} Y_1\left(\sqrt{|M_{\text{eff}}^2|} b\right) & M_{\text{eff}}^2 < 0 \end{cases} .
\end{aligned} \tag{298}$$

At the end we only need the asymptotic solution for $b \to b_\infty$ to obtain the c_2-coefficients

$$\text{Re}(c_{2,\psi}) = -\lim_{b\to\infty} \text{Re}\left(\frac{\psi_1^{(p)}(b)}{\psi_1^{(2)}(b)}\right) = -\frac{\psi_{1,r}^{(p)}(b_\infty)\psi_{1,r}^{(2)}(b_\infty) + \psi_{1,i}^{(p)}(b_\infty)\psi_{1,i}^{(2)}(b_\infty)}{\left(\psi_{1,r}^{(2)}(b_\infty)\right)^2 + \left(\psi_{1,i}^{(2)}(b_\infty)\right)^2}, \tag{299}$$

$$\text{Im}(c_{2,h}) = -\lim_{b\to\infty} \text{Im}\left(\frac{h_1^{(p)}(b)}{h_1^{(2)}(b)}\right) = -\frac{h_{1,i}^{(p)}(b_\infty)h_{1,r}^{(2)}(b_\infty) - h_{1,r}^{(p)}(b_\infty)h_{1,i}^{(2)}(b_\infty)}{\left(h_{1,r}^{(2)}(b_\infty)\right)^2 + \left(h_{1,i}^{(2)}(b_\infty)\right)^2}. \tag{300}$$

We do now have all equations at hand to obtain the c_2-coefficients. These equations can be solved using standard technics as for example Runge-Kutta methods. Further a numerical integration method can be used to solve the σ-integrals

$$\sigma_\psi(\omega, p_\parallel) := \int_{-\infty}^{\infty} \frac{\mathcal{F}(p_\parallel, k_\parallel)}{k_\parallel - p_\parallel} \text{Re}(c_{2,\psi}(\omega, p_\parallel, k_\parallel)) \frac{dk_\parallel}{2\pi}, \tag{301}$$

$$\sigma_h(\omega, p_\parallel) := \int_{-\infty}^{\infty} \frac{\mathcal{F}(p_\parallel, k_\parallel)}{4k_\parallel^2(k_\parallel - p_\parallel)} \text{Im}(c_{2,h}(\omega, p_\parallel, k_\parallel)) \frac{dk_\parallel}{2\pi}. \tag{302}$$

The numerical details and the program structure will be presented in section 8 together with the results.

7 Approximation of the gauge corrected Lepton Number Matrix

In section 5 we found the following result of the gauge corrected lepton number matrix L_{ii}

$$L_{ii}(t,t) = -\frac{24}{\pi^2}\lambda_{ii}\int_0^t\int_0^t\int_0^{t_2}\int_{-\infty}^{\infty}\int_{-\infty}^{\infty}\int_0^{\infty}\frac{M}{\omega_{\vec{p}}}\cos(\omega_{\vec{p}}y_{13})f_F(\omega_{\vec{p}})f_F(\omega_{21})e^{-\Gamma_{\vec{p}}\frac{t_1+t_3}{2}}\mathrm{Re}\left[e^{-i(\omega_{21}y_{21}+\omega_{23}y_{23})}\right] \tag{303}$$

$$[\sigma_h(\omega_{21},p)\sigma_h(\omega_{23},p)+\sigma_\psi(\omega_{21},p)\sigma_\psi(\omega_{23},p)]\,p^2dp\frac{d\omega_{21}}{2\pi}\frac{d\omega_{23}}{2\pi}dt_3dt_2dt_1.$$

Obviously the lepton number matrix has to be calculated numerically since it depends on the c_2-coefficients appearing in the σ-contributions as well as in the decay width $\Gamma_{\vec{p}}$.

Counting the integral dimensions including the two "hidden" integrals in the σ-contribution leads to a total number of 8 dimensions. On top of that for each point the integrand function is evaluated an asymptotic solution of the ODEs for ψ and h has to be calculated to obtain the c_2-coefficients. All together an enormous amount of computational effort has to be made. As a result calculating the full integral using Monte Carlo is not only slow but also one has to take care of the approximations made previously when developing the resummation scheme for the gauge corrections in section 3. For this it is useful to investigate the regions with the largest contribution. Based on that a systematic approximation of the lepton number matrix will be presented in the following.

7.1 Symmetry Observations

The result of the lepton number matrix can be simplified further by making use of symmetry properties of the self energy Σ.

In section 3.4.2 and 4.4 we had seen that the self energy could be written in the following form

$$\mathrm{Im}\Sigma^{\mathrm{ret}}_{\vec{p}}(\omega_{21}) = \begin{pmatrix} 0 & \mathrm{Im}\Sigma^{\mathrm{ret},R}_{\vec{p}}(\omega_{21}) \\ \mathrm{Im}\Sigma^{\mathrm{ret},L}_{\vec{p}}(\omega_{21}) & 0 \end{pmatrix}, \tag{304}$$

with the symmetry

$$\mathrm{Im}\Sigma^{\mathrm{ret},R}_{-\vec{p}}(\omega_{21}) = \mathrm{Im}\Sigma^{\mathrm{ret},L}_{\vec{p}}(\omega_{21}). \tag{305}$$

The result for the right-handed gauge corrected self energy developed in section 5 had the following form (compare to equation (235))

$$\mathrm{Im}\Sigma^{\mathrm{ret},R}_{\vec{p}}(\omega_{21}) \overset{\vec{p}_\perp=0}{=} \begin{pmatrix} \sigma_\psi(\omega_{21},p_\parallel) & 0 \\ 0 & \sigma_h(\omega_{21},p_\parallel) \end{pmatrix}. \tag{306}$$

Recalling the expression from section 4.4 [Ani+11, p. 19] for $\vec{p}_\perp = 0$

$$\mathrm{Im}\Sigma^{\mathrm{ret}}_{\vec{p}}(\omega_{21}) \overset{\vec{p}_\perp=0}{=} \frac{1}{2}\begin{pmatrix} 0 & a_{\vec{p}}(\omega_{21})\mathbb{1}_{2\times2}+b_{\vec{p}}(\omega_{21})p_3\sigma^3 \\ a_{\vec{p}}(\omega_{21})\mathbb{1}_{2\times2}-b_{\vec{p}}(\omega_{21})p_3\sigma^3 & 0 \end{pmatrix} \tag{307}$$

and comparing both expressions of the right-handed self energy then leads to

$$\mathrm{Im}\Sigma^{\mathrm{ret},R}_{\vec{p}}(\omega_{21}) \overset{\vec{p}_\perp=0}{=} \frac{1}{2}\begin{pmatrix} a_{\vec{p}}(\omega_{21})+p_3b_{\vec{p}}(\omega_{21}) & 0 \\ 0 & a_{\vec{p}}(\omega_{21})-p_3b_{\vec{p}}(\omega_{21}) \end{pmatrix} = \begin{pmatrix} \sigma_\psi(\omega_{21},p_\parallel) & 0 \\ 0 & \sigma_h(\omega_{21},p_\parallel) \end{pmatrix}. \tag{308}$$

Changing from $\vec{p} \to -\vec{p}$ we obtain the left-handed self energy in the following form

$$\mathrm{Im}\Sigma^{\mathrm{ret},L}_{\vec{p}}(\omega_{21}) \overset{\vec{p}_\perp=0}{=} \frac{1}{2}\begin{pmatrix} a_{\vec{p}}(\omega_{21})-p_3b_{\vec{p}}(\omega_{21}) & 0 \\ 0 & a_{\vec{p}}(\omega_{21})+p_3b_{\vec{p}}(\omega_{21}) \end{pmatrix} = \begin{pmatrix} \sigma_h(\omega_{21},p_\parallel) & 0 \\ 0 & \sigma_\psi(\omega_{21},p_\parallel) \end{pmatrix}. \tag{309}$$

We can conclude the following symmetry of the σ-part

$$\sigma_\psi(\omega_{21}, -p_\parallel) = \sigma_h(\omega_{21}, p_\parallel). \tag{310}$$

Further in [Ani+11, p. 19] has been shown that

$$\begin{aligned} a_{\vec{p}}(\omega_{21}) &= a_{\vec{p}}(-\omega_{21}) \\ b_{\vec{p}}(\omega_{21}) &= -b_{\vec{p}}(-\omega_{21}). \end{aligned} \tag{311}$$

Recalling again the Ansatz for the self energy, we arrive at another symmetry of the system

$$\begin{aligned} \mathrm{Im}\Sigma^{\mathrm{ret},R}_{\vec{p}}(-\omega_{21}) &\overset{\vec{p}_\perp=0}{=} \frac{1}{2}\begin{pmatrix} a_{\vec{p}}(-\omega_{21}) + p_3 b_{\vec{p}}(-\omega_{21}) & 0 \\ 0 & a_{\vec{p}}(-\omega_{21}) - p_3 b_{\vec{p}}(-\omega_{21}) \end{pmatrix} \\ &= \frac{1}{2}\begin{pmatrix} a_{\vec{p}}(\omega_{21}) - p_3 b_{\vec{p}}(\omega_{21}) & 0 \\ 0 & a_{\vec{p}}(\omega_{21}) + p_3 b_{\vec{p}}(\omega_{21}) \end{pmatrix} \equiv \mathrm{Im}\Sigma^{\mathrm{ret},L}_{\vec{p}}(\omega_{21}). \end{aligned} \tag{312}$$

Continuing in the same way as presented before we arrive at the following symmetry

$$\sigma_h(-\omega_{21}, p_\parallel) = \sigma_\psi(\omega_{21}, p_\parallel). \tag{313}$$

Combining now both observations leads to

$$\begin{aligned} \mathrm{Im}\Sigma^{\mathrm{ret},R}_{-\vec{p}}(-\omega_{21}) &= \mathrm{Im}\Sigma^{\mathrm{ret},R}_{\vec{p}}(\omega_{21}), \\ \mathrm{Im}\Sigma^{\mathrm{ret},L}_{-\vec{p}}(-\omega_{21}) &= \mathrm{Im}\Sigma^{\mathrm{ret},L}_{\vec{p}}(\omega_{21}), \\ \Rightarrow \mathrm{Im}\Sigma^{\mathrm{ret}}_{-\vec{p}}(-\omega_{21}) &= \mathrm{Im}\Sigma^{\mathrm{ret}}_{\vec{p}}(\omega_{21}). \end{aligned} \tag{314}$$

This is in agreement with the invariance under time reflection pointed out in [Bes10, p. 47].

7.2 Time Integration and the infinite Time Limit

Recalling the expression of the lepton number matrix from section 5.4 it can be noticed that it is possible to solve the time integrals analytically. The only time dependent part is of the following form

$$\begin{aligned} L_{ii}(t,t) = -\frac{24}{\pi^2}\lambda_{ii} \int_{-\infty}^{\infty}\int_{-\infty}^{\infty}\int_{0}^{\infty} \frac{M}{\omega_{\vec{p}}} f_F(\omega_{\vec{p}}) f_F(\omega_{21}) \underbrace{\int_0^t\int_0^t\int_0^{t_2} \cos(\omega_{\vec{p}} y_{13}) e^{-\Gamma_{\vec{p}}\frac{t_1+t_3}{2}} \mathrm{Re}\left[e^{-i(\omega_{21}y_{21}+\omega_{23}y_{23})}\right] dt_3 dt_2 dt_1}_{\text{time dependent part } T(t)} \\ \left[\sigma_h(\omega_{21},p)\sigma_h(\omega_{23},p) + \sigma_\psi(\omega_{21},p)\sigma_\psi(\omega_{23},p)\right] p^2 dp \frac{d\omega_{21}}{2\pi}\frac{d\omega_{23}}{2\pi}. \end{aligned} \tag{315}$$

This time dependent part $T(t)$ can be solved using *mathematica* [Wol17]

$$\begin{aligned} T(t) &= \int_0^t\int_0^t\int_0^{t_2} \cos(\omega_{\vec{p}} y_{13}) e^{-\Gamma_{\vec{p}}\frac{t_1+t_3}{2}} \mathrm{Re}\left[e^{-i(\omega_{21}y_{21}+\omega_{23}y_{23})}\right] dt_3 dt_2 dt_1 \\ &= \int_0^t\int_0^t\int_0^{t_2} \cos(\omega_{\vec{p}}(t_1-t_3)) e^{-\Gamma_{\vec{p}}\frac{t_1+t_3}{2}} \\ &\qquad [\cos(\omega_{21}(t_2-t_1))\cos(\omega_{23}(t_2-t_3)) - \sin(\omega_{21}(t_2-t_1))\sin(\omega_{23}(t_2-t_3))] dt_3 dt_2 dt_1. \end{aligned} \tag{316}$$

Unluckily the calculation leads to a very lengthy result, the detailed result will be given in appendix C.

An interesting case is the limit $t \to \infty$ corresponding to a completely thermalized result

$$\begin{aligned}
\lim_{t\to\infty} T(t) &= \mathrm{Re}\left[\int_0^\infty\int_0^\infty\int_0^{t_2} \cos(\omega_{\vec{p}} y_{13}) e^{-\Gamma_{\vec{p}}\frac{t_1+t_3}{2}} e^{-i(\omega_{21}y_{21}+\omega_{23}y_{23})} dt_3 dt_2 dt_1\right] \qquad (317)\\
&= \mathrm{Re}\left[\int_0^\infty\int_0^\infty e^{-\Gamma_{\vec{p}}\frac{t_1+t_2}{2}} \left(\frac{\left(-2e^{\mathrm{i}t_2\omega_{23}}(-2\mathrm{i}\omega_{23}+\Gamma_{\vec{p}})\cos(\omega_{\vec{p}}(t_1-t_2)) - 4e^{\mathrm{i}t_2\omega_{23}}\omega_{\vec{p}}\sin(\omega_{\vec{p}}(t_1-t_2))\right)}{4\omega_{\vec{p}}^2-(2\omega_{23}+\mathrm{i}\Gamma_{\vec{p}})^2}\right.\right.\\
&\qquad \left.\left. + \frac{2e^{\Gamma_{\vec{p}}\frac{t_2}{2}}\left((-2\mathrm{i}\omega_{23}+\Gamma_{\vec{p}})\cos(\omega_{\vec{p}}t_1)+2\omega_{\vec{p}}\sin(\omega_{\vec{p}}t_1)\right)}{4\omega_{\vec{p}}^2-(2\omega_{23}+\mathrm{i}\Gamma_{\vec{p}})^2}\right) e^{\mathrm{i}\omega_{21}t_1} e^{-\mathrm{i}(\omega_{21}+\omega_{23})t_2} dt_2 dt_1\right]\\
&:= \mathrm{Re}\left[\int_0^\infty\int_0^\infty F_{t_3}(\omega_{\vec{p}},\omega_{21},\omega_{23},t_2,t_1,\Gamma_{\vec{p}}) e^{\mathrm{i}\omega_{21}t_1} e^{-\mathrm{i}(\omega_{21}+\omega_{23})t_2} dt_2 dt_1\right].
\end{aligned}$$

It is possible to solve the integral by including Heaviside step functions to change the integration limits and interpreting the new result as a Fourier transformation

$$\begin{aligned}
\lim_{t\to\infty} T(t) &= \mathrm{Re}\left[\int_{-\infty}^\infty\int_{-\infty}^\infty F_{t_3}(\omega_{\vec{p}},\omega_{21},\omega_{23},t_2,t_1,\Gamma_{\vec{p}})\Theta(t_1)\Theta(t_2) e^{\mathrm{i}\omega_{21}t_1} e^{-\mathrm{i}(\omega_{21}+\omega_{23})t_2} dt_2 dt_1\right] \qquad (318)\\
&= 4\pi \frac{(\Gamma_{\vec{p}}^2+4\omega_{\vec{p}}^2-4\omega_{21}\omega_{23})(\Gamma_{\vec{p}}^4+16(\omega_{\vec{p}}-\omega_{21})(\omega_{\vec{p}}+\omega_{21})(\omega_{\vec{p}}-\omega_{23})(\omega_{\vec{p}}+\omega_{23})+4\Gamma_{\vec{p}}^2(2\omega_{\vec{p}}^2+\omega_{21}^2+\omega_{23}^2))}{(\Gamma_{\vec{p}}^4+16(\omega_{\vec{p}}^2-\omega_{21}^2)^2+8\Gamma_{\omega_{\vec{p}}}^2(\omega_{\vec{p}}^2+\omega_{21}^2))(\Gamma_{\vec{p}}^4+16(\omega_{\vec{p}}^2-\omega_{23}^2)^2+8\Gamma_{\vec{p}}^2(\omega_{\vec{p}}^2+\omega_{23}^2))}\\
&\quad \times \delta(\omega_{21}+\omega_{23}),
\end{aligned}$$

where the real part has already been taken. Note that the result is proportional to $\delta(\omega_{21}+\omega_{23})$. In the thermalized limit only the region with $\omega_{21} = -\omega_{23}$ contributes. Because of continuity this gives information about large contributions to the integral in general that will be investigated further in the following. In fact this will play an important role when approximating the integrand of the lepton number matrix later.

Because of the delta function it is now possible to solve the ω_{23} integral in the thermalized expression of L_{ii} leading to

$$\begin{aligned}
\lim_{t\to\infty} L_{ii}(t,t) = -\frac{48}{\pi^2}\lambda_{ii}\int_{-\infty}^\infty\int_0^\infty \frac{M}{\omega_{\vec{p}}} f_F(\omega_{\vec{p}}) f_F(\omega_{21}) \frac{(\Gamma_{\vec{p}}^2+4(\omega_{\vec{p}}^2+\omega_{21}^2))}{\Gamma_{\vec{p}}^4+16(\omega_{\vec{p}}^2-\omega_{21}^2)^2+8\Gamma_{\vec{p}}^2(\omega_{\vec{p}}^2+\omega_{21}^2)}\\
[\sigma_h(\omega_{21},p)\sigma_h(-\omega_{21},p)+\sigma_\psi(\omega_{21},p)\sigma_\psi(-\omega_{21},p)]\, p^2 dp \frac{d\omega_{21}}{2\pi}. \qquad (319)
\end{aligned}$$

We can simplify further using $\sigma_h(-\omega_{21},p) = \sigma_\psi(\omega_{21},p)$ as derived in the last section, leading to a final result for the full gauge corrected thermalized lepton number matrix

$$\begin{aligned}
\lim_{t\to\infty} L_{ii}(t,t) &= -\frac{48}{\pi^3}\lambda_{ii}\int_{-\infty}^\infty\int_0^\infty \frac{M}{\omega_{\vec{p}}} \frac{f_F(\omega_{\vec{p}}) f_F(\omega_{21})(\Gamma_{\vec{p}}^2+4(\omega_{\vec{p}}^2+\omega_{21}^2))}{\Gamma_{\vec{p}}^4+16(\omega_{\vec{p}}^2-\omega_{21}^2)^2+8\Gamma_{\vec{p}}^2(\omega_{\vec{p}}^2+\omega_{21}^2)} \sigma_\psi(\omega_{21},p)\sigma_h(\omega_{21},p) p^2 dp d\omega_{21} \qquad (320)\\
&= -\frac{48}{\pi^3}\lambda_{ii}\int_0^\infty \frac{M}{\omega_{\vec{p}}} \frac{f_F(\omega_{\vec{p}})(\Gamma_{\vec{p}}^2+4(\omega_{\vec{p}}^2+\omega_{21}^2))}{\Gamma_{\vec{p}}^4+16(\omega_{\vec{p}}^2-\omega_{21}^2)^2+8\Gamma_{\vec{p}}^2(\omega_{\vec{p}}^2+\omega_{21}^2)}\\
&\qquad \left(\int_0^\infty f_F(\omega_{21})\sigma_\psi(\omega_{21},p)\sigma_h(\omega_{21},p) d\omega_{21} + \int_{-\infty}^0 f_F(\omega_{21})\sigma_\psi(\omega_{21},p)\sigma_h(\omega_{21},p) d\omega_{21}\right) p^2 dp\\
&= -\frac{48\lambda_{ii}}{\pi^3}\int_0^\infty\int_0^\infty \underbrace{[f_F(\omega_{21})+f_F(-\omega_{21})]}_{=1} \frac{M}{\omega_{\vec{p}}} \frac{f_F(\omega_{\vec{p}})(\Gamma_{\vec{p}}^2+4(\omega_{\vec{p}}^2+\omega_{21}^2))(\sigma_\psi(\omega_{21},p)\sigma_h(\omega_{21},p))}{\Gamma_{\vec{p}}^4+16(\omega_{\vec{p}}^2-\omega_{21}^2)^2+8\Gamma_{\vec{p}}^2(\omega_{\vec{p}}^2+\omega_{21}^2)} p^2\, d\omega_{21} dp\\
&= -\frac{48}{\pi^3}\lambda_{ii}\int_0^\infty\int_0^\infty \frac{M}{\omega_{\vec{p}}} \frac{f_F(\omega_{\vec{p}})(\Gamma_{\vec{p}}^2+4(\omega_{\vec{p}}^2+\omega_{21}^2))}{\Gamma_{\vec{p}}^4+16(\omega_{\vec{p}}^2-\omega_{21}^2)^2+8\Gamma_{\vec{p}}^2(\omega_{\vec{p}}^2+\omega_{21}^2)} \sigma_\psi(\omega_{21},p)\sigma_h(\omega_{21},p) p^2\, d\omega_{21} dp.
\end{aligned}$$

7.3 Dominating Part of the gauge corrected Lepton Number Matrix

In this section we are going to investigate the ω dependent parts of the lepton number matrix to identify the regions with the largest contribution. The results can then be used to approximate L_{ii} leading to an expression that can be calculated numerically.

At first it is useful to have a closer look at the thermalized expression calculated in the last section

$$\lim_{t\to\infty} L_{ii}(t,t) = -\frac{96}{\pi^3}\int_0^\infty\int_0^\infty \frac{M}{\omega_{\vec{p}}} f_F(\omega_{\vec{p}}) \underbrace{\frac{(\Gamma_{\vec{p}}^2 + 4(\omega_{\vec{p}}^2+\omega_{21}^2))}{\Gamma_{\vec{p}}^4 + 16(\omega_{\vec{p}}^2-\omega_{21}^2)^2 + 8\Gamma_{\vec{p}}^2(\omega_{\vec{p}}^2+\omega_{21}^2)}}_{:=S(\omega_{21},\omega_{\vec{p}},\Gamma_{\vec{p}})} \sigma_\psi(\omega_{21},p)\sigma_h(\omega_{21},p)p^2\, d\omega_{21}dp. \tag{321}$$

The prefactor $S(\omega_{21},\omega_{\vec{p}},\Gamma_{\vec{p}})$ is plotted as a function of ω_{21} for different values of $\omega_{\vec{p}}$ with the corresponding thermal width $\Gamma_{\vec{p}}$.

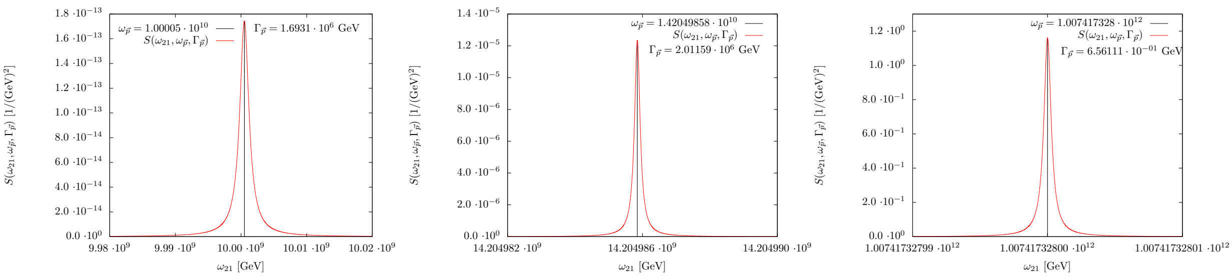

Figure 19: $S(\omega_{21},\omega_{\vec{p}},\Gamma_{\vec{p}})$ for different $\omega_{\vec{p}}$ and the corresponding thermal width $\Gamma_{\vec{p}}$ plotted as function of ω_{21}.

It can clearly be noticed that $S(\omega_{21},\omega_{\vec{p}},\Gamma_{\vec{p}})$ is narrowly peaked at $\omega_{21}\sim\omega_{\vec{p}}$. On top of that the width of the peak is smaller then $100\cdot\Gamma_{\vec{p}}$. It seems reasonable to approximate $\omega_{21}\approx\omega_{\vec{p}}$, but to do so one has to investigate the deviation of σ_ψ and σ_h around $\omega_{21}\sim\omega_{\vec{p}}$.

For this purpose we are having a closer look at σ_ψ and σ_h for $\omega_{21}\in\{\omega_{\vec{p}}-100\cdot\Gamma_{\vec{p}},\omega_{\vec{p}}+100\cdot\Gamma_{\vec{p}}\}$.

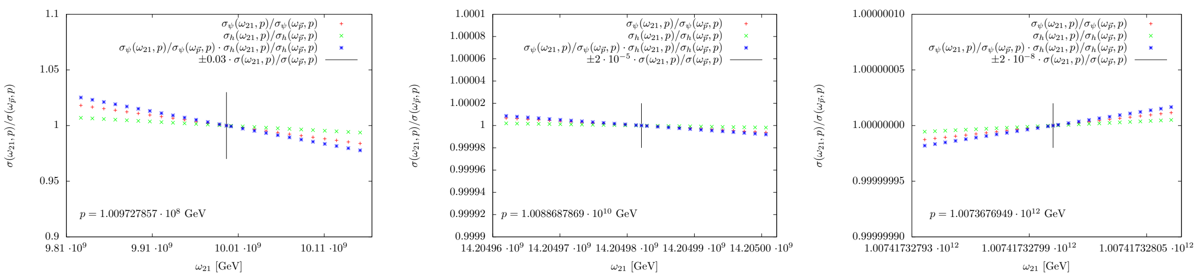

Figure 20: Deviation of the σ-contributions from the value of σ at $\omega_{21}=\omega_{\vec{p}}$ plotted for different $\omega_{\vec{p}}$ as a function of $\omega_{21}\in\{\omega_{\vec{p}}-100\cdot\Gamma_{\vec{p}},\omega_{\vec{p}}+100\cdot\Gamma_{\vec{p}}\}$.

One notices that the σ-parts do not vary much around their value at $\omega_{21}=\omega_{\vec{p}}$. The deviation becomes even smaller for large momenta $\vec{p}$.

Finally we are having a closer look at the complete integrand function denoted as $L_{ii}^{\text{integrand}}(t, \omega_{21}, p)$. It is plotted as a function of p while keeping $\omega_{21} = \omega_{\vec{p}}$ fixed.

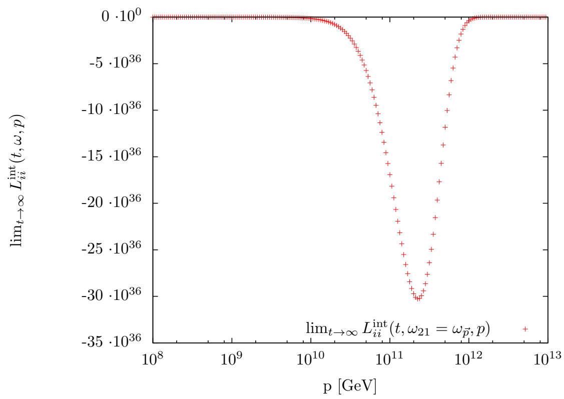

Figure 21: Integrand $L_{ii}^{\text{integrand}}(t, \omega_{21}, p)$ plotted as a function of p for fixed $\omega_{21} = \omega_{\vec{p}}$.

From the plot it becomes clear that the main contribution is given at large momenta $p \in \{10^{10}, 10^{12}\}$[7]. Previously we have seen that the σ-contribution does not vary much around $\omega_{21} \sim \omega_{\vec{p}}$. Combining now both results we can conclude that the sigma-part varies only around $2 \cdot 10^{-5}$ from its 'on-shell' value at $\omega_{21} = \omega_{\vec{p}}$ in the regions with the main contribution to the integral.

All in all this motivates to approximate the self energy part the following way: $\sigma_h(\omega_{21}, p_{\|}) \approx \sigma_h(\omega_{\vec{p}}, p_{\|})$, as well as $\sigma_\psi(\omega_{21}, p_{\|}) \approx \sigma_\psi(\omega_{\vec{p}}, p_{\|})$. Nevertheless we have only studied the thermalized lepton number matrix yet, for completeness we need to check this again with the time integrated non-thermalized version.

Solving the time integrals in the non-thermalized version leads to a lengthy prefactor $T(t)$ given in Appendix C. The denominator of the expression has the following form

$$(\omega_{23}^2 - \omega_{21}^2)(\Gamma_{\vec{p}}^2 + 4(\omega_{23} - \omega_{\vec{p}})^2)(\Gamma_{\vec{p}}^2 + 4(\omega_{23} + \omega_{\vec{p}})^2)(\Gamma_{\vec{p}}^2 + 4(\omega_{21} - \omega_{\vec{p}})^2)(\Gamma_{\vec{p}}^2 + 4(\omega_{21} + \omega_{\vec{p}})^2). \tag{322}$$

The peaks are located at $\omega_{21} = \pm\omega_{23} = \pm\omega_{\vec{p}}$. Note that this includes the dominant case $\omega_{21} \sim -\omega_{23} \sim \pm\omega_{\vec{p}}$ of the thermalized version.

At first we are going to investigate the peaks. From the resummation process of our self energy the thermal width is of order $\Gamma_{\vec{p}} \sim \mathcal{O}(\lambda^2 T)$ [Bes10, p. 33]. With the time dependence being proportional to $e^{\Gamma_{\vec{p}} t}$ a timescale $t \sim \mathcal{O}(\lambda^{-2} T^{-1})$ is implied otherwise for larger times $t > 1/\Gamma_{\vec{p}}$ the thermalized version of L_{ii} is sufficient[8]. For the peaks we have to consider two limits:

1. $\omega_{21} \to \omega_{23}$, $\omega_{23} \to \pm\omega_{\vec{p}}$.
   It is sufficient to consider $+\omega_{\vec{p}}$ since the result is symmetric under sign changes of $\omega_{\vec{p}}$ after the first limit. Calculating both limits using the full time expression given in appendix C leads to

$$\lim_{\omega_{23}\to\omega_{\vec{p}}} \lim_{\omega_{21}\to\omega_{23}} T(t) = \frac{2e^{\Gamma_{\vec{p}} t}(e^{\Gamma_{\vec{p}} t} - 1)}{\Gamma_{\vec{p}}\omega_{\vec{p}}(\Gamma_{\vec{p}}^2 + 16\omega_{\vec{p}}^2)} \left[4\omega_{\vec{p}} + e^{\frac{1}{2}\Gamma_{\vec{p}} t}(-4\omega_{\vec{p}}\cos(2\omega_{\vec{p}} t) + \Gamma_{\vec{p}}\sin(2\omega_{\vec{p}} t))\right]. \tag{323}$$

   The relevant scale is $\omega_{\vec{p}} \sim \mathcal{O}(T)$ where $\Gamma_{\vec{p}}$ is small. So it is possible to approximate $(\Gamma_{\vec{p}}^2 + 16\omega_{\vec{p}}^2) \approx 16\omega_{\vec{p}}^2$. Counting orders then leads to $\sim \mathcal{O}(\lambda^2 T^4)$ for the denominator. In the numerator the leading part is given by the first two terms of order $\sim \mathcal{O}(T)$. All in all the dependence is $\sim \mathcal{O}(\lambda^{-2} T^{-3})$.

[7]Note that this fits to $p \sim \mathcal{O}(T)$.
[8]These estimates need to be understood for the dominating part of the integral at $p \sim \omega_{\vec{p}} \sim \mathcal{O}(T)$.

2. $\omega_{21} \to -\omega_{23}$, $\omega_{23} \to \pm\omega_{\vec{p}}$.
   Considering now the negative sign in the first limit leads to

$$\lim_{\omega_{23}\to\omega_{\vec{p}}} \lim_{\omega_{21}\to-\omega_{23}} T(t) = \frac{e^{-\Gamma_{\vec{p}}t}}{\Gamma_{\vec{p}}^3(\Gamma_{\vec{p}}^2+16\omega_{\vec{p}}^2)^2}\Big[-8(\Gamma_{\vec{p}}^4+16\Gamma_{\vec{p}}^2\omega_{\vec{p}}^2+128\omega_{\vec{p}}^4) \tag{324}$$
$$+4e^{\Gamma_{\vec{p}}t}\Big(\Gamma_{\vec{p}}^4(\Gamma_{\vec{p}}t-2)+8(3\Gamma_{\vec{p}}t-4)\Gamma_{\vec{p}}^2\omega_{\vec{p}}^2+128(\Gamma_{\vec{p}}t-2)\omega_{\vec{p}}^4\Big)$$
$$-2e^{\frac{1}{2}\Gamma_{\vec{p}}t}\Big((\Gamma_{\vec{p}}t-4)(\Gamma_{\vec{p}}^2+16\omega_{\vec{p}}^2)^2+\Gamma_{\vec{p}}^3(\Gamma_{\vec{p}}(\Gamma_{\vec{p}}t-4)+16\omega_{\vec{p}}^2t)\Big)$$
$$\times\cos(2\omega_{\vec{p}}t)\Big].$$

   The dominating part of the denominator is of order $\sim\mathcal{O}(\lambda^6T^7)$ and the dominating part of the numerator is of order $\sim\mathcal{O}(T^4)$. So all in all the expression in this case is of order $\sim\mathcal{O}(\lambda^{-6}T^{-3})$.

Further we have to investigate the regions away from the peaks. In analogy to [ABB11, p. 35] we perform the limit $\Gamma_{\vec{p}}\to 0$ while keeping $\Gamma_{\vec{p}}t$ fixed[9]. Performing the limit leads to the following result for $T(t)$

$$\frac{e^{-\frac{1}{2}\Gamma_{\vec{p}}t}}{(\omega_{21}+\omega_{23})(\omega_{21}^2-\omega_{\vec{p}}^2)(\omega_{23}^2-\omega_{\vec{p}}^2)}\Big[(\omega_{21}\omega_{23}-\omega_{\vec{p}}^2)\Big[\cos(\omega_{\vec{p}}t)(\sin(\omega_{21}t)+\sin(\omega_{23}t))-e^{\frac{1}{2}\Gamma_{\vec{p}}t}\sin((\omega_{21}+\omega_{23})t)\Big]$$
$$+(\omega_{21}-\omega_{23})\omega_{\vec{p}}(\cos(\omega_{21}t)-\cos(\omega_{23}t))\sin(\omega_{\vec{p}}t)\Big]. \tag{325}$$

First note that the result is symmetric under the exchange of ω_{23} and ω_{21}, therefore we assume $\omega_{21}>\omega_{23}$ to reduce the number of regions we have to investigate. If doing so we can approximate $(\omega_{21}+\omega_{23})\approx\omega_{21}$. There are the following cases of interest:

1. $\omega_{21},\omega_{23}>\omega_{\vec{p}}$: In this case we can approximate $(\omega_{\vec{p}}^2-\omega_{21}^2)\approx-\omega_{21}^2$, respectively $(\omega_{\vec{p}}^2-\omega_{23}^2)\approx-\omega_{23}^2$ in the denominator. Further in analogy to the first case we now approximate $(\omega_{21}\omega_{23}-\omega_{\vec{p}})\approx\omega_{21}\omega_{23}$ in the numerator. Counting the order leads to $\sim\mathcal{O}(\omega_{21}^{-2}\omega_{23}^{-1})$ and since $\omega_{21},\omega_{23}>\omega_{\vec{p}}\sim\mathcal{O}(T)$ to a small contribution.

2. $\omega_{21}>\omega_{\vec{p}}$ but $\omega_{23}<\omega_{\vec{p}}$: Again we make the following approximations $(\omega_{\vec{p}}^2-\omega_{21}^2)\approx-\omega_{21}^2$, but now $(\omega_{\vec{p}}^2-\omega_{23}^2)\approx\omega_{\vec{p}}^2$ in the denominator. In this case we can not approximate the numerator further. Counting orders then leads to the following result for the largest contribution $\sim\mathcal{O}(\omega_{21}^{-2}T^{-1})$ and since $\omega_{21}>\omega_{\vec{p}}\sim\mathcal{O}(T)$ this is small again.

3. Finally we are looking at the case $\omega_{21},\omega_{23}<\omega_{\vec{p}}$: In this case we can approximate $(\omega_{\vec{p}}^2-\omega_{21}^2)\approx\omega_{\vec{p}}^2$ in the denominator as well for ω_{23}. In the nominator we approximate $(\omega_{21}\omega_{23}-\omega_{\vec{p}}^2)\approx-\omega_{\vec{p}}^2$. By keeping $\Gamma_{\vec{p}}t$ constant when performing the limit and $\omega_{21},\omega_{23}<\omega_{\vec{p}}\sim\mathcal{O}(T)$ we can neglect all terms but

$$\sim\frac{-\omega_{\vec{p}}^2\Big[\cos(\omega_{\vec{p}}t)(\sin(\omega_{21}t)+\sin(\omega_{23}t))-e^{\frac{1}{2}\Gamma_{\vec{p}}t}\sin(\omega_{21}t)\Big]}{\omega_{21}\omega_{\vec{p}}^4}\sim\frac{1}{\omega_{21}\omega_{\vec{p}}^2}\sim o(\omega_{21}^{-1}T^{-2}). \tag{326}$$

   For very small ω_{21} (and since $\omega_{21}>\omega_{23}$ also small ω_{23}) it is possible to expand the $\sin(\omega_{21}t)$ contributions leading to the following expression

$$\sim\frac{-\cos(\omega_{\vec{p}}t)t-e^{\frac{1}{2}\Gamma_{\vec{p}}t}t}{\omega_{\vec{p}}^2}. \tag{327}$$

   As discussed in the beginning the timescale of the finite time result is of order $t\sim1/\Gamma_{\vec{p}}\sim\mathcal{O}(\lambda^{-2}T^{-1})$ so we arrive at $\mathcal{O}(\lambda^{-2}T^{-3})$ for the whole expression, which is similar to the observation made when investigating the first peak.

Comparing all results leads to the largest contribution given at $\omega_{21}=-\omega_{23}=\pm\omega_{\vec{p}}$ since the contribution is of order $\mathcal{O}(\lambda^{-6}T^{-3})$ with the small coupling λ_{ii}.

[9] The first limit has to be understood in the sense $\Gamma_{\vec{p}}/\omega_{\vec{p}}\to0$. Further since $\Gamma_{\vec{p}}$ depends on p we investigate the regions with the largest contribution given by $p\sim\mathcal{O}(T)$.

The observed behavior is in very good agreement to the observation made for the thermalized result. In the thermalized case we even obtained a delta function that forced $\omega_{23} = -\omega_{21}$. Further we have shown in the beginning that the largest contribution is given around the "on-shell" value obtained by fixing ω_{21} and ω_{23} at $\omega_{\vec{p}}$ in the thermalized case. In this case the prefactor of the integrand showed a narrowly peaked behavior.

This can also be observed in the finite time case by directly looking at the time dependent part $T(t, \omega_{21}, \omega_{23}, \Gamma_{\vec{p}})$. For this purpose we plot the prefactor with $t = 10^{-2}$ 1/GeV and fixed momentum p as a function of $\omega_{21} \in \{\omega_{\vec{p}} - 10 \cdot \Gamma_{\vec{p}}, \omega_{\vec{p}} + 10 \cdot \Gamma_{\vec{p}}\}$ and $\omega_{23} \in \{-\omega_{\vec{p}} - 10 \cdot \Gamma_{\vec{p}}, -\omega_{\vec{p}} + 10 \cdot \Gamma_{\vec{p}}\}$.

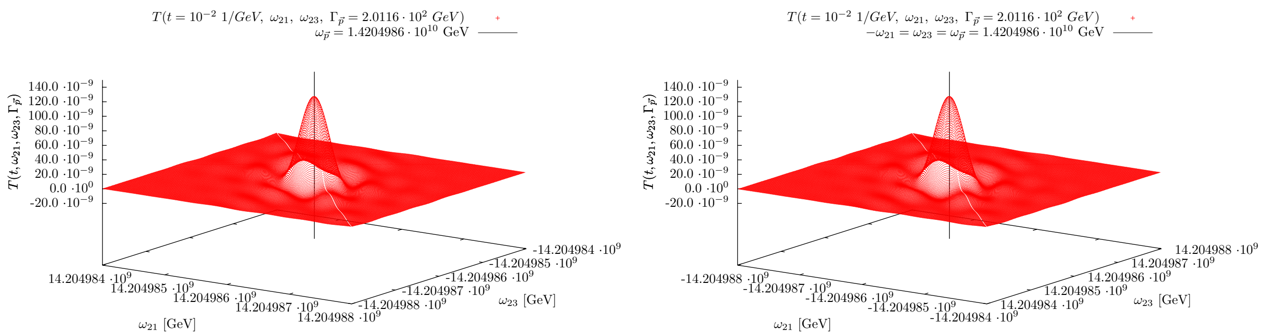

Figure 22: $T(t, \omega_{21}, \omega_{23}, \Gamma_{\vec{p}})$ plotted for $\omega_{21} \in \{\omega_{\vec{p}} - 10 \cdot \Gamma_{\vec{p}}, \omega_{\vec{p}} + 10 \cdot \Gamma_{\vec{p}}\}$ and $\omega_{23} \in \{-\omega_{\vec{p}} - 10 \cdot \Gamma_{\vec{p}}, -\omega_{\vec{p}} + 10 \cdot \Gamma_{\vec{p}}\}$ on the left side and $\omega_{21} \in \{-\omega_{\vec{p}} - 10 \cdot \Gamma_{\vec{p}}, -\omega_{\vec{p}} + 10 \cdot \Gamma_{\vec{p}}\}$ and $\omega_{23} \in \{\omega_{\vec{p}} - 10 \cdot \Gamma_{\vec{p}}, \omega_{\vec{p}} + 10 \cdot \Gamma_{\vec{p}}\}$ on the right side at fixed $\omega_{\vec{p}}$ for $t = 10^{-2}$ 1/GeV.

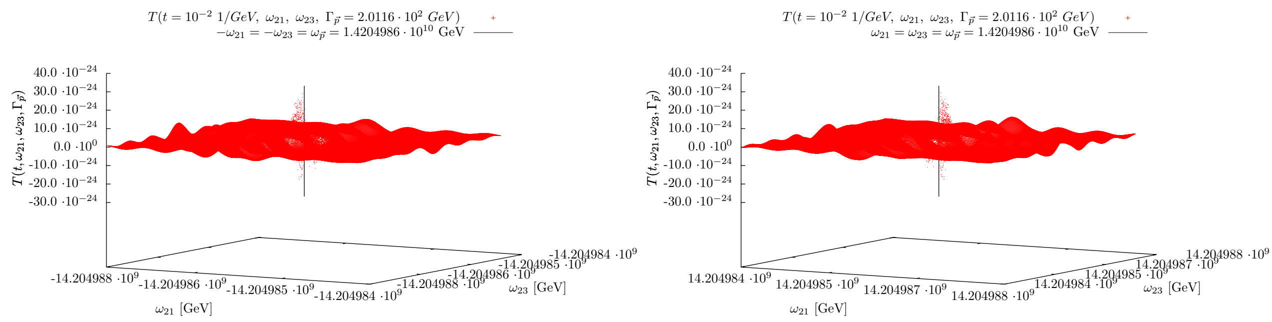

Figure 23: $T(t, \omega_{21}, \omega_{23}, \Gamma_{\vec{p}})$ plotted for $\omega_{21} \in \{-\omega_{\vec{p}} - 10 \cdot \Gamma_{\vec{p}}, -\omega_{\vec{p}} + 10 \cdot \Gamma_{\vec{p}}\}$ and $\omega_{23} \in \{-\omega_{\vec{p}} - 10 \cdot \Gamma_{\vec{p}}, -\omega_{\vec{p}} + 10 \cdot \Gamma_{\vec{p}}\}$ on the left side and $\omega_{21} \in \{\omega_{\vec{p}} - 10 \cdot \Gamma_{\vec{p}}, \omega_{\vec{p}} + 10 \cdot \Gamma_{\vec{p}}\}$ and $\omega_{23} \in \{\omega_{\vec{p}} - 10 \cdot \Gamma_{\vec{p}}, \omega_{\vec{p}} + 10 \cdot \Gamma_{\vec{p}}\}$ on the right side at fixed $\omega_{\vec{p}}$ for $t = 10^{-2}$ 1/GeV.

From the plot it is clear that the main contributions are given at $\omega_{21} \approx \pm\omega_{\vec{p}}$ and $\omega_{23} \approx \mp\omega_{\vec{p}}$ corresponding to our expectation motivated by the estimate presented before.

All in all these observations motivate to approximate $\omega_{21} \approx \pm\omega_{\vec{p}}$ and $\omega_{23} \approx \mp\omega_{\vec{p}}$. Further we have seen that the width of the peaks is determined by multiples of $\Gamma_{\vec{p}}$ and therefore of order $\sim \mathcal{O}(\lambda^2 T)$ making it possible to cross check results as explained in the next section.

7.4 Approximating the gauge corrected Lepton Number Matrix

We are now able to use the results from the last section to approximate the gauge corrected lepton number matrix

$$L_{ii}(t,t) = -\frac{24}{\pi^2}\lambda_{ii}\int_0^t\int_0^t\int_0^{t_2}\int_{-\infty}^{\infty}\int_{-\infty}^{\infty}\int_0^{\infty}\frac{M}{\omega_{\vec{p}}}\cos(\omega_{\vec{p}}y_{13})f_F(\omega_{\vec{p}})f_F(\omega_{21})e^{-\Gamma_{\vec{p}}(\omega_{\vec{p}})\frac{t_1+t_3}{2}}\mathrm{Re}\left[e^{-i(\omega_{21}y_{21}+\omega_{23}y_{23})}\right] \quad (328)$$

$$[\sigma_h(\omega_{21},p)\sigma_h(\omega_{23},p)+\sigma_\psi(\omega_{21},p)\sigma_\psi(\omega_{23},p)]\,p^2dp\frac{d\omega_{21}}{2\pi}\frac{d\omega_{23}}{2\pi}dt_3dt_2dt_1.$$

The ω_{21}, ω_{23} dependent part of the full expression is given as

$$W(\omega_{21},\omega_{23}) := \int_{-\infty}^{\infty}\int_{-\infty}^{\infty} f_F(\omega_{21})\mathrm{Re}\left[e^{-\mathrm{i}(\omega_{21}y_{21}+\omega_{23}y_3)}\right][\sigma_h(\omega_{21},p)\sigma_h(\omega_{23},p)+\sigma_\psi(\omega_{21},p)\sigma_\psi(\omega_{23},p)]\frac{d\omega_{21}}{2\pi}\frac{d\omega_{23}}{2\pi}. \quad (329)$$

In the previous section we have shown that the main contribution to L_{ii} is given by setting $\omega_{23}\to-\omega_{21}\pm a$ with the width a given by multiples of $\Gamma_{\vec{p}}$. For this purpose we set the integration boundaries of the ω_{23} integration to $-\omega_{21}-a$ and $-\omega_{21}+a$ with $a>\Gamma_{\vec{p}}$ but $a<\omega_{21}$

$$W(\omega_{21},\omega_{23}) := \int_{-\infty}^{\infty}\int_{-\omega_{21}-a}^{-\omega_{21}+a} f_F(\omega_{21})\mathrm{Re}\left[e^{-\mathrm{i}(\omega_{21}y_{21}+\omega_{23}y_3)}\right][\sigma_h(\omega_{21},p)\sigma_h(\omega_{23},p)+\sigma_\psi(\omega_{21},p)\sigma_\psi(\omega_{23},p)]\frac{d\omega_{21}}{2\pi}\frac{d\omega_{23}}{2\pi} \quad (330)$$

$$= \int_0^{\infty}\int_{-\omega_{21}-a}^{-\omega_{21}+a} f_F(\omega_{21})\mathrm{Re}\left[e^{-\mathrm{i}(\omega_{21}y_{21}+\omega_{23}y_3)}\right][\sigma_h(\omega_{21},p)\sigma_h(\omega_{23},p)+\sigma_\psi(\omega_{21},p)\sigma_\psi(\omega_{23},p)]\frac{d\omega_{21}}{2\pi}\frac{d\omega_{23}}{2\pi}$$
$$+\int_{-\infty}^{0}\int_{-\omega_{21}-a}^{-\omega_{21}+a} f_F(\omega_{21})\mathrm{Re}\left[e^{-\mathrm{i}(\omega_{21}y_{21}+\omega_{23}y_3)}\right][\sigma_h(\omega_{21},p)\sigma_h(\omega_{23},p)+\sigma_\psi(\omega_{21},p)\sigma_\psi(\omega_{23},p)]\frac{d\omega_{21}}{2\pi}\frac{d\omega_{23}}{2\pi}.$$

Changing first $\omega_{21}\to-\omega_{21}$ and then $\omega_{23}\to-\omega_{23}$ in the second integral leads to

$$\int_{-\infty}^{0}\int_{-\omega_{21}-a}^{-\omega_{21}+a} f_F(\omega_{21})\mathrm{Re}\left[e^{-\mathrm{i}(\omega_{21}y_{21}+\omega_{23}y_3)}\right][\sigma_h(\omega_{21},p)\sigma_h(\omega_{23},p)+\sigma_\psi(\omega_{21},p)\sigma_\psi(\omega_{23},p)]\frac{d\omega_{21}}{2\pi}\frac{d\omega_{23}}{2\pi} \quad (331)$$

$$= \int_0^{\infty}\int_{\omega_{21}-a}^{\omega_{21}+a} f_F(-\omega_{21})\mathrm{Re}\left[e^{-\mathrm{i}(-\omega_{21}y_{21}+\omega_{23}y_3)}\right]\underbrace{[\sigma_h(-\omega_{21},p)\sigma_h(\omega_{23},p)+\sigma_\psi(-\omega_{21},p)\sigma_\psi(\omega_{23},p)]}_{=[\sigma_\psi(\omega_{21},p)\sigma_h(\omega_{23},p)+\sigma_h(\omega_{21},p)\sigma_\psi(\omega_{23},p)]}\frac{d\omega_{21}}{2\pi}\frac{d\omega_{23}}{2\pi}$$

$$= \int_0^{\infty}\int_{-\omega_{21}-a}^{-\omega_{21}+a} f_F(-\omega_{21})\mathrm{Re}\left[e^{\mathrm{i}(\omega_{21}y_{21}+\omega_{23}y_3)}\right]\underbrace{[\sigma_\psi(\omega_{21},p)\sigma_h(-\omega_{23},p)+\sigma_h(\omega_{21},p)\sigma_\psi(-\omega_{23},p)]}_{=[\sigma_\psi(\omega_{21},p)\sigma_\psi(\omega_{23},p)+\sigma_h(\omega_{21},p)\sigma_h(\omega_{23},p)]}\frac{d\omega_{21}}{2\pi}\frac{d\omega_{23}}{2\pi}.$$

All in all we arrive at

$$W(\omega_{21},\omega_{23}) = \int_0^{\infty}\int_{-\omega_{21}-a}^{-\omega_{21}+a}\mathrm{Re}\left(f_F(\omega_{21})e^{-\mathrm{i}(\omega_{21}y_{21}+\omega_{23}y_{23})}+f_F(-\omega_{21})e^{\mathrm{i}(\omega_{21}y_{21}+\omega_{23}y_{23})}\right) \quad (332)$$

$$[\sigma_h(\omega_{21},p)\sigma_h(\omega_{23},p)+\sigma_\psi(\omega_{21},p)\sigma_\psi(\omega_{23},p)]\frac{d\omega_{21}}{2\pi}\frac{d\omega_{23}}{2\pi}$$

$$= \int_0^{\infty}\int_{-\omega_{21}-a}^{-\omega_{21}+a}\cos(\omega_{21}y_{21}+\omega_{23}y_{23})\,[\sigma_h(\omega_{21},p)\sigma_h(\omega_{23},p)+\sigma_\psi(\omega_{21},p)\sigma_\psi(\omega_{23},p)]\frac{d\omega_{21}}{2\pi}\frac{d\omega_{23}}{2\pi}.$$

Further we have seen in the last section that the main contribution is given for $\omega_{21} \approx -\omega_{23} \approx \pm\omega_{\vec{p}}$. Since the coefficients $\sigma_\psi(\omega, p)$ and $\sigma_h(\omega, p)$ do not vary much for $\omega \in \{\omega_{\vec{p}} - a, \omega_{\vec{p}} + a\}$ with $a = a(\Gamma_{\vec{p}})$ we can approximate[10]

$$\begin{aligned}\sigma_h(\omega_{21}, p) &\approx \sigma(\omega_{\vec{p}}, p),\\ \sigma_\psi(\omega_{21}, p) &\approx \sigma_\psi(\omega_{\vec{p}}, p).\end{aligned} \tag{333}$$

On top of that we have $\omega_{23} \in \{-\omega_{21} - a, -\omega_{21} + a\}$, so when approximating $\sigma(\omega_{21}, p) \approx \sigma(\omega_{\vec{p}}, p)$ we can further approximate

$$\begin{aligned}\sigma_h(\omega_{23}, p) &\approx \sigma_h(-\omega_{\vec{p}}, p) = \sigma_\psi(\omega_{\vec{p}}, p),\\ \sigma_\psi(\omega_{23}, p) &\approx \sigma_\psi(-\omega_{\vec{p}}, p) = \sigma_h(\omega_{\vec{p}}, p).\end{aligned} \tag{334}$$

Putting everything together leads to the following result

$$\begin{aligned}W(\omega_{21}, \omega_{23}) &\approx 2 \int_0^\infty \int_{-\omega_{21}-a}^{-\omega_{21}+a} \cos(\omega_{21} y_{21} + \omega_{23} y_{23}) \frac{d\omega_{21}}{2\pi} \frac{d\omega_{23}}{2\pi} \left[\sigma_h(\omega_{\vec{p}}, p)\sigma_\psi(\omega_{\vec{p}}, p)\right]\\ &= 2 \int_0^\infty 2 \frac{\cos(\omega_{21}(y_{21} - y_{23}))\sin(a y_{23})}{y_{23}} \frac{1}{2\pi} \frac{d\omega_{21}}{2\pi} \left[\sigma_h(\omega_{\vec{p}}, p)\sigma_\psi(\omega_{\vec{p}}, p)\right].\end{aligned} \tag{335}$$

Note that this can be written as

$$2\frac{\cos(\omega_{21}(y_{21} - y_{23}))\sin(a y_{23})}{y_{23}} = \frac{\sin(a y_{23})}{y_{23}} \left(e^{\mathrm{i}\omega_{21}(y_{21}-y_{23})} + e^{-\mathrm{i}\omega_{23}(y_{21}-y_{23})}\right), \tag{336}$$

making it possible to solve the remaining ω_{21} integral

$$\begin{aligned}\int_0^\infty e^{\mathrm{i}\omega_{21}(y_{21}-y_{23})} \frac{d\omega_{21}}{2\pi} &= \int_{-\infty}^\infty \Theta(\omega_{21}) e^{\mathrm{i}\omega_{21}(y_{21}-y_{23})} \frac{d\omega_{21}}{2\pi} = \frac{\mathrm{i}}{2\pi(y_{21} - y_{23})} + \frac{1}{2}\delta(y_{21} - y_{23}),\\ \int_0^\infty e^{-\mathrm{i}\omega_{21}(y_{21}-y_{23})} \frac{d\omega_{21}}{2\pi} &= \int_{-\infty}^\infty \Theta(\omega_{21}) e^{-\mathrm{i}\omega_{21}(y_{21}-y_{23})} \frac{d\omega_{21}}{2\pi} = \frac{-\mathrm{i}}{2\pi(y_{21} - y_{23})} + \frac{1}{2}\delta(y_{21} - y_{23}).\end{aligned} \tag{337}$$

Finally we end up with

$$\begin{aligned}W(\omega_{21}, \omega_{23}) &= \int_0^\infty \frac{\sin(a y_{23})}{\pi y_{23}} \left(e^{\mathrm{i}\omega_{21}(y_{21}-y_{23})} + e^{-\mathrm{i}\omega_{23}(y_{21}-y_{23})}\right) \frac{d\omega_{21}}{2\pi} \left[\sigma_h(\omega_{\vec{p}}, p)\sigma_\psi(\omega_{\vec{p}}, p)\right]\\ &= \frac{\sin(a(t_2 - t_3))}{\pi(t_2 - t_3)} \delta(t_3 - t_1) \times \left[\sigma_h(\omega_{\vec{p}}, p)\sigma_\psi(\omega_{\vec{p}}, p)\right].\end{aligned} \tag{338}$$

We can now solve the time integrals of the lepton number matrix L_{ii}.

$$\begin{aligned}L_{ii}(t, t) &= -\frac{24}{\pi^2}\lambda_{ii} \int_0^t \int_0^t \int_0^{t_2} \int_0^\infty \frac{M}{\omega_{\vec{p}}} \cos(\omega_{\vec{p}} y_{13}) f_F(\omega_{\vec{p}}) e^{-\Gamma_{\vec{p}}(\omega_{\vec{p}})\frac{t_1+t_3}{2}} W(\omega_{21}, \omega_{23}) p^2 dp dt_3 dt_2 dt_1\\ &= -\frac{24}{\pi^2}\lambda_{ii} \int_0^\infty \int_0^t \int_0^t \int_0^{t_2} \frac{M}{\omega_{\vec{p}}} \cos(\omega_{\vec{p}} y_{13}) f_F(\omega_{\vec{p}}) e^{-\Gamma_{\vec{p}}(\omega_{\vec{p}})\frac{t_1+t_3}{2}} \frac{\sin(a(t_2 - t_3))}{\pi(t_2 - t_3)} \delta(t_3 - t_1) dt_3 dt_2 dt_1\\ &\quad \times \left[\sigma_h(\omega_{\vec{p}}, p)\sigma_\psi(\omega_{\vec{p}}, p)\right] p^2 dp.\end{aligned} \tag{339}$$

[10] Remember that $\omega_{21} \in \{0, \infty\}$ now after using some symmetry properties.

The time part can be solved using *mathematica* [Wol17] leading to

$$L_{ii} = -\frac{48}{\pi^2}\lambda_{ii}\int_0^\infty \frac{M}{\omega_{\vec{p}}} f_F(\omega_{\vec{p}})\frac{1}{4\Gamma_{\vec{p}}} e^{-\Gamma_{\vec{p}}t}\Big(2\mathrm{i}(-\mathrm{CoshIntegral}[t(-\mathrm{i}a+\Gamma_{\vec{p}})] + \mathrm{CoshIntegral}[t(\mathrm{i}a+\Gamma_{\vec{p}})] \\ +\ln[-\mathrm{i}a+\Gamma_{\vec{p}}] - \ln[\mathrm{i}a+\Gamma_{\vec{p}}] + \mathrm{SinhIntegral}[t(\mathrm{i}a+\Gamma_{\vec{p}})] + \mathrm{SinhIntegral}[t(\mathrm{i}a-\Gamma_{\vec{p}})]) \\ + 4e^{\Gamma_{\vec{p}}t}\mathrm{SinIntegral}[at]\Big) \times [\sigma_h(\omega_{\vec{p}},p)\sigma_\psi(\omega_{\vec{p}},p)]\, p^2 dp. \tag{340}$$

Finally it is even possible to investigate the limit $at \to \infty$ while keeping $\Gamma_{\vec{p}}t$ fixed leading to an a-independent result of the lepton number matrix. In practice this corresponds to the case $a \gg \Gamma_{\vec{p}}$. Performing the limit leads to

$$L_{ii}(t,t) = -\frac{48}{(2\pi)^2}\lambda_{ii}\int\limits_0^\infty \frac{Mp^2}{\omega_{\vec{p}}} f_F(\omega_{\vec{p}})\frac{1-e^{-\Gamma_{\vec{p}}t}}{\Gamma_{\vec{p}}} \times [\sigma_h(\omega_{\vec{p}},p)\sigma_\psi(\omega_{\vec{p}},p)]\, dp. \tag{341}$$

As explained previously this is only valid for $t \gtrsim 1/\Gamma_{\vec{p}}$ with the relevant momentum of order $p \sim \mathcal{O}(T)$ because the σ-coefficients do not vary much from their "on-shell" value at $\omega = \omega_{\vec{p}}$.

7.5 Interpreting the Result

The obtained result is remarkable due to the following points:

At first we can have a look at the limit $t \to \infty$ arriving at

$$\lim_{t\to\infty} L_{ii}(t,t) = -\frac{48}{(2\pi)^2}\lambda_{ii}\int\limits_0^\infty \frac{Mp^2}{\omega_{\vec{p}}} f_F(\omega_{\vec{p}})\frac{1}{\Gamma_{\vec{p}}} \times [\sigma_h(\omega_{\vec{p}},p)\sigma_\psi(\omega_{\vec{p}},p)]\, dp. \tag{342}$$

In section 7.3 we found

$$\lim_{t\to\infty} L_{ii}(t,t) = -\frac{48}{\pi^3}\int\limits_{-\infty}^\infty\int\limits_0^\infty \frac{M}{\omega_{\vec{p}}}\frac{f_F(\omega_{\vec{p}})(\Gamma_{\vec{p}}^2+4(\omega_{\vec{p}}^2+\omega_{21}^2))}{\Gamma_{\vec{p}}^4+16(\omega_{\vec{p}}^2-\omega_{21}^2)^2+8\Gamma_{\vec{p}}^2(\omega_{\vec{p}}^2+\omega_{21}^2)}\sigma_\psi(\omega_{21},p)\sigma_h(\omega_{21},p)p^2\; d\omega_{21}dp. \tag{343}$$

Approximating now the σ-coefficients as done previously makes it possible to integrate out the ω_{21} dependent part

$$\sigma_h(\omega_{21},p) \approx \sigma_h(\omega_{\vec{p}},p) \\ \sigma_\psi(\omega_{21},p) \approx \sigma_\psi(\omega_{\vec{p}},p), \tag{344}$$

$$\int\limits_{-\infty}^\infty \frac{(\Gamma_{\vec{p}}^2+4(\omega_{\vec{p}}^2+\omega_{21}^2))}{\Gamma_{\vec{p}}^4+16(\omega_{\vec{p}}^2-\omega_{21}^2)^2+8\Gamma_{\vec{p}}^2(\omega_{\vec{p}}^2+\omega_{21}^2)}\frac{d\omega_{21}}{2\pi} = \frac{1}{8\Gamma_{\vec{p}}}. \tag{345}$$

All in all we end up with

$$\lim_{t\to\infty} L_{ii}(t,t) = -\frac{48}{(2\pi)^2}\lambda_{ii}\int\limits_0^\infty \frac{Mp^2}{\omega_{\vec{p}}} f_F(\omega_{\vec{p}})\frac{1}{\Gamma_{\vec{p}}} \times [\sigma_h(\omega_{\vec{p}},p)\sigma_\psi(\omega_{\vec{p}},p)]\, dp. \tag{346}$$

This is exactly the same result we found after applying the approximation first and integrating out both ω dependent parts and performing the limit $t \to \infty$ afterwards.

Further the time dependent part of the result has the same structure as the solution of the Boltzmann equation given in section 1.4. The Kadanoff-Baym calculation presented in [Ani+11] could also reproduce this time dependence by introducing thermal widths for SM propagators "by hand" [Ani+11, p. 27]. In our case we have used a much more rigorous procedure to systematically include gauge corrections using resummation also arriving at the same time dependence known from Boltzmann analysis. This not only legitimates a Boltzmann

Ansatz but also it could be proven that gauge corrections are essential to arrive at this kind of time dependence in a quantum mechanical approach.

Though it should be mentioned once again that the obtained approximated result is only valid for times $t \gtrsim 1/\Gamma_{\vec{p}}$. For smaller times memory and off-shell effects play a more important role making the restriction $\omega_{21} = -\omega_{23} = \pm\omega_{\vec{p}}$ too strict. For small times smaller momenta become more important and the σ-coefficients deviate much stronger from their "on-shell" value around $\omega \approx \omega_{\vec{p}}$. Nevertheless it is possible to investigate the effect of gauge corrections for sufficiently large times $t \gtrsim \mathcal{O}(\lambda^{-2}T^{-1})$.

As mentioned previously it is possible to test the approximation further using the following approach. We motivated the approximation by investigating the main contributions to the integral, given at $\omega_{21} \approx -\omega_{23}$ and $\omega_{21} \in \{\pm\omega_{\vec{p}} - a, \pm\omega_{\vec{p}} + a\}$ with $a = a(\Gamma_{\vec{p}})$ $a \gtrsim \Gamma_{\vec{p}}$. Instead of approximating the σ-coefficients directly we can also keep the restricted integral boundaries. We arrive at the following expression that should lead to similar results ($|a| < \omega_{\vec{p}}$)

$$
\begin{aligned}
L_{ii}(t,t) = -\frac{24}{\pi^2}\lambda_{ii}\int\limits_0^\infty \Bigg[& \int\limits_{\omega_{\vec{p}}-a}^{\omega_{\vec{p}}+a}\int\limits_{-\omega_{\vec{p}}-a}^{-\omega_{\vec{p}}+a} \frac{M}{\omega_{\vec{p}}} T(t,\omega_{21},\omega_{23},\omega_{\vec{p}},p) f_F(\omega_{\vec{p}}) f_F(\omega_{21}) \\
& [\sigma_h(\omega_{21},p)\sigma_h(\omega_{23},p) + \sigma_\psi(\omega_{21},p)\sigma_\psi(\omega_{23},p)] \frac{d\omega_{21}}{2\pi}\frac{d\omega_{23}}{2\pi} \\
& \int\limits_{-\omega_{\vec{p}}-a}^{-\omega_{\vec{p}}+a}\int\limits_{\omega_{\vec{p}}-a}^{\omega_{\vec{p}}+a} \frac{M}{\omega_{\vec{p}}} T(t,\omega_{21},\omega_{23},\omega_{\vec{p}},p) f_F(\omega_{\vec{p}}) f_F(\omega_{21}) \\
& [+\sigma_h(\omega_{21},p)\sigma_h(\omega_{23},p) + \sigma_\psi(\omega_{21},p)\sigma_\psi(\omega_{23},p)] \frac{d\omega_{21}}{2\pi}\frac{d\omega_{23}}{2\pi} \Bigg] p^2 dp.
\end{aligned} \tag{347}
$$

Unluckily a numerical treatment is much more involving in this case. That is why we only perform it in one case for less points to make a cross check of results.

For a better numerical treatment it is convenient to simplify the expression by changing $\omega_{23} \to -\omega_{23}$ in the first and $\omega_{21} \to -\omega_{21}$ in the second integral

$$
\begin{aligned}
L_{ii}(t,t) = -\frac{24}{\pi^2}\lambda_{ii}\int\limits_0^\infty \Bigg[& \int\limits_{\omega_{\vec{p}}-a}^{\omega_{\vec{p}}+a}\int\limits_{\omega_{\vec{p}}-a}^{\omega_{\vec{p}}+a} \frac{M}{\omega_{\vec{p}}} T(t,\omega_{21},-\omega_{23},\omega_{\vec{p}},p) f_F(\omega_{\vec{p}}) f_F(\omega_{21}) \\
& [+\sigma_h(\omega_{21},p)\sigma_\psi(\omega_{23},p) + \sigma_\psi(\omega_{21},p)\sigma_h(\omega_{23},p)] \frac{d\omega_{21}}{2\pi}\frac{d\omega_{23}}{2\pi} \\
& \int\limits_{\omega_{\vec{p}}-a}^{\omega_{\vec{p}}+a}\int\limits_{\omega_{\vec{p}}-a}^{\omega_{\vec{p}}+a} \frac{M}{\omega_{\vec{p}}} T(t,-\omega_{21},\omega_{23},\omega_{\vec{p}},p) f_F(\omega_{\vec{p}}) f_F(-\omega_{21}) \\
& [\sigma_h(\omega_{21},p)\sigma_\psi(\omega_{23},p) + \sigma_\psi(\omega_{21},p)\sigma_h(\omega_{23},p)] \frac{d\omega_{21}}{2\pi}\frac{d\omega_{23}}{2\pi} \Bigg] p^2 dp.
\end{aligned} \tag{348}
$$

Here we have used the symmetries of $\sigma(\omega,p)$ from section 7.1 again.

At the end one could think of a Taylor expansion of σ around $\omega_{\vec{p}}$. This is not possible because linear and higher order contributions of ω_{21} and ω_{23} appear in the integrand leading to divergent integral expressions. This gives evidence that it is not possible to expand the σ-parts in a straight forward Taylor expansion. Maybe it would be possible to restrict the calculation onto a small interval around the expansion point $\omega_{\vec{p}}$ and perform an expansion on a compact interval to calculate corrections and obtain a reasonable result. Regarding previous results it should be expected that such a calculation requires a difficult and especially costly numerical treatment.

8 Numerical Results

In the following the results from numerical calculations of the approximated gauge corrected lepton number matrix will be presented. At first the time dependence of the lepton number matrix at fixed parameters $T = 10^{11}$ GeV and $M = 10^{10}$ GeV is investigated to learn about the thermalization of the result. Next we are going to have a closer look at the temperature dependence of the gauge corrections. Hereby the time is left fixed by looking at the infinite time limit. Finally the results are compared to the result of the lepton number matrix as presented in [Ani+11, p.] to determine the effect of gauge corrections.

8.1 Numerical Setup

Before starting with the presentation of results several details of the numerical algorithms have to be pointed out.

8.1.1 Model Parameters

As explained in the Introduction our work is based on the model first considered in [Ani+11]. We want to observe the effect of gauge corrections in this scenario. To compare our results to [Ani+11] we are working with a heavy neutrino mass of $M = 10^{10}$ GeV. Further as presented in section 3 and 5 the inclusion of gauge corrections is based on a the method presented in [ABB11]. In analogy we choose the coupling of the decay width to be $|\lambda|^2 = 10^{-8}$. Indeed the choice of coupling is not determined since the only term of our result containing the gauge corrected decay width has the form

$$T(t) = \frac{1 - e^{-\Gamma_{\vec{p}} t}}{\Gamma_{\vec{p}}} \tag{349}$$

It is possible to rescale t such that $|\lambda|^2 t$ is left constant, so the result can be given easily for any other value of $|\lambda|^2$.

Since the heavy neutrino has not been observed yet, the weakness of the coupling λ_{ii} is yet unknown. Instead of working with an estimate all results will be given without the coupling L_{ii}/λ_{ii} because it can be factorized out.

8.1.2 Standard Model Couplings

All other parameters are well known from the standard model. We are working with the following standard model parameters [Pat+16]

$$\begin{aligned}
\mu_Z := m_Z &= 91.1876(21) \text{ GeV}, \\
\alpha_{em}(\tau_Z) &= 1/127.950(17), \\
\alpha_s(\tau_Z) &= 0.1182(16), \\
\sin^2(\Theta_W(\tau_Z)) &= 0.23129(5), \\
m_t &= 173.21(1.22) \text{ GeV}, \\
m_H &= 125.09(24) \text{ GeV}, \\
G_F &= 1.1663787(6) \cdot 10^{-5} \text{ GeV}^{-2},
\end{aligned} \tag{350}$$

denoting $\tau_Z = \ln(\mu_Z/\mu_0)$. The scale of the system has been set at $\mu_0 = 2\pi T_R$ with reheating temperature $T_R = 10^9$ GeV in analogy to [ABB11]. Using these parameters the renormalization group equations can be solved to obtain renormalized SM couplings.

In analogy to [ABB11] the renormalization group equations from [SW96; Ara+92] are taken

$$\begin{aligned}
\frac{dg_1^2}{d\tau} &= \frac{g_1^4}{8\pi^2}\frac{41}{10} + \mathcal{O}\left(g^6\right), \\
\frac{dg_2^2}{d\tau} &= \frac{g_2^4}{8\pi^2}\left(-\frac{19}{6}\right) + \mathcal{O}\left(g^6\right), \\
\frac{dg_3^2}{d\tau} &= \frac{g_3^4}{8\pi^2}(-7) + \mathcal{O}\left(g^6\right), \\
\frac{d\lambda_t^2}{d\tau} &= \frac{\lambda_t^2}{8\pi^2}\left(\frac{9}{2}\lambda_t^2 - \frac{17}{20}g_1^2 - \frac{9}{4}g_2^2 - 8g_3^2\right) + \mathcal{O}\left(g^6\right), \\
\frac{d\Lambda}{d\tau} &= \frac{1}{16\pi^2}\left(\frac{27}{200}g_1^4 + \frac{9}{20}g_1^2 g_2^2 + \frac{9}{8}g_2^4 - \frac{9}{5}g_1^2\Lambda - 9g_2^2\Lambda - 6\lambda_t^4 + 12\lambda_t^2\Lambda + 24\Lambda^2\right) + \mathcal{O}\left(g^6\right).
\end{aligned} \tag{351}$$

Here τ is given as $\tau := \ln(\mu/\mu_0)$. The notation $\mathcal{O}(g^6)$ implies any combination of SM couplings up to the estimated order, note that Λ is of order $\Lambda \sim \mathcal{O}\left(g^2\right)$. In section 5 we introduced the couplings g and g' in context of the Debeye masses. They can now be identified as $g_1 \equiv g$ and $g_2 \equiv g'$. The SM parameters and the renormalization group equations are related via

$$\begin{aligned}
\alpha_1(\tau_Z) &:= \frac{g_1^2(\tau_Z)}{4\pi} = \frac{\alpha_{em}(\tau_Z)}{\cos^2(\Theta_W(\tau_Z))}, \\
\alpha_2(\tau_Z) &:= \frac{g_2^2(\tau_Z)}{4\pi} = \frac{\alpha_{em}(\tau_Z)}{\sin^2(\Theta_W(\tau_Z))}, \\
\alpha_3(\tau_Z) &:= \frac{g_3^2(\tau_Z)}{4\pi} = \alpha_s(\tau_Z), \\
\lambda_t(\tau_Z) &:= g_t^2(\tau_Z) = 2\sqrt{2}m_t^2 G_F, \\
\Lambda(\tau_Z) &:= g_\Lambda^2(\tau_Z) = \frac{\sqrt{2}}{2}m_H G_F.
\end{aligned} \tag{352}$$

The renormalization group equations for g_1, g_2 ad g_3 can be solved analytically leading to

$$g_i^2(\tau) = \frac{c_i}{d_i - \tau}, \tag{353}$$

where the coefficients c_i are given as

$$\begin{aligned}
c_1 &= \frac{80\pi^2}{41}, \quad & d_1 &= \frac{20\pi(1-\sin^2(\Theta_W(\tau_Z)))}{41\alpha_{em}(\tau_Z)} + \tau_Z, \\
c_2 &= \frac{48\pi^2}{19}, \quad & d_2 &= \frac{12\pi\sin^2(\Theta_W(\tau_Z))}{19\alpha_{em}(\tau_Z)} - \tau_Z, \\
c_3 &= \frac{8\pi^2}{7}, \quad & d_3 &= \frac{2\pi}{7\alpha_s(\tau_Z)} - \tau_Z.
\end{aligned} \tag{354}$$

The remaining equations for λ_t and Λ have to be solved numerically. This is done using a Boolirsch-Stoer algorithm from the *BOOST* C++ library [Boo15].

8.1.3 Structure of the Program

The program is written in C++ and structured the following way:

After setting up the temperature and mass M of the heavy neutrino the renormalization group equations are solved to obtain the standard model couplings. Next an integration routine is called to solve the lepton number matrix. For a cross check we have tested various routines from different libraries including the CUBA library [Hah05] and the GSL library [Con10].

The integration routine calls a routine calculating the integrand and returning its value. Besides a constant prefactor the integrand has three parts:

$$L_{ii}(t,t) = -\frac{48}{(2\pi)^2}\lambda_{ii}\int_0^\infty \underbrace{\frac{Mp^2}{\omega_{\vec{p}}} f_F(\omega_{\vec{p}})}_{\text{"statistics-part"}} \underbrace{\frac{1-e^{-\Gamma_{\vec{p}}t}}{\Gamma_{\vec{p}}}}_{\text{"time-part"}} \times \underbrace{[\sigma_h(\omega_{\vec{p}},p)\sigma_\psi(\omega_{\vec{p}},p)]}_{"self-energy-part"} dp. \tag{355}$$

Since the integral has infinity as upper bound it is convenient to check if the integrand function reaches zero for large momenta and therefore a upper bound below infinity exists. To emphasize this the integrand function is plotted at fixed time $t = 10^{-1}$ 1/GeV leading to

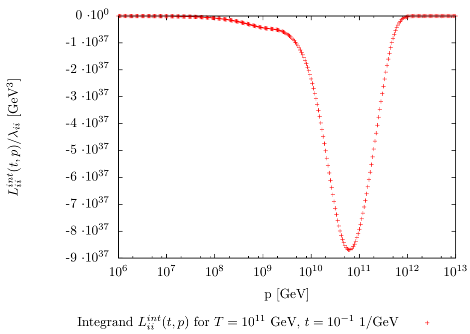

Figure 24: Integrand $L_{ii}^{\text{int}}(t,t)$ at fixed $t = 10^{-1}$ 1/GeV

Obviously it is possible to identify an upper bound and the result is finite. The different parts of the integrand function are calculated the following way:

- **Statistics-Part:** The statistics part is just given by equilibrium distribution functions and constant parameters that can be solved easily.
- **Time-Part:** The time dependent part is a function of the gauge corrected decay width. Depending on the chosen integration algorithm the decay width is implemented in two different ways:

  From section 5.1 we know that the gauge corrected decay width can be written as a function of the σ-coefficients

  $$\Gamma_{\vec{p}}(\omega_{\vec{p}}) = -\frac{|\lambda|^2 d(r)}{2\omega_{\vec{p}}}\left((\omega_{\vec{p}}+p_\parallel)\sigma_h(\omega_{\vec{p}},p_\parallel) + (\omega_{\vec{p}}-p_\parallel)\sigma_\psi(\omega_{\vec{p}},p_\parallel)\right). \tag{356}$$

  As a consequence it can be calculated in the same way as the self energy part. Especially when calculating L_{ii} as a function of T this is very useful since the decay width and the self energy part can be calculated in one step.

  When calculating L_{ii} as a function of t with fixed temperature $T = 10^{11}$ GeV, the decay width has been calculated separately and stored in a grid file. The grid file is created with an overall accuracy of $acc = 5.0 \cdot 10^{-2}$ starting at $p_\parallel = 2.741556 \cdot 10^4$ GeV with a value of $\Gamma_{\vec{p}} = 1.57099006 \cdot 10^{10}$ GeV. The width turned out to be sufficiently small at $p_\parallel \approx 6.34 \cdot 10^{12}$ GeV reaching $\Gamma_{\vec{p}} \approx 1.700775 \cdot 10^{-1}$ GeV marking the last value of the grid file.

- **Self-Energy-Part:** The calculation of the σ-coefficients is the most involving part. Recalling their expression from section 5.3 shows that a one dimensional integral has to be solved

$$\sigma_h(\omega, p_\parallel) := \int_{-\infty}^{\infty} \frac{\mathcal{F}(p_\parallel, k_\parallel)}{4k_\parallel^2(k_\parallel - p_\parallel)} \mathrm{Im}(c_{2,h}(\omega, p_\parallel, k_\parallel)) \frac{dk_\parallel}{2\pi}, \tag{357}$$

$$\sigma_\psi(\omega, p_\parallel) := \int_{-\infty}^{\infty} \frac{\mathcal{F}(p_\parallel, k_\parallel)}{k_\parallel - p_\parallel} \mathrm{Re}(c_{2,\psi}(\omega, p_\parallel, k_\parallel)) \frac{dk_\parallel}{2\pi}.$$

The integrand function of the σ-coefficients depends on the c_2-coefficients. To obtain the c_2-values an asymptotic solution of the differential equations for ψ and h presented in section 6 is needed. This has to be done for every point the integrand function needs to be evaluated leading to some numerical effort. The c_2-coefficients are then given as

$$\mathrm{Re}(c_{2,\psi}) = -\lim_{b\to\infty} \mathrm{Re}\left(\frac{\psi_1^{(p)}(b)}{\psi_1^{(2)}(b)}\right) = -\frac{\psi_{1,r}^{(p)}(b_\infty)\psi_{1,r}^{(2)}(b_\infty) + \psi_{1,i}^{(p)}(b_\infty)\psi_{1,i}^{(2)}(b_\infty)}{\left(\psi_{1,r}^{(2)}(b_\infty)\right)^2 + \left(\psi_{1,i}^{(2)}(b_\infty)\right)^2}, \tag{358}$$

$$\mathrm{Im}(c_{2,h}) = -\lim_{b\to\infty} \mathrm{Im}\left(\frac{h_1^{(p)}(b)}{h_1^{(2)}(b)}\right) = -\frac{h_{1,i}^{(p)}(b_\infty)h_{1,r}^{(2)}(b_\infty) - h_{1,r}^{(p)}(b_\infty)h_{1,i}^{(2)}(b_\infty)}{\left(h_{1,r}^{(2)}(b_\infty)\right)^2 + \left(h_{1,i}^{(2)}(b_\infty)\right)^2}. \tag{359}$$

The program module calculating the c_2-coefficients consists of two parts: One part calculating $c_{2,\psi}$ and the other $c_{2,h}$. The solution of the differential equations is done by making use of a Runge-Kutta-Cash-Sharp (4,5) method which turned out to be the fastest and most stable Runge-Kutta method. The algorithm is implemented from the open source library *GNU scientific library* [Con10]. It turned out that $b_0 = 10^{-5}/T$ for $\psi(0) = \psi(b_0)$ is a good initial value [Hüt13, p. 80].

The value of b_∞ is obtained the following way:

The program starts with $b_\infty = 0.1/T$ and calculates the c_2-coefficient. Afterwards the value of b_∞ is increased via the iteration

$$\begin{aligned} b_\infty &= b_\infty + 0.1/T \quad \text{the first 20 counts}, \\ b_\infty &= b_\infty + 2./T \quad \text{until 80 counts}, \\ b_\infty &= b_\infty + 10./T \quad \text{until 20000/T}. \end{aligned} \tag{360}$$

The loop ends if a plateau for c_2 is reached. This is done by comparing the last four c_2-values with each other and if the plateau tolerance $h_{\text{plt}} = 10^{-3}$ is reached the final value is taken as result. If more than $20000/T$ iterations are needed the program gives a warning and uses the mean value of the last four c_2-coefficients as result. This only appears for very high momenta which have no large contribution to L_{ii}.

The Runge-Kutta solver works at a relative tolerance of $tol_{\text{rel}} = 10^{-6}$ with the first integration step given by $h_{\text{start}} = 10^{-10}$.

To obtain σ the one dimensional integral over $k_\parallel$ needs to be solved. This is done using an integration routine from the *GNU Scientific Library* [Con10] named *QAG adaptive integration*. Since we need to solve an integral with infinite boundaries again an upper and lower bound has to be found by investigating the integrand function. For this purpose the integrand function is scanned in positive and negative direction starting at $k_\parallel = \pm 10^{10}$ GeV to find a bound by increasing the momentum $k_\parallel = 1.8 \cdot k_\parallel$ each step until the integrand value $I(k_\parallel)$ is below $I(\pm k_{\parallel,\text{cut}}) < 10^{-10}$. Afterwards the integration algorithm is started with the corresponding integral bounds k_{cut}. To demonstrate that this is possible an example of the integrand of σ_h and σ_ψ is plotted.

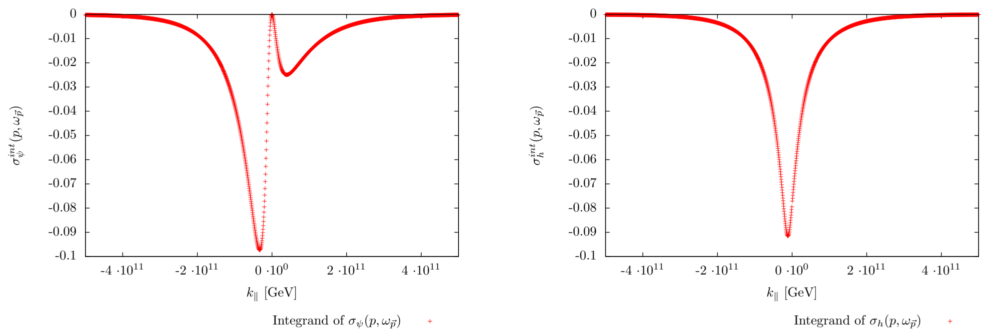

Figure 25: Integrand function of $\sigma_\psi(p,\omega_{\vec{p}})$ left and $\sigma_\psi(p,\omega_{\vec{p}})$ right for $M = 10^{10}$ GeV, $T = 10^{11}$ GeV at fixed $\omega_{\vec{p}} = 1.0074 \cdot 10^{12}$ GeV as a function of $k_\parallel$.

The integration routine works with a relative tolerance of $tol_{\text{rel}} = 10^{-2}$.

For a better understanding the program structure is shown in the following visualization:

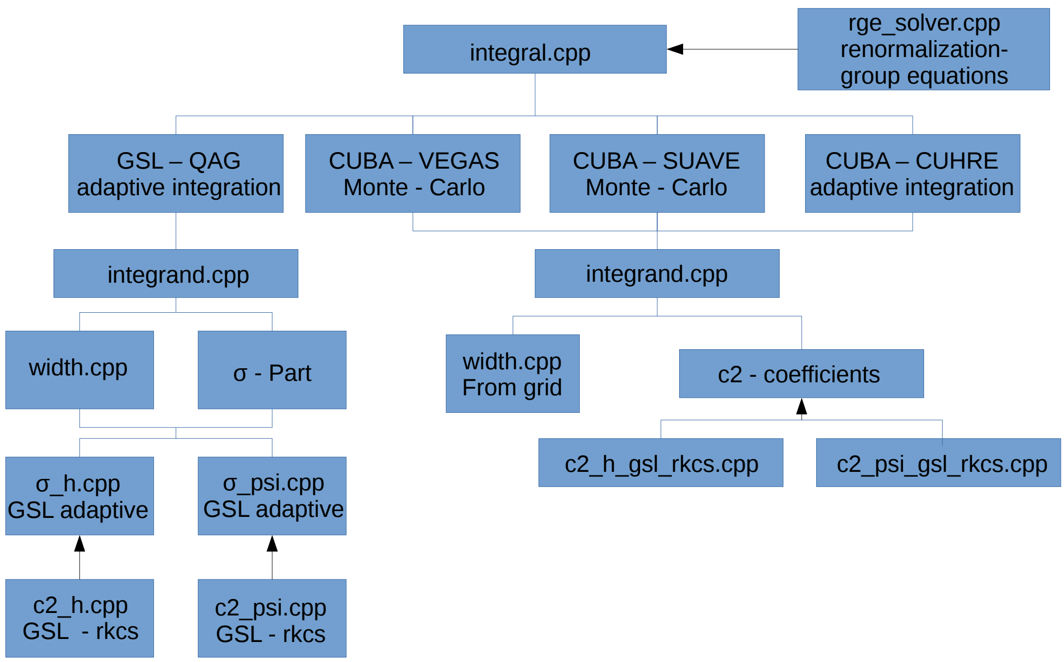

Figure 26: Structure of the C++ program, rkcs stands for the ODE method Runge-Kutta-Cash-Sharp.

8.2 Thermalization of L_{ii}

At first the result of $L_{ii}(t,t)$ as a function of t for fixed $M = 10^{10}$ GeV and $T = 10^{11}$ GeV is presented. To prove the independence on the choice of algorithm the calculation is performed using different integration algorithms from the open source libraries GSL [Con10] and CUBA [Hah05].

8.2.1 GSL - QAG adaptive Integration

The result is calculated using the *QAG adaptive integration* algorithm from the *GNU scientific library* [Con10]. This is the same algorithm used to calculate the σ-contributions. The integral to solve has the following form known from the previous section

$$L_{ii}(t,t) = -\frac{48}{(2\pi)^2}\lambda_{ii}\int_0^\infty \frac{Mp^2}{\omega_{\vec{p}}} f_F(\omega_{\vec{p}}) \frac{1-e^{-\Gamma_{\vec{p}}t}}{\Gamma_{\vec{p}}} \times [\sigma_h(\omega_{\vec{p}},p)\sigma_\psi(\omega_{\vec{p}},p)]\, dp. \tag{361}$$

Note that in this case the decay width of the Majorana neutrino can directly be computed by making use of the */sigma*-coefficients calculated in the integrand function. The integrator works at a relative tolerance of $tol_{\mathrm{rel}} = 10^{-2}$.

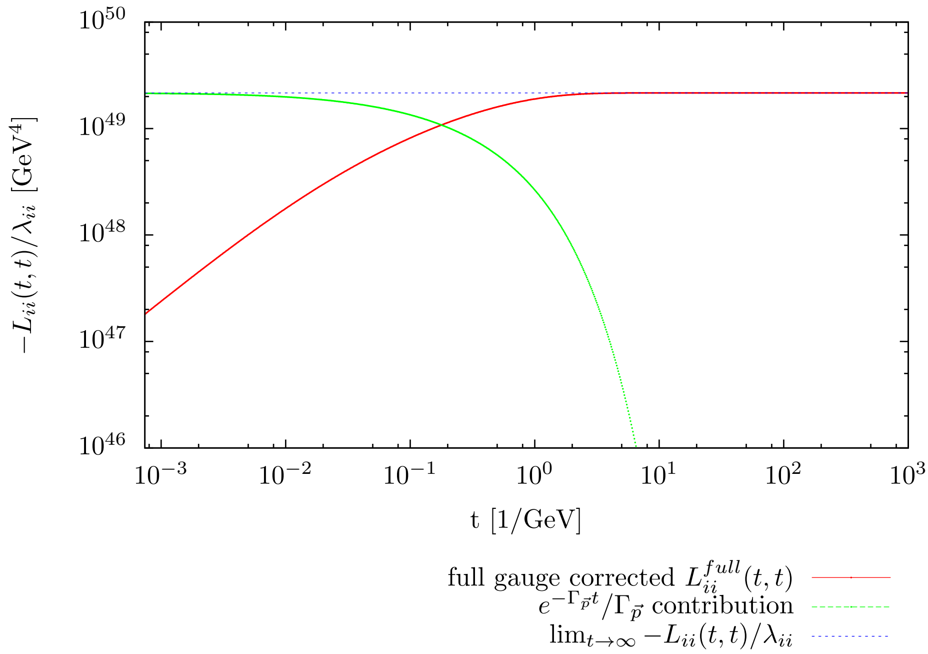

Figure 27: Result for $M = 10^{10}$ GeV, $T = 10^{11}$ GeV using the GSL QAG adaptive integration algorithm with a relative tolerance of $tol_{\mathrm{rel}} = 10^{-2}$.

Note that we have taken $-L_{ii}$ to plot our results. This is not surprising since keeping $B - L =$ constant while changing $B + L$ as it is the case when converting the lepton asymmetry to a baryon asymmetry via the sphaleron processes requires an extend of antileptons over leptons.[11]

[11] This can easily be checked with a simple example by starting with an extend of antileptons over leptons $L = l - \bar{l} < 0$ and a vanishing baryon number $B = b - \bar{b} = 0$ and shifting the asymmetry while keeping $B - L =$ constant.

8.2.2 CUBA - VEGAS adaptive Monte Carlo Integration

As a first cross-check $L_{ii}(t,t)$ is calculated using the adaptive Monte Carlo algorithm *VEGAS* provided by the *CUBA* library [Hah05]. Monte Carlo algorithms are most efficient for multidimensional integrals, in fact the algorithm provided by *CUBA* only works for at least $d \gtrsim 2$ integral dimensions. This is why the σ-terms need to be replaced by their explicit expression known from section 5.3 leading to a three dimensional integral

$$L_{ii}(t,t) = -\frac{48}{(2\pi)^2}\lambda_{ii}\int\limits_0^\infty\int\limits_{-\infty}^\infty\int\limits_{-\infty}^\infty \frac{Mp^2}{\omega_{\vec{p}}} f_F(\omega_{\vec{p}})\frac{1-e^{-\Gamma_{\vec{p}}t}}{\Gamma_{\vec{p}}} \times \left[\frac{\mathcal{F}(p,k_\parallel)}{4k_\parallel^2(k_\parallel - p)}\mathrm{Im}(c_{2,h}(\omega_{\vec{p}},p,k_\parallel))\frac{\mathcal{F}(p,k_\parallel)}{k_\parallel - p}\mathrm{Re}(c_{2,\psi}(\omega_{\vec{p}},p,k_\parallel))\right]\frac{dk_\parallel}{2\pi}\frac{dk_\parallel}{2\pi}dp. \tag{362}$$

Now the c_2-coefficients are computed instead of the $/sigma$-coefficients. As a result it is not possible to calculate the decay width directly because it would slow down the computation dramatically. This is why the width is calculated separately and stored in a grid file. In the calculation the data can then be read from the grid file.

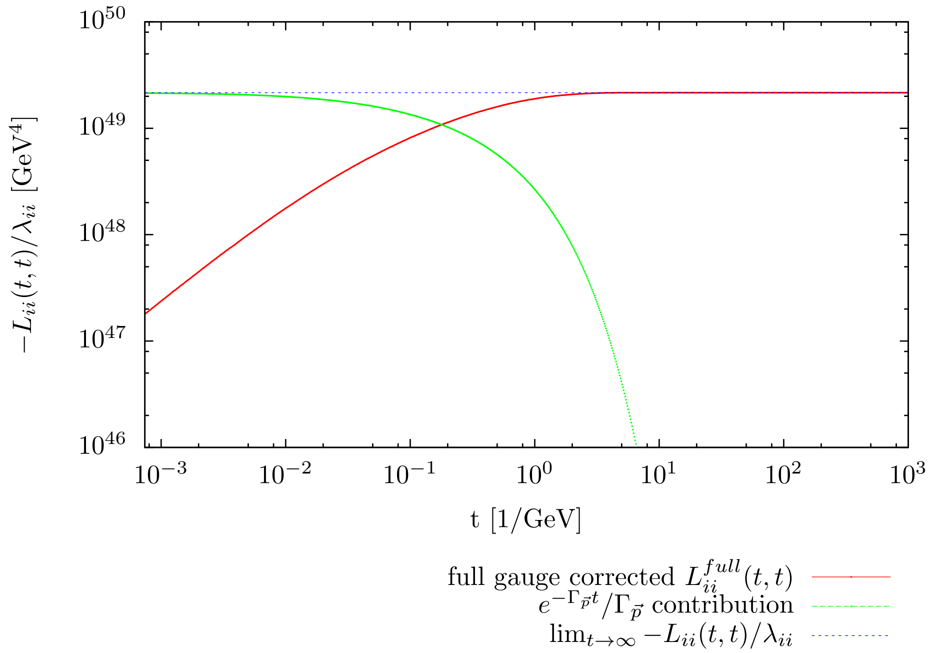

Figure 28: Result for $M = 10^{10}$ GeV, $T = 10^{11}$ GeV using the VEGAS Monte Carlo algorithm from the CUBA library with a relative tolerance of $tol_{\mathrm{rel}} = 10^{-2}$.

8.2.3 CUBA - CUHRE multidimensional Integration

As a second cross-check $L_{ii}(t,t)$ is calculated using the multidimensional adaptive integration algorithm *CUHRE* also provided by the *CUBA* library [Hah05]. The expression calculated has the same form as presented in the last section. Again we have to make use of the grid file for the Majorana decay width.

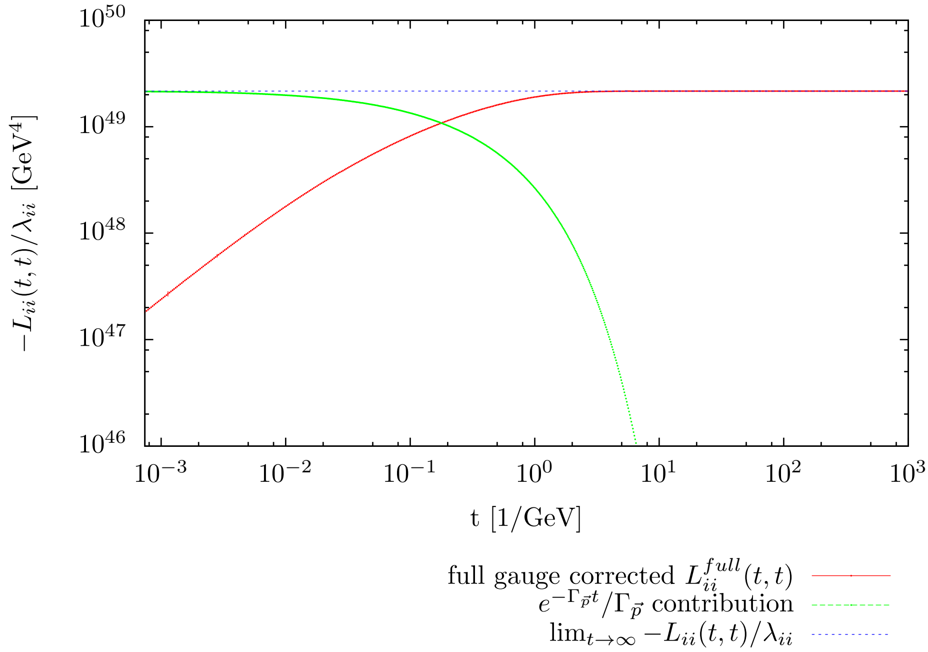

Figure 29: Result for $M = 10^{10}$ GeV, $T = 10^{11}$ GeV using the GSL QAG adaptive integration algorithm with a relative tolerance of $tol_{\text{rel}} = 10^{-1}$.

The CUHRE algorithm converges much slower and it was only possible to calculate L_{ii} up to a relative tolerance of $tol_{\text{rel}} = 10^{-1}$.

The three results for the gauge corrected lepton number matrix calculated with three different integration algorithms show very good agreement. The integration algorithms are implemented correctly and the result does not depend on the choice of algorithm. For the following calculations we choose the *QAG* algorithm provided by the *GSL* library, because no grid file for the decay width is needed. This is very useful when calculating L_{ii} as a function of temperature T because the decay width itself is a function of T, making the use of a grid file not possible or very unlikely.

The presented results for the lepton number thermalize fast. Thermalization is reached at times around $t \gtrsim 1/GeV$ exactly as expected from previous considerations in section 7. On top of that we expected that for times larger then $t > 1/\Gamma_{\vec{p}}$ it is sufficient to work with the thermalized lepton number matrix $\lim_{t\to\infty} L_{ii}(t,t)$. The thermalized result is shown as dotted blue line in the plots and we can see that it is indeed sufficient to use it for times $t > 1/\Gamma_{\vec{p}}$. In section 7.3 we pointed out that the dominant regions of the integral are given at momenta $p \sim T$. In this region the decay width has the value $1/\Gamma_{\vec{p}} \lesssim 1/GeV$. The corresponding timescale of thermalization was given as $t \gtrsim 1/\Gamma_{\vec{p}} \sim \mathcal{O}(\lambda^{-2}T^{-1})$. This could now be proven to be the case. For smaller times t the $e^{-\Gamma_{\vec{p}}t}/\Gamma_{\vec{p}}$ contribution has a bigger impact on the integral value. This can also be observed in the plots by looking at the green line. When increasing time the $e^{-\Gamma_{\vec{p}}t}/\Gamma_{\vec{p}}$ contribution becomes smaller and the remaining time independent part proportional to $1/\Gamma_{\vec{p}}$ is dominant. Recalling that in the limit $t \to \infty$ only the $1/\Gamma_{\vec{p}}$ contribution remains explains the perfect agreement of $L_{ii}(t,t)$ and $L_{ii}(t \to \infty)$ for large times.

8.2.4 Crosscheck via restricted Integration Boundaries using SUAVE

Finally we want to compare the result of the approximated lepton number matrix L_{ii} to the expression with restricted integration boundaries for ω_{21} and ω_{23} from section 7.5

$$L_{ii}(t,t) = -\frac{24}{\pi^2}\lambda_{ii}\int\limits_0^\infty \Bigg[\int\limits_{\omega_{\vec{p}}-a}^{\omega_{\vec{p}}+a}\int\limits_{\omega_{\vec{p}}-a}^{\omega_{\vec{p}}+a}\frac{M}{\omega_{\vec{p}}}T(t,\omega_{21},-\omega_{23},\omega_{\vec{p}},p)f_F(\omega_{\vec{p}})f_F(\omega_{21}) \tag{363}$$

$$[\sigma_h(\omega_{21},p)\sigma_\psi(\omega_{23},p)+\sigma_\psi(\omega_{21},p)\sigma_h(\omega_{23},p)]\,\frac{d\omega_{21}}{2\pi}\frac{d\omega_{23}}{2\pi}$$

$$\int\limits_{\omega_{\vec{p}}-a}^{\omega_{\vec{p}}+a}\int\limits_{\omega_{\vec{p}}-a}^{\omega_{\vec{p}}+a}\frac{M}{\omega_{\vec{p}}}T(t,-\omega_{21},\omega_{23},\omega_{\vec{p}},p)f_F(\omega_{\vec{p}})f_F(-\omega_{21})$$

$$[\sigma_h(\omega_{21},p)\sigma_\psi(\omega_{23},p)+\sigma_\psi(\omega_{21},p)\sigma_h(\omega_{23},p)]\,\frac{d\omega_{21}}{2\pi}\frac{d\omega_{23}}{2\pi}\Bigg]p^2dp.$$

In section 7.3 we have seen that choosing $a = 100\cdot\Gamma_{\vec{p}}$ seems to be sufficient but nevertheless we have chosen $a = 1000\cdot\Gamma_{\vec{p}}$ in the calculation to be on the safe side. For small momenta this choice of a leads to $|a| > \omega_{\vec{p}} \to \omega_{\vec{p}} - a < 0$. In this regions the prefactor 1000 is divided by 10 until $\omega_{\vec{p}} - a \geq 0$. It should be mentioned that these regions do not contribute significantly to the integral.

The calculation is much more involving than previous calculations because several σ values have to be calculated. On top of that as pointed out in section 7.3 the integrand is narrowly peaked, leading to a high numerical sensitivity of the problem. It turned out that calculating the integral after reinserting the expressions for σ_h and σ_ψ is much more efficient. All in all the following 5 dimensional integral is calculated

$$L_{ii}(t,t) = -\frac{24}{\pi^2}\lambda_{ii}\int\limits_0^\infty\int\limits_{-\infty}^\infty\int\limits_{-\infty}^\infty \Bigg[\int\limits_{\omega_{\vec{p}}-a}^{\omega_{\vec{p}}+a}\int\limits_{\omega_{\vec{p}}-a}^{\omega_{\vec{p}}+a}\frac{M}{\omega_{\vec{p}}}T(t,\omega_{21},-\omega_{23},\omega_{\vec{p}},p)f_F(\omega_{\vec{p}})f_F(\omega_{21}) \tag{364}$$

$$\Bigg(\frac{\mathcal{F}(p_\parallel,k_\parallel)}{4k_\parallel^2(k_\parallel-p_\parallel)}\frac{\mathcal{F}(p_\parallel,k'_\parallel)}{(k'_\parallel-p_\parallel)}\mathrm{Im}(c_{2,h}(\omega_{21},p_\parallel,k_\parallel))\mathrm{Re}(c_{2,\psi}(\omega_{23},p_\parallel,k'_\parallel))$$

$$\frac{\mathcal{F}(p_\parallel,k_\parallel)}{(k_\parallel-p_\parallel)}\frac{\mathcal{F}(p_\parallel,k'_\parallel)}{4k'^2_\parallel(k'_\parallel-p_\parallel)}\mathrm{Re}(c_{2,\psi}(\omega_{21},p_\parallel,k_\parallel))\mathrm{Im}(c_{2,h}(\omega_{23},p_\parallel,k'_\parallel))\Bigg)\frac{d\omega_{21}}{2\pi}\frac{d\omega_{23}}{2\pi}$$

$$\int\limits_{\omega_{\vec{p}}-a}^{\omega_{\vec{p}}+a}\int\limits_{\omega_{\vec{p}}-a}^{\omega_{\vec{p}}+a}\frac{M}{\omega_{\vec{p}}}T(t,-\omega_{21},\omega_{23},\omega_{\vec{p}},p)f_F(\omega_{\vec{p}})f_F(-\omega_{21})$$

$$\Bigg(\frac{\mathcal{F}(p_\parallel,k_\parallel)}{4k_\parallel^2(k_\parallel-p_\parallel)}\frac{\mathcal{F}(p_\parallel,k'_\parallel)}{(k'_\parallel-p_\parallel)}\mathrm{Im}(c_{2,h}(\omega_{21},p_\parallel,k_\parallel))\mathrm{Re}(c_{2,\psi}(\omega_{23},p_\parallel,k'_\parallel))$$

$$\frac{\mathcal{F}(p_\parallel,k_\parallel)}{(k_\parallel-p_\parallel)}\frac{\mathcal{F}(p_\parallel,k'_\parallel)}{4k'^2_\parallel(k'_\parallel-p_\parallel)}\mathrm{Re}(c_{2,\psi}(\omega_{21},p_\parallel,k_\parallel))\mathrm{Im}(c_{2,h}(\omega_{23},p_\parallel,k'_\parallel))\Bigg)\frac{d\omega_{21}}{2\pi}\frac{d\omega_{23}}{2\pi}\Bigg]\frac{dk_\parallel}{2\pi}\frac{dk'_\parallel}{2\pi}p^2dp.$$

The integration has been performed by making use of the adaptive Monte Carlo algorithm *SUAVE* provided by the *CUBA* library. In contrast to the *VEGAS* algorithm, *SUAVE* splits the integral into subintervals to find the largest contributions by sampling points in these subintervals. Unluckily the calculation becomes more slow in this case but a positive effect on convergence is achieved. Never the less a large number of points needs to be calculated to obtain a convergent result.

The result of the calculation is shown in the following plot and compared to the approximated result calculated using *GSL* from section 8.2.1.

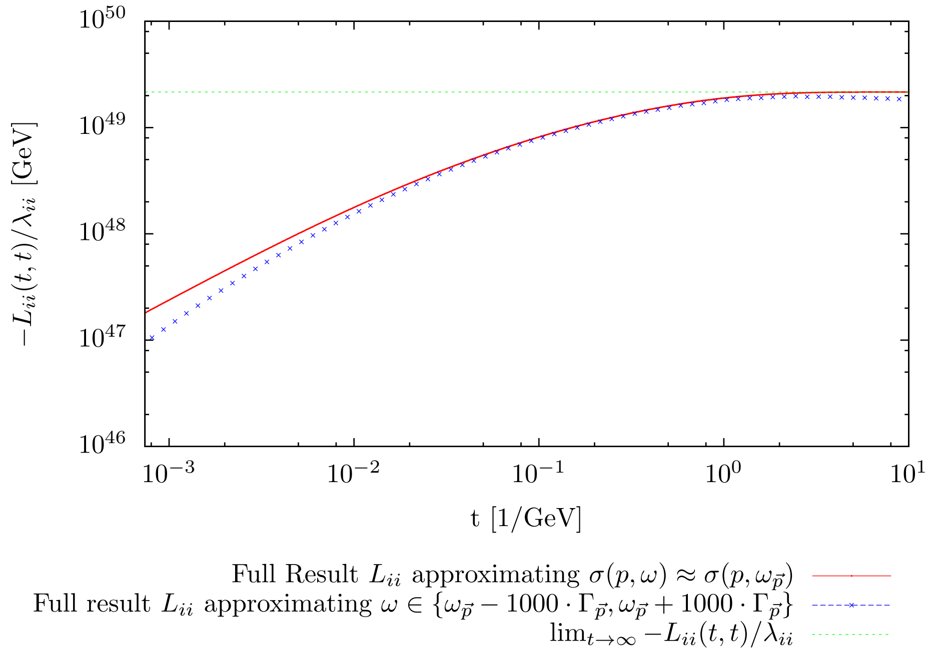

Figure 30: Result for $M = 10^{10}$ GeV, $T = 10^{11}$ GeV with restricted integral boundaries for $\omega_{23} = -\omega_{21}$ and $\omega_{21} \in \{\pm\omega_{\vec{p}} - 1000 \cdot \Gamma_{\vec{p}}, \pm\omega_{\vec{p}} + 1000 \cdot \Gamma_{\vec{p}}\}$ calculated using the *SUAVE* adaptive Monte Carlo algorithm provided by the *CUBA* library. The computations are done with a relative tolerance of $tol_{\text{rel}} = 10^{-2}$ and compared to the approximated result of L_{ii} from section 8.2.1 calculated with the *QAG* adaptive integration algorithm provided by the *GSL* library.

The results slightly differ for small times t. This is not surprising since the approximation of the σ-coefficients is best for large times $t \gtrsim 1/\Gamma_{\vec{p}}$ because they do not vary much from their value at $\omega = \omega_{\vec{p}}$. On top of that the narrowly peaked behavior of the integrand function increases when increasing time. It can be observed that around the thermalization time $t \sim 1/\Gamma_{\vec{p}}$ the results from both calculations fit the best. Especially around $t \in \{10^{-2}/GeV, 1/GeV\}$ the results fit pretty good. For small times the results are still at the same order of magnitude so that the result with approximated σ-coefficients gives reasonable information about the effect of gauge corrections.

Large times are numerically very costly since the prefactor $T(t)$ given in Appendix C is very narrowly peaked. As a result it is very difficult for the algorithm to identify the subintervals with the largest contributions for large times. The error seems to be underestimated and for even larger times no convergence is achieved.

All in all this is the first result for L_{ii} up to one loop order where gauge corrections are systematically included.

8.3 The thermalized Result

To observe the effect of gauge corrections on the lepton number matrix it is interesting to look at the thermalized result given by the limit $t \to \infty$. Up to now gauge corrections have only be investigated by adding thermal damping widths 'per hand' to the SM propagators [Ani+11]

$$\Delta^{\pm,eq}_{\vec{k}}(y) = \Delta^{\pm}_{\vec{k}}(y)e^{-\gamma_\phi|y|}, \qquad S^{\pm,eq}_{\vec{k}}(y) = S^{\pm}_{\vec{k}}(y)e^{-\gamma_l|y|}. \tag{365}$$

To investigate the effect of our systematic approach on gauge corrections we are going to compare our result to the result of [Ani+11, p. 36-37]

$$\begin{aligned} L_{ii}(t,t) = -\frac{3\lambda_{ii}M}{16\pi^3} \int_0^\infty \int_0^\infty \int_{k'_{\min}(p)}^{k'_{\max}(p)} \int_{q_-}^{q_+} \int_{q'_-}^{q'_+} \frac{1}{\omega_{\vec{p}}} \left(1 - \frac{p^2+k^2-q^2}{2pk}\frac{p^2+k'^2-q'^2}{2pk'}\right) f_{l,\phi}(k,q) f_{l,\phi}(k',q') f_N^{eq}(\omega_{\vec{p}}) \\ \times \frac{\gamma\gamma'}{((\omega_{\vec{p}}-k-q)^2+\gamma^2)((\omega_{\vec{p}}-k'-q')^2+\gamma'^2} \underbrace{\frac{1-e^{-\Gamma t}}{\Gamma}}_{\overset{t\to\infty}{=}\frac{1}{\Gamma}} kk'dq'dqdk'dkdp, \end{aligned} \tag{366}$$

where we have defined $\gamma(k,q) = \gamma_l + \gamma_\phi$, $\gamma' = \gamma(k',q')$. The integration boundaries have the following form

$$\begin{aligned} k'_{\min} &= \frac{\omega_{\vec{p}} - p}{2}, \qquad k'_{\min} = \frac{\omega_{\vec{p}} + p}{2}, \\ q_\pm &= |p \pm k|, \qquad q'_\pm = |p \pm k'|. \end{aligned} \tag{367}$$

Further details on the calculation can be found in Appendix D or in [Ani+11, App. C]. We have integrated out the k dependence in the result of [Ani+11] to compare it to our result for the gauge corrected lepton number matrix.

In [Ani+11] the SM thermal damping widths are estimated to be $\gamma = \gamma' \sim \frac{6g^2}{8\pi}T \sim 0.1T$ [Bel11]. On top of that we are going to vary the thermal widths γ to investigate the behavior of the [Ani+11] result as a function of γ and to fit it to the result of our systematic approach. Further, sticking to the formulation of [Ani+11, p. 41], the Majorana decay width is estimated to be $\Gamma \sim 10^{-7}M$ as pointed out in [BPY05]. Similar to our considerations for the SM widths γ we are going to investigate the effect on the result when varying Γ. The 5 dimensional integral is solved with the *VEGAS* adaptive Monte-Carlo algorithm provided by the *CUBA* library [Hah05].

The result with systematic corrections is again calculated using the *QAG* adaptive integration algorithm provided by *GSL* [Con10]

$$L_{ii}(t \to \infty) = -\frac{48}{(2\pi)^2}\lambda_{ii} \int_0^\infty \frac{Mp^2}{\omega_{\vec{p}}} f_F(\omega_{\vec{p}}) \frac{1}{\Gamma_{\vec{p}}} \times [\sigma_h(\omega_{\vec{p}},p)\sigma_\psi(\omega_{\vec{p}},p)]\, dp. \tag{368}$$

Since we are working at fixed time $t \to \infty$ we are going to have a look at the result as a function of temperature T. We would expect that gauge corrections (especially when looking at the corrections to the CP- violating diagram from section 4) play an important role for temperatures beyond the heavy neutrino mass $T > M$.

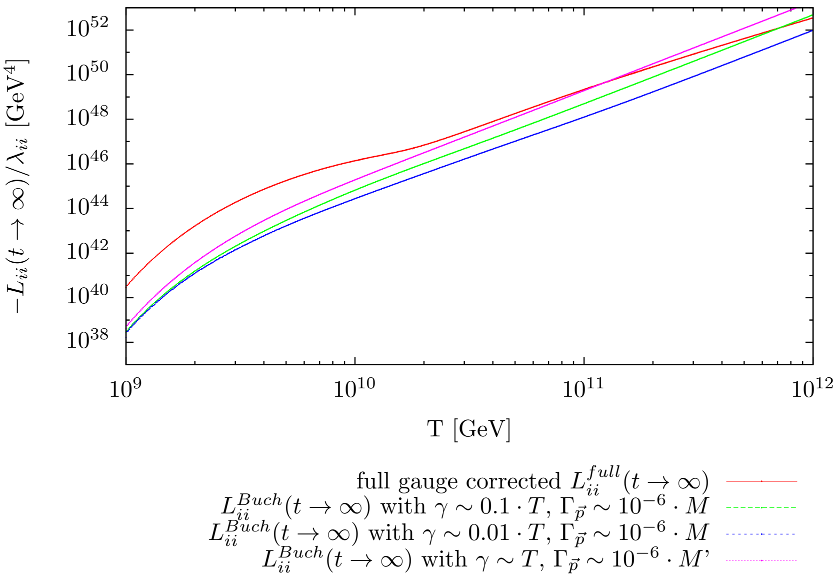

Figure 31: Result for $M = 10^{10}$ GeV, $\Gamma \sim 10^{-6} \cdot M$ using the *GSL QAG* adaptive integration algorithm to compute the full result and the *CUBA VEGAS* Monte Carlo algorithm to compute the expression of [Ani+11]. Both integrator work at a relative tolerance of $tol_{\text{rel}} = 10^{-2}$.

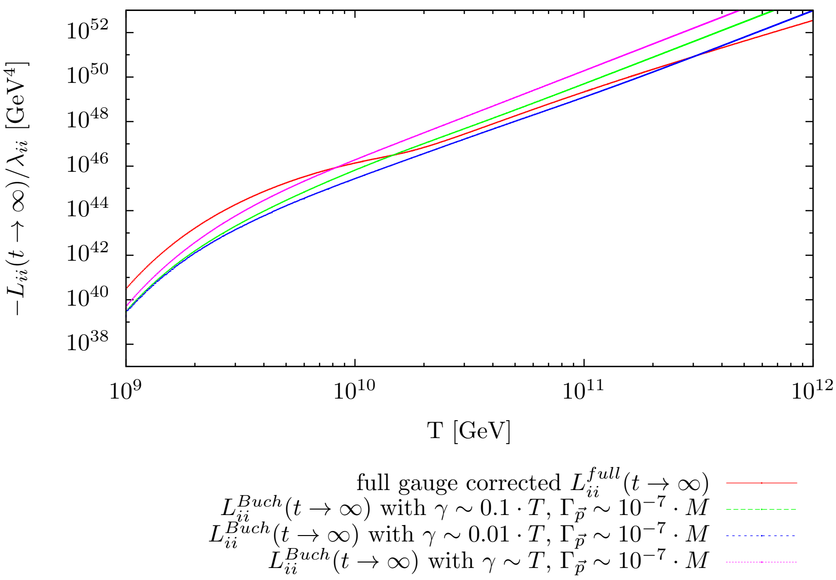

Figure 32: Result for $M = 10^{10}$ GeV, $\Gamma \sim 10^{-7} \cdot M$ using the *GSL QAG* adaptive integration algorithm to compute the full result and the *CUBA VEGAS* Monte Carlo algorithm to compute the expression of [Ani+11]. Both integrator work at a relative tolerance of $tol_{\text{rel}} = 10^{-2}$.

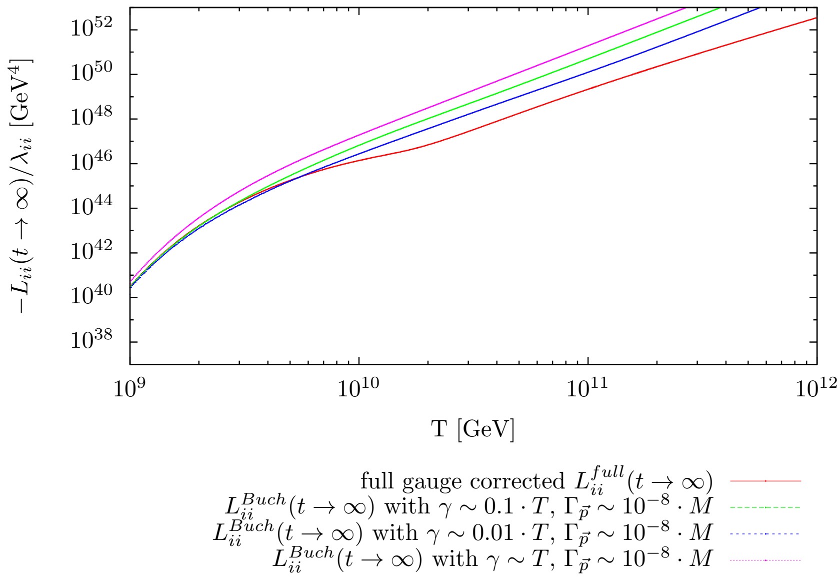

Figure 33: Result for $M = 10^{10}$ GeV, $\Gamma \sim 10^{-8} \cdot M$ using the *GSL QAG* adaptive integration algorithm to compute the full result and the *CUBA VEGAS* Monte Carlo algorithm to compute the expression of [Ani+11]. Both integrator work at a relative tolerance of $tol_{\text{rel}} = 10^{-2}$.

All 3 plots make clear that the systemically gauge corrected result of L_{ii} and the result from [Ani+11] lead to comparable results in the order of magnitude. Systematic gauge corrections do lead to a deviation but not to a dramatically new situation. This is especially interesting for vertex corrections that are taken into account when calculating the cylindrical diagram. Such corrections are not included properly in the Ansatz of thermal damping widths for SM propagators.

The shape of the full corrected result of L_{ii} shows an interesting behavior at temperatures $T \sim M$ underlining our expectation that gauge corrections are important at temperatures above the heavy neutrino mass $T \gtrsim M$. This becomes even more clear when comparing the shape of the systematically gauge corrected L_{ii} and the shape of L_{ii}^{Buch}. The important difference between the two graphs is that the L_{ii}^{Buch} shape does not flatten at $T \sim M$. Just from comparing the shapes the Ansatz of thermal damping widths for SM propagators seems reasonable for temperatures below the neutrino mass $T \lesssim M$.

This becomes even more clear comparing the different results for different thermal damping widths γ and neutrino decay widths Γ. The estimate of $\Gamma_{\vec{p}} \approx 10^{-7} \cdot M$ and $\gamma \approx 0.1 \cdot T$, as motivated by [Ani+11], is plotted in the second graph as green line. It intersects the red line denoting our full result of L_{ii} at a temperature slightly larger then $T \sim M$. As introduced in section 1 the parameters $M = 10^{10}$ GeV and $T = 10^{11}$ GeV are connected to the physical scenario. The green line stays close to the red line for temperatures above $T > M$ making it possible to conclude that the estimate made for the parameters $\Gamma_{\vec{p}}$ and γ is reasonable. Nevertheless the effect is even a little overestimated because reducing γ to $\gamma \sim 0.01 \cdot T$ leads to the blue line in the second graph. The blue line intersects the red line at temperatures slightly above $T > 10^{11}$ GeV and is even closer to the full gauge corrected result at $T = 10^{11}$ GeV leaving the effect only a little underestimated. We can conclude that the optimal value is somewhere between $\gamma \approx 0.1 - 0.01 \cdot T$. When increasing γ the effect is clearly overestimated for $T = 10^{11}$ GeV and $M = 10^{10}$ GeV, but the results fit better for low temperatures.

We have further investigated the behavior of L_{ii}^{Buch} when varying the Majorana decay width $\Gamma_{\vec{p}}$. For a larger width $\Gamma_{\vec{p}} \sim 10^{-6} \cdot M$ it is still possible to fit the result to the value of L_{ii} at $M = 10^{10}$ GeV and $T = 10^{11}$ GeV by increasing γ as seen from the pink line in the first graph. But in general the difference between the red L_{ii} and L_{ii}^{Buch} seems to be to large. More interesting is to investigate a smaller decay width as $\Gamma_{\vec{p}} \sim 10^{-8} \cdot M \sim 10^{-2}$ GeV. Note that this value for $\Gamma_{\vec{p}}$ is in good correspondence to the value of the gauge corrected decay width at the relevant momentum scale $o(T)$. For small temperatures $T < M$ the full result of L_{ii} and the result of

L_{ii}^{Buch} with $\Gamma_{\vec{p}} = 10^{-8} \cdot M$ and $\gamma = 0.01 \cdot T$ denoted as blue line in the third plot do agree nearly perfectly. On top of that one can clearly notice that non trivial corrections become important for temperatures beyond the heavy neutrino mass $T \geq M$, because the results start to differ above $T \gtrsim M$.

All in all we can conclude that gauge corrections have an impact on the thermalized result of the lepton number matrix. Especially for temperatures beyond the heavy neutrino mass $T \gtrsim M$ non-linear gauge corrections as for example vertex corrections are important. A similar dependence of gauge corrections for $T \gtrsim M$ has been found by Frederik Depta in his Master thesis by investigating the effect of propagator and vertex corrections separately.

8.4 Time dependent Result

In this section we are going to compare the time dependent result of section 8.2 for fixed temperature $T = 10^{11}$ GeV and fixed mass $M = 10^{10}$ GeV to the time dependence of the result found in [Ani+11]. Our aim is to investigate for which choice of parameters $\Gamma_{\vec{p}}$ and γ a similar time dependence of both results is achieved. On top of that we have calculated the result of [Ani+11] using the gauge corrected decay width of the heavy neutrino as developed in section 5.1. In this case we only need to estimate γ.

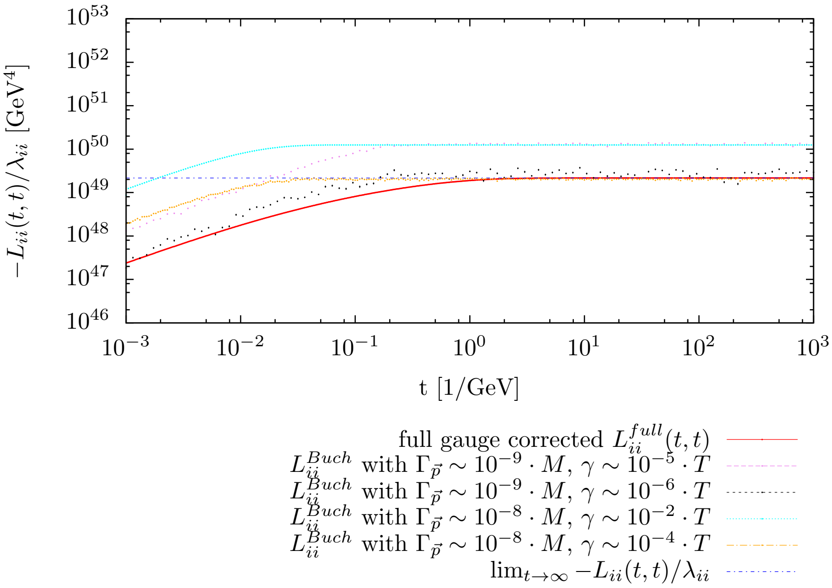

Figure 34: Time dependent result of L_{ii} with fixed $M = 10^{10}$ GeV and $T = 10^{11}$ GeV compared to L_{ii}^{Buch} for different $\Gamma_{\vec{p}}$ and γ. L_{ii} calculated using *GSL QAG* and L_{ii}^{Buch} using *CUBA VEGAS* both with a relative tolerance of $tol_{\mathrm{rel}} = 10^{-2}$.

Looking at the orange and the cyan graph it becomes clear that the result thermalizes faster as the full gauge corrected result given as the red line. The reason for that can be understood easily recalling our results from section 8.2. The orange and the cyan graph are both dealing with a decay width of $\Gamma_{\vec{p}} \sim 10^{-8} \cdot M \sim 10^2$ GeV. As explained in section 8.2 a corresponding timescale for thermalization is then given as $t \sim 1/\Gamma_{\vec{p}} \sim 10^{-2}$ 1/GeV. This fits very well to the observation made: The result thermalizes for times $t \sim 10^{-2}$ 1/GeV.

In section 8.2 we have seen that the full gauge corrected result thermalizes for times $t \sim 1$ GeV, because of that we have a closer look at the result of [Ani+11] for a smaller Majorana decay width of $\Gamma_{\vec{p}} \sim 10^{-9} \cdot M \sim 10$ GeV. The results given as black and violet line in the plot show that thermalization is reached later now comparing better to the red full gauge corrected result.

Varying only the decay width of the heavy neutrino is not sufficient. Moreover we have to vary the thermal damping widths of SM propagators γ as well. It shows that a smaller $\Gamma_{\vec{p}}$ requires a smaller γ because otherwise the effect is overestimated. This becomes clear when comparing the cyan and the violet line to the other lines.

Unluckily as smaller $\Gamma_{\vec{p}}$ and γ get as more difficult is a numerical treatment. It can clearly be noticed that the noise increases and the error is underestimated. Increasing the number of calculated points has only a marginal effect on the result making it most likely that machine precision has been reached. This is also the reason why a discussion for even smaller decay widths is left out.

Finally we are having a look at the result calculated with a gauge corrected heavy Majorana decay width. In this case the values of $\Gamma_{\vec{p}}$ are taken from the grid file introduced earlier.

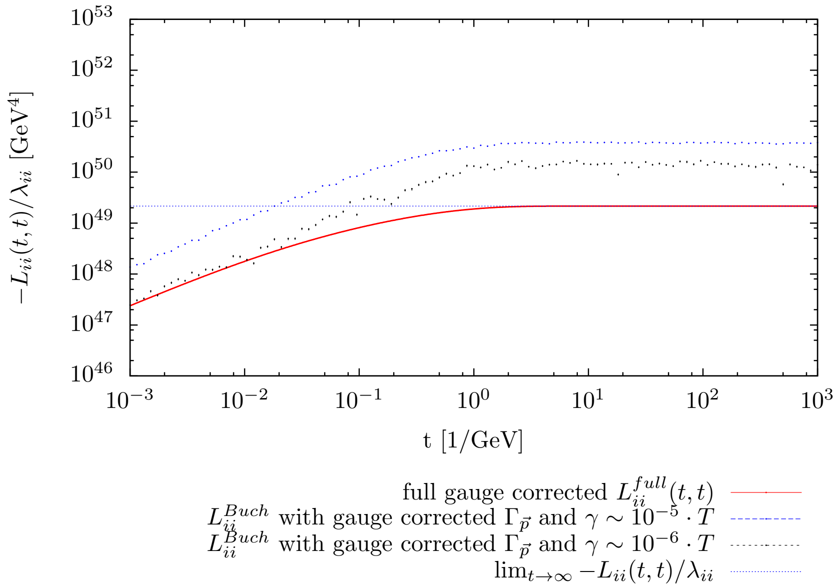

Figure 35: Time dependent result of L_{ii} with fixed $M = 10^{10}$ GeV and $T = 10^{11}$ GeV compared to L_{ii}^{Buch} with gauge corrected $\Gamma_{\vec{p}}$ and different values of γ. L_{ii} calculated using *GSL QAG* and L_{ii}^{Buch} using *CUBA VEGAS* both with a relative tolerance of $tol_{\text{rel}} = 10^{-2}$.

As expected the timescale for thermalization is identical now because all results are working with the full gauge corrected Majorana decay width. More interesting is the final value of L_{ii} that is reached after thermalization. In both cases for $\gamma \sim 10^{-5} \cdot T$ and $\gamma \sim 10^{-6} \cdot T$ the final value lies above the full value of L_{ii}. Lowering γ has the effect that the final value becomes smaller, but still the results do not fit. On the other hand for small times t the result with $\gamma \sim 10^{-6} \cdot T$ fits pretty good to the full gauge corrected result.

From this observation we can conclude that it is not sufficient to work only with a gauge corrected Majorana decay width. In fact when working with a gauge corrected decay width non trivial gauge corrections to the self energy part of the lepton matrix are indispensable. It is interesting to see that the result of [Ani+11] can be 'fitted' better to the result involving a systematic treatment of gauge corrections when leaving $\Gamma_{\vec{p}}$ constant. This constant value has to be small $\Gamma_{\vec{p}} \lesssim 10^{-9} \cdot M$ to reproduce the correct time dependence as seen in the beginning.

For completeness it should be mentioned that the data of L_{ii}^{Buch} with a gauge corrected decay width again shows increasing numerical noise for smaller γ. In this case calculating more points is even slower and also only marginal improvement is observed. Again it seems that machine precision has been reached. Keep in mind that the whole discussion depends on the choice of coupling $|\lambda|^2 = 10^{-8}$ in the calculation of the Majorana neutrino decay width. Choosing a smaller value shifts thermalization to later times whereas a larger value results in earlier thermalization. The actual physical value is unknown since the particle has not been detected yet.

8.5 Temperature and Time dependent Result

Finally for completeness we are going to investigate the gauge corrected lepton number matrix as a function of temperature T and time t. As done previously the calculations are performed with the QAG adaptive integration algorithm provided by the GSL library.

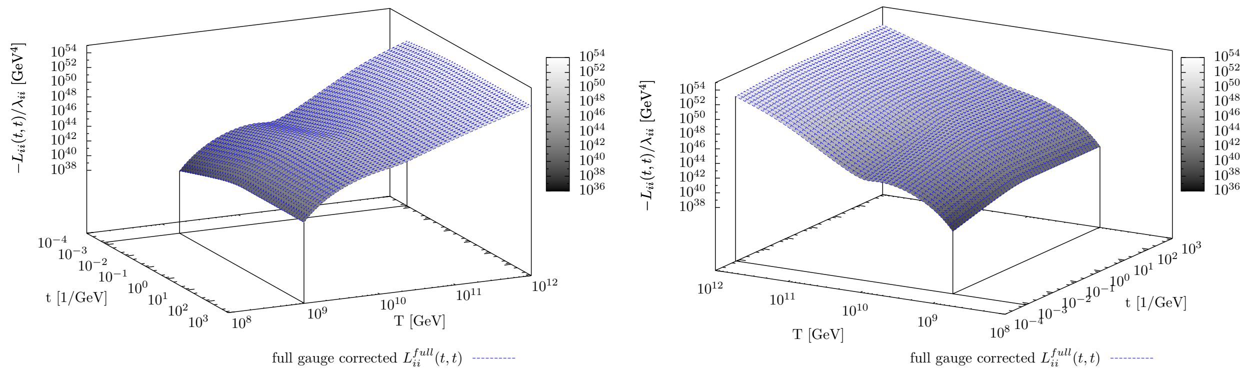

Figure 36: Result of the full gauge corrected lepton number matrix $L_{ii}^{\text{full}}(t,t)$ at fixed $M = 10^{10}$ GeV as a function of T and t using the GSL QAG adaptive integration algorithm with a relative tolerance of $tol_{\text{rel}} = 10^{-2}$.

Again it is possible to recognize a thermalization at times $t \sim 1/\Gamma_{\vec{p}} \gtrsim 1/GeV$. On top of that for temperatures beyond the heavy neutrino mass $T \gtrsim M$ a bump in the shape can be noticed, as observed previously for the thermalized lepton number matrix. For small times t this effect is even more visible. The reason for that has to be connected to the importance of gauge corrections to the decay width of the neutrino since it is the only part of the integral with an explicit time dependence. For small times the $e^{-\Gamma_{\vec{p}}t}/\Gamma_{\vec{p}}$ term has a larger contribution to the integral. This corresponds to the observation made in section 8.1 at fixed temperature. Plotting the dependence explicitly leads to the following graph.

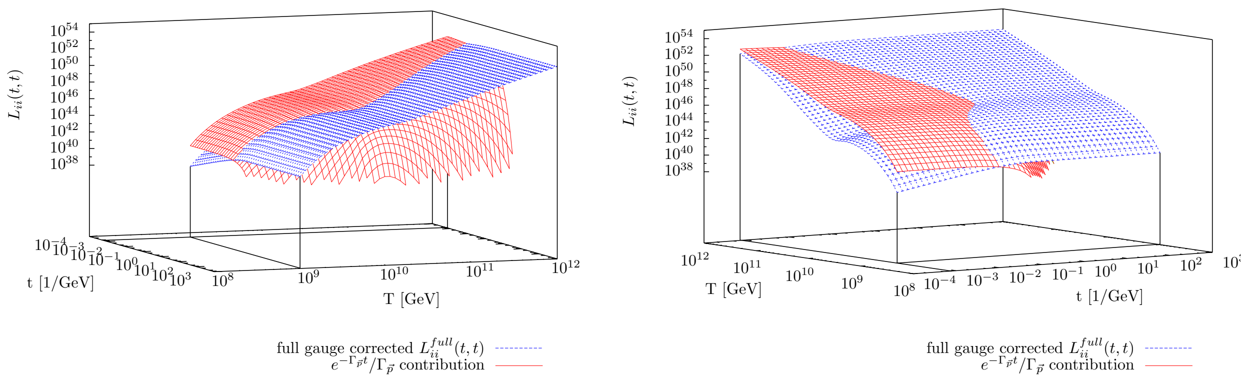

Figure 37: Result of the full gauge corrected lepton number matrix $L_{ii}^{\text{full}}(t,t)$ and the $\sim e^{-\Gamma_{\vec{p}}t}/\Gamma_{\vec{p}}$ contribution at fixed $M = 10^{10}$ GeV. Calculated using the GSL QAG adaptive integration algorithm with a relative tolerance of $tol_{\text{rel}} = 10^{-2}$.

Now the temperature and time dependent L_{ii} is plotted in comparison to L_{ii}^{Buch} for different γ and $\Gamma_{\vec{p}}$.

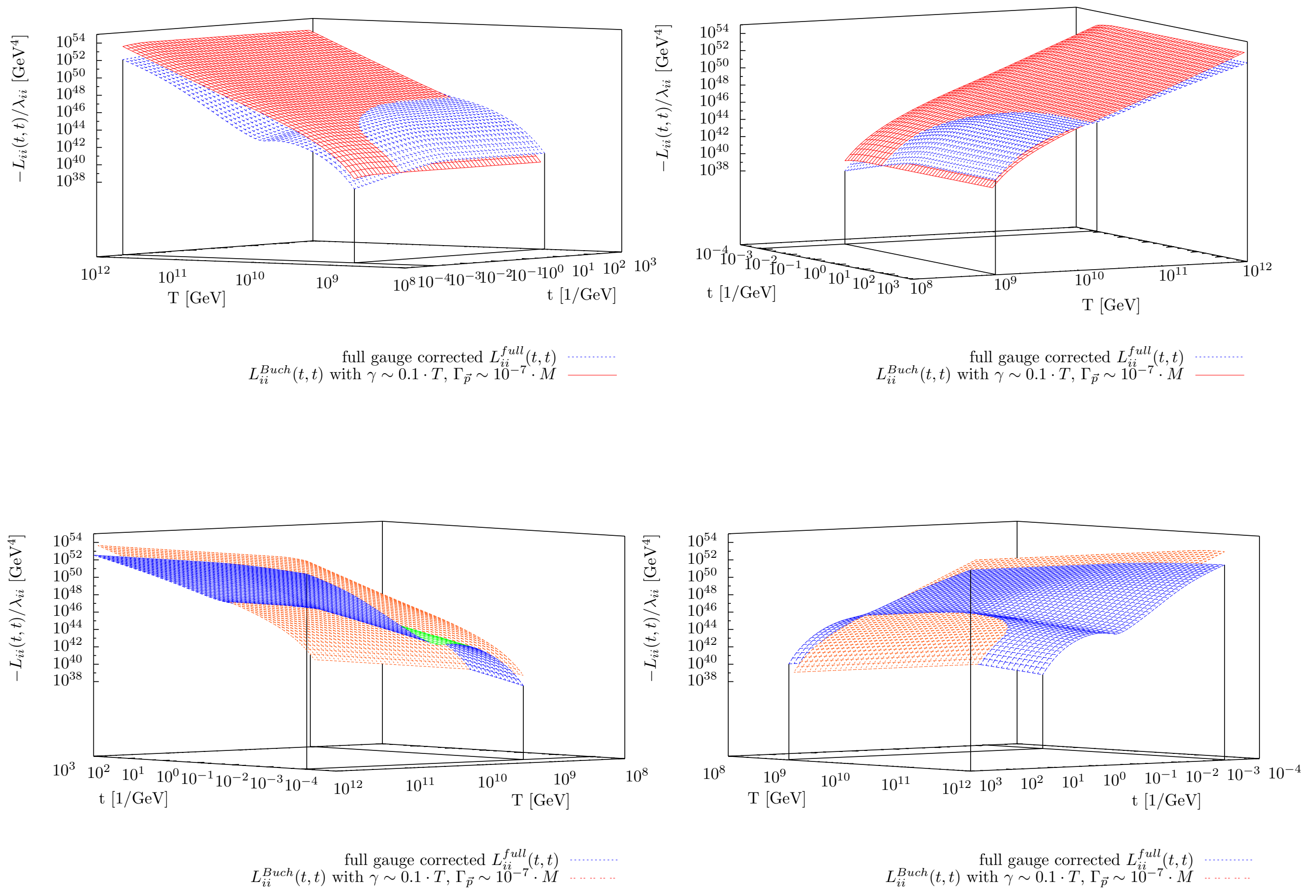

Figure 38: Four different views of the result of $L_{ii}^{\text{full}}(t,t)$ compared to $L_{ii}^{\text{Buch}}(t,t)$ at fixed $M = 10^{10}$ GeV and $\gamma \sim 0.1 \cdot T$, $\Gamma_{\vec{p}} \sim 10^{-7} \cdot M$. Both calculated with a relative tolerance of $tol_{\text{rel}} = 10^{-2}$.

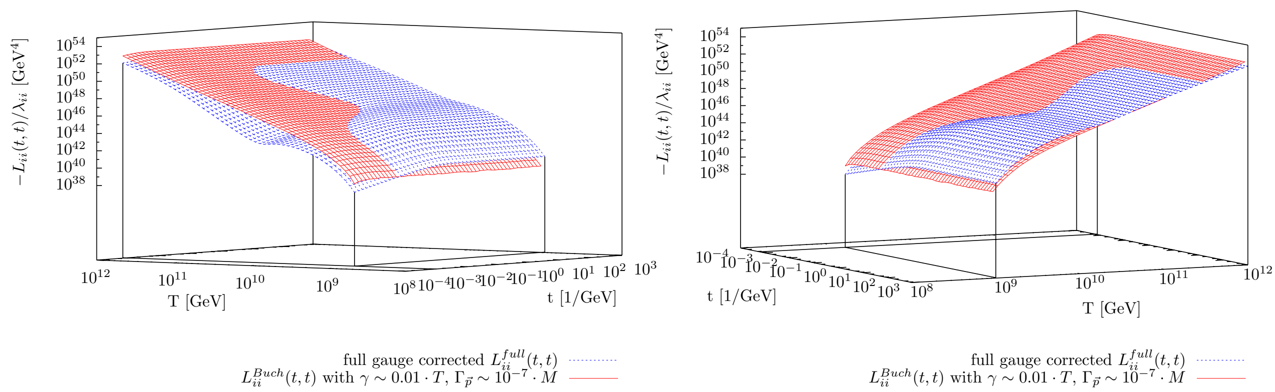

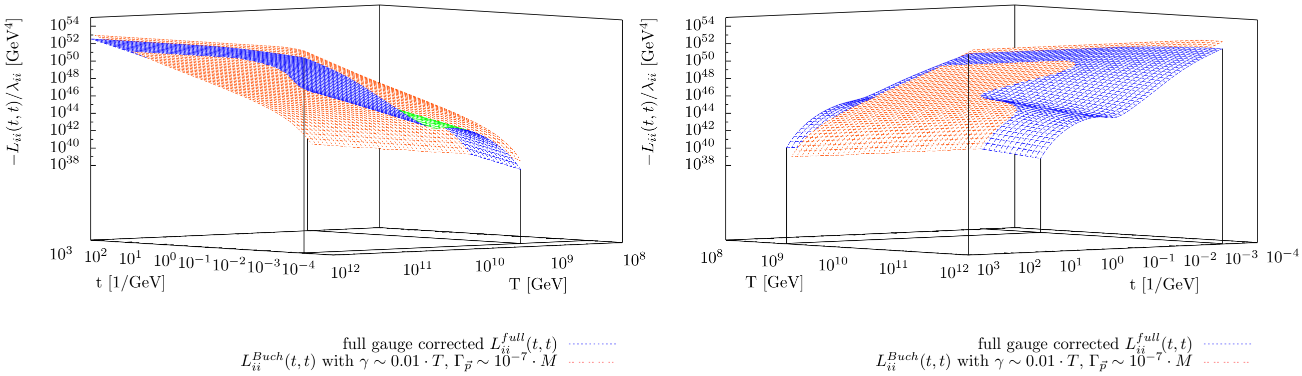

Figure 39: Four different views of the result of $L_{ii}^{\text{full}}(t,t)$ compared to $L_{ii}^{\text{Buch}}(t,t)$ at fixed $M = 10^{10}$ GeV and $\gamma \sim 0.01 \cdot T$, $\Gamma_{\vec{p}} \sim 10^{-7} \cdot M$. Both calculated with a relative tolerance of $tol_{\text{rel}} = 10^{-2}$.

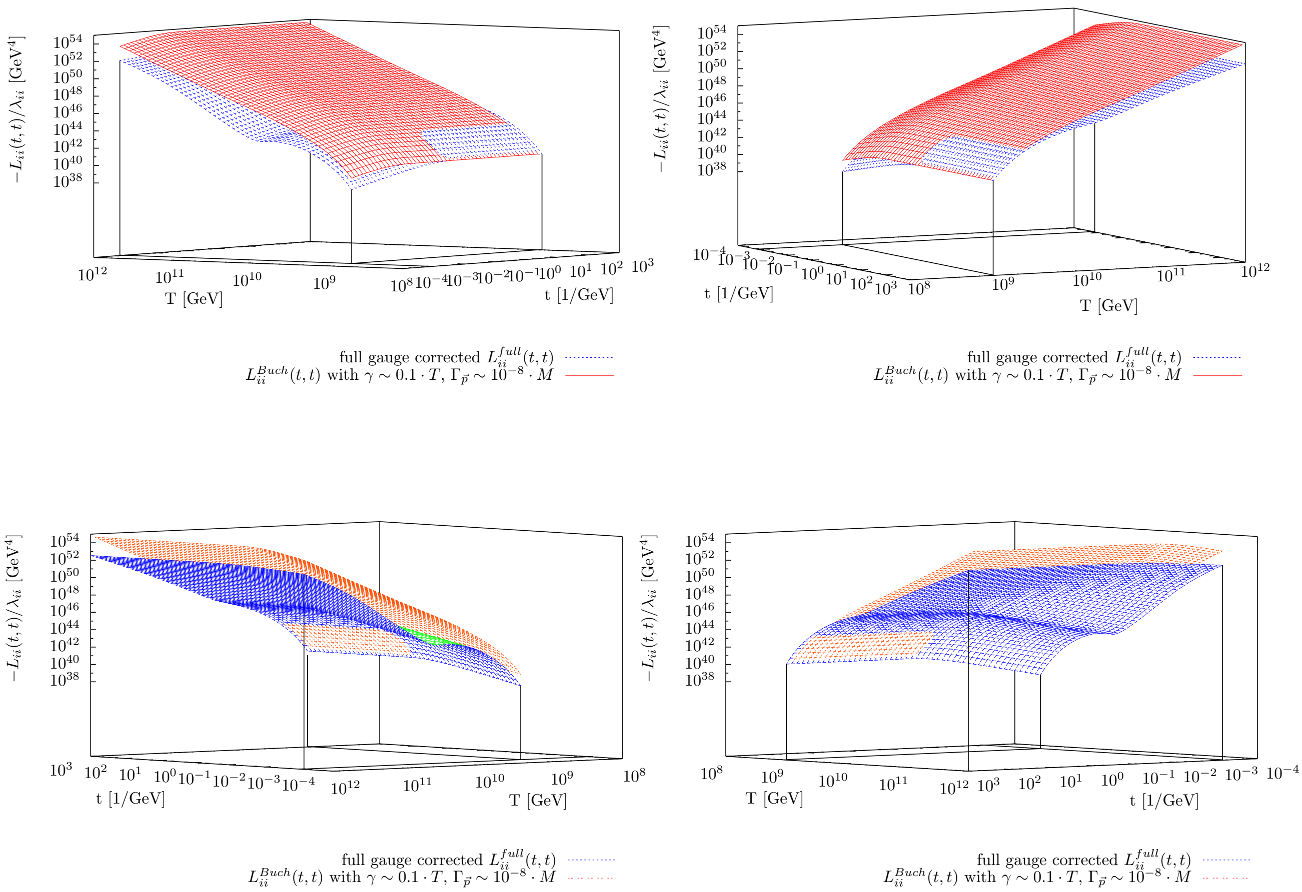

Figure 40: Four different views of the result of $L_{ii}^{\text{full}}(t,t)$ compared to $L_{ii}^{\text{Buch}}(t,t)$ at fixed $M = 10^{10}$ GeV and $\gamma \sim 0.1 \cdot T$, $\Gamma_{\vec{p}} \sim 10^{-8} \cdot M$. Both calculated with a relative tolerance of $tol_{\text{rel}} = 10^{-2}$.

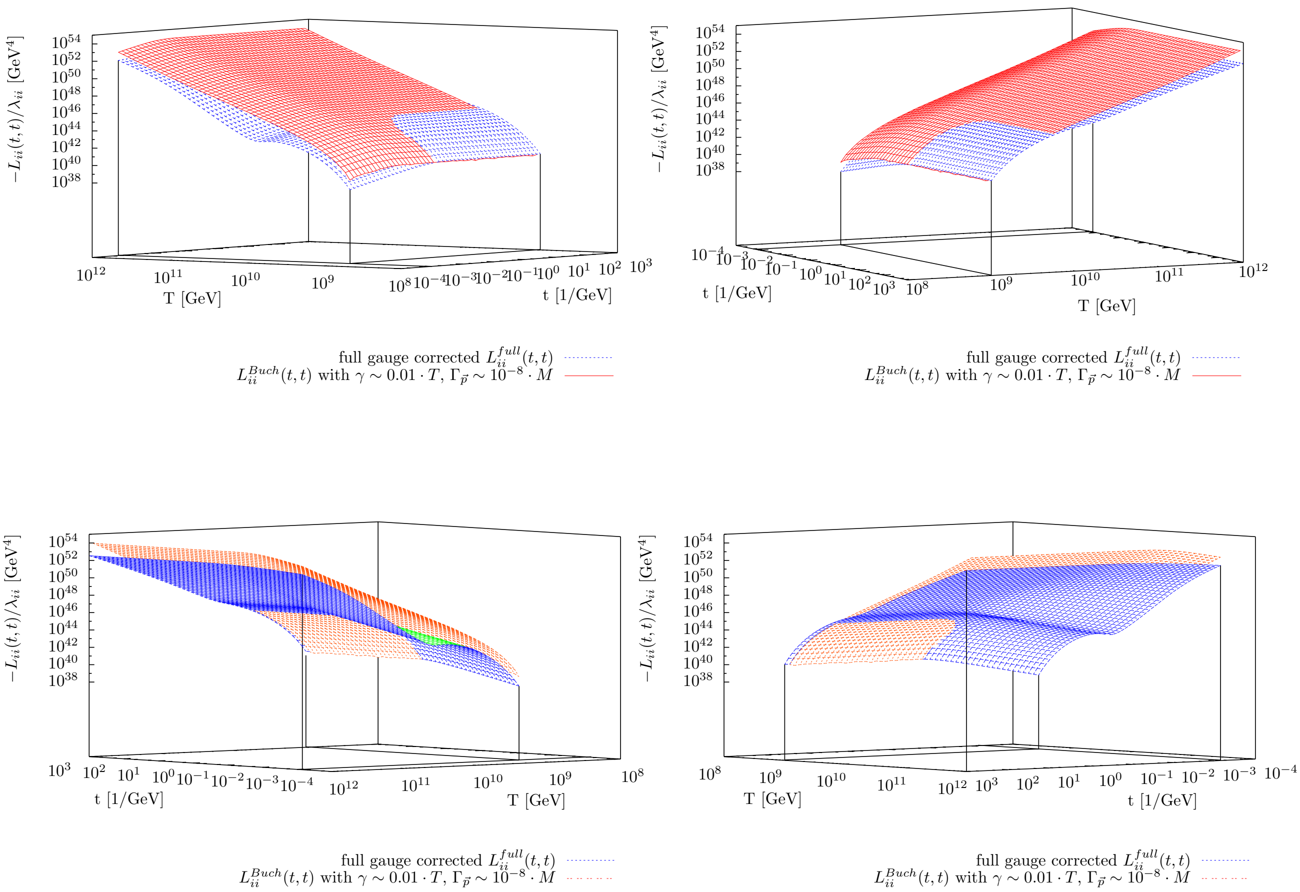

Figure 41: Four different views of the result of $L_{ii}^{\text{full}}(t,t)$ compared to $L_{ii}^{\text{Buch}}(t,t)$ at fixed $M = 10^{10}$ GeV and $\gamma \sim 0.01 \cdot T$, $\Gamma_{\vec{p}} \sim 10^{-8} \cdot M$. Both calculated with a relative tolerance of $tol_{\text{rel}} = 10^{-2}$.

As observed in the thermalized case in section 8.2 the estimated result for L_{ii} presented in [Ani+11] compares well to our systematic approach. Both results do not differ much in the order of magnitude. Nevertheless there are some important differences that can also be noticed now for running temperature and time.

At first the shapes of the results differ. As pointed out in the beginning this can be observed very well in all 4 graphs, especially for small times. The reason for that has already been given earlier: Since the only time dependent part of the gauge corrected lepton number matrix is connected to the Majorana decay width, a gauge corrected decay width becomes crucial, making especially non trivial gauge corrections, as for example vertex corrections to the Majorana self energy, more important for small times t.

We have calculated 4 cases: two with a Majorana decay width of $\Gamma_{\vec{p}} \sim 10^{-7} \cdot M$ and two different thermal widths of SM propagators $\gamma \sim 0.1 \cdot T$ and $\gamma \sim 0.01 \cdot T$ and two with a decay width of $\Gamma_{\vec{p}} \sim 10^{-8} \cdot M$ and again two different thermal damping widths $\gamma \sim 0.1 \cdot T$ and $\gamma \sim 0.01 \cdot T$. We have left out an investigation of the lepton number matrix with $\Gamma_{\vec{p}} \sim 10^{-6} \cdot M$ and $\gamma \sim T$ because in section 8.2 we could observe that the effect of gauge corrections is overestimated for this choice of parameters by comparing the results. Investigating now the intersections between the calculated results makes it possible to observe the effect of systematical gauge corrections.

For standard parameters, as motivated by [Ani+11], $\gamma \sim 0.1 \cdot T$ and $\Gamma_{\vec{p}} \sim 10^{-7} \cdot M$ the deviation between the systematically corrected result and the result with SM damping widths increases for smaller times t. For large times $t \gtrsim 1/\Gamma_{\vec{p}}$ thermalization is reached and we have the same situation investigated previously in section 8.3. Comparing this to the smaller thermal damping width $\gamma \sim 0.01 \cdot T$ shows that the intersection between the results is shifted to the left. As a result the deviation for small times becomes smaller giving evidence that the effect is a little smaller than estimated in [Ani+11]. This fits well to our observations from section 8.3. When comparing the shape of the graphs in temporal direction one notices that the result of L_{ii}^{Buch} is more flat. Since the only time dependent part of the lepton number matrix is proportional to the heavy neutrino decay width $\sim e^{-\Gamma_{\vec{p}} t}$ this gives evidence that the estimate for the non-corrected decay width is to big.

For this reason it is reasonable to look at a smaller decay width estimating $\Gamma_{\vec{p}} \sim 10^{-8} \cdot M$. As pointed out in section 8.3 this is in better correspondence to the value of the gauge corrected $\Gamma_{\vec{p}}$ at the relevant momentum scale $p \sim \mathcal{O}(T)$. Comparing now the shape of the two results in t-direction shows that the red line is not as flat as in the previous case for a larger Majorana decay width and therefore the shapes fit better. Nevertheless for small times the result still seems to be a little overestimated.

Further we are looking at two cases for the SM damping widths γ. Comparing both results shows that the result with $\gamma \sim 0.1 \cdot T$ has a bigger deviation from our systematic gauge corrected result than the result with $\gamma \sim 0.01 \cdot T$. In correspondence to previous observations made in section 8.3 the two results fit very well for large times and small temperatures below the heavy neutrino mass $T < M$, especially in the case $\gamma \sim 0.01 \cdot T$. Again it can clearly be noticed that the deviation increases for temperatures above the heavy neutrino mass $T \geq M$. In analogy to the observation made for a bigger Majorana decay width this is even more visible for small times t. Again this is because the time dependent part of the lepton number matrix is connected to the Majorana decay width $\Gamma_{\vec{p}}$. In section 7.3 we have seen that the dominating part of the integral is given at momenta $p \sim \mathcal{O}(T)$. In this region the gauge corrected heavy Majorana decay width is small, such that estimating a small value for the decay width leads to reasonable results. Considering now small times has the effect that the $\sim e^{-\Gamma_{\vec{p}} t}$ part in the integrand plays a more important role such that already lower momenta contribute compared to the thermalized case. As a result a gauge corrected decay width becomes more important because the decay width can not be kept at a small constant value. On the other hand the σ-contributions are time independent and give the same values independently on t, but since we have seen now that lower momenta become more important for small times since they are not suppressed by $\sim e^{-\Gamma_{\vec{p}} t}$ anymore, gauge corrections to the σ-part play a more important role for small times. For this reason it is possible to understand that corrections have a bigger effect on the result for temperatures $T > M$ when considering small times, making them more visible in our results.

Finally we can conclude three things:

Non trivial gauge corrections are important for temperatures beyond the heavy neutrino mass $T > M$. This could not only be proven to be the case when looking at the thermalized version of L_{ii}, for small times t the effect is even more visible.
Further we have seen that a smaller heavy Majorana decay width $\Gamma_{\vec{p}}$ than the estimate $\Gamma_{\vec{p}} \sim 10^{-7} \cdot M$ leads not only to a better result when comparing the time dependence of the results but also the value compares better to the value of the full gauge corrected decay width at relevant momentum $p \sim \mathcal{O}(T)$. Never the less this depends on the choice of $|\lambda|^2$ in the calculation of the gauge corrected Majorana decay width.
Finally the value $\gamma \sim 0.1 \cdot T$ seems to overestimate the effect of gauge corrections a little, especially when dealing with a small decay width $\Gamma_{\vec{p}}$. We have seen that a smaller value as $\gamma \sim 0.01 \cdot T$ leads to a behavior that compares better. Nevertheless the estimate $\Gamma_{\vec{p}} \sim 10^{-7} \cdot M$ and $\gamma \sim 0.1 \cdot T$ presented in [Ani+11] is a good approximation for the thermalized lepton number matrix.

9 Conclusion and Research Perspectives

In this thesis the effect of gauge corrections on a Leptogenesis scenario has been investigated. This has been done by systematically including gauge corrections in a full quantum mechanical treatment involving nonequilibrium Kadanoff-Baym equations. Our calculation was motivated by previous analysis done by Anisimov, Buchmüller et al. [Ani+11]. Their results were briefly repeated in section 2 and 4 in this thesis. In analogy to [Ani+11] we considered an effective theory where 2 of 3 heavy neutrinos were integrated out. The remaining Majorana neutrino is considered to be an out-of-equilibrium particle weakly coupled to a thermal bath of SM leptons and Higgs fields. In this scenario it was possible to start from a zero initial abundance of the heavy neutrino and based on that it was possible to solve the Kadanoff-Baym equations for the heavy Majorana neutrino obtaining an out-of-equilibrium propagator. The lepton asymmetry is now caused by the CP-violating out-of-equilibrium decay of the heavy neutrino. For this purpose the CP-violating diagrams needed to be identified in section 4. With these diagrams at hand a measure for the lepton asymmetry could be calculated referred to as lepton number matrix.

Gauge corrections could be included to the lepton number matrix in two steps: First by calculating a gauge corrected decay width of the heavy neutrino, second by making use of a cylindrical diagram that systematically includes all propagator and vertex corrections to the CP-violating diagrams. The idea of the cylindrical diagram has first been proposed in [Hüt13]. It appeared that in both cases a resummation of the Majorana self energy is needed. In section 3 such a resummation scheme for the self energy has been presented based on previous works by Anisimov, Bödecker et al. [ABB11]. It was pointed out that not only propagator corrections could be included by making use of asymptotic masses for SM equilibrium propagators, but also a systematic resummation for the Majorana self energy had to be performed. For this purpose the procedure of CTL resummation has been presented in section 3 leading to a recursion relation making it possible to calculate a ladder diagram for the Majorana self energy [ABB11].

Based on the results of section 3 and 4 it was now possible to formulate a systematic gauge corrected lepton number matrix in section 5. Note that the final result slightly differs from the expression found in previous analysis made by [Hüt13].

After presenting a numerical procedure to calculate the gauge corrections in section 6 an approximation for the gauge corrected lepton number matrix has been presented in section 7. By investigating the thermalized limit $t \to \infty$ we have shown that the integrand function of the full expression is narrowly peaked. As a result it was possible to restrict the calculation on the regions with the largest contributions leading to a much simpler form of the gauge corrected lepton number matrix. After applying the approximation it could be shown that the final result has the same time dependence as observed previously using Boltzmann equations to calculate the asymmetry. This is very interesting to see because for Anisimov, Buchmüller et al. it was only possible to arrive at this kind of time dependence in a quantum mechanical approach by including thermal widths γ for SM propagators 'by hand' [Ani+11]. A systematic treatment was still missing. We could now not only present a systematic gauge corrected result of the lepton number matrix calculated purely quantum mechanical but also the approximated result reproduces the same time dependence known from Boltzmann analysis and the approach taken by [Ani+11]. In fact we could show that gauge effects do lead to a result for the lepton number matrix that compares to the Boltzmann case as supposed by Anisimov and Buchmüller. On top of that this proves that Boltzmann analysis is indeed possible.

The final section 8 presented the numerical results obtained by solving the approximated integral from section 7. Sticking to the model of [Ani+11] we first investigated the time dependence of the result at fixed temperature $T \sim 10^{11}$ GeV and fixed heavy neutrino mass $M \sim 10^{10}$ GeV. It could be shown that the result thermalizes on a timescale given by $t \sim 1/\Gamma_{\vec{p}} \sim 1/GeV$ with the value of the Majorana decay width $\Gamma_{\vec{p}} \sim 1$ GeV given at relevant momentum $p \sim \mathcal{O}(T)$. The calculation has been tested using various numerical algorithms all leading to the same result. Further it was possible to show that the approximation is best for times $t \gtrsim 1/\Gamma_{\vec{p}} \sim 1/GeV$. Next we investigated the temperature dependence of the gauge corrections at fixed time $t \to \infty$ corresponding to the thermalized version of the integral. It was possible to show that gauge corrections are important especially for temperatures beyond the heavy neutrino mass $T \geq M$. Further we compared the full result to the result from [Ani+11]. Doing this it was possible to search for an optimal set of the parameters $\Gamma_{\vec{p}}$ and γ used in the result of [Ani+11]. We could show that $\Gamma_{\vec{p}} \sim 10^{-7} \cdot M$ and $\gamma \sim 0.1 \cdot T$ is the best global approximation for all temperatures of the full result, but using $\Gamma_{\vec{p}} \sim 10^{-8} \cdot M$ and $\gamma \sim 0.01 \cdot T$ reproduces the behavior of the full result for small temperatures T nearly perfectly. This underlines again the argument that gauge corrections are most important for temperatures $T \geq M$. By investigating the time dependence of the result for fixed $T = 10^{11}$ GeV and $M = 10^{10}$ GeV once again and comparing it to the result from [Ani+11] we could additionally show that a smaller value for $\Gamma_{\vec{p}} \lesssim 10^{-8} \cdot M$ compares better to the value of the full gauge corrected decay width at relevant momentum $p \sim \mathcal{O}(T)$ and to the timescale of thermalization of the full gauge corrected lepton number matrix. Nevertheless this depends of course on the choice of coupling $|\lambda|^2 = 10^{-8}$ in the calculation of the gauge corrected heavy Majorana neutrino decay width. On top of that we calculated the result from [Ani+11] using the gauge corrected heavy Majorana neutrino decay width. By doing so we could show that working only with a gauge corrected decay width but leaving out the systematic treatment via the cylindrical diagram is not sufficient. Of course the result has the correct thermalization behavior but it is not possible to fit it to the full gauge corrected result by making a correct guess for the SM damping width γ. A full treatment especially involving non trivial gauge corrections to the CP-violating diagrams as for example vertex corrections is inevitable. Finally we could underline these results by investigating both the temperature and time dependence. In general the choice of $\Gamma_{\vec{p}} \sim 10^{-7} \cdot M$ and $\gamma \sim 0.1 \cdot T$ overestimates the corrections a little, but especially for temperatures $T \geq M$ non-trivial gauge corrections become important as for example corrections to the CP-violating diagrams. This effect could also be investigated by Frederik Depta in his Master thesis on the subject.

We provided a result for a Leptogenesis scenario that systematically includes gauge corrections and showed that gauge corrections have an effect especially for $T \geq M$ in this thesis. Nevertheless our results did not lead to a dramatically new situation and we could show that Boltzmann analysis is indeed possible. On top of that there are still some open questions that could be addressed in future work:

It might be possible to drop some of the approximations made in the quantum mechanical treatment of the problem. We have worked with an effective theory where 2 of 3 heavy neutrinos where integrated out, thus it could be interesting to investigate a model with 2 or even all 3 heavy neutrinos. Especially the model of resonant Leptogenesis could be of interest (for a recent review see [Dev+17]). On top of that only the two-loop diagrams contributing to CP-violation were taken into account. In a future work one could of course investigate higher loop order corrections.
Further in the framework of this thesis Hubble expansion was neglected. It is possible to formulate the Kadanoff-Baym equations including a Hubble term, a formulation can for example be found in [Men10]. Never the less it remains questionable if these equations are solvable especially it is unlikely to find an analytic solution as it was possible in our case without Hubble expansion.
Another neglected effect in our model is washout. There a numerous loop diagrams that have to be included in a systematic treatment of washout. Such a treatment will lead to highly complicated expressions that can probably only be treated numerically.
We have shown that gauge corrections in a quantum mechanical treatment do not rule out a treatment using Boltzmann equations due to memory effects or other specific effects of nonequilibrium QFT. As a result it could be interesting to investigate the scenario further using Boltzmann equations instead of a Kadanoff-Baym treatment. Especially the effect of Hubble expansion can be included much easier in a Boltzmann treatment of the problem.
Finally latest models have considered a combination of GUT Baryogenesis and Leptogenesis and it would be interesting to investigate how both models work together. The same holds for Leptogenesis and the frequently discussed model of electroweak Baryogenesis.

10 Appendix A - Feynman Rules

In the following the Feynman rules for propagators and vertices will be given [Hüt13]

- Majorana neutrino propagator:

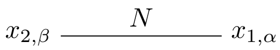

$\mathrm{i}G_{\alpha\beta}(x_1 x_2)$

- Lepton propagator:

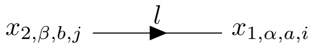

$\mathrm{i}\delta_{ij}\delta_{ab}S_{\alpha\beta}(x_1, x_2)$

- Scalar propagator:

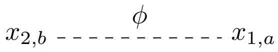

$\mathrm{i}\delta_{ab}\Delta(x_1, x_2)$

- Majorana-lepton-Higgs vertices:

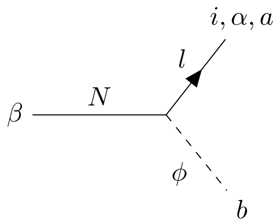

$\mathrm{i}\lambda^*_{i1}\epsilon_{ab}(P_R)_{\alpha\beta}$

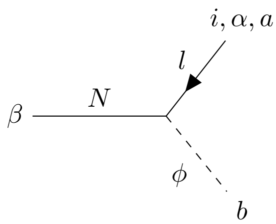

$\mathrm{i}\lambda_{i1}\epsilon_{ab}(CP_L)_{\beta\alpha}$

- Lepton-lepton-Higgs-Higgs effective vertices

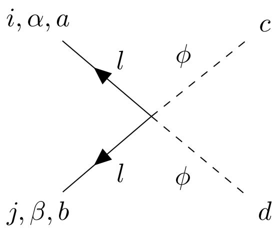

$\mathrm{i}\eta^*_{ij}(\epsilon_{ac}\epsilon_{bd} + \epsilon_{ad}\epsilon_{bc})(P_R C)_{\alpha\beta}$

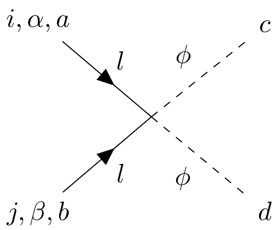

$\mathrm{i}\eta_{ij}(\epsilon_{ac}\epsilon_{bd} + \epsilon_{ad}\epsilon_{bc})(CP_L)_{\alpha\beta}$

with the chiral projectors $P_R = \frac{1}{2}(1 + \gamma_5)$ and $P_L = \frac{1}{2}(1 - \gamma_5)$ and the Levi-Civita tensor in 2 dimensions $\epsilon_{ab} = -\epsilon_{ba}$.

11 Appendix B - List of Propagators

The following propagators can also be found in [Ani+11, App. A]. They are given as a function of relative time $y = t_1 - t_2$ and total time $t = (t_1 + t_2)/2$.

- Free massive scalar propagators with on-shell momentum $\omega_{\vec{q}} = \sqrt{m^2 + \vec{q}^2}$,

$$\Delta_{\vec{q}}(y)^- = \frac{1}{\omega_{\vec{q}}} \sin(\omega_{\vec{q}} y), \tag{369}$$

$$\Delta^+_{\vec{q}}(y) = \frac{1}{2\omega_{\vec{q}}} \coth\left(\frac{\beta\omega_{\vec{q}}}{2}\right) \cos(\omega_{\vec{q}} y), \tag{370}$$

$$\Delta^>_{\vec{q}}(y) = \frac{1}{2\omega_{\vec{q}}} \left(\coth\left(\frac{\beta\omega_{\vec{q}}}{2}\right) \cos(\omega_{\vec{q}} y) - \mathrm{i}\sin(\omega_{\vec{q}} y)\right), \tag{371}$$

$$\Delta^<_{\vec{q}}(y) = \frac{1}{2\omega_{\vec{q}}} \left(\coth\left(\frac{\beta\omega_{\vec{q}}}{2}\right) \cos(\omega_{\vec{q}} y) + \mathrm{i}\sin(\omega_{\vec{q}} y)\right). \tag{372}$$

- Free massive Dirac fermion propagators with on-shell momentum $\omega_{\vec{k}} = \sqrt{m^2 + \vec{k}^2}$

$$S^-_{\vec{k}}(y) = \mathrm{i}\gamma_0 \cos(\omega_{\vec{k}} y) + \frac{m - \vec{k}\cdot\vec{\gamma}}{\omega_{\vec{k}}} \sin(\omega_{\vec{k}} y), \tag{373}$$

$$S^+_{\vec{k}}(y) = -\frac{1}{2}\tanh\left(\frac{\beta\omega_{\vec{k}}}{2}\right) \left(\mathrm{i}\gamma_0 \sin(\omega_{\vec{k}} y) - \frac{m - \vec{k}\cdot\vec{\gamma}}{\omega_{\vec{k}}} \cos(\omega_{\vec{k}} y)\right), \tag{374}$$

$$S^>_{\vec{k}}(y) = \frac{\gamma_0}{2} \left(\cos(\omega_{\vec{k}} y) - \mathrm{i}\tanh\left(\frac{\beta\omega_{\vec{k}}}{2}\right) \sin(\omega_{\vec{k}} y)\right) + \frac{m - \vec{k}\vec{\gamma}}{2\omega_{\vec{k}}} \left(\tanh\left(\frac{\beta\omega_{\vec{k}}}{2}\right) \cos(\omega_{\vec{k}} y) - \mathrm{i}\sin(\omega_{\vec{k}} y)\right), \tag{375}$$

$$S^<_{\vec{k}}(y) = \frac{\gamma_0}{2} \left(\cos(\omega_{\vec{k}} y) - \mathrm{i}\tanh\left(\frac{\beta\omega_{\vec{k}}}{2}\right) \sin(\omega_{\vec{k}} y)\right) + \frac{m - \vec{k}\vec{\gamma}}{2\omega_{\vec{k}}} \left(\tanh\left(\frac{\beta\omega_{\vec{k}}}{2}\right) \cos(\omega_{\vec{k}} y) + \mathrm{i}\sin(\omega_{\vec{k}} y)\right). \tag{376}$$

- Nonequilibrium massive Majorana fermion $\omega_{\vec{p}} = \sqrt{M^2 + \vec{p}^2}$

$$G^-_{\vec{p}}(t, y) = \left(\mathrm{i}\gamma_0 \cos(\omega_{\vec{p}} y) + \frac{M - \vec{p}\vec{\gamma}}{\omega_{\vec{p}}} \sin(\omega_{\vec{p}} y)\right) e^{-\Gamma_{\vec{p}}|y|/2} C^{-1}, \tag{377}$$

$$G^+_{\vec{p}}(t, y) = -\left(\mathrm{i}\gamma_0 \sin(\omega_{\vec{p}} y) - \frac{M - \vec{p}\vec{\gamma}}{\omega_{\vec{p}}} \cos(\omega_{\vec{p}} y)\right) \times \left(\frac{1}{2}\tanh\left(\frac{\beta\omega_{\vec{p}}}{2}\right) e^{-\Gamma_{\vec{p}}|y|/2} + f^{eq}_N(\omega_{\vec{p}}) e^{-\Gamma_{\vec{p}} t}\right) C^{-1}, \tag{378}$$

$$G^>_{\vec{p}}(t, y) = G^+_{\vec{p}}(t, y) - \frac{\mathrm{i}}{2} G^-_{\vec{p}}(t, y), \tag{379}$$

$$G^<_{\vec{p}}(t, y) = G^+_{\vec{p}}(t, y) + \frac{\mathrm{i}}{2} G^-_{\vec{p}}(t, y). \tag{380}$$

12 Appendix C - Full time integrated Lepton Number Matrix

The full expression of the time integral

$$\begin{aligned}
T(t) &= \int_0^t \int_0^t \int_0^{t_2} \cos(\omega_{\vec{p}} y_{13}) e^{-\Gamma_{\vec{p}}(\omega_{\vec{p}})\frac{t_1+t_3}{2}} \mathrm{Re}\left[e^{-i(\omega_{21}y_{21}+\omega_{23}y_{23})}\right] dt_3 dt_2 dt_1 \\
&= \int_0^t \int_0^t \int_0^{t_2} \cos(\omega_{\vec{p}}(t_1-t_3)) e^{-\Gamma_{\vec{p}}(\omega_{\vec{p}})\frac{t_1+t_3}{2}} \\
&\qquad [\cos(\omega_{21}(t_2-t_1))\cos(\omega_{23}(t_2-t_3)) - \sin(\omega_{21}(t_2-t_1))\sin(\omega_{23}(t_2-t_3))] dt_3 dt_2 dt_1
\end{aligned} \tag{381}$$

will be given. Using *mathematica* [Wol17] one ends up with

$$\begin{aligned}
T(t) =& \frac{4e^{-\frac{1}{2}\Gamma_{\vec{p}}t}(\omega_{21}-\omega_{23})}{(\omega_{23}^2-\omega_{21}^2)(\Gamma_{\vec{p}}^2+4(\omega_{23}-\omega_{\vec{p}})^2)(\Gamma_{\vec{p}}^2+4(\omega_{23}+\omega_{\vec{p}})^2)(\Gamma_{\vec{p}}^2+4(\omega_{21}-\omega_{\vec{p}})^2)(\Gamma_{\vec{p}}^2+4(\omega_{21}+\omega_{\vec{p}})^2)} \\
&\Bigg\{ 2\Gamma_{\vec{p}}(\omega_{21}+\omega_{23})\Big[8\omega_{\vec{p}}^2(\Gamma_{\vec{p}}^2+2(\omega_{21}^2-4\omega_{21}\omega_{23}+\omega_{23}^2)) + (\Gamma_{\vec{p}}^2+4\omega_{21}^2)(\Gamma_{\vec{p}}^2+4\omega_{23}^2)+16\omega_{\vec{p}}^4\Big] \\
&\quad \times \Big[e^{\frac{1}{2}\Gamma_{\vec{p}}t}\cos(\omega_{21}t)\cos(\omega_{23}t) - \cos(\omega_{\vec{p}}t)(\cos(\omega_{21}t)+\cos(\omega_{23}t))\Big] \\
&- 32\Gamma_{\vec{p}}\omega_{\vec{p}}(\omega_{21}-\omega_{23})(\omega_{21}+\omega_{23})\sin(\omega_{\vec{p}}t)(\Gamma_{\vec{p}}^2-4\omega_{21}\omega_{23}+4\omega_{\vec{p}})\sin\left(\frac{1}{2}(\omega_{21}-\omega_{23})t\right)\cos\left(\frac{1}{2}(\omega_{21}+\omega_{23})t\right) \\
&+ 8\omega_{\vec{p}}(\omega_{21}-\omega_{23})\sin(\omega_{\vec{p}}t)\Big[\Gamma_{\vec{p}}^4-4\Gamma_{\vec{p}}^2(\omega_{21}^2+4\omega_{21}\omega_{23}+\omega_{23}^2-2\omega_{\vec{p}}^2)+16(\omega_{21}^2-\omega_{\vec{p}}^2)(\omega_{23}^2-\omega_{\vec{p}}^2)\Big] \\
&\quad \times \sin\left(\frac{1}{2}(\omega_{21}-\omega_{23})t\right)\sin\left(\frac{1}{2}(\omega_{21}+\omega_{23})t\right) \\
&+ (\Gamma_{\vec{p}}^2-4\omega_{21}\omega_{23}+4\omega_{\vec{p}}^2)\times\Big[\Gamma_{\vec{p}}^4+4\Gamma_{\vec{p}}^2(\omega_{21}^2+\omega_{23}^2+2\omega_{\vec{p}}^2)+16(\omega_{21}^2-\omega_{\vec{p}}^2)(\omega_{23}^2-\omega_{\vec{p}}^2)\Big] \\
&\quad \times \Big[\cos(\omega_{\vec{p}}t)(\sin(\omega_{21}t)+\sin(\omega_{23}t)) - e^{\frac{1}{2}\Gamma_{\vec{p}}t}\cos(\omega_{21}t)\sin(\omega_{23}t)\Big] \\
&+ \sinh\left(\frac{1}{2}\Gamma_{\vec{p}}t\right)\times\Big[\sin(\omega_{21}t)\cos(\omega_{23}t)(-\Gamma_{\vec{p}}^2+4\omega_{21}\omega_{23}-4\omega_{\vec{p}}^2) \\
&\quad \times\Big(\Gamma_{\vec{p}}^4+4\Gamma_{\vec{p}}^2(\omega_{21}^2+\omega_{23}^2+2\omega_{\vec{p}}^2)+16(\omega_{21}^2-\omega_{\vec{p}}^2)(\omega_{23}^2-\omega_{\vec{p}}^2)\Big) - 2\Gamma_{\vec{p}}(\omega_{21}+\omega_{23})(\sin(\omega_{21}t)\sin(\omega_{23}t)+1) \\
&\quad \times\Big(8\omega_{\vec{p}}^2(\Gamma_{\vec{p}}^2+2(\omega_{21}^2-4\omega_{21}\omega_{23}+\omega_{23}^2)+(\Gamma_{\vec{p}}^2+4\omega_{21}^2)(\Gamma_{\vec{p}}^2+4\omega_{23}^2)+16\omega_{\vec{p}}^4\Big)\Big] \\
&+ \cosh\left(\frac{1}{2}\Gamma_{\vec{p}}t\right)\times\Big[\sin(\omega_{21}t)\cos(\omega_{23}t)(-\Gamma_{\vec{p}}^2+4\omega_{21}\omega_{23}-4\omega_{\vec{p}}^2) \\
&\quad \times\Big(\Gamma_{\vec{p}}^4+4\Gamma_{\vec{p}}^2(\omega_{21}^2+\omega_{23}^2+2\omega_{\vec{p}}^2)+16(\omega_{21}^2-\omega_{\vec{p}}^2)(\omega_{23}^2-\omega_{\vec{p}}^2)\Big) - 2\Gamma_{\vec{p}}(\omega_{21}+\omega_{23})(\sin(\omega_{21}t)\sin(\omega_{23}t)-1) \\
&\quad \times\Big(8\omega_{\vec{p}}^2(\Gamma_{\vec{p}}^2+2(\omega_{21}^2-4\omega_{21}\omega_{23}+\omega_{23}^2)+(\Gamma_{\vec{p}}^2+4\omega_{21}^2)(\Gamma_{\vec{p}}^2+4\omega_{23}^2)+16\omega_{\vec{p}}^4\Big)\Big]\Bigg\}.
\end{aligned} \tag{382}$$

13 Appendix D - Result for L_{ii} as calculated in [Ani+11]

In this Appendix we want to have a closer look at the result of L_{ii} presented in [Ani+11]. We have used it to compare it to our full gauge corrected result. Starting point is the following expression of the lepton number matrix given in [Ani+11, p. 32]

$$L_{\vec{k},ii}(t,t) = -3\lambda_{ii}M\int_{\vec{q},\vec{q}'}\frac{k\cdot k'}{kk'\omega_{\vec{p}}}\frac{\gamma\gamma'}{((\omega_{\vec{p}}-k-q)^2+\gamma^2)((\omega_{\vec{p}}-k'-a')^2+(\gamma')^2}$$
$$f_{l,\phi}(k,q)f_{l,\phi}(k',q')f_N^{eq}(\omega_{\vec{p}})\frac{1-e^{-\Gamma t}}{\Gamma}. \tag{383}$$

To arrive at this result SM propagators with thermal damping widths have been used

$$\Delta_{\vec{k}}^{\pm,eq}(y) = \Delta_{\vec{k}}^{\pm}(y)e^{-\gamma_\phi|y|}, \qquad S_{\vec{k}}^{\pm,eq}(y) = S_{\vec{k}}^{\pm}(y)e^{-\gamma_l|y|}, \tag{384}$$

denoting $\gamma = \gamma(k,q) = \gamma_\phi + \gamma_l$, $\gamma' = \gamma(k',q')$.

Following [Ani+11] we define the angles with respect to the momentum $\vec{p}$: $\theta = \angle(\vec{k},\vec{p})$, $\theta' = \angle(\vec{k}',\vec{p})$ and $\varphi' = \angle(\vec{k}_\perp,\vec{k}'_\perp)$. In this case the perpendicular mark denotes perpendicular to $\vec{p}$.
We choose the following coordinate system

$$\hat{\vec{k}} = \begin{pmatrix}\cos\theta\\ \sin\theta\\ 0\end{pmatrix}, \qquad \hat{\vec{k}}' = \begin{pmatrix}\cos\theta'\\ \sin\theta'\cos\varphi'\\ \sin\theta'\sin\varphi'\end{pmatrix}. \tag{385}$$

The product of 4-vectors can then be written as

$$k\cdot k' = kk'(1-\hat{\vec{k}}\hat{\vec{k}}') = kk'(1-(\cos\theta\cos\theta'+\sin\theta\sin\theta'\cos\varphi')). \tag{386}$$

Since we are interested in the integrated lepton number matrix L_{ii} we have to look at the following expression

$$L_{ii}(t,t) = -3\lambda_{ii}M\int_{\Omega_{\vec{k}}}\int_0^\infty\int_{\vec{q},\vec{q}'}\frac{1-\cos\theta\cos\theta'-\sin\theta\sin\theta'\cos\varphi'}{\omega_{\vec{p}}}\frac{\gamma\gamma'}{((\omega_{\vec{p}}-k-q)^2+\gamma^2)((\omega_{\vec{p}}-k'-a')^2+(\gamma')^2}$$
$$f_{l,\phi}(k,q)f_{l,\phi}(k',q')f_N^{eq}(\omega_{\vec{p}})\frac{1-e^{-\Gamma t}}{\Gamma}k^2dkd\Omega_{\vec{k}}. \tag{387}$$

Following [Ani+11] we change variables $(\vec{q},\vec{q}')\to(\vec{p},\vec{k}')$

$$\begin{aligned}L_{ii} &\sim \int\int(1-\cos\theta\cos\theta'-\sin\theta\sin\theta'\cos\varphi')F(\theta,\theta',...)d\Omega_{\vec{k}}d\Omega_{\vec{k}'} \\ &= \int_{-1}^{1}\int_{-1}^{1}\int_0^{2\pi}\int_0^{2\pi}(1-\cos\theta\cos\theta'-\sin\theta\sin\theta'\cos\varphi')F(\theta,\theta',...)d\phi d\phi' d\cos(\theta)d\cos(\theta') \\ &= (2\pi)^2\int_{-1}^{1}\int_{-1}^{1}(1-\cos\theta\cos\theta')F(\theta,\theta',...)d\cos(\theta)d\cos(\theta').\end{aligned} \tag{388}$$

We have used that the integrand function $F(\theta,\theta',...)$ does not depend on φ'.

The integral has the following form now

$$L_{ii}(t,t) = -3\lambda_{ii}\frac{M}{16\pi^3}\int_{-1}^{1}\int_{-1}^{1}\int_0^\infty\int_0^\infty\int_0^\infty\frac{1-\cos\theta\cos\theta'}{qq'\omega_{\vec{p}}}\frac{\gamma\gamma'}{((\omega_{\vec{p}}-k-q)^2+\gamma^2)((\omega_{\vec{p}}-k'-a')^2+(\gamma')^2} \tag{389}$$
$$f_{l,\phi}(k,q)f_{l,\phi}(k',q')f_N^{eq}(\omega_{\vec{p}})\frac{1-e^{-\Gamma t}}{\Gamma}p^2dpk^2dkk'^2dk'd\cos\theta d\cos\theta'.$$

Recall that in [Ani+11] the notation of the integrals had been defined as

$$\int_{\vec{q}} = \int \frac{d^3q}{2(2\pi)^3 q_0}. \tag{390}$$

Changing the variables the following way

$$\begin{aligned} q &= |\vec{p} - \vec{k}| = (p^2 + k^2 - 2pk\cos\theta)^{\frac{1}{2}}, \\ q' &= |\vec{p} - \vec{k}'| = (p^2 + k^{'2} - 2pk'\cos\theta)^{\frac{1}{2}}, \\ -\frac{q}{pk}dq &= d\cos\theta, \qquad -\frac{q'}{pk'} = d\cos\theta', \end{aligned} \tag{391}$$

leads to

$$\begin{aligned} L_{ii}(t,t) = -\frac{3\lambda_{ii}M}{16\pi^3} \int_0^\infty \int_0^\infty \int_{k'_{\min}(p)}^{k'_{\max}(p)} \int_{q_-}^{q_+} \int_{q'_-}^{q'_+} \frac{1}{\omega_{\vec{p}}} \left(1 - \frac{p^2 + k^2 - q^2}{2pk} \frac{p^2 + k^{'2} - q^{'2}}{2pk'}\right) f_{l,\phi}(k,q) f_{l,\phi}(k',q') f_N^{eq}(\omega_{\vec{p}}) \\ \times \frac{\gamma\gamma'}{((\omega_{\vec{p}} - k - q)^2 + \gamma^2)((\omega_{\vec{p}} - k' - q')^2 + \gamma^{'2}} \frac{1 - e^{-\Gamma t}}{\Gamma} kk'dq'dqdk'dkdp. \end{aligned} \tag{392}$$

The integration boundaries are chosen similar to [Ani+11] given as the maximal value of q and q' connected to the change of variables

$$q_\pm = |k \pm p|, \qquad q'_\pm = |k' \pm p|. \tag{393}$$

Further the constraint $p > (M^2 - 4k^{'2})/(4k')$ [Ani+11, p. 49] leads to

$$k' > \frac{\omega_{\vec{p}} - p}{2} := k'_{\min}(p), \qquad k' < \frac{\omega_{\vec{p}} + p}{2} := k'_{\max}(p). \tag{394}$$

This is the result simulated in section 8.3. For more details see [Ani+11, App. C].

References

[ABB11] Alexey Anisimov, Denis Besak, and Dietrich Bodeker. "Thermal production of relativistic Majorana neutrinos: Strong enhancement by multiple soft scattering". In: *JCAP* 1103 (2011), p. 042. DOI: 10.1088/1475-7516/2011/03/042. arXiv: 1012.3784 [hep-ph] (cit. on pp. 5, 21, 24–29, 39, 48, 49, 51, 63, 69, 70, 90).

[AD85] Ian Affleck and Michael Dine. "A New Mechanism for Baryogenesis". In: *Nucl. Phys.* B249 (1985), pp. 361–380. DOI: 10.1016/0550-3213(85)90021-5 (cit. on p. 8).

[Ani+10] A. Anisimov, W. Buchmuller, M. Drewes, and S. Mendizabal. "Leptogenesis from Quantum Interference in a Thermal Bath". In: *Phys. Rev. Lett.* 104 (2010), p. 121102. DOI: 10.1103/PhysRevLett.104.121102. arXiv: 1001.3856 [hep-ph] (cit. on p. 19).

[Ani+11] A. Anisimov, W. Buchmüller, M. Drewes, and S. Mendizabal. "Quantum Leptogenesis I". In: *Annals Phys.* 326 (2011). [Erratum: Annals Phys.338,376(2011)], pp. 1998–2038. DOI: 10.1016/j.aop.2011.02.002,10.1016/j.aop.2013.05.00. arXiv: 1012.5821 [hep-ph] (cit. on pp. 4, 5, 11, 13, 15–21, 30–32, 35–37, 58, 59, 67, 69, 79–83, 88–91, 93, 95, 96).

[Ara+92] H. Arason, D. J. Castano, B. Keszthelyi, S. Mikaelian, E. J. Piard, Pierre Ramond, and B. D. Wright. "Renormalization group study of the standard model and its extensions. 1. The Standard model". In: *Phys. Rev.* D46 (1992), pp. 3945–3965. DOI: 10.1103/PhysRevD.46.3945 (cit. on p. 70).

[Aur+02] P. Aurenche, F. Gelis, G. D. Moore, and H. Zaraket. "Landau-Pomeranchuk-Migdal resummation for dilepton production". In: *JHEP* 12 (2002), p. 006. DOI: 10.1088/1126-6708/2002/12/006. arXiv: hep-ph/0211036 [hep-ph] (cit. on p. 29).

[Bah+99] Neta A. Bahcall, Jeremiah P. Ostriker, Saul Perlmutter, and Paul J. Steinhardt. "The Cosmic triangle: Assessing the state of the universe". In: *Science* 284 (1999), pp. 1481–1488. DOI: 10.1126/science.284.5419.1481. arXiv: astro-ph/9906463 [astro-ph] (cit. on p. 4).

[Bam+12] Kazuharu Bamba, Salvatore Capozziello, Shin'ichi Nojiri, and Sergei D. Odintsov. "Dark energy cosmology: the equivalent description via different theoretical models and cosmography tests". In: *Astrophys. Space Sci.* 342 (2012), pp. 155–228. DOI: 10.1007/s10509-012-1181-8. arXiv: 1205.3421 [gr-qc] (cit. on p. 4).

[Bar+00] Riccardo Barbieri, Paolo Creminelli, Alessandro Strumia, and Nikolaos Tetradis. "Baryogenesis through leptogenesis". In: *Nucl. Phys.* B575 (2000), pp. 61–77. DOI: 10.1016/S0550-3213(00)00011-0. arXiv: hep-ph/9911315 [hep-ph] (cit. on p. 10).

[BB10] Denis Besak and Dietrich Bodeker. "Hard Thermal Loops for Soft or Collinear External Momenta". In: *JHEP* 05 (2010), p. 007. DOI: 10.1007/JHEP05(2010)007. arXiv: 1002.0022 [hep-ph] (cit. on pp. 5, 21, 22, 24–26, 28).

[BDP02] W. Buchmuller, P. Di Bari, and M. Plumacher. "Cosmic microwave background, matter - antimatter asymmetry and neutrino masses". In: *Nucl. Phys.* B643 (2002). [Erratum: Nucl. Phys.B793,362(2008)], pp. 367–390. DOI: 10.1016/S0550-3213(02)00737-X,10.1016/j.nuclphysb.2007.11.030. arXiv: hep-ph/0205349 [hep-ph] (cit. on pp. 10, 11).

[BDP03] W. Buchmuller, P. Di Bari, and M. Plumacher. "The Neutrino mass window for baryogenesis". In: *Nucl. Phys.* B665 (2003), pp. 445–468. DOI: 10.1016/S0550-3213(03)00449-8. arXiv: hep-ph/0302092 [hep-ph] (cit. on p. 9).

[BDP05] W. Buchmuller, P. Di Bari, and M. Plumacher. "Leptogenesis for pedestrians". In: *Annals Phys.* 315 (2005), pp. 305–351. DOI: 10.1016/j.aop.2004.02.003. arXiv: hep-ph/0401240 [hep-ph] (cit. on p. 10).

[Bel11] Michel Le Bellac. *Thermal Field Theory*. Cambridge University Press, 2011. ISBN: 9780511885068, 9780521654777. URL: http://www.cambridge.org/mw/academic/subjects/physics/theoretical-physics-and-mathematical-physics/thermal-field-theory?format=AR (cit. on pp. 15–17, 21, 34, 35, 79).

[Bes10] Denis Besak. "Thermal particle production in the early universe". PhD thesis. 2010 (cit. on pp. 21–24, 28, 59, 62).

[BF00] Wilfried Buchmuller and Stefan Fredenhagen. “Quantum mechanics of baryogenesis”. In: *Phys. Lett.* B483 (2000), pp. 217–224. DOI: 10.1016/S0370-2693(00)00573-6. arXiv: hep-ph/0004145 [hep-ph] (cit. on pp. 10, 12).

[Bio+17] Simone Biondini et al. “Status of rates and rate equations for thermal leptogenesis”. In: (2017). arXiv: 1711.02864 [hep-ph] (cit. on p. 11).

[Boo15] Boost. *Boost C++ Libraries*. http://www.boost.org/. Last accessed 2015-06-30. 2015 (cit. on p. 70).

[BPY05] W. Buchmuller, R. D. Peccei, and T. Yanagida. “Leptogenesis as the origin of matter”. In: *Ann. Rev. Nucl. Part. Sci.* 55 (2005), pp. 311–355. DOI: 10.1146/annurev.nucl.55.090704.151558. arXiv: hep-ph/0502169 [hep-ph] (cit. on pp. 8, 9, 79).

[CFH99] F. Csikor, Z. Fodor, and J. Heitger. “Where does the hot electroweak phase transition end?” In: *Nucl. Phys. Proc. Suppl.* 73 (1999), pp. 659–661. DOI: 10.1016/S0920-5632(99)85166-4. arXiv: hep-ph/9809293 [hep-ph] (cit. on p. 7).

[Con10] GSL Project Contributors. *GSL - GNU Scientific Library - GNU Project - Free Software Foundation (FSF)*. http://www.gnu.org/software/gsl/. 2010. URL: http://www.gnu.org/software/gsl/ (cit. on pp. 71–74, 79).

[CRV96] Laura Covi, Esteban Roulet, and Francesco Vissani. “CP violating decays in leptogenesis scenarios”. In: *Phys. Lett.* B384 (1996), pp. 169–174. DOI: 10.1016/0370-2693(96)00817-9. arXiv: hep-ph/9605319 [hep-ph] (cit. on p. 9).

[Dev+17] Bhupal Dev, Mathias Garny, Juraj Klaric, Peter Millington, and Daniele Teresi. “Resonant enhancement in leptogenesis”. In: (2017). arXiv: 1711.02863 [hep-ph] (cit. on pp. 34, 91).

[DK03] Michael Dine and Alexander Kusenko. “The Origin of the matter - antimatter asymmetry”. In: *Rev. Mod. Phys.* 76 (2003), p. 1. DOI: 10.1103/RevModPhys.76.1. arXiv: hep-ph/0303065 [hep-ph] (cit. on p. 6).

[Fan+99] V. Fanti et al. “A New measurement of direct CP violation in two pion decays of the neutral kaon”. In: *Phys. Lett.* B465 (1999), pp. 335–348. DOI: 10.1016/S0370-2693(99)01030-8. arXiv: hep-ex/9909022 [hep-ex] (cit. on p. 7).

[FY86] M. Fukugita and T. Yanagida. “Baryogenesis Without Grand Unification”. In: *Phys. Lett.* B174 (1986), pp. 45–47. DOI: 10.1016/0370-2693(86)91126-3 (cit. on p. 8).

[Gar+10] M. Garny, A. Hohenegger, A. Kartavtsev, and M. Lindner. “Systematic approach to leptogenesis in nonequilibrium QFT: Self-energy contribution to the CP-violating parameter”. In: *Phys. Rev.* D81 (2010), p. 085027. DOI: 10.1103/PhysRevD.81.085027. arXiv: 0911.4122 [hep-ph] (cit. on p. 31).

[GHK10] M. Garny, A. Hohenegger, and A. Kartavtsev. “Medium corrections to the CP-violating parameter in leptogenesis”. In: *Phys. Rev.* D81 (2010), p. 085028. DOI: 10.1103/PhysRevD.81.085028. arXiv: 1002.0331 [hep-ph] (cit. on p. 9).

[Hah05] T. Hahn. “CUBA: A Library for multidimensional numerical integration”. In: *Comput. Phys. Commun.* 168 (2005), pp. 78–95. DOI: 10.1016/j.cpc.2005.01.010. arXiv: hep-ph/0404043 [hep-ph] (cit. on pp. 71, 74–76, 79).

[Hal+76] A. Halprin, P. Minkowski, H. Primakoff, and Simon Peter Rosen. “Double-beta Decay and a Massive Majorana Neutrino”. In: *Phys. Rev.* D13 (1976), p. 2567. DOI: 10.1103/PhysRevD.13.2567 (cit. on p. 9).

[HPW09] F. Hahn-Woernle, M. Plumacher, and Y. Y. Y. Wong. “Full Boltzmann equations for leptogenesis including scattering”. In: *JCAP* 0908 (2009), p. 028. DOI: 10.1088/1475-7516/2009/08/028. arXiv: 0907.0205 [hep-ph] (cit. on p. 12).

[HS95] Patrick Huet and Eric Sather. “Electroweak baryogenesis and standard model CP violation”. In: *Phys. Rev.* D51 (1995), pp. 379–394. DOI: 10.1103/PhysRevD.51.379. arXiv: hep-ph/9404302 [hep-ph] (cit. on p. 7).

[Hub29] Edwin Hubble. “A relation between distance and radial velocity among extra-galactic nebulae”. In: *Proc. Nat. Acad. Sci.* 15 (1929), pp. 168–173. DOI: 10.1073/pnas.15.3.168 (cit. on p. 4).

[Hüt13] J. Hütig. "Including gauge corrections to thermal leptogenesis". PhD thesis. Frankfurt U., 2013. URL: http://inspirehep.net/record/1240734/files/Thesis-2013-Hutig.pdf (cit. on pp. 5, 7, 9, 11, 14, 16, 22, 32, 38, 40–42, 44–47, 51–53, 55, 72, 90, 92).

[KB62] L.P. Kadanoff and G. Baym. *Quantum Statistical Mechanics*. New York: W.A. Benjamin Inc., 1962 (cit. on p. 4).

[Kel64] L. V. Keldysh. "Diagram technique for nonequilibrium processes". In: *Zh. Eksp. Teor. Fiz.* 47 (1964). [Sov. Phys. JETP20,1018(1965)], pp. 1515–1527 (cit. on pp. 4, 14).

[Kom+11] E. Komatsu et al. "Seven-Year Wilkinson Microwave Anisotropy Probe (WMAP) Observations: Cosmological Interpretation". In: *Astrophys. J. Suppl.* 192 (2011), p. 18. DOI: 10.1088/0067-0049/192/2/18. arXiv: 1001.4538 [astro-ph.CO] (cit. on p. 6).

[KP12a] Clemens Kiessig and Michael Plumacher. "Hard-Thermal-Loop Corrections in Leptogenesis I: CP-Asymmetries". In: *JCAP* 1207 (2012), p. 014. DOI: 10.1088/1475-7516/2012/07/014. arXiv: 1111.1231 [hep-ph] (cit. on p. 9).

[KP12b] Clemens Kiessig and Michael Plumacher. "Hard-Thermal-Loop Corrections in Leptogenesis II: Solving the Boltzmann Equations". In: *JCAP* 1209 (2012), p. 012. DOI: 10.1088/1475-7516/2012/09/012. arXiv: 1111.1235 [hep-ph] (cit. on p. 9).

[KT90] Edward W. Kolb and Michael S. Turner. "The Early Universe". In: *Front. Phys.* 69 (1990), pp. 1–547 (cit. on p. 6).

[Lan81] Paul Langacker. "Grand Unified Theories and Proton Decay". In: *Phys. Rept.* 72 (1981), p. 185. DOI: 10.1016/0370-1573(81)90059-4 (cit. on p. 7).

[Lem27] Georges Lemaitre. "A Homogeneous Universe of Constant Mass and Growing Radius Accounting for the Radial Velocity of Extragalactic Nebulae". In: *Annales Soc. Sci. Bruxelles A* 47 (1927). [Gen. Rel. Grav.45,no.8,1635(2013)], pp. 49–59. DOI: 10.1007/s10714-013-1548-3 (cit. on p. 4).

[LP53] L. D. Landau and I. Pomeranchuk. "Limits of applicability of the theory of bremsstrahlung electrons and pair production at high-energies". In: *Dokl. Akad. Nauk Ser. Fiz.* 92 (1953), pp. 535–536 (cit. on p. 24).

[Men10] Sebastian Mendizabal Cofre. "Quantum mechanics of leptogenesis". PhD thesis. Hamburg U., 2010. URL: http://www-library.desy.de/cgi-bin/showprep.pl?thesis10-029 (cit. on pp. 13, 91).

[Mig56] Arkady B. Migdal. "Bremsstrahlung and pair production in condensed media at high-energies". In: *Phys. Rev.* 103 (1956), pp. 1811–1820. DOI: 10.1103/PhysRev.103.1811 (cit. on p. 24).

[MR12] David E. Morrissey and Michael J. Ramsey-Musolf. "Electroweak baryogenesis". In: *New J. Phys.* 14 (2012), p. 125003. DOI: 10.1088/1367-2630/14/12/125003. arXiv: 1206.2942 [hep-ph] (cit. on p. 7).

[Pat+16] C. Patrignani et al. "Review of Particle Physics". In: *Chin. Phys.* C40.10 (2016), p. 100001. DOI: 10.1088/1674-1137/40/10/100001 (cit. on pp. 7, 69).

[Sak67] A. D. Sakharov. "Violation of CP Invariance, c Asymmetry, and Baryon Asymmetry of the Universe". In: *Pisma Zh. Eksp. Teor. Fiz.* 5 (1967). [Usp. Fiz. Nauk161,61(1991)], pp. 32–35. DOI: 10.1070/PU1991v034n05ABEH002497 (cit. on pp. 4, 6).

[Sch14] Matthew D. Schwartz. *Quantum Field Theory and the Standard Model*. Cambridge University Press, 2014. ISBN: 1107034736, 9781107034730. URL: http://www.cambridge.org/us/academic/subjects/physics/theoretical-physics-and-mathematical-physics/quantum-field-theory-and-standard-model (cit. on p. 18).

[Sch61] Julian S. Schwinger. "Brownian motion of a quantum oscillator". In: *J. Math. Phys.* 2 (1961), pp. 407–432. DOI: 10.1063/1.1703727 (cit. on p. 4).

[SW96] Barbara Schrempp and Michael Wimmer. "Top quark and Higgs boson masses: Interplay between infrared and ultraviolet physics". In: *Prog. Part. Nucl. Phys.* 37 (1996), pp. 1–90. DOI: 10.1016/0146-6410(96)00059-2. arXiv: hep-ph/9606386 [hep-ph] (cit. on p. 70).

[t H76a] Gerard 't Hooft. "Computation of the Quantum Effects Due to a Four-Dimensional Pseudoparticle". In: *Phys. Rev.* D14 (1976). [Erratum: Phys. Rev.D18,2199(1978)], pp. 3432–3450. DOI: 10.1103/PhysRevD.18.2199.3,10.1103/PhysRevD.14.3432 (cit. on p. 7).

[t H76b] Gerard 't Hooft. "Symmetry Breaking Through Bell-Jackiw Anomalies". In: *Phys. Rev. Lett.* 37 (1976), pp. 8–11. DOI: 10.1103/PhysRevLett.37.8 (cit. on p. 7).

[Wel83] H. Arthur Weldon. "Simple Rules for Discontinuities in Finite Temperature Field Theory". In: *Phys. Rev.* D28 (1983), p. 2007. DOI: 10.1103/PhysRevD.28.2007 (cit. on p. 19).

[Wol17] Wolfram Research, Inc. *Mathematica 11.0*. Version 11.2. 2017. URL: https://www.wolfram.com (cit. on pp. 59, 67, 94).

Selbständigkeitserklärung

Gemäß §30 (12) der Ordnung des Fachbereichs Physik an der Johann Wolf- gang von Goethe Universität für den Bachelor- und Masterstudiengang Physik vom 24.04.2013 versichere ich, dass ich die vorliegende Arbeit selbständig und ohne Benutzung anderer als der angegebenen Quellen und Hilfsmittel verfasst habe. Ferner erkläre ich, dass diese Arbeit, auch nicht auszugsweise, für eine andere Prüfung oder Studienleistung verwendet worden ist.

Andreas Halsch